



VOL
G.W.-OSC. OFF ON
CW-OSC ADJUST
OFF-M.V.C.-A.V.C.
REC. SEND
FUSE
FUSE
FUSE
MICRO
SPEAKER 200 8000
PUSHES 200 8000
PUSHES 200 8000
LOCK
400u OHMS

THE OPTICAL PROPERTIES OF THIN GLASS-LIKE FILMS
GRANT
1966

72
清永 上

AD 619 071

THE OPTICAL PROPERTIES OF THIN GERMANIUM
FILMS

Paul Michael Grant

June 1965

DISTRIBUTED BY:

CLEARINGHOUSE

FOR FEDERAL SCIENTIFIC AND TECHNICAL INFORMATION

U. S. DEPARTMENT OF COMMERCE / NATIONAL BUREAU OF STANDARDS / INSTITUTE FOR APPLIED TECHNOLOGY



REPORT selection aids

Pinpointing R & D reports for industry

Clearinghouse, Springfield, Va. 22151

U.S. GOVERNMENT RESEARCH AND DEVELOPMENT REPORTS (USGRDR)---SEMI-MONTHLY JOURNAL ANNOUNCING R&D REPORTS. ANNUAL SUBSCRIPTION \$30.00 (\$37.50 FOREIGN MAILING). SINGLE COPY \$3.00.

U.S. GOVERNMENT RESEARCH AND DEVELOPMENT REPORTS INDEX---SEMI-MONTHLY INDEX TO U.S. GOVERNMENT RESEARCH AND DEVELOPMENT REPORTS. ANNUAL SUBSCRIPTION \$22.00 (\$27.50 FOREIGN MAILING). SINGLE COPY \$3.00.

FAST ANNOUNCEMENT SERVICE---SUMMARIES OF SELECTED R&D REPORTS COMPILED AND MAILED BY SUBJECT CATEGORIES. ANNUAL SUBSCRIPTION \$5.00, TWO YEARS: \$9.00, AND THREE YEARS: \$12.00. WRITE FOR AN APPLICATION FORM.

DOCUMENT PRICES---ALMOST ALL OF THE DOCUMENTS IN THE CLEARINGHOUSE COLLECTION ARE PRICED AT \$3.00 FOR PAPER COPIES AND 65 CENTS FOR COPIES IN MICROFICHE.

COUPONS---THE CLEARINGHOUSE PREPAID DOCUMENT COUPON SALES SYSTEM FOR PURCHASING PAPER COPIES AND MICROFICHE PROVIDES FASTER, MORE EFFICIENT SERVICE ON DOCUMENT REQUESTS. THE PREPAID COUPON IS A TABULATING CARD WITH A FACE VALUE OF THE PURCHASE PRICE OF A CLEARINGHOUSE DOCUMENT (\$3.00 PAPER COPY OR 65 CENTS MICROFICHE). IT IS YOUR METHOD OF PAYMENT, ORDER FORM, SHIPPING LABEL, AND RECEIPT OF SALE.

COUPONS FOR PAPER COPY (HC) DOCUMENTS ARE AVAILABLE AT \$3.00 EACH OR IN BOOKS OF 10 COUPONS FOR \$30.00. COUPONS FOR MICROFICHE COPIES OF CLEARINGHOUSE DOCUMENTS ARE AVAILABLE IN BOOKS OF 50 COUPONS FOR \$32.50. WRITE FOR A COUPON ORDER FORM.

AD619071

Office of Naval Research

Contract Nonr-1866 (10)

NR-017-308

THE OPTICAL PROPERTIES OF THIN
GERMANIUM FILMS



COPY _____ OF _____ 16
HARD COPY \$ 6.00
MICROFICHE \$ 1.50
2131

DDC
REPRODUCED
AUG 17 1965
RESOLVED
DDC-IRA E

By

Paul Michael Grant

June, 1965

Technical Report No. HP-14

Gordon McKay Laboratory
Division of Engineering and Applied Physics
Harvard University • Cambridge, Massachusetts

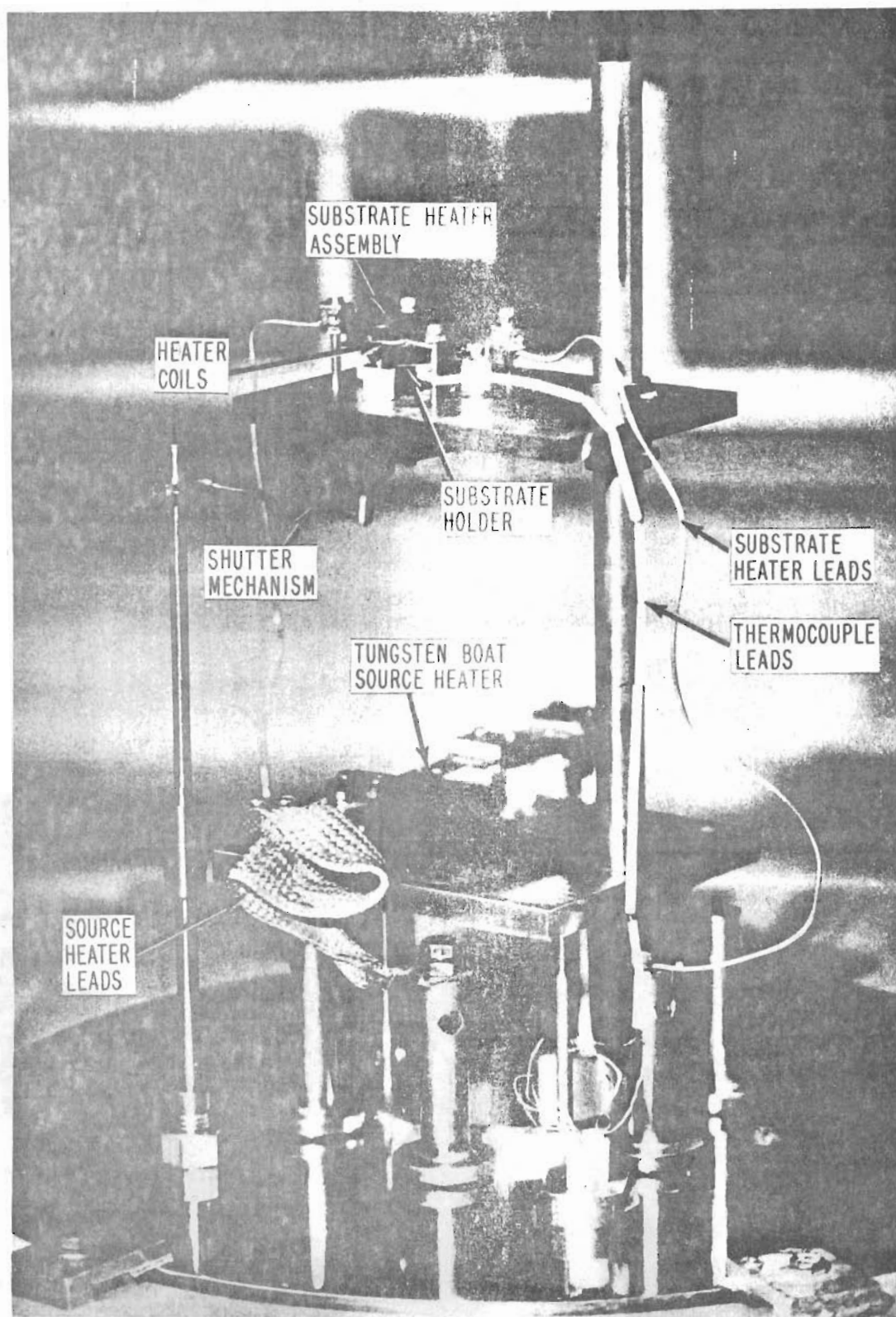


FIG. 2-2 THE HARVARD EVAPORATION APPARATUS

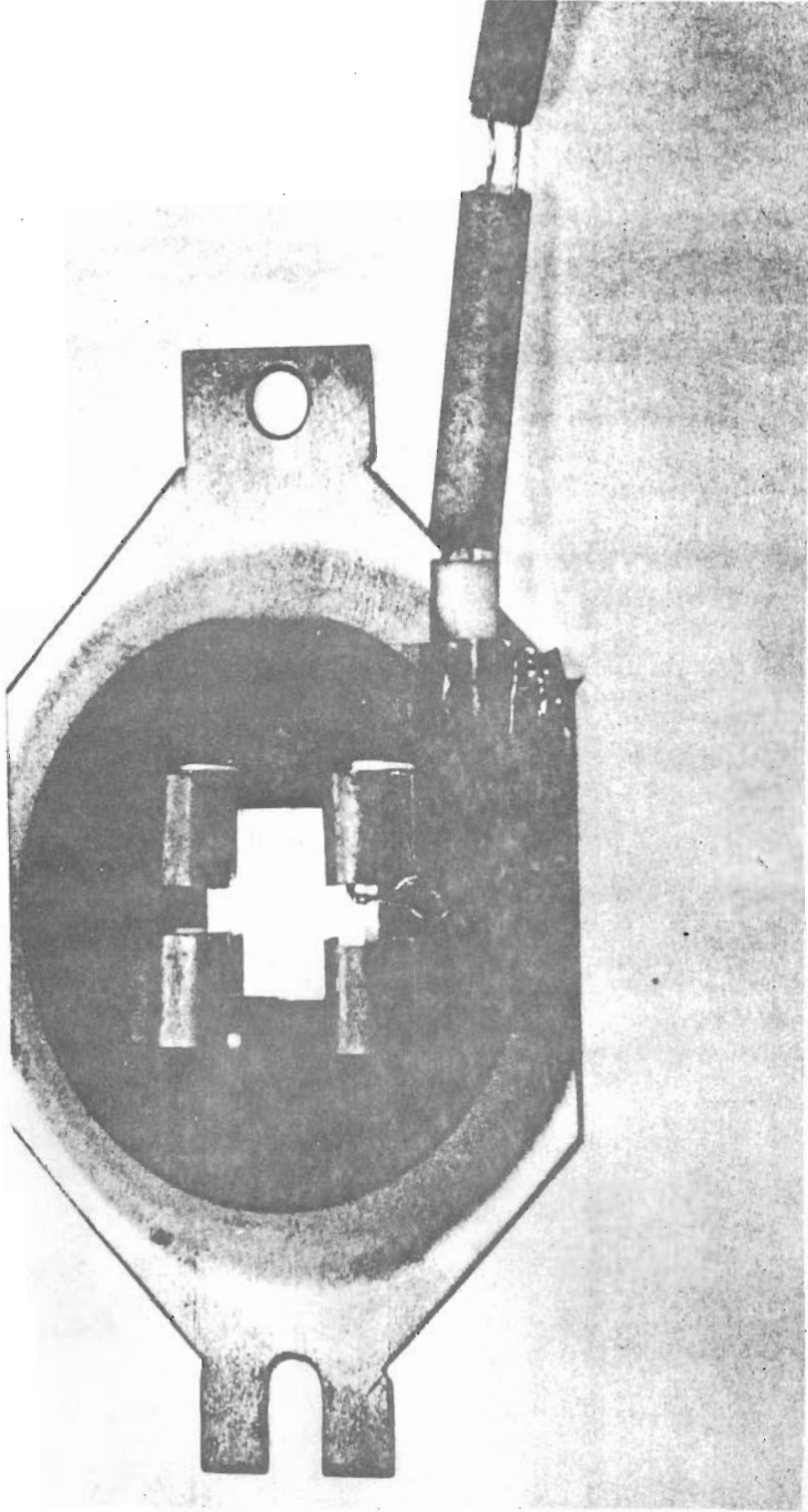
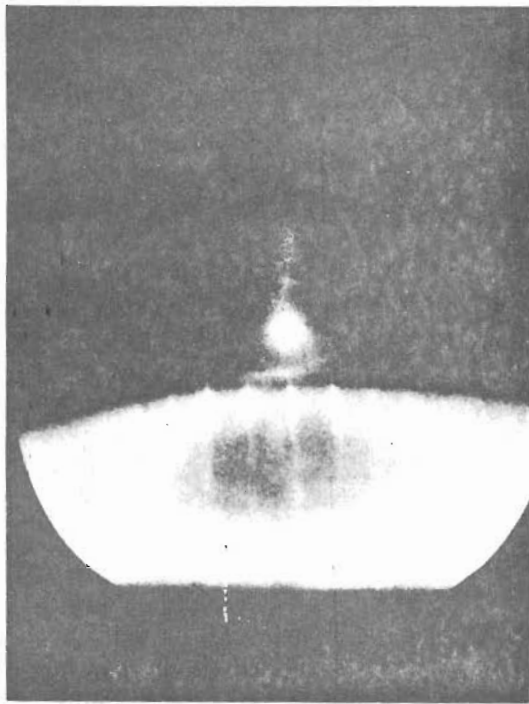


FIG. 2-3 DETAILS OF THE SUBSTRATE HOLDER SHOWING SUBSTRATE AND THERMOCOUPLE IN POSITION

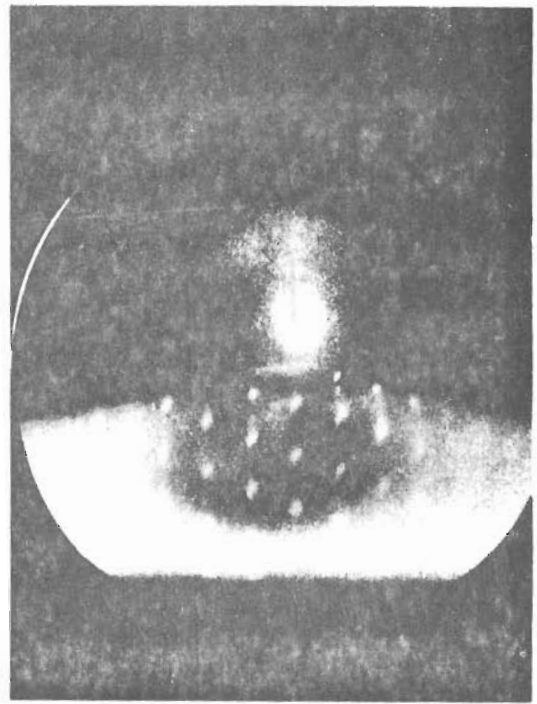


FIG. 2-4 TYPICAL GERMANIUM FILM SAMPLE ON CLEAVED CaF_2

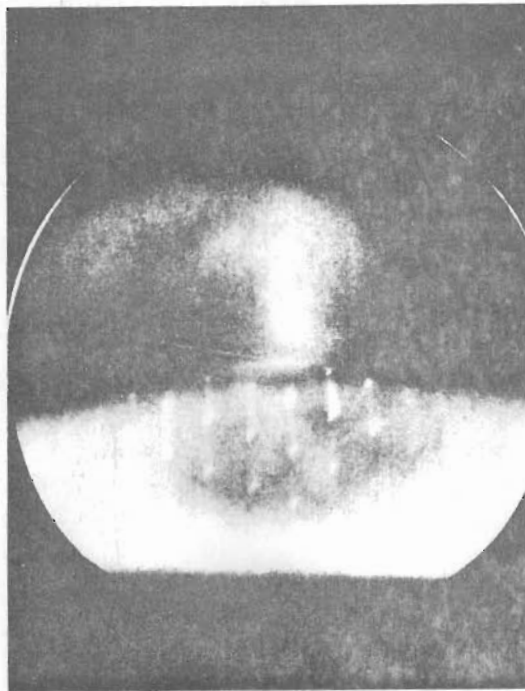
602 071



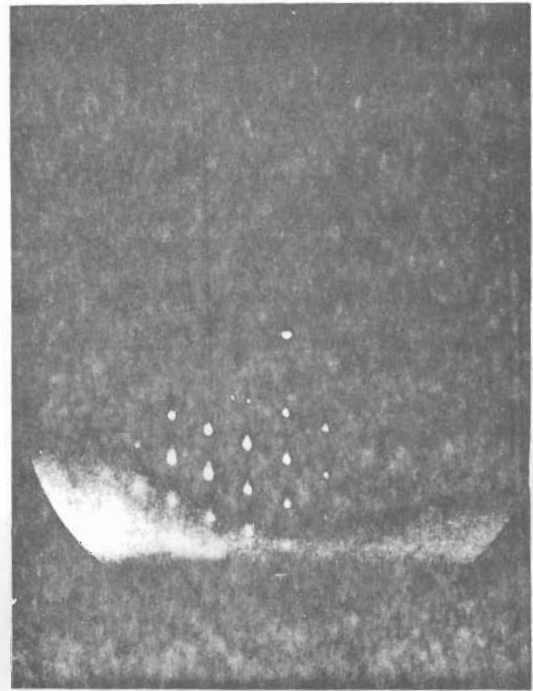
(a) Substrate Before Opening Shutter



(b) Pattern After 15 Seconds Growth



(c) 3 Minutes Growth



(d) 5 Minutes Growth

FIG. 2-6 TIME SEQUENCE REFLECTION ELECTRON DIFFRACTOGRAMS SHOWING EPITAXIAL GROWTH OF GERMANIUM FILM ON CaF_2

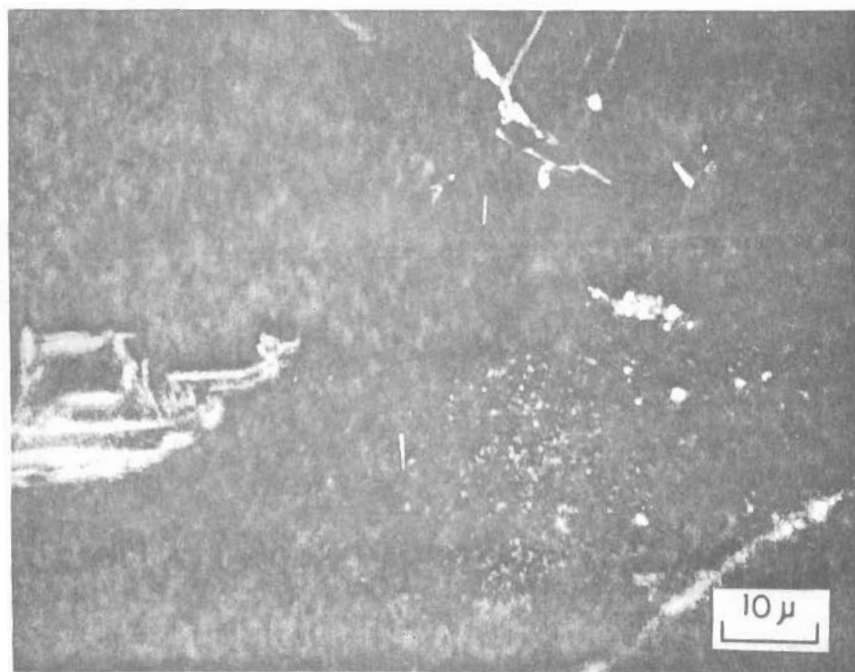


FIG. 2-7 SURFACE PHOTOMICROGRAPH OF
EPITAXIAL Ge FILM ON CLEAVED CaF₂

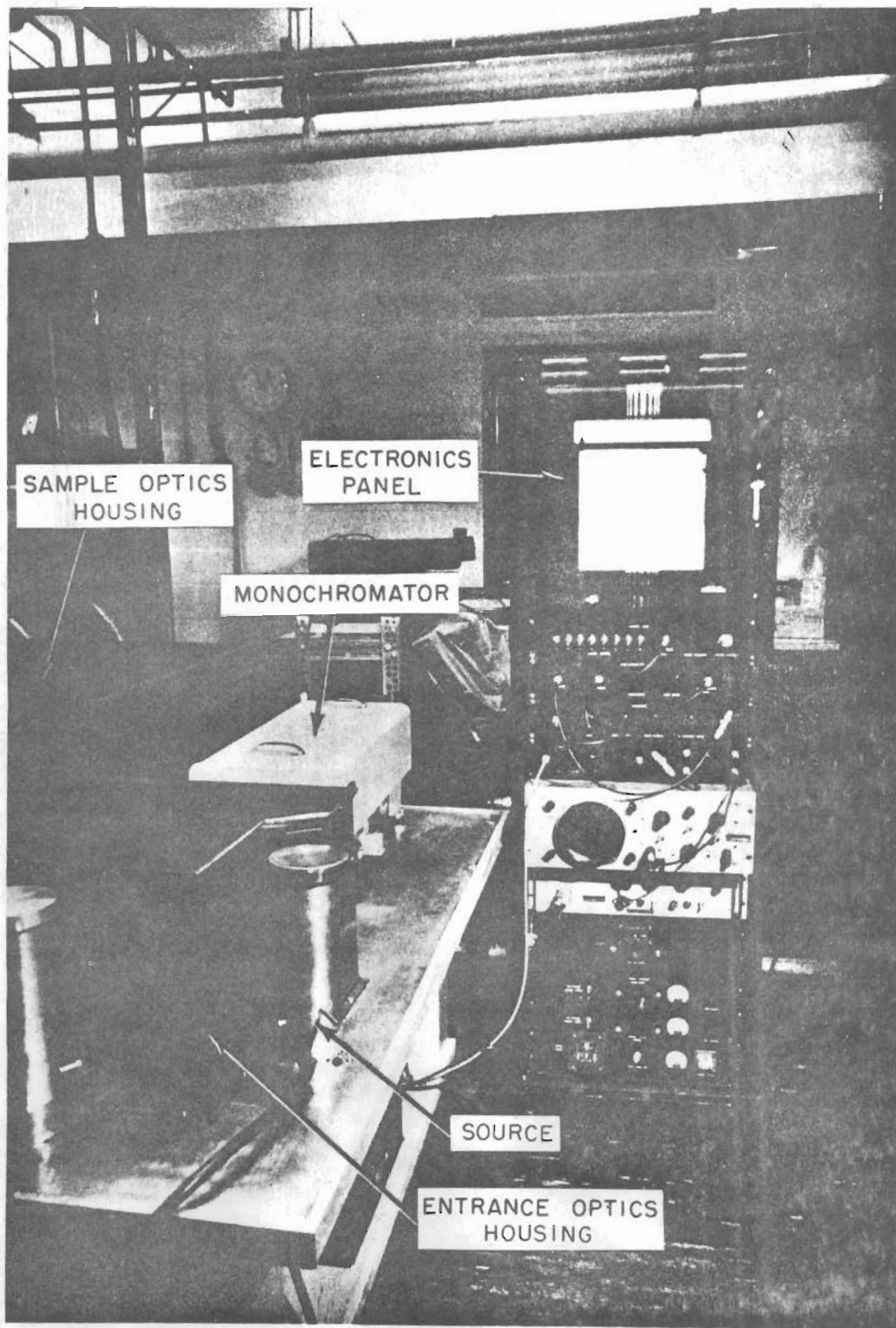


FIG. 4-2 PHOTOGRAPH OF THE SPECTROPHOTOMETER

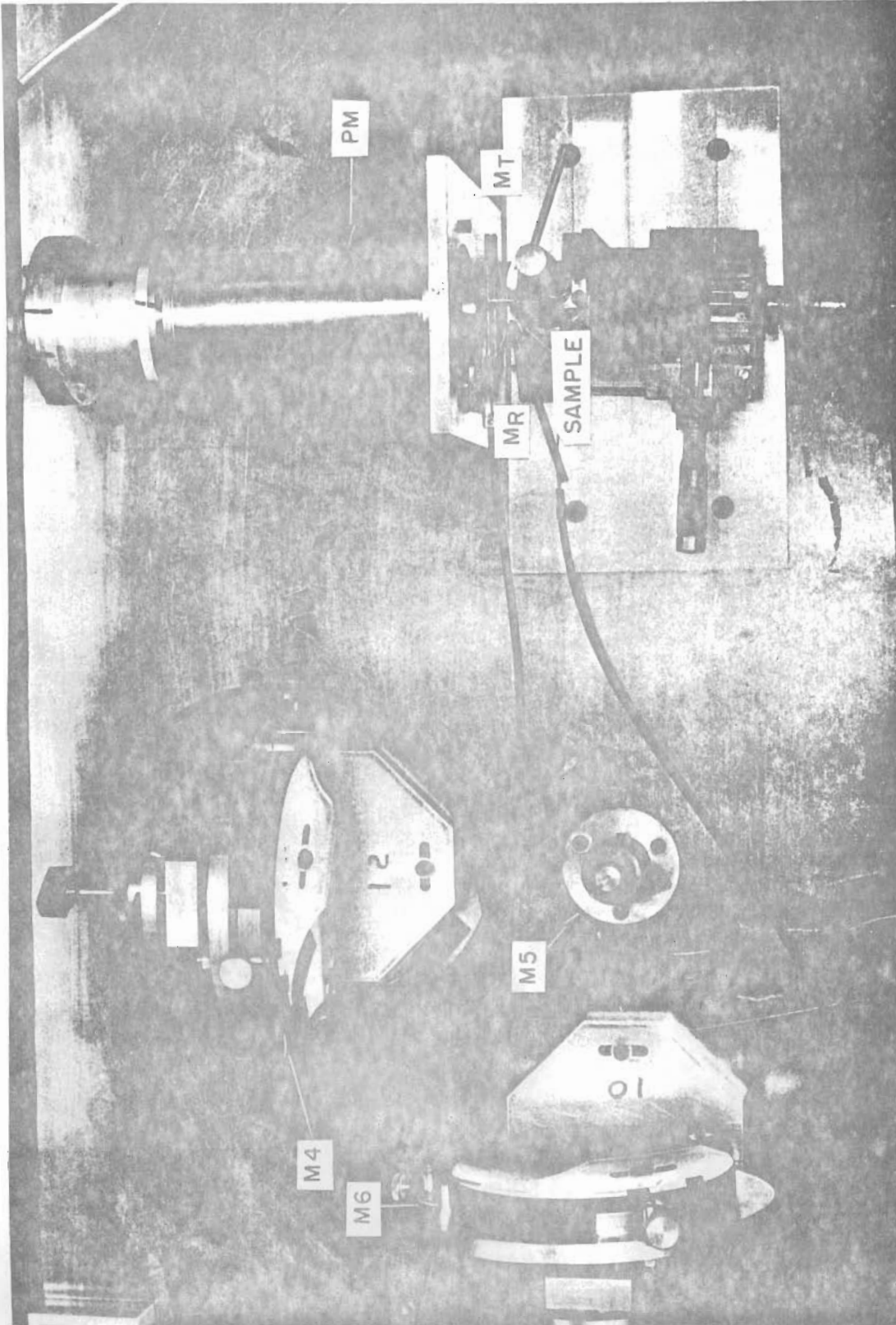
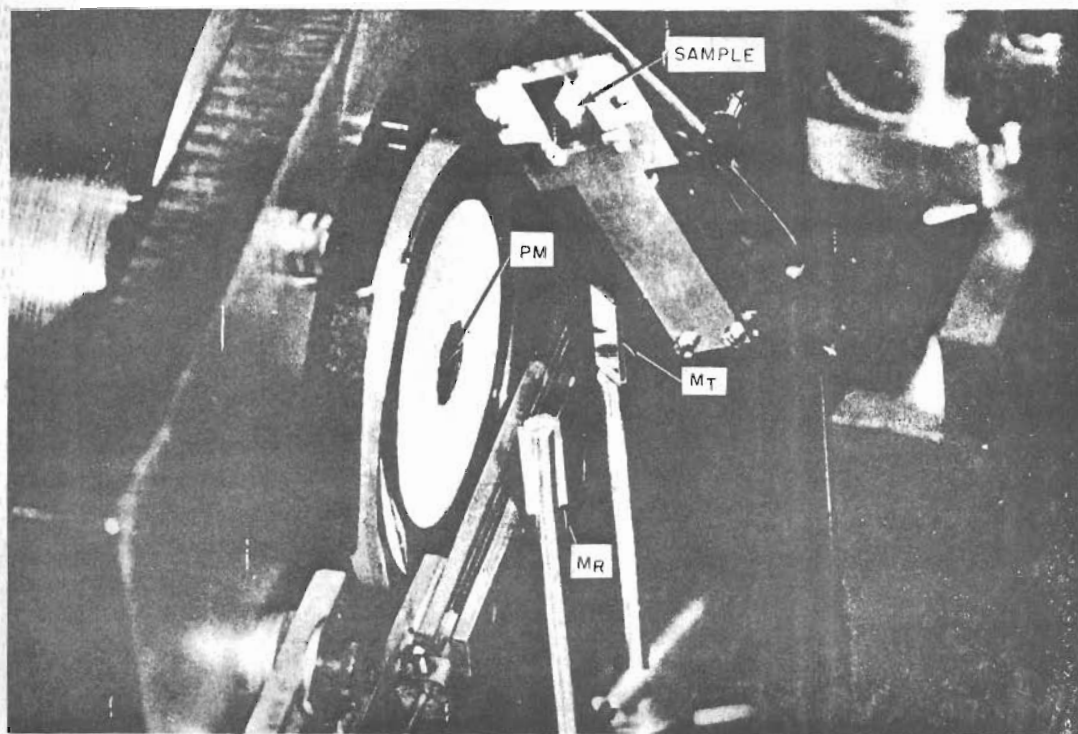
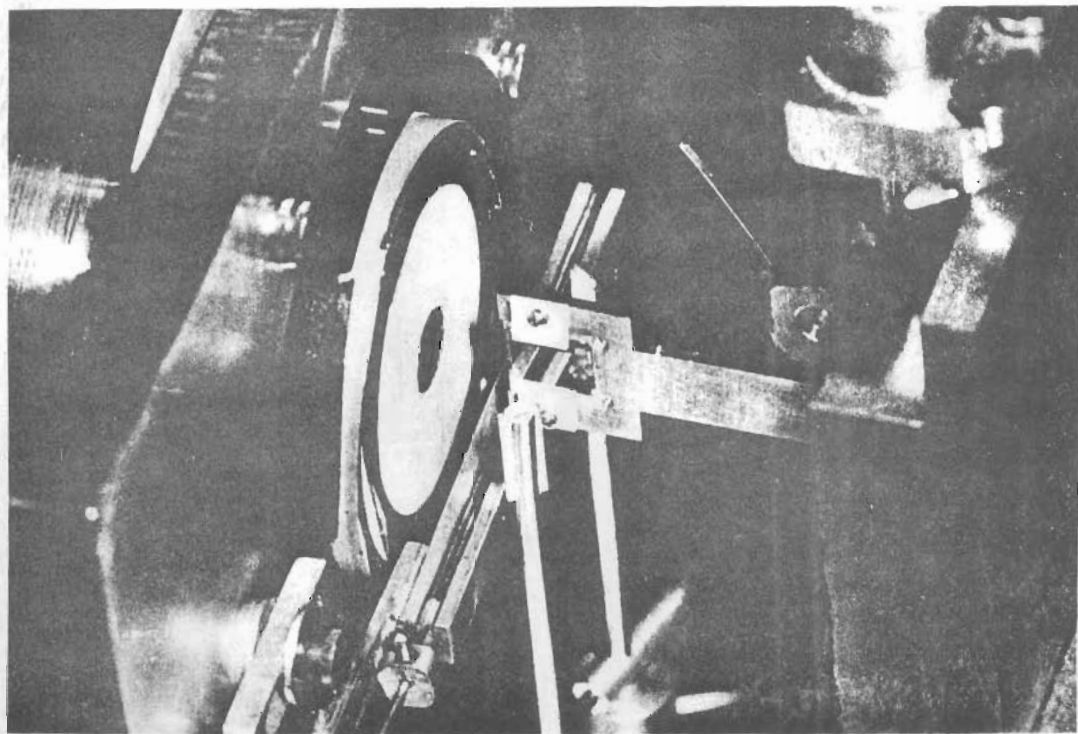


FIG. 4-3 PHOTOGRAPH OF SAMPLE OPTICS



(a) SAMPLE OUT

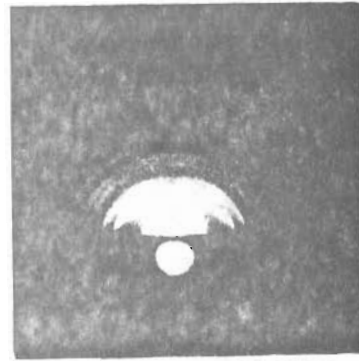


(b) SAMPLE IN

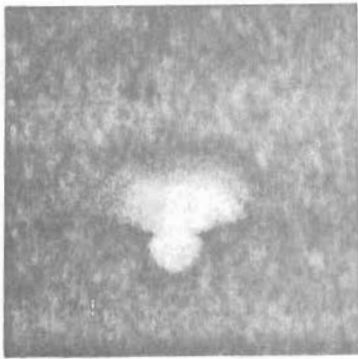
FIG. 4-4 DETAILS OF SAMPLE OPTICS



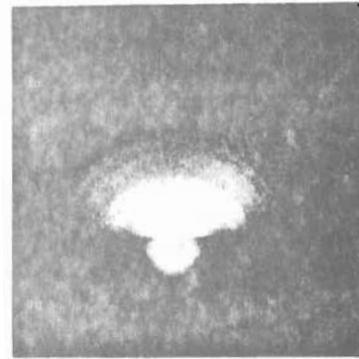
1. 780°C



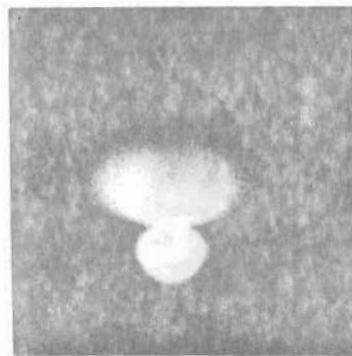
2. 600°C



3. 450°C



4. 300°C

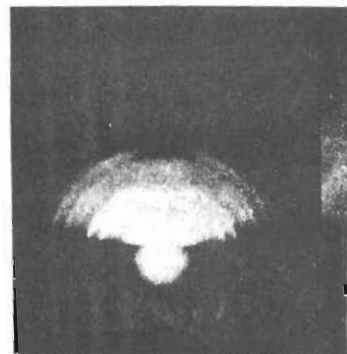


5. 25°C

FIG. 4-6 RED PATTERNS FOR Ge FILMS ON FUZED QUARTZ FOR VARIOUS SUBSTRATE TEMPERATURES, T_s . Δ APPROXIMATELY CONSTANT.



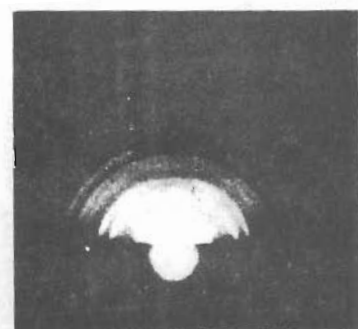
1. 3850Å/min



2. 1600Å/min

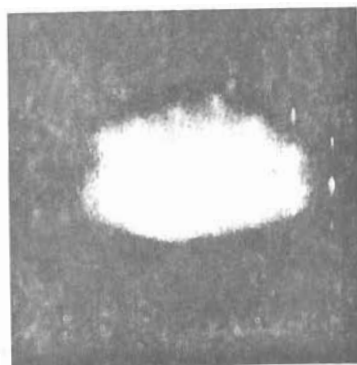


3. 670Å/min

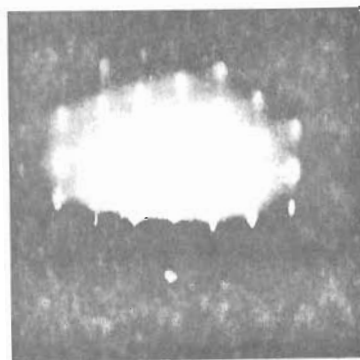


4. 154Å/min

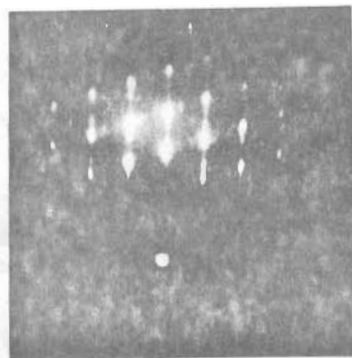
FIG. 4-8 RED PATTERNS FOR Ge FILMS ON FUZED QUARTZ FOR VARIOUS DEPOSITION RATES, Δ . $T_s = 600^\circ\text{C}$.



$T_s = 600^\circ\text{C}$
 $\Delta = 925 \text{ \AA}/\text{min}$
 $\alpha = 1850 \text{ \AA}$



$T_s = 600^\circ\text{C}$
 $\Delta = 750 \text{ \AA}/\text{min}$
 $\alpha = 250 \text{ \AA}$



$T_s = 620^\circ\text{C}$
 $\Delta = 810 \text{ \AA}/\text{min}$
 $\alpha = 135 \text{ \AA}$

FIG. 4--10 RED PATTERNS FOR Ge FILMS ON CaF₂.

019 071

Office of Naval Research

Contract Nonr-1866(10)

NR - 017 - 308

THE OPTICAL PROPERTIES OF THIN GERMANIUM FILMS

by

Paul Michael Grant

June, 1965

The research reported in this document was made possible through support extended the Division of Engineering and Applied Physics, Harvard University, by the Office of Naval Research, under Contract Nonr-1866(10). Reproduction in whole or in part is permitted for any purpose of the United States Government.

Technical Report HP-14

Gordon Mc Kay Laboratory

Division of Engineering and Applied Physics

Harvard University

Cambridge, Massachusetts

TABLE OF CONTENTS

	Page
TABLE OF CONTENTS	iii
LIST OF FIGURES	vii
LIST OF TABLES	xi
ABSTRACT	xiii

Chapter One

INTRODUCTION

A. OBJECTIVES OF RESEARCH. PRELIMINARY REMARKS.	1-1
B. REVIEW OF THE MACROSCOPIC AND MICROSCOPIC THEORIES OF THE OPTICAL PROPERTIES OF SOLIDS.	1-3
1. Theory of the Optical Response of Materials According to the Electromagnetic Theory of Light.	1-3
2. Quantum Mechanical Theory of the Optical Constants.	1-12
C. THE BAND STRUCTURE OF GERMANIUM.	1-15
D. REVIEW OF THE METHODS OF DETERMINING THE OPTICAL CONSTANTS OF SOLIDS.	1-18
1. Polarimetric Measurements.	1-18
2. Dispersion Theory. Kramers-Kronig Analysis.	1-19
3. Photometric Measurements.	1-22
E. REVIEW OF THE ATTEMPTS TO DETERMINE THE OPTICAL CONSTANTS OF GERMANIUM THIN FILMS.	1-24
1. Skin Depth of Germanium.	1-24
2. Preparation of Thin Films.	1-24
3. Results Prior to 1950.	1-25
4. Results After 1950.	1-26
BIBLIOGRAPHY.	1-28

Chapter Two

THIN FILM FABRICATION.

A. REVIEW OF METHODS OF FABRICATING THIN GERMANIUM FILMS.	2-1
1. Pre-Epitaxial Methods.	2-1
2. Post-Epitaxial Methods.	2-3
3. Suitability of Various Methods for Producing Films for Optical Studies.	2-5
B. THE TECHNIQUE OF VACUUM DEPOSITION OF EPITAXIAL GERMANIUM FILMS ON CaF ₂ SUBSTRATES.	2-5
1. Reasons for Choice of CaF ₂ . Substrate Preparation.	2-5
2. The Apparatus of Via.	2-9
3. The Harvard Apparatus. Deposition Procedure.	2-10
4. Physical Appearance of the Deposited Films.	2-13
C. REFLECTION ELECTRON DIFFRACTION (RED) ANALYSIS.	2-15
D. FILM SURFACE TOPOGRAPHY STUDIES.	2-21
E. MEASUREMENT OF FILM THICKNESS.	2-21
BIBLIOGRAPHY.	2-23

Chapter Three

THE THEORY OF THE DETERMINATION OF THE OPTICAL CONSTANTS OF SEMICONDUCTOR THIN FILMS FROM PHOTOMETRIC MEASUREMENTS.

A. THE REFLECTIVITY-TRANSMISSIVITY (RT) METHOD.	3-1
1. Theoretical Development.	3-1
2. The First Order Error Derivatives for Germanium Thin Films.	3-10
B. THE TWO THICKNESS, TWO TRANSMISSION METHOD.	3-17
1. Theoretical Development.	3-17
2. Error Derivatives.	3-18
C. CONCLUSION.	3-21
BIBLIOGRAPHY.	3-24

Chapter FourMEASUREMENT OF THE REFLECTIVITY AND TRANSMISSIVITY
COEFFICIENTS OF THIN GERMANIUM FILMS.

A. SPECTROPHOTOMETRIC APPARATUS.	4-1
1. Principles of Design and Operation.	4-1
2. Description of Experimental Procedures. Test and Calibration by Measurement of Bulk Reflectivity.	4-8
B. RESULTS FOR THE REFLECTIVITY AND TRANSMISSIVITY COEFFICIENTS.	4-12
1. Results for Fused Quartz Substrates.	4-12
2. Results for Cleaved CaF ₂ Substrates.	4-13
C. INTERPRETATION OF RESULTS.	4-15
1. Effect of Film Crystalline Perfection.	4-15
2. Effect of Surface Topography and Film Thickness.	4-19
3. Effect of Induced Strains in the Films.	4-24
4. Comparison with Other Work.	4-29
BIBLIOGRAPHY.	4-31

Chapter Five

ANALYSIS OF EXPERIMENTAL RESULTS.

A. NUMERICAL ANALYSIS AND PROGRAMMING TECHNIQUES.	5-1
1. The Newton-Raphson Method.	5-1
2. Programming Operations.	5-3
B. THE OPTICAL CONSTANTS OF THIN GERMANIUM FILMS	5-5
C. CONCLUSIONS.	5-7
BIBLIOGRAPHY.	5-12

ACKNOWLEDGEMENTS.

LIST OF FIGURES

	<u>After Page</u>
Fig. 1-1. Reflection and Transmission of an Electromagnetic Wave at the Boundary between Two Media.	1-10
Fig. 1-2. Pseudopotential Energy Bands of Germanium as Calculated by Brust with some of the Principal Transitions Indicated.	1-16
Fig. 1-3. (a) Reflectivity of Bulk Germanium; (b) The Kramers-Kronig Results for the Optical Constants of Germanium	1-22
Fig. 1-4. Skin Depth of Germanium as a Function of Wavelength.	1-24
Fig. 1-5. Optical Constants Obtained by Other Workers from Germanium Thin Films; (a) O'Bryan, 1936; (b) Brattain and Briggs, 1949; (c) Gebbie, 1952; (d) Lukes, 1960.	1-26
Fig. 2-1. Schematic Diagram of the Arrangement of the Components in the Evaporation Chamber.	2-10
Fig. 2-2. The Harvard Evaporation Apparatus.	2-10
Fig. 2-3. Details of the Substrate Holder Showing Substrate and Thermocouple in Position.	2-10
Fig. 2-4. Typical Germanium Film Sample on Cleaved CaF_2 .	2-14
Fig. 2-5. Ewald's Construction in the Reciprocal Lattice.	2-16
Fig. 2-6. Time Sequence Reflection Electron Diffractograms Showing Epitaxial Growth of Germanium Film on CaF_2 .	2-16
Fig. 2-7. Surface Photomicrograph of Epitaxial Ge Film on Cleaved CaF_2 .	2-20

After Page

- Fig. 3-1. Model for the Case of an Absorbing Thin Film on a Semi-infinite Non-absorbing Substrate. 3-2
- Fig. 3-2. Intensity Addition Model for a Thin Absorbing Film on a Thick Non-absorbing Substrate. 3-6
- Fig. 3-3. The Transmission of Germanium Thin Films on CaF_2 Substrates Using the Optical Constants Derived by Philipp. 3-6
- Fig. 3-4. The Reflectivity of Germanium Thin Films on CaF_2 Substrates Using the Optical Constants Derived by Philipp. 3-6
- Fig. 3-5. A T vs R Representation Using Relation (3-12) and R and T for a 300\AA Ge Film Calculated From Equations (3-9a) and (3-10). 3-10
- Fig. 3-6. The Root-Locus Diagram for the R-T Model of a 50\AA Ge Film on CaF_2 ; (a) $\lambda = 2500\text{\AA}$, $a = 50\text{\AA}$; (b) $\lambda = 3000\text{\AA}$, $a = 50\text{\AA}$; (c) $\lambda = 5500\text{\AA}$, $a = 50\text{\AA}$. 3-16
- Fig. 3-7. The Root-Locus Diagram for the R-T Model of a 150\AA Ge Film on CaF_2 ; (a) $\lambda = 2500\text{\AA}$, $a = 150\text{\AA}$; (b) $\lambda = 3000\text{\AA}$, $a = 150\text{\AA}$; (c) $\lambda = 5500\text{\AA}$, $a = 150\text{\AA}$. 3-16
- Fig. 3-8. The Root-Locus Diagram for the R-T Model of a 300\AA Ge Film on CaF_2 ; (a) $\lambda = 2500\text{\AA}$, $a = 300\text{\AA}$; (b) $\lambda = 3000\text{\AA}$, $a = 300\text{\AA}$; (c) $\lambda = 5500\text{\AA}$, $a = 300\text{\AA}$; (d) $\lambda = 3900\text{\AA}$, $a = 300\text{\AA}$. 3-16
- Fig. 3-9. The Root-Locus Diagram for the R-T Model of a 500\AA Ge Film on CaF_2 ; (a) $\lambda = 2500\text{\AA}$, $a = 500\text{\AA}$; (b) $\lambda = 3000\text{\AA}$, $a = 500\text{\AA}$; (c) $\lambda = 5500\text{\AA}$, $a = 500\text{\AA}$. 3-16
- Fig. 3-10. The Angle of Root-Locus Intersections θ_{RT} , vs. λ for the R-T Model of a Ge Film on CaF_2 . 3-16
- Fig. 3-11. The Index of Refraction Error Derivatives vs. λ for the R-T Model of a Ge Film on CaF_2 ; (a) $|\partial n/\partial R|$; (b) $T|\partial n/\partial T|$; (c) $|\partial n/\partial a|$. 3-16

	<u>After Page</u>
Fig. 3-12. The Extinction Coefficient Error Derivatives vs. λ for the R-T Model of a Ge Film on CaF_2 ; (a) $ \partial k/\partial R $; (b) $T \partial k/\partial T $; (c) $ \partial k/\partial a $.	3-16
Fig. 3-13. Wavelength Region Where $ \theta_{RT} \leq 10^\circ$ for the R-T Model of a Ge Film on CaF_2 .	3-16
Fig. 3-14. (a) Wavelength Region Where $ \partial n/\partial R \geq 20$ for the R-T Model of a Ge Film on CaF_2 ; (b) $T \partial n/\partial T \geq 5$; (c) $ \partial n/\partial a \geq 5 \cdot 10^{-2}/\text{\AA}$.	3-16
Fig. 3-15. (a) Wavelength Region Where $ \partial k/\partial R \geq 20$ for the R-T Model of a Ge Film on CaF_2 ; (b) $T \partial k/\partial T \geq 5$; (c) $ \partial k/\partial a \geq 5 \cdot 10^{-2}/\text{\AA}$.	3-16
Fig. 3-16. The Index of Refraction Combined Transmission Error Derivatives vs. λ for Two Thickness, Two Transmission Method for Ge Films on CaF_2 ; (a) a' paired with $a = 50 \text{\AA}$; (b) a' paired with $a = 100 \text{\AA}$; (c) a' paired with $a = 200 \text{\AA}$; (d) a' paired with $a = 300 \text{\AA}$ and 400\AA .	3-20
Fig. 3-17. The Index of Refraction Combined Thickness Error Derivatives vs. λ for Two Thickness, Two Transmission Method for Ge Films on CaF_2 ; (a) a' paired with $a = 50 \text{\AA}$; (b) a' paired with $a = 100 \text{\AA}$; (c) a' paired with $a = 200 \text{\AA}$; (d) a' paired with $a = 300 \text{\AA}$ and 400\AA .	3-20
Fig. 4-1. (a) Schematic Diagram of the Optical Signal Path; (b) Block Diagram of the Electronic Signal Path.	4-2
Fig. 4-2. Photograph of the Spectrophotometer.	4-2
Fig. 4-3. Photograph of Sample Optics.	4-2
Fig. 4-4. Details of Sample Optics; (a) Sample Out; (b) Sample In.	4-2
Fig. 4-5. Reflectivity of Etched Single Crystal Bulk Germanium.	4-12

After Page

Fig. 4-6.	RED Patterns for Ge Films on Fused Quartz for Various Substrate Temperatures T_S . Δ Approximately Constant.	4-12
Fig. 4-7.	Reflectivity of Ge Films on Fused Quartz for Various Substrate Temperatures, T_S .	4-12
Fig. 4-8.	RED Patterns for Ge Films on Fused Quartz for Various Deposition Rates, Δ . $T_S = 600^\circ\text{C}$.	4-12
Fig. 4-9.	Reflectivity of Ge Films on Fused Quartz for Various Deposition Rates, Δ .	4-12
Fig. 4-10.	RED Patterns for Ge Films on CaF_2 .	4-14
Fig. 4-11.	Reflectivity of a 1850 Å Epitaxial Germanium Film Compared with that of Bulk Germanium.	4-14
Fig. 4-12.	(a) Reflectivity of a 250 Å Epitaxial Germanium Film on CaF_2 ; (b) Transmission of a 250 Å Epitaxial Germanium Film on CaF_2 .	4-14
Fig. 4-13.	(a) Reflectivity of a 135 Å Epitaxial Germanium Film on CaF_2 ; (b) Transmission of a 135 Å Epitaxial Germanium Film on CaF_2 .	4-14
Fig. 4-14.	Roughness Plot for the 1850 Å Epitaxial Ge Film on CaF_2 .	4-22
Fig. 4-15.	Effect of Film Stress on Reflectivity Peaks.	4-28
Fig. 5-1.	Flow Chart of Optical Constant Calculation Program.	5-4
Fig. 5-2.	Optical Constants of a 250 Å Epitaxial Germanium Film.	5-6

LIST OF TABLES

	Page
Table 2-1. The pertinent physical properties of possible substrate materials suitable for the epitaxial deposition of germanium films.	2-14
Table 3-1. Wavelength and energy at which $n^2 = k^2 + 1$ or $\epsilon_1 = 1$ for several common semiconductor materials.	3-23

ABSTRACT

This report describes an investigation into the optical properties of thin germanium films. The central topic is the deduction of the optical constants from photometric measurements on epitaxial films on CaF_2 in the wavelength range 2000 - 6000 Å. Methods of film production are discussed, and the effect of deposition parameters on the crystallinity and reflectivity of films on fused quartz and CaF_2 are reported. The principal conclusion is that epitaxial films give excellent agreement with bulk single crystal material as regards interband transition structure in their reflectivity and transmissivity coefficients R and T. However, the over-all amplitudes of R and T for films are strongly governed by residual surface roughness effects. These cause the magnitude of R, in the region 2000 - 3500 Å, to depart considerably from that of carefully prepared bulk surfaces.

Theoretical studies are carried out on the accuracy of derivation of the optical constants n and k from measurements of normal incidence R and T on a single film. Another model also considered is the recovery of n and k from measurements of the transmissivities of two films of different thicknesses. For each of these methods, the first order dependence of n and k on the photometric quantities was calculated using appropriate theoretical equations and optical constants from dispersion analyses. The

results indicate that for the R and T method, in the wavelength regions where $n \approx k$, the error in the derived optical constants becomes intolerably large for the usual experimental errors in R and T. For the two thickness, two transmission method, however, certain judicious choices of thicknesses can reduce the sensitivity to experimental error to reasonable values over the entire wavelength range considered here.

A review is given of previous investigations and measurements of the optical properties and constants of germanium thin films. This review shows that the results are much at variance among themselves due to lack of crystalline perfection in the samples studied. The results for n and k reported in this work were computed from measurements of R and T on a 250 Å epitaxial germanium film on CaF_2 . They are shown to give much better agreement with optical constants from dispersion analysis than those of earlier workers. In addition, with the inclusion of experimental error, the present results overlap those of the dispersion analysis in those wavelength ranges in which it was possible to obtain roots.

Thus, the conclusions of this research may be summarized as follows:

- (1) The optical properties of epitaxial germanium films replicate bulk single crystals to a degree sufficient to justify

their consideration as vehicles for further optical research into the high energy, high absorption spectral regions.

(2) The use of epitaxial semiconductor films to calculate optical constants will supplement, but not supplant, other methods such as polarimetry and dispersion analysis.

Chapter One

INTRODUCTION

A. OBJECTIVES OF RESEARCH. PRELIMINARY REMARKS.

"It will be clear to anyone who has contemplated the measurement of optical constants that this is no easy task. The apparent values of optical constants shown by a film or surface depend critically on the state of the first few layers. The measurements involved are not easy to make with high accuracy; and it would appear from much early work on the n , k values for thin films that different methods may yield results differing by unhealthily large factors from those of other people. Such large differences may, however, be generally attributed to differences in method of preparation of the film. Both sets of figures may well be correct for the different systems. If the film structures are widely different, agreement in n , k values would not be expected. Unless the state of the film is closely specified, the results for n , k are likely to be of little value unless determined by a method which takes account of the structure of the film."

This remark by O. S. Heavens in his book Optical Properties of Thin Solid Films [25] well expresses the attitude toward the study of the optical properties of films before the advent of epitaxial single crystal layers deposited on substrates of the

alkali-alkaline earth halides. It is the purpose of this report to demonstrate that the use of epitaxial films, although by no means a panacea, now allows the measurement of the optical properties of materials in the film state which can be extended to and correlated with the optical properties of materials in the bulk state. The problem undertaken for detailed study was the determination of the optical constants of germanium from measurements of the reflection and transmission of thin epitaxial films. The results are compared with those of other experimental methods to calibrate the accuracy of the film optical constants and illustrate the strengths and weaknesses of the film method.

This chapter will be concerned on the one hand with supplying the theoretical foundation for the research and on the other with reviewing attempts which have been made in the past to determine the optical constants of germanium films. The experimental and theoretical work explored the wavelength range 2000 Å to 6000 Å.

Chapter Two describes the techniques of film production, especially those yielding epitaxial films. Analysis of the film crystal structure by reflection electron diffraction (RED) techniques, and examination of the film surface topography by optical microscopy are also discussed.

In Chapter Three the full theoretical development of two photometric methods for the calculation of optical constants of

thin films is given and the consequences discussed. Chapter Four describes the measurement of the reflectivity and transmissivity coefficients. The results are interpreted in light of the film deposition parameters. In Chapter Five we analyze the reflectance and transmittance in terms of the theory of Chapter Three in order to deduce the optical constants. Comparisons with the results of others are made and the conclusions discussed.

B. REVIEW OF THE MACROSCOPIC AND MICROSCOPIC THEORIES OF THE OPTICAL PROPERTIES OF SOLIDS.

1. Theory of the Optical Response of Materials According to the Electromagnetic Theory of Light.

A modern discussion of the electromagnetic theory of light in a framework suitable for solids has been given by Stern [1]. The development presented here will parallel that of Stern but will be much more brief in scope. In cgs units and in the presence of a material medium, Maxwell's equations may be written as follows:

$$\nabla \times \underline{E} = -1/c \frac{\partial \underline{B}}{\partial t} \tag{1-1a}$$

$$\nabla \times \underline{H} = \frac{4\pi}{c} \underline{J} + \frac{1}{c} \frac{\partial \underline{D}}{\partial t} \tag{1-1b}$$

$$\nabla \cdot \underline{D} = 4\pi \rho \tag{1-1c}$$

$$\nabla \cdot \underline{B} = 0 \tag{1-1d}$$

where \underline{E} and \underline{H} are the electric and magnetic field vectors respectively, \underline{D} and \underline{B} their modifications by an intervening material medium, \underline{J} is

the total current density, and ρ the total charge density. The equation expressing the conservation of charge is

$$\nabla \cdot \underline{J} = - \frac{\partial \rho}{\partial t} \quad (1-2)$$

and the power flow is given by Poynting's vector, viz.,

$$\underline{S} = \frac{c}{4\pi} (\text{Re}\underline{E} \times \text{Re}\underline{H}) . \quad (1-3)$$

Expressions giving the relationship between the electromagnetic field vectors on each side of a discontinuity in the material medium will be needed in order to derive the optical response coefficients. The appropriate equations are [1]:

$$\underline{l} \cdot (\underline{B}_2 - \underline{B}_1) = 0 \quad (1-4a)$$

$$\underline{l} \times (\underline{E}_2 - \underline{E}_1) = 0 \quad (1-4b)$$

$$\underline{l} \times (\underline{H}_2 - \underline{H}_1) = \underline{j}_s \quad (1-4c)$$

$$\underline{l} \cdot (\underline{D}_2 - \underline{D}_1) = \rho_s \quad (1-4d)$$

where \underline{l} is the normal unit vector from medium 1 to medium 2, \underline{j}_s is the surface current density, and ρ_s is the surface charge density, both being externally introduced quantities. In this work, we will only consider radiation incident on boundaries containing no such charges or currents.

In order to introduce in an explicit way the manner in which the material medium generates \underline{D} and \underline{B} from \underline{E} and \underline{H} , the following relationships are usually defined:

$$\underline{J} = \sigma \underline{E} \quad (1-5a)$$

$$\underline{D} = \epsilon \underline{E} \quad (1-5b)$$

$$\underline{B} = \mu \underline{H} \quad (1-5c)$$

where σ is the conductivity tensor and equation (1-5a) expresses Ohm's law, ϵ is the dielectric constant tensor, and μ is the permeability tensor. The equations (1-5) are valid when $|\underline{E}|$ and $|\underline{H}|$ are weak. In view of the fact that the materials we consider are non-magnetic, we will hence take μ to be equal to unity.

Equations (1-5a) and (1-5b) together with equation (1-1b) suggest the following simplification. Suppose we consider a new displacement field defined by

$$\begin{aligned} \underline{D}' &\equiv \underline{D} + 4\pi \int \underline{J} \, dt \\ &= \epsilon \underline{E} + 4\pi\sigma \int \underline{E} \, dt . \end{aligned} \quad (1-6)$$

Equation (1-6) then leads directly to a new material response parameter, the dielectric constant linear operator; given by the equations:

$$\underline{D}' = \tilde{\epsilon} \underline{E} \quad (1-7)$$

where

$$\tilde{\epsilon} = \epsilon + 4\pi\sigma \int dt . \quad (1-8)$$

The explicit form of this linear operator will depend upon the form of the time dependency of the field vectors and the type of transformation calculus used to analyze this dependency. For example, if the time dependency of \underline{E} is of the form $\exp(-i\omega t)$, the

dielectric constant linear operator becomes the well-known complex dielectric constant,

$$\tilde{\epsilon} = \epsilon + i \frac{4\pi\sigma}{\omega} . \quad (1-9)$$

The same analysis can be carried out for the conductivity by defining a new current density by the relation,

$$\begin{aligned} \underline{J}' &= \underline{J} + \frac{1}{4\pi} \frac{\partial D}{\partial t} \\ &= \sigma \underline{E} + \frac{1}{4\pi} \epsilon \frac{\partial \underline{E}}{\partial t} \end{aligned} \quad (1-10)$$

which leads to the equations:

$$\underline{J}' = \tilde{\sigma} \underline{E} \quad (1-11)$$

$$\tilde{\sigma} = \sigma + \frac{\epsilon}{4\pi} \frac{\partial}{\partial t} \quad (1-12)$$

and for $\underline{E} \sim \exp(-i\omega t)$,

$$\tilde{\sigma} = \sigma - i \frac{\omega\epsilon}{4\pi} . \quad (1-13)$$

The relationship between the dielectric and conductivity operators can then be found from equation (1-1b) to be:

$$\tilde{\sigma} = \frac{\tilde{\epsilon}}{4\pi} \frac{\partial}{\partial t} . \quad (1-14)$$

We will now apply a plane wave solution to Maxwell's equations (1-1) of the form

$$\underline{E} = \underline{E}_0 e^{i(\tilde{k} \cdot \underline{r} - \omega t)} \quad (1-15a)$$

$$\underline{H} = \underline{H}_0 e^{i(\tilde{k} \cdot \underline{r} - \omega t)} . \quad (1-15b)$$

One consequence of this choice of solution is that whereas previously the tilde symbol denoted an operator, it will now represent a complex number or variable whenever there is a chance for ambiguity in the notation, otherwise it will be omitted. The plane waves (1-15) are traveling waves moving in the direction of increasing r with wave vector $\tilde{\mathbf{k}}$ which will be in general complex. The form of the exponential in (1-15) is important as it will fix sign conventions for many of the formulas to follow. Introducing the further assumption that we will deal only with isotropic, homogeneous media, substitution of (1-15) into (1-1) yields:

$$\tilde{\mathbf{k}} \times \underline{\mathbf{E}}_0 = \frac{\omega}{c} \underline{\mathbf{H}}_0 \quad (1-16a)$$

$$\tilde{\mathbf{k}} \times \underline{\mathbf{H}}_0 = -\frac{\omega}{c} \tilde{\epsilon} \underline{\mathbf{E}}_0 \quad (1-16b)$$

$$\tilde{\mathbf{k}} \cdot \underline{\mathbf{E}}_0 = 0 \quad (1-16c)$$

$$\tilde{\mathbf{k}} \cdot \underline{\mathbf{H}}_0 = 0 \quad (1-16d)$$

It is seen from equations (1-16) that the vectors $\tilde{\mathbf{k}}$, $\underline{\mathbf{E}}_0$, and $\underline{\mathbf{H}}_0$ form a mutually orthogonal set.

We now form:

$$\begin{aligned} \tilde{\mathbf{k}} \times (\tilde{\mathbf{k}} \times \underline{\mathbf{E}}_0) &= \frac{\omega}{c} \tilde{\mathbf{k}} \times \underline{\mathbf{H}}_0 = (\tilde{\mathbf{k}} \cdot \underline{\mathbf{E}}_0) \tilde{\mathbf{k}} - (\tilde{\mathbf{k}} \cdot \tilde{\mathbf{k}}) \underline{\mathbf{E}}_0 \\ &= -(\tilde{\mathbf{k}} \cdot \tilde{\mathbf{k}}) \underline{\mathbf{E}}_0 \end{aligned} \quad (1-17)$$

or:

$$\tilde{\mathbf{k}} \cdot \tilde{\mathbf{k}} = \frac{\omega^2}{c^2} \tilde{\epsilon} \quad (1-18)$$

Equation (1-18) shows that the wave vector \tilde{k} must be complex. By analogy to the case of plane waves in dielectric media we may define the complex index of refraction through the relation:

$$\tilde{k} \equiv (n + ik) \frac{\omega}{c} \underline{1}_k = \tilde{n} \frac{\omega}{c} \underline{1}_k \quad (1-19)$$

where $\underline{1}_k$ is the unit vector in the direction of propagation of the wave, n is the real part of the complex index of refraction, or simply, the index of refraction, and k is the extinction coefficient. Unfortunately, there now arises a notational difficulty between \tilde{k} the wave vector and k the extinction coefficient. However, it should be noted that almost always the context of the discussion should be sufficient to allow one to differentiate between the two. Substitution of (1-19) into (1-18) yields:

$$\tilde{n}^2 = \tilde{\epsilon} . \quad (1-20)$$

If we write $\tilde{\epsilon} = \epsilon_1 + i \epsilon_2$, we obtain:

$$\epsilon_1 = n^2 - k^2 \quad (1-21a)$$

$$\epsilon_2 = 2nk . \quad (1-21b)$$

Relations (1-21) are very useful as it will be seen that optical measurements are better interpreted in terms of n and k while ϵ_1 and ϵ_2 more easily describe the properties of the media in terms of its microscopic structure. The inverse equations for (1-21) are:

$$n = \left[\frac{\epsilon_1}{2} + \frac{1}{2} [\epsilon_1^2 - \epsilon_2^2]^{\frac{1}{2}} \right]^{\frac{1}{2}} \quad (1-22a)$$

$$k = \left[-\frac{\epsilon_1}{2} + \frac{1}{2} [\epsilon_1^2 - \epsilon_2^2]^{\frac{1}{2}} \right]^{\frac{1}{2}} \quad (1-22b)$$

The sign choice in the root-taking process was governed by the requirement that k be real and greater than zero and that $n \rightarrow \epsilon_1^{\frac{1}{2}}$ as $\epsilon_2 \rightarrow 0$.

In optics, the experimentally measurable quantity is the light intensity which is proportional to the time average and vector magnitude of the Poynting vector as follows:

$$I \propto \left| \lim_{T \rightarrow \infty} \frac{1}{T} \int_0^T \left(\frac{c}{4\pi} \operatorname{Re} \underline{E} \times \operatorname{Re} \underline{H} \right) dt \right| \quad (1-23)$$

which for the case of plane waves of the form (1-15) propagating in the x direction becomes

$$I \propto \frac{nc}{8\pi} E_0^2 e^{-2 \frac{\omega}{c} kx} \quad (1-24)$$

We see that in an absorbing medium the light intensity is attenuated by the factor $e^{-2 \frac{\omega}{c} kx}$. It is sometimes convenient to define the absorption constant α and the skin depth δ by the following relations:

$$\alpha \equiv \frac{4\pi k}{\lambda}$$

$$\delta \equiv 1/\alpha = \frac{\lambda}{4\pi k} \quad (1-25b)$$

where we have used the well-known formula for the wavelength

$$\lambda = \frac{\omega}{2\pi c}$$

The derivation of the optical response parameters, the reflectivity and transmissivity coefficients, from the boundary conditions (1-4) will now be considered. In view of the fact that all of the optical measurements in this work were taken near normal incidence, only the normal incidence case will be explicitly derived. It provides a very good approximation for angles of incidence up to 10° and even further if the light is unpolarized [2]. Referring to Figure 1-1, it is seen that the appropriate field vectors are as follows:

$$\underline{E}_1 = \underline{1}_y [E_i e^{i\tilde{k}_1 x} + E_r e^{-i\tilde{k}_1 x}] \quad (1-26a)$$

$$\underline{H}_1 = \underline{1}_z [H_i e^{i\tilde{k}_1 x} + H_r e^{-i\tilde{k}_1 x}] \quad (1-26b)$$

$$\underline{E}_2 = \underline{1}_y E_t e^{i\tilde{k}_2 x} \quad (1-26c)$$

$$\underline{H}_2 = \underline{1}_z H_t e^{i\tilde{k}_2 x} \quad (1-26d)$$

where the subscripts 1 and 2 denote the medium, and the subscripts i, r, and t the incident, reflected, and transmitted complex amplitudes, respectively. Application of boundary condition (1-4b) yields

$$E_t - E_i - E_r = 0 \quad , \quad (1-27)$$

and application of boundary condition (1-4c) in conjunction with equation (1-16a) gives:

$$\tilde{k}_2 E_t - \tilde{k}_1 E_i + \tilde{k}_1 E_r = 0 \quad . \quad (1-28)$$

MEDIUM 1

MEDIUM 2

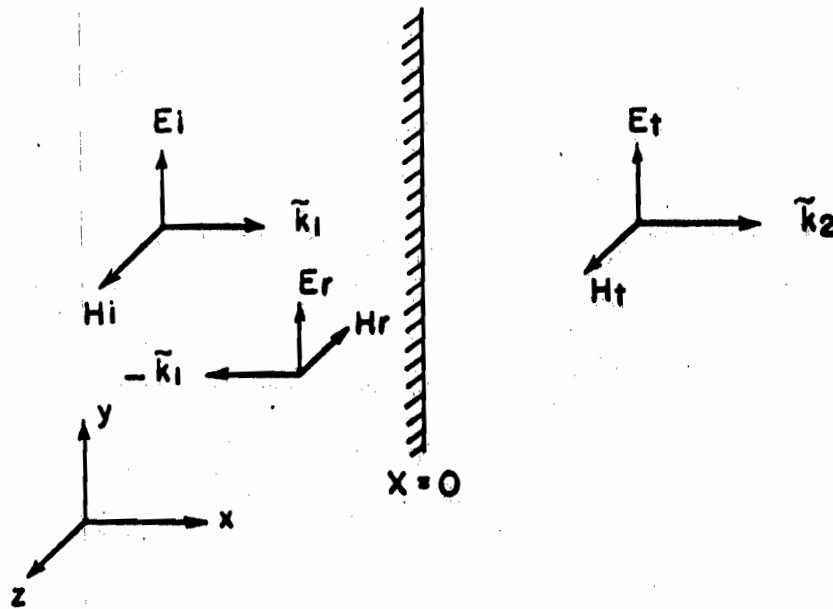


FIG. 1-1 REFLECTION AND TRANSMISSION OF AN ELECTROMAGNETIC WAVE AT THE BOUNDARY BETWEEN TWO MEDIA.

In view of equation (1-24), we need only consider the optical response parameters for the electric vector. Defining the complex reflectivity and transmissivity coefficients as

$$\rho \equiv \frac{E_r}{E_i} \quad (1-29a)$$

$$\tau \equiv \frac{E_t}{E_i} \quad (1-29b)$$

respectively, we have immediately from equations (1-27), (1-28), and (1-19):

$$\rho = \frac{\tilde{k}_1 - \tilde{k}_2}{\tilde{k}_1 + \tilde{k}_2} = \frac{\tilde{n}_1 - \tilde{n}_2}{\tilde{n}_1 + \tilde{n}_2} \quad (1-30a)$$

$$\tau = \frac{2\tilde{k}_1}{\tilde{k}_1 + \tilde{k}_2} = \frac{2\tilde{n}_1}{\tilde{n}_1 + \tilde{n}_2} \quad (1-30b)$$

The present work is concerned with the situation where medium 1 is a dielectric with index of refraction n_s and medium 2 is a conductor with complex index of refraction \tilde{n} . Also, we will now concentrate on ρ alone as τ and ρ are related by the expression $\tau - \rho = 1$. We then have:

$$\rho = \frac{n_s - \tilde{n} - ik}{n_s + \tilde{n} + ik} \quad (1-31)$$

If medium 2 is a dielectric with greater optical density than medium 1, then we see that ρ is negative. This implies that under this condition the reflected electric vector undergoes a phase change of 180° . It will be convenient for the development

of the theory in Chapter Three if we express ρ in polar form. However, in doing this one must be extremely careful as ρ is then no longer unique. That is, care must be taken to define the argument of the polar form in its principal value range and to specify the positive root as being implied when any square roots are taken. With this in mind, we have immediately from equation (1-31):

$$\rho \equiv -R^{\frac{1}{2}} e^{i\psi} \quad (1-32a)$$

$$R = \frac{(n_s - n)^2 + k^2}{(n_s + n)^2 + k^2} \quad (1-32b)$$

$$\psi = \tan^{-1} \frac{2n_s k}{n^2 + k^2 - n_s^2} \quad (1-32c)$$

It may be inferred from equations (1-23) and (1-24) that the ratio of the reflected light intensity to the incident light intensity is given by $\rho\rho^*$ or is the quantity R of equation (1-32b). The equations (1-32) are the principal result of this section and will be used extensively in Chapter Three.

2. Quantum Mechanical Theory of the Optical Constants.

A detailed inquiry into the derivation of the optical constants from quantum mechanical principles is outside the purpose of this work. Therefore, only the briefest outline of the procedure used will be given. There are essentially two approaches to the problem, namely, the many body formulation [11], and the one-electron formulation. We will direct our attention to the latter.

The one-electron formulation makes contact with the macroscopic theory through the definition of the quantum mechanical current density:

$$\underline{J}' \equiv \left\langle \frac{e}{m} \left(\underline{p} + \frac{e}{c} \underline{A} \right) \right\rangle \quad (1-33)$$

and through the assumption that the \underline{J}' of this equation is identical to that of equation (1-11). Here e is the electronic charge and m its mass, while \underline{p} is the momentum and \underline{A} is the vector potential of the local field. The procedure is then to calculate the expectation value of the canonical momentum $\underline{p} + \frac{e}{c} \underline{A}$ in a suitable representation to terms linear in the electric field and apply equations (1-11) and (1-14) to obtain $\tilde{\epsilon}$ from which the optical constants can be found by equation (1-22). The right-hand side of equation (1-33) has been evaluated by Ehrenreich and Cohen using density matrix methods [12]. Their method included many body effects by describing them as the interaction of a single electron with a self-consistent electromagnetic field. The dielectric constant which results for a Bloch representation and an incident field whose wavelength is much greater than the interatomic spacing is as follows [12]:

$$\begin{aligned} \tilde{\epsilon}(\omega) = & 1 - \frac{(e/\pi)^2}{m} \int d^3k \sum'_{\ell\ell'} f_{\ell}(\underline{k}) f_{\ell',\ell}^{\mu} \\ & \times \frac{(\omega^2 - \omega_{\ell\ell'}^2) - \tau_{\ell\ell'}^{-2} - i 2\omega \tau_{\ell\ell'}^{-1}}{[(\omega - \omega_{\ell\ell'})^2 + \tau_{\ell\ell'}^{-2}][(\omega + \omega_{\ell\ell'})^2 + \tau_{\ell\ell'}^{-2}]} \end{aligned} \quad (1-34)$$

where

$\hbar\omega_{\ell\ell'} = E_{\ell'}(\underline{k}) - E_{\ell}(\underline{k})$, $E_{\ell}(\underline{k})$ being the energy of an electron with wave vector \underline{k} in band ℓ , $f_{\ell}(\underline{k})$ is the Fermi distribution for band ℓ ,

$f_{\ell\ell'}^{\mu} = (2/\pi\hbar\omega_{\ell\ell'}) |\langle \ell' \underline{k} | p^{\mu} | \ell \underline{k} \rangle|^2$, $|\ell \underline{k} \rangle$ being the cell-periodic part of a Bloch function for an electron with wave vector \underline{k} in band ℓ and p^{μ} its momentum component in the direction of propagation of the incident radiation,

and

$\tau_{\ell\ell'}$ is a phenomenologically introduced lifetime.

Equation (1-34) therefore expresses the dependence of the complex dielectric constant on interband transitions. It was mentioned above that equation (1-33) is written in terms of the local field. One may well ask whether or not equation (1-34) must be modified in accordance with the Clausius-Mossotti relation in order to include the difference between the local field and the externally applied field [13]. However, Nozières and Pines [11] have found that if the electrons in the crystal are loosely bound, as they are for semiconductors, then local field corrections can be neglected.

C. THE BAND STRUCTURE OF GERMANIUM

The band theory of covalent semiconductors has become well established during the past decade. It appears to give an excellent description of their optical properties for energies at least up to 20 eV. Much of our knowledge about the band structure of materials has been gained through experiment; however, we have usually been limited to exploring only those portions of the band that lie near symmetry points of the first Brillouin zone. The advent of the pseudopotential method [14] now allows a fairly accurate theoretical description of the band structure in a region of about 10 eV about the energy gap. These calculations have been a great aid in the interpretation of the visible and ultraviolet optical spectra of semiconductors [15].

The pseudopotential energy bands of germanium have been calculated by Brust [15] and are shown in Fig. 1-2. The notation used to label the bands and symmetry points is that of Bouckaert, Smoluchowski, and Wigner [16]. Also shown in Fig. 1-2 are some of the important interband transitions. In order to demonstrate their connection with the reflectivity spectra of bulk germanium shown in Fig. 1-3a, we will outline how one proceeds from the theoretical band structure to the deduction of the optical constants. Let us consider the following simplifications to equation (1-34):

(1) We will assume conditions of absolute zero temperature and that transitions take place only between a valence band l' and several conduction bands l .

(2) We will assume that $\tau_{ll'} \rightarrow \infty$.

(3) We will assume that matrix element $|\langle l' \underline{k} | p^\mu | l \underline{k} \rangle|^2$ is independent of \underline{k} . According to the results of the pseudopotential theory, this appears to be a valid approximation[17].

We then obtain for ϵ_2 :

$$\epsilon_2(\omega) = \pi^{-1} (e/m \omega)^2 \sum_{l > l'} |\langle l' \underline{k} | p^\mu | l \underline{k} \rangle|^2 \int d^3k \delta(\omega_{ll'} - \omega) \quad (1-35)$$

where we have written out $f_{ll'}^\mu$, in full. If the \underline{k} -space integral in equation (1-35) is transformed to an energy representation, we obtain:

$$\epsilon_2(\omega) = 4\pi^2 (e/m \omega)^2 \sum_{l > l'} J_{ll'}(\omega) |\langle l' \underline{k} | p^\mu | l \underline{k} \rangle|^2 \quad (1-36)$$

where

$$J_{ll'}(\omega) = \frac{2}{(2\pi)^2} \int_{\omega_{ll'} = \omega} \frac{dS_{\underline{k}}}{|\nabla_{\underline{k}} \omega_{ll'}|} \quad (1-37)$$

This equation defines the so-called joint density of states [15] in which the integral is taken over a constant $\omega = \omega_{ll'}$ surface. Van Hove [18] has investigated the behavior of equation (1-37) and has found that certain points in the Brillouin zone produce analytic singularities in (1-37) due to the vanishing of the denominator of the integrand. These points are called critical points

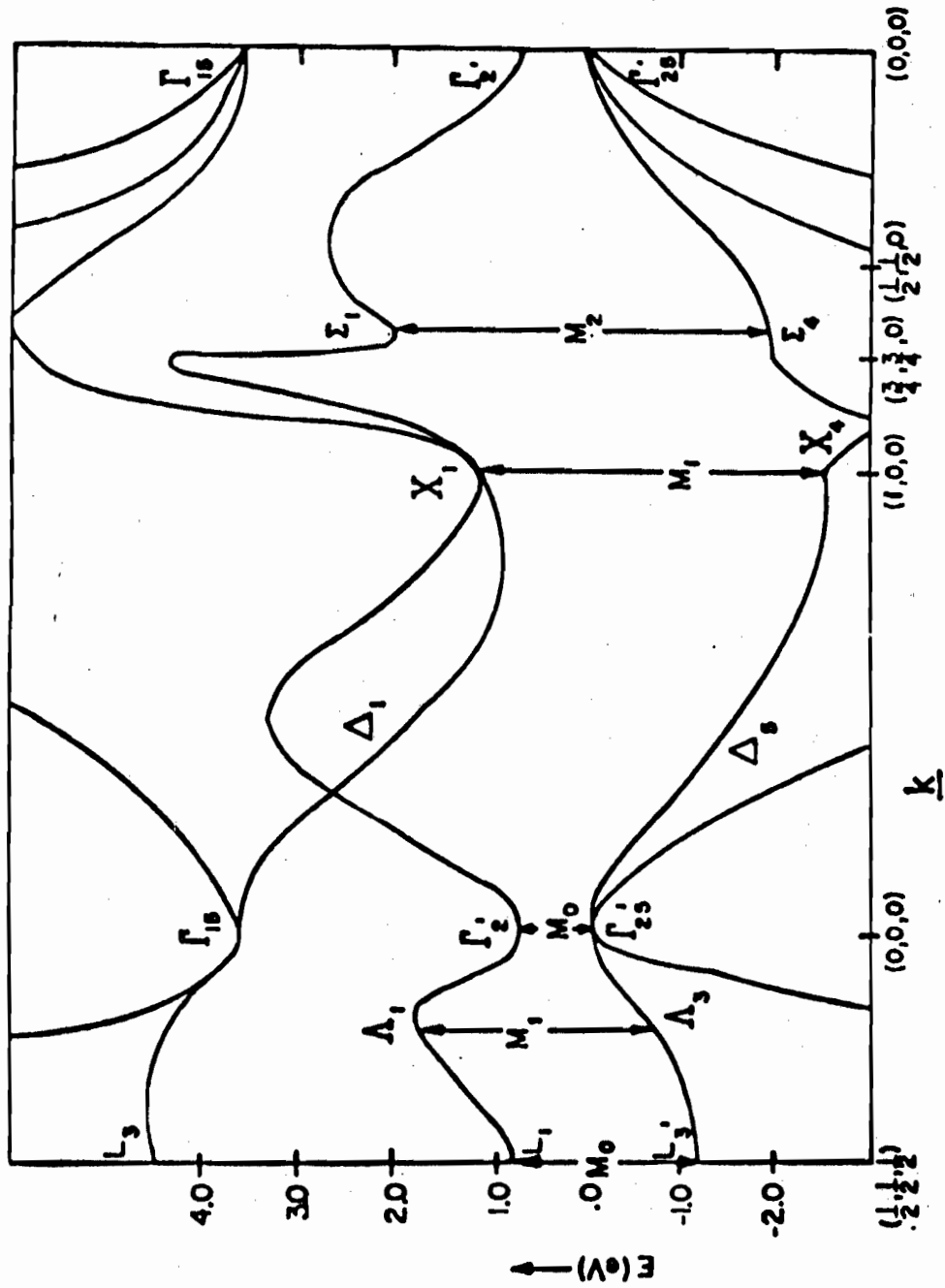


FIG. 1-2 PSEUDOPOTENTIAL ENERGY BANDS OF GERMANIUM AS CALCULATED BY BRUST WITH SOME OF THE PRINCIPAL TRANSITIONS INDICATED.

and their presence strongly influences the ω -dependence of $J_{ll'}$, and thus ϵ_2 . Now, $J_{ll'}$ can readily be calculated using the pseudopotential bands. This allows the deduction of a theoretical ϵ_2 to be compared with an experimental ϵ_2 determined, for example, by a dispersion analysis of reflectivity data. In this way, structure in the reflectivity spectrum of a semiconductor can be traced back to definite interband transitions at particular points of the Brillouin zone.

The important critical point transitions, or Van Hove singularities, are shown in Fig. 1-2. M_0 , M_1 , and M_2 designate the type of critical point behavior and are explained in reference 15. The $\Gamma'_{25} \rightarrow \Gamma'_2$ transition is the well-known direct "optical gap" transition between the valence and conduction bands. The $L'_3 \rightarrow L_1$ and $\Lambda_3 \rightarrow \Lambda_1$ transitions are responsible for the reflectivity peaks near 6000\AA shown in Fig. 1-3a. The L transition is thought to cause the onset of these peaks, while the peaks themselves are due to the Λ transition. The reason two peaks appear in the reflectivity spectrum is because of the spin-orbit splitting of the Λ_3 valence band [19]. Spin-orbit splitting was not included in the pseudopotential calculation. The main peak near 2000\AA is caused by the combined effect of the $X_4 \rightarrow X_1$ and $\Sigma_4 \rightarrow \Sigma_1$ transitions. The shape of their respective joint density of state functions is such that

this reflectivity peak is very sharp. The small peak near 2100\AA has tentatively been assigned to the $L_{3,1} \rightarrow L_{3,2}$ transition, which is not explicitly shown in Fig. 1-2.

D. REVIEW OF THE METHODS OF DETERMINING THE OPTICAL CONSTANTS OF SOLIDS

1. Polarimetric Measurements.

This method was originally formulated by Drude [20] and has been used by Archer [21] to obtain the optical constants of germanium over a limited wavelength range. It involves the use of a beam of plane polarized monochromatic light in 45° azimuth obliquely incident on a reflecting surface. This beam may be thought of as two in-phase orthogonal plane wave components of equal amplitude; one in the plane of incidence and the other normal to it. After reflection, these components will be out of phase by the angle Δ and the ratio of their amplitudes can be expressed by the quantity $\tan \psi$. The dependence of these quantities on the optical constants is given by [21]:

$$\frac{1 - e^{i\Delta} \tan \psi}{1 + e^{i\Delta} \tan \psi} = \left\{ \frac{n^2 - k^2 \sin^2 \phi - i 2nk}{\tan \phi \sin \phi} \right\}^{\frac{1}{2}} \quad (1-38)$$

where ϕ is the angle of incidence. The reflected components are brought back into phase by a Babinet-Soleil compensator which is essentially a tunable quarter-wave plate. This yields Δ while rotating an analyzer to an extinction position for the now plane

polarized beam gives ψ . This was the technique employed by many early workers to determine the optical constants of metals. A more complex, although analogous, approach has been used for thin absorbing films [22].

The principal limitation of polarimetric measurements of this type is probably the wavelength range of commercially available compensators and polarizers. The compensators in particular seem to be restricted to the wavelength region between 3500\AA and $1.5\ \mu$. As far as is known, no theoretical investigation of this method has been performed to determine the effect of experimental errors on the derived optical constants; however, Archer's results agree well with those of workers using dispersion analysis. It is to be noted that the spin-orbit splitting [19] near 6000\AA is missing in Archer's data, which emphasizes another limitation of this technique, namely, the ability to scan continuously with wavelength to uncover fine structure is missing.

2. Dispersion Theory. Kramers-Kronig Analysis.

The concept of a response function has long been known to workers in the field of linear systems analysis. The response function expresses the linear relation between the input and output of a system in which causality requires that the output cannot precede the input. An example of such a system is one in which

the input may be a current and the output a voltage, the response function thereby being an impedance. The system equations are usually written in terms of their Fourier transforms, namely, $E(\omega) = Z(\omega) I(\omega)$, where in general all three quantities are complex functions of the complex variable ω . However, the real and imaginary parts of the impedance are by no means independent of one another [23]. This is because the condition of causality requires that $Z(\omega)$ be analytic in some half-plane of the complex ω plane, thus allowing us to integrate the Cauchy-Riemann equations, which express the real and imaginary parts of $Z(\omega)$ in terms of each other, by means of Cauchy's integral formula. In optics, we can consider equation (1-29a) as being analogous to our Ohm's law above, with ρ being the linear response function. If we express ρ in the form of equation (1-32a), enforce the physical requirement that its inverse Fourier transform be real, and apply the reasoning outlined above, it can be shown that [1]:

$$\psi(\omega) = \frac{\omega}{\pi} \int_0^{\infty} \frac{\ln \frac{R(\omega')}{R(\omega)}}{\omega'^2 - \omega^2} d\omega' \quad (1-39a)$$

$$\ln R(\omega) = \frac{4}{\pi} \int_0^{\infty} \frac{\omega' \psi(\omega') - \omega \psi(\omega)}{\omega'^2 - \omega^2} d\omega' \quad (1-39b)$$

Furthermore, equations (1-32b) and (1-32c) can be inverted to give:

$$n = (1 - R)/(1 + R - 2 \sqrt{R} \cos \psi) \quad (1-40a)$$

$$k = 2 \sqrt{R} \sin \psi / (1 + R - 2 \sqrt{R} \cos \psi) . \quad (1-40b)$$

Equations of the type (1-39) are known in optics as dispersion relations or Kramers-Kronig relations. We see that (1-39a) in conjunction with equations (1-40) can be used to determine n and k if we know the entire spectral response of R . What is done in practice is to measure the reflectivity of a substance over as wide a range of frequency (energy) as possible and then to use some suitable extrapolation procedure to cover the rest. Equation (1-39) is then evaluated numerically and n and k calculated therefrom. The various extrapolations that are used are fully discussed in Stern [1]; they consist primarily of fitting a smooth analytic curve to the high frequency end of the R spectrum which approaches $R = 0$ as $\omega \rightarrow \infty$. The extrapolation function has a parameter which is chosen to make n and k equal to known, independently measured values in the infrared.

The optical constants of germanium have been calculated from reflectivity data in this manner by Philipp and Taft [4] and are shown in Fig. 1-3b. As with the polarimetric method, it is not known whether or not there exists a detailed theoretical investigation into the effect of variations in R and the extrapolation procedure on the derived n and k . However, Philipp [6] has recalculated the germanium optical constants from the data of Donovan, et al.

[3], and these constants are also given in Fig. 1-3b along with the previous values. Therefore, by comparing the reflectivities shown in Fig. 1-3a with the optical constants derived therefrom in Fig. 1-3b, we can say that for germanium at least, it appears that variations of 2% to 5% absolute in the reflectivity will cause variations up to one-half of an optical constant in the Kramers-Kronig result.

The dispersion analysis method is presently being widely used to obtain the optical constants of solids. It has the disadvantage that one has to use extrapolation procedures, but it remains to be seen how sensitive the results really are to them. In addition, surface conditions can vary widely. In Fig. 1-3a, Philipp's and Taft's data were taken from a polished and etched sample as was that of Tauc and Abraham; whereas, the data of Donovan,et al., were obtained from an electropolished sample whose surface was of both high optical and crystalline quality. The reflectivity data of Donovan,et al., can be considered authoritative and the optical constants calculated from them by Philipp will be taken as the standard for this work.

3. Photometric Measurements.

By photometric measurements we will mean those methods which measure light intensity ratios such as reflectivity and transmission.

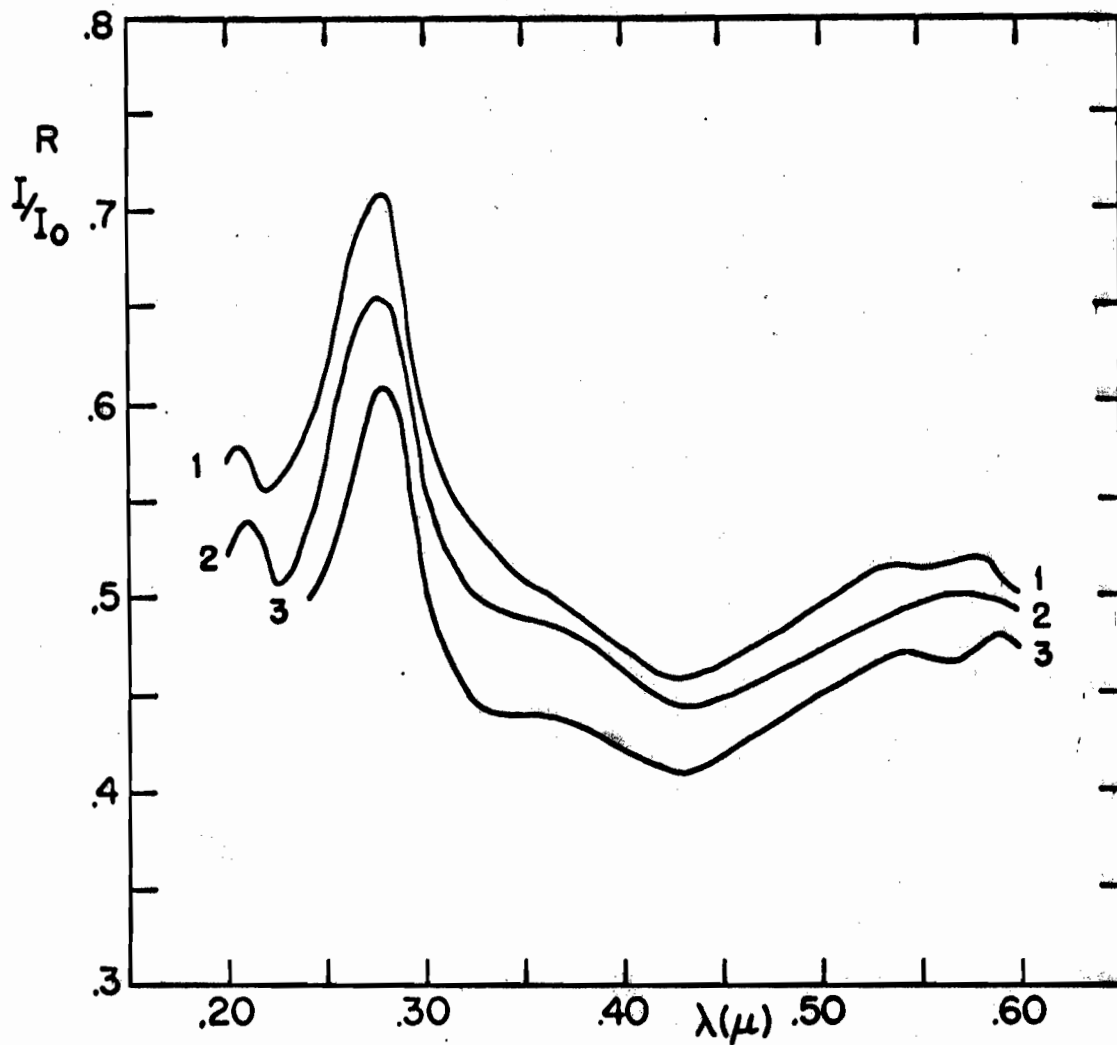


FIG. 1-3a REFLECTIVITY OF BULK GERMANIUM.

1. DONOVAN, et al. (3)
2. PHILIPP AND TAFT (4)
3. TAUC AND ABRAHAM (5)

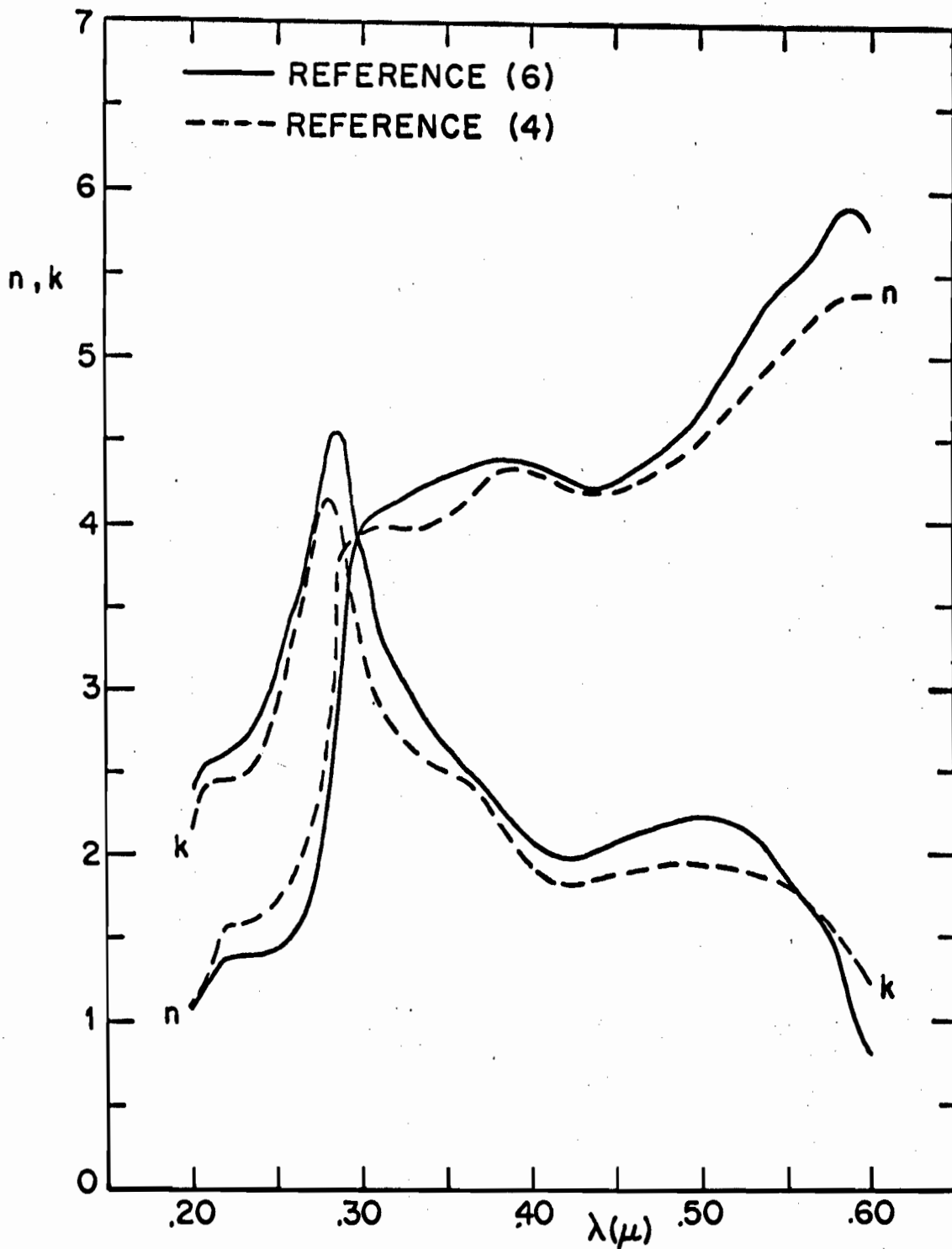


FIG. 1-3b THE KRAMERS-KRONIG RESULTS FOR THE OPTICAL CONSTANTS OF GERMANIUM.

The optical constants can then be calculated, via the theory of Section B-1, from two independent measurements of these quantities at a given wavelength. For example, one could use for data the reflectivity and transmission of a slab of given thickness, or the transmissivities of two slabs of different thicknesses, or the reflectivities at two different angles of incidence, and so forth. These and other photometric methods are discussed by Heavens [24]. Again, there apparently has been no extensive investigation into which method yields optical constants least sensitive to experimental error. Ultimately, such considerations will condition not only the choice of photometric method, but also the choice of photometric over polarimetric or dispersion analysis, or vice versa. However, it is doubtful that any method mentioned here will be capable of rendering the high degree of accuracy expected from the classical measurements of the index of refraction of dielectrics by refraction and interference techniques. For this work, we have emphasized the photometric measurement of reflection and transmission for the determination of the optical constants of thin films primarily because of its historical interest, its physical interest, and its esthetic interest through its close subjective connection with the visual conception we have of our environment.

E. REVIEW OF THE ATTEMPTS TO DETERMINE THE OPTICAL CONSTANTS OF GERMANIUM THIN FILMS

1. Skin Depth of Germanium.

In order to gain an appreciation of the sample thicknesses that must be considered when contemplating the transmission of light through germanium, Fig. 1-4 was constructed from the data of reference 6. The skin depth was calculated directly from k with equation (1-25b). We see that at the Σ , X transition at 2800\AA , the skin depth is only about 40\AA which for germanium is merely eight interatomic distances. Assuming a lower limit for the measurement of transmission of 10^{-3} imposes a maximum sample thickness of about 300\AA or 60 atoms. Obviously such samples are impossible to obtain through reduction of the bulk material by conventional grinding and polishing.

2. Preparation of Thin Films.

The main discussion of this topic will be given in Chapter Two. Here we wish briefly to indicate how the problem of preparing thin samples is overcome. The general procedure is to heat a piece of bulk germanium in a vacuum to such a temperature that it begins to vaporize appreciably. A suitable transparent substrate is placed in the vapor stream so as to cause a film of germanium to be deposited on it. The thickness is varied by varying the exposure time. This procedure is that which was used in the work to

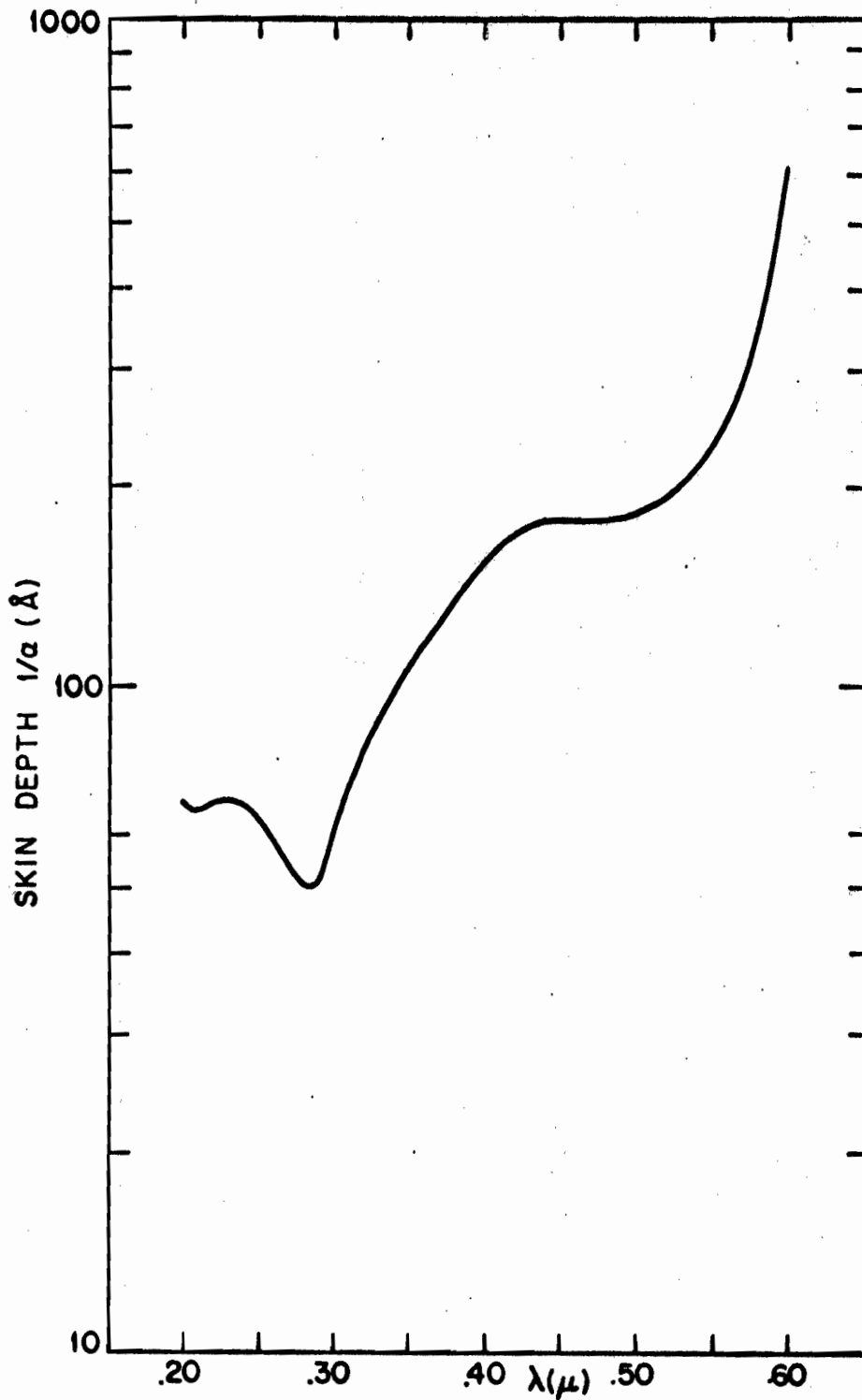


FIG. 1-4 SKIN DEPTH OF GERMANIUM AS A FUNCTION OF WAVE LENGTH.

be discussed in the next two subsections.

3. Results Prior to 1950.

This date roughly marks the beginning of the period when the importance of the crystal structure of the films with regard to their optical properties started to be stressed. The results prior to this date are now discussed.

The first results reported for the optical constants of germanium thin films were by O'Bryan [7] and are displayed in Fig. 1-5a with those of reference 6. They bear little resemblance to each other. O'Bryan's work was quite early (1936) and his films were of undetermined crystalline quality (probably amorphous). He calculated the optical constants from reflectivity measurements at different angles of incidence.

The next data were taken by Brattain and Briggs in 1949 [8]; they are shown in Fig. 1-5b. Again we have depressingly little correspondence with the later Kramers-Kronig results. Their films were deposited on glass, quartz, and CaF_2 slides which were sometimes heated to 150°C during evaporation. After deposition, the films were post-annealed at 400°C but no attempt was made to measure the influence on crystalline perfection (the results of Chapter Four indicate that these films were probably amorphous or nearly so). The optical constants were calculated from the film reflectance and transmittance.

4. Results After 1950.

The first worker to study the effect of crystallinity on the optical constants of germanium films was Gebbie in 1952 [9]. He annealed his films after deposition up to temperatures of 525°C for several hours. The electron diffraction pattern then showed fine rings characteristic of the polycrystalline state (see Chapter Two, Section C-1). The optical constants for such a film are given in Fig. 1-5c. Here the qualitative agreement among the values of k is tolerable, but n appears to oscillate wildly. Since this work is unpublished, we cannot be sure of the method used to obtain n and k . However, it is reported by Heavens [26] that Gebbie employed the transmittances of two or more films to deduce the optical constants. If this is the case, then the theory of Chapter Three, Section B provides an explanation for the oscillatory behavior of n which shows it to be an effect of the method of calculation and not an intrinsic property of the film.

The most recent results are those of Lukes (1960) [10], which are shown in Fig. 1-5d. These have fair qualitative agreement with the dispersion results in the **wavelength region indicated**. This is somewhat surprising in view of the fact that his films were neither deposited on hot substrates nor post-annealed to improve their crystallinity. That the crystallinity was indeed poor can be seen from his Fig. 5, which shows the reflectivity of one

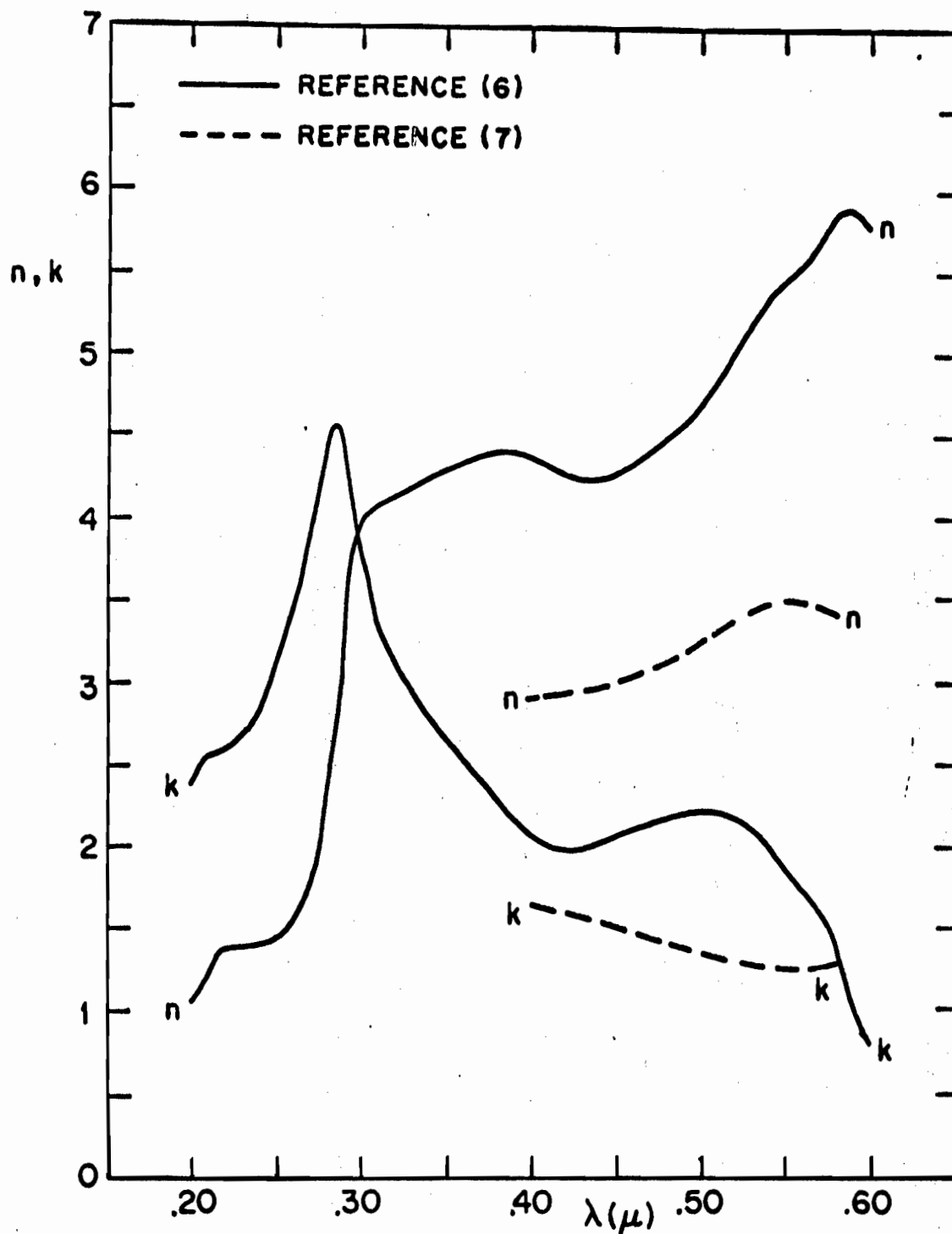


FIG. 1-5a OPTICAL CONSTANTS OBTAINED BY OTHER WORKERS FROM GERMANIUM THIN FILMS.
 a. O'BRYAN, 1936 (7).

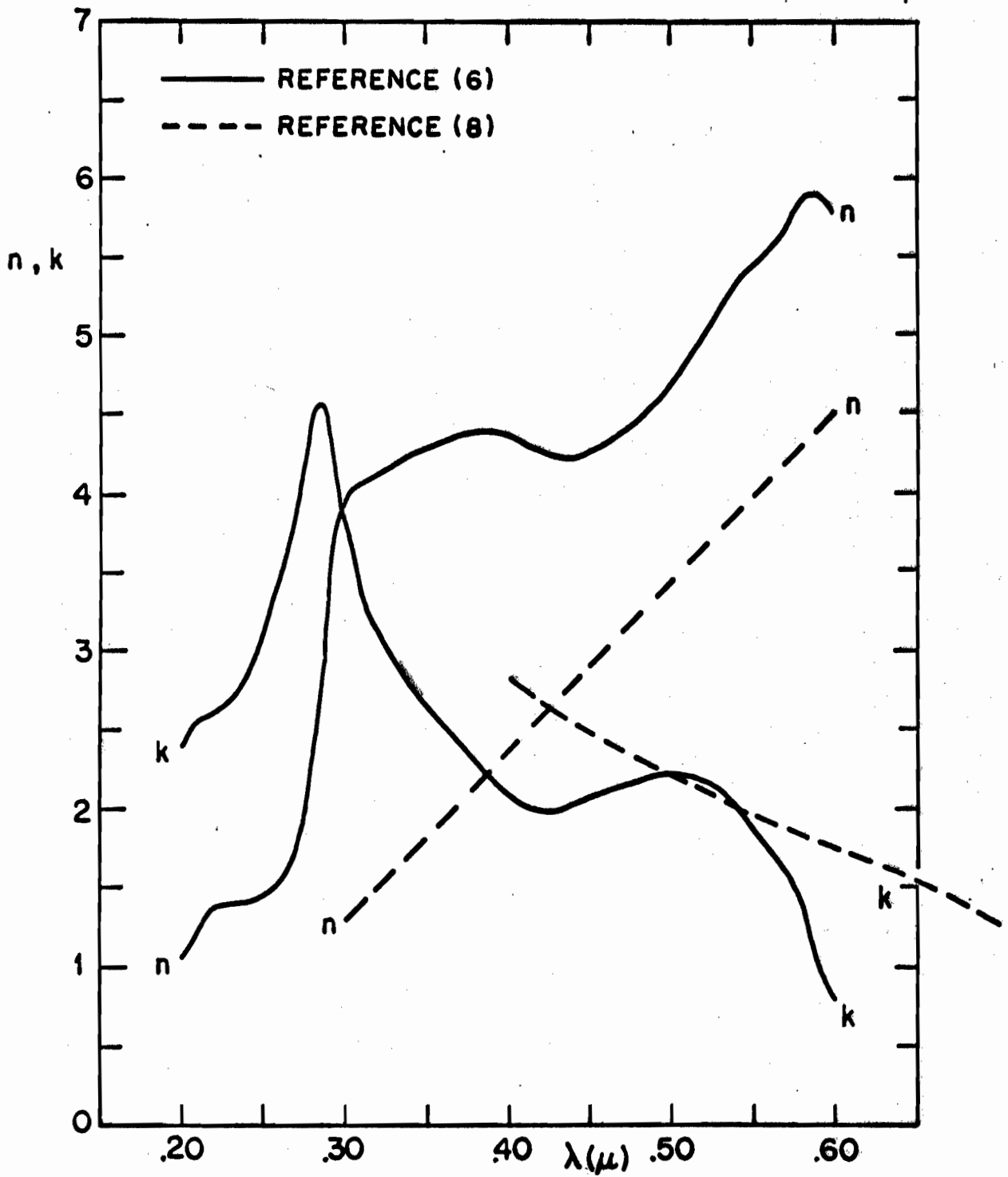


FIG. 1-5b BRATTAIN AND BRIGGS, 1949 (8).

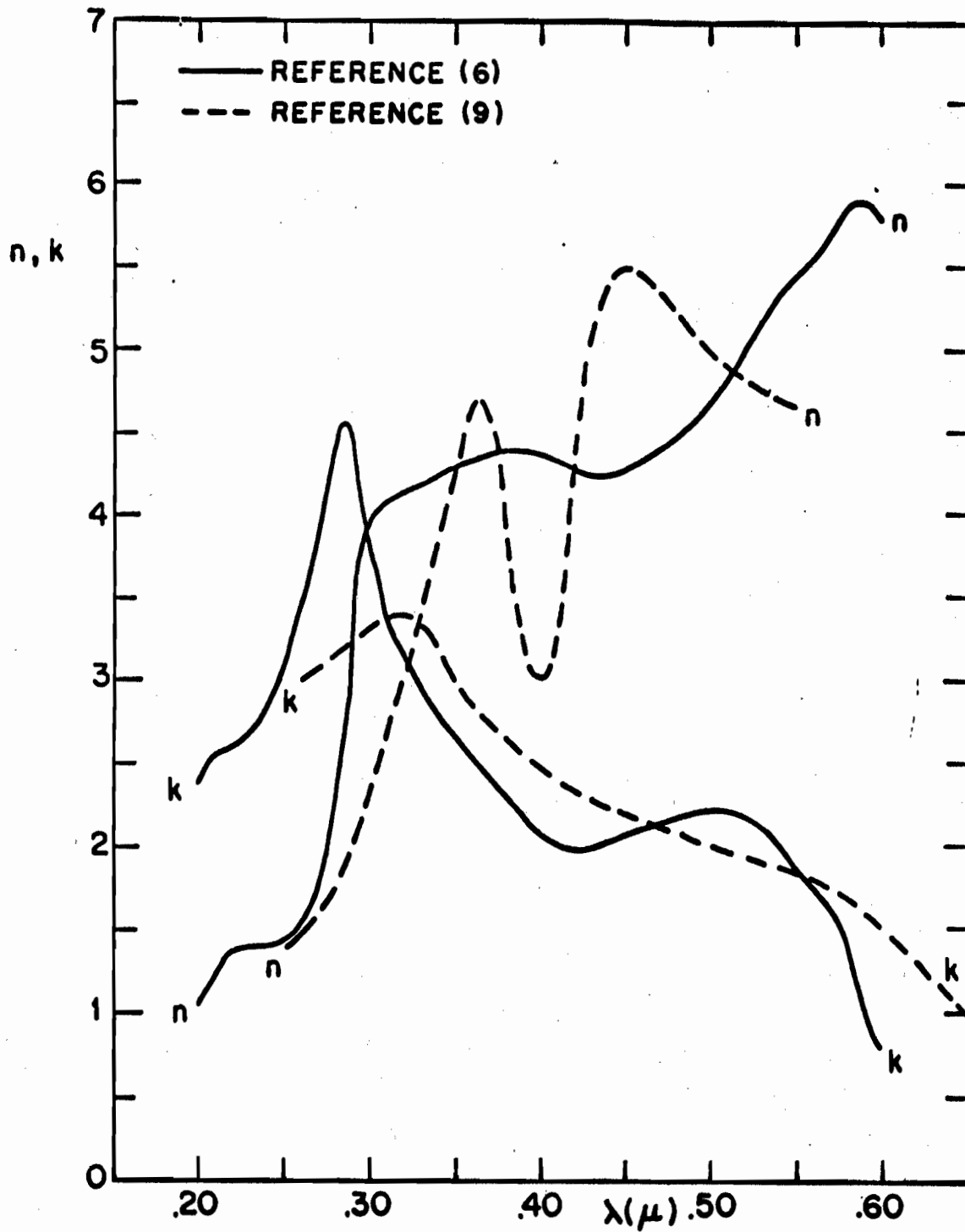


FIG. 1-5c GEBBIE, 1952 (9).

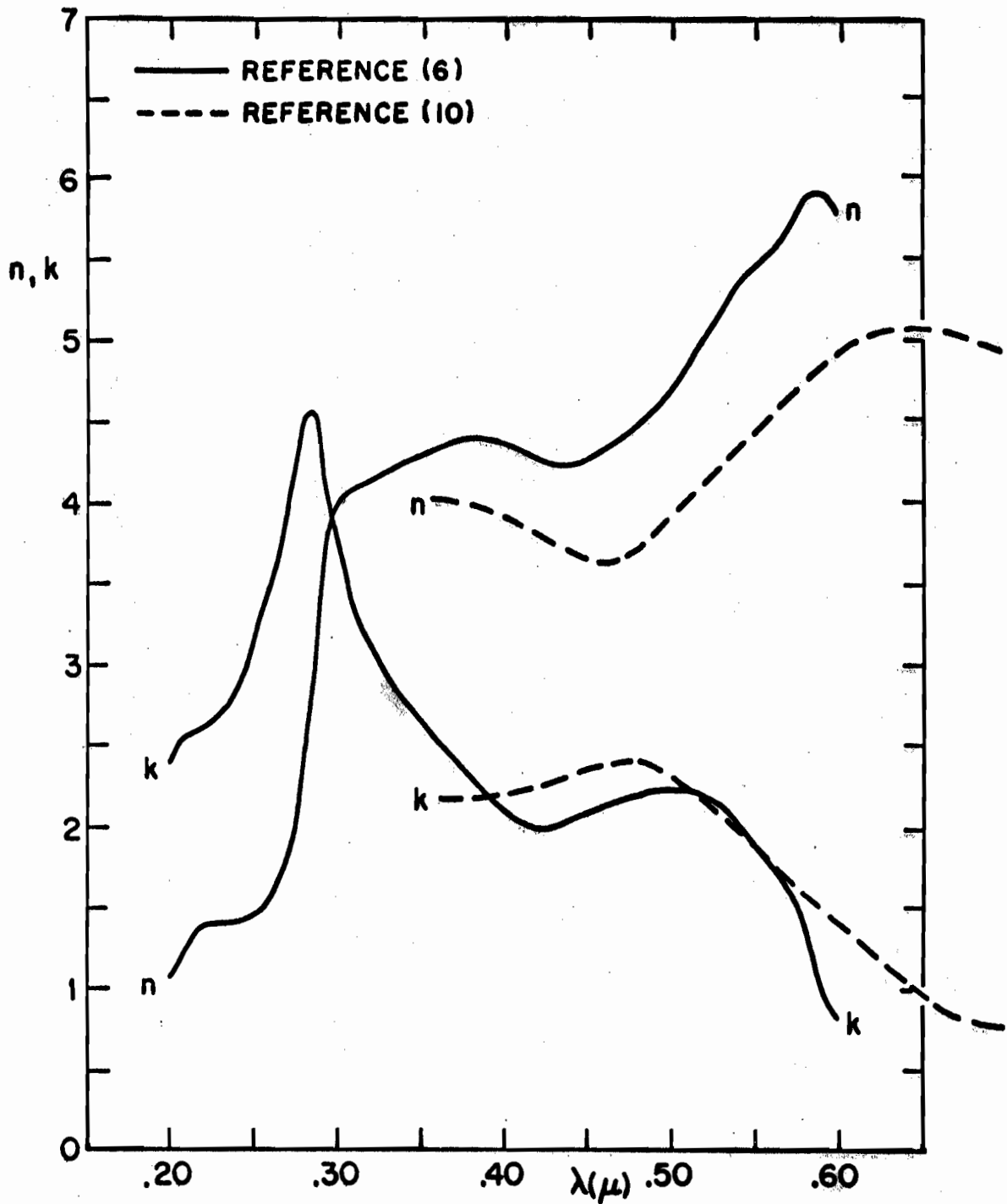


FIG. 1-5d LUKESŤ, 1960 (10).



of his films. It corresponds roughly to our result for a film on fused quartz shown by curve 4 of Fig. 4-7 which is definitely known to be of poor crystalline quality. Lukes calculated n and k from measurements of R and T .

Recently several works have appeared in which either the reflectance or transmittance of germanium films has been measured but the optical constants were not computed. These works will be covered in Chapter Four where our own results are discussed.

In conclusion, we see that the data of previous work do not agree very well with the dispersion analysis results. This is due mainly to a lack of appreciation on the part of early workers of the importance of improving the crystalline quality of the films to the highest degree possible before any meaningful optical measurements could be made on them. What makes this hard to understand is that RED techniques and methods of producing epitaxial films of many materials (although not germanium) were known by 1936. Today, however, we are greatly aided by the extensive knowledge of the germanium band structure, improved bulk reflectivity measurements, optical constants from dispersion analyses, and high speed digital computers, all of which were not available to the early researchers. In spite of this, optical properties of germanium films are still being reported in which the data were taken on amorphous films with no consideration of crystallinity and which were interpreted in apparent ignorance of modern band theory [27].

Chapter One

BIBLIOGRAPHY

- [1] F. Stern, Elementary Theory of the Optical Properties of Solids, Solid State Physics, vol. 15, ed. by F. Seitz and D. Turnbull (Academic Press, New York, 1963).
- [2] R. W. Ditchburn, Light (Interscience Publishers Inc., New York, 1953), Fig. 15.1, p. 444.
- [3] T. M. Donovan, E. J. Ashley, and H. E. Bennett, J. Opt. Soc. Am. 53, 1403 (1963).
- [4] H. R. Philipp and E. A. Taft, Phys. Rev. 113, 1002 (1959).
- [5] J. Tauc and A. Abraham, Proceedings of the International Conference on Semiconductor Physics, Prague, 1960 (Czechoslovakian Academy of Sciences, Prague, 1961), p. 375; J. Phys. Chem. Solids 20, 190 (1961).
- [6] H. R. Philipp, private communication, Nov. 16, 1964.
- [7] H. M. O'Bryan, J. Opt. Soc. Am. 26, 122 (1936).
- [8] W. H. Brattain and H. B. Briggs, Phys. Rev. 75, 1705 (1949).
- [9] H. A. Gebbie, Ph.D. Thesis, Reading, 1952 (unpublished), according to [10].
- [10] F. Lukes, Czech. J. Phys. B10, 59 (1960).
- [11] P. Nozières and D. Pines, Phys. Rev. 109, 762 (1958); Il Nuovo Cimento 9, 470 (1958).
- [12] H. Ehrenreich and M. H. Cohen, Phys. Rev. 115, 786 (1959); H. R. Philipp and H. Ehrenreich, Phys. Rev. 129, 1550 (1963).
- [13] C. Kittel, Introduction to Solid State Physics (Wiley, New York, 1956).
- [14] J. C. Phillips and L. Kleinman, Phys. Rev. 116, 287 (1959); for a concise discussion of the pseudo-potential method, see R. Zallen, Technical Report No. HP-12, Gordon McKay Laboratory of Applied Science, Harvard University, 1964 (unpublished).

- [15] D. Brust, Phys. Rev. 134, A1337 (1964).
- [16] Bouckaert, Smoluchowski, and Wigner, Phys. Rev. 50, 58 (1936).
- [17] D. Brust, J. C. Phillips, and F. Bassani, Phys. Rev. Letters 9, 94 (1962).
- [18] L. Van Hove, Phys. Rev. 89, 1189 (1953).
- [19] J. Tauc and E. Antoncik, Phys. Rev. Letters 5, 253 (1960).
- [20] P. Drude, The Theory of Optics (Dover, New York, 1959).
- [21] R. J. Archer, Phys. Rev. 110, 354 (1958).
- [22] O. S. Heavens, Measurement of Optical Constants of Thin Films, Physics of Thin Films, vol. 2, ed. by G. Hass and R. E. Thun (Academic Press, New York, 1964).
- [23] H. Bode, Network Analysis and Feedback Amplifier Design (D. Van Nostrand Company, New York, 1945).
- [24] O. S. Heavens, Optical Properties of Thin Solid Films (Butterworths Scientific Publications, London, 1953).
- [25] Ibid., p. 148.
- [26] Ibid., p. 137
- [27] J. Richard, C.R. Acad. Sci. (France) 256, 1093 (1963).

Chapter Two

THIN FILM FABRICATION

A. REVIEW OF METHODS OF FABRICATING THIN GERMANIUM FILMS

1. Pre-Epitaxial Methods.

The development of methods for the production of thin films for optical studies prior to the pre-epitaxial period is discussed by Heavens [1] and Holland [2]. These methods, which have much in common with post-epitaxial methods, consist of primarily three techniques, which, listed in their historical order, are electrolytic deposition, cathodic sputtering, and vacuum deposition.

Let us first, however, define precisely what we mean by the term "epitaxial." An epitaxial film is one whose azimuthal orientation and normal direction of that crystallographic plane which lies parallel to the substrate surface is congruent to the same crystallographic plane in the substrate. For example, if one has a slab of CaF_2 , whose crystal symmetry is cubic, in which the surface crystallographic plane is of the $\{111\}$ family with a $\langle 111 \rangle$ type direction normal to the surface and $\langle 110 \rangle$ and $\langle 211 \rangle$ type directions lying in the surface, the crystallographic orientation of a germanium film grown epitaxially on such a surface will be defined by these exact same indices. Sometimes the term "single crystal" instead of epitaxial is used; however, in view of the

agglomerate nature of film growth (to be discussed), this term is a misnomer.

Films formed by electrolytic deposition use the principle of electrolysis in which a film, usually a metal, is deposited out on the cathode by the decomposition of an electrolyte containing a solution of a soluble salt of the metal. The method has the disadvantage that the film properties depend on a large number of difficult-to-control factors. This technique is not too widespread for the production of films for research purposes.

The process of cathodic sputtering involves the maintenance of a gaseous discharge between two electrodes with the cathode being the material to be sputtered. The bombardment of the cathode by the gas ions drives off atoms which are then diffused throughout the sputtering chamber and deposited on any exposed surfaces. Thus one has here a means with which to form films of hard-to-evaporate materials such as the refractory metals. Until recently, this method had been in decline for some years. However, it is now returning as an important technique for the formation of epitaxial films.

The technique of vacuum deposition by thermal evaporation consists of the thermal decomposition under vacua of at least 10^{-4} torr, of some source material from which the film will be formed. The path of the evaporated atoms will be relatively unhindered and will hence form a beam whose geometry is determined by the



geometry of the source arrangement. The substrate which will support the film is then placed in this beam so as to intercept the evaporated atoms and allow them to be deposited thereon. In this method, the deposition parameters can be fairly easily controlled and it has been this technique which was the overwhelming choice for the production of germanium films in the pre-epitaxial period.

2. Post-Epitaxial Methods.

The expression "epitaxial" has been defined above. There is presently no completely satisfactory theory of epitaxial growth, although the body of experimental data is growing rapidly [3, 4]. However, the following qualitative observations seem to be substantiated by the experimental results:

(a) Epitaxial growth is almost never effected without heating the substrate. Therefore, it seems plausible that growth initially occurs because the deposited atoms are given enough mobility so that they may arrange themselves according to the pattern set by the substrate crystal symmetry.

(b) The film and substrate lattice structure and lattice constants must match each other to a degree that seems to depend on the extent to which the bonding of the film material is ionic. That is, it appears that the greater the ionicity of the valence bonds of the film, the greater is the lattice mismatch with the

substrate that can be tolerated. For example, it is far easier to obtain epitaxial growth of the alkali-halides than of germanium.

(c) The film grows by the formation of discrete nuclei with the bulk lattice structure which are scattered over the substrate surface. The growth continues by the enlargement of these nuclei until they grow together forming a more or less homogeneous film [3].

At present, three techniques are used to produce epitaxial films. These are vapor deposition, cathodic sputtering and vacuum deposition. Vapor deposition involves a chemical reaction between an appropriate substrate and a gas atmosphere containing a compound of the material to be deposited as a film. One of the more popular methods uses the breakdown of a halide gas of Ge or Si at the surface of a substrate of similar material [5]. This technique works well when the film-substrate system is among the group 4 or 3-5 semiconductors. As mentioned before, cathodic sputtering is making a comeback as a means of producing epitaxial films [6]; however, the predominant method is still vacuum deposition. The only major change in this method that has occurred since the pre-epitaxial era has been to heat the substrate. It has been successful for a very large number of materials besides semiconductors [7].

3. Suitability of Various Methods for Producing Films for Optical Studies.

The selection of a suitable technique from the ones mentioned above which will provide films for optical transmission studies will now be discussed. Vapor deposition must be ruled out at least for the present because of its inability to make depositions on transparent crystals. Although both cathodic sputtering and vacuum deposition will satisfy this condition, it is still too early to determine which will eventually become the superior technique. Therefore, vacuum deposition was chosen as the preparation vehicle for the films to be examined in this work primarily because of the wealth of previous experience with this technique reported by many workers.

B. THE TECHNIQUE OF VACUUM DEPOSITION OF
EPITAXIAL GERMANIUM FILMS ON CaF_2 SUBSTRATES

1. Reasons for Choice of CaF_2 . Substrate Preparation.

We now examine the various criteria pertinent to the selection of a suitable substrate upon which to grow epitaxial germanium films. With reference to Table 2-1, they are as follows:

(a) The substrate material must have a lattice configuration that is as geometrically similar as possible to that of germanium. The space group for germanium is O_h^7 , the well-known diamond structure.

The space group O_h^5 , common to the alkali-alkaline earth halides, is of two types. For the alkali halides we have the so-called NaCl structure, while for the alkaline earth halides we have the CaF_2 structure. The CaF_2 structure is the same as the diamond structure, except that now the empty quarter-diagonal positions of the latter are occupied in the former. Both structures are suitable for the epitaxial growth of germanium; however, because the CaF_2 structure has a {111} type cleavage which is the natural direction of growth for germanium, it is slightly more preferable than the NaCl structure which has a {100} type cleavage.

(b) As the germanium bond is non-ionic in character, a reasonable match of its lattice constant to that of the substrate is to be demanded. Just how close we have to be can only be found by experiment; however, other considerations being equal, the closer we can come, the better.

(c) Because the substrate must be heated, it must be able to withstand the temperature necessary for epitaxial growth without undue deterioration. Since this temperature runs between 500° and $700^\circ C$, the melting point of the substrate should be considerably above this range. Unfortunately, many of the alkali-halides undergo appreciable evaporation well before their melting points.

(d) Again because the substrate must be heated, its linear thermal expansion coefficient becomes an important parameter.

This is due to the fact that, after the film has been formed, the film-substrate system is cooled to room temperature. If the film-substrate difference thermal expansion coefficient is large, then large stresses are induced into the film. They may be so large that the film wrinkles and breaks away from the substrate.

(e) Finally, the useful optical transmission range is of overriding importance to this work. It is mandatory that whatever substrate is chosen, it must be transparent to radiation with wavelength between 2000\AA and 6000\AA .

In compiling Table 2-1, any candidate that flagrantly violated any of the above conditions was eliminated. Of the remaining choices, it is apparent that CaF_2 and SrF_2 are in the lead. We chose CaF_2 over SrF_2 primarily because there exists much more experience with this material as a substrate for germanium films. As far as is known, there has been no attempt to deposit epitaxial films of germanium on SrF_2 ; however, there is no reason to expect that such an attempt would not be quite successful.

The CaF_2 used as substrate material for this research was purchased in single crystal blocks 1 cm square by 5 cm long from Optovac, Inc., North Brookfield, Mass. The $\langle 111 \rangle$ crystallographic direction was oriented parallel to the long direction of the block. The material was high purity laser-grade stock. At first, a substrate was prepared by cleaning a 1 mm thick slab from this block

and then polishing both sides by the usual technique for preparing optical flats. Films deposited on such substrates were found to be of good crystalline quality but of very poor optical quality. Microscopic examination of these polished substrates showed that although they appeared highly polished to the naked eye they invariably possessed a surface roughness comparable in size to the final grit that was used in the polishing operation. This roughness had a highly degrading effect on the ultraviolet optical properties of a film deposited thereon (see Chapter Four for additional information). It appears as if crystalline materials with highly ionic bonds cannot be polished by conventional methods. We therefore decided to use cleaved slabs as our substrate medium. Although these substrate surfaces are rough macroscopically due to the presence of many cleavage steps, they are smooth microscopically on the exposed atomic planes. The cleavage steps cause at the most a constant error in the optical response of the film which can be minimized by carefully aligning the sample in the optical apparatus (see Chapter Four). The cleavage operation is performed by holding the block firmly in suitably jiggling, aligning a razor blade parallel to the cleavage plane at the required point along the length of the crystal, and striking it sharply with a small hammer. Sometimes several attempts were required

to obtain a fairly smooth substrate surface. These substrates were usually used immediately, but at other times several days elapsed. This did not seem to make any difference in the growth of the film.

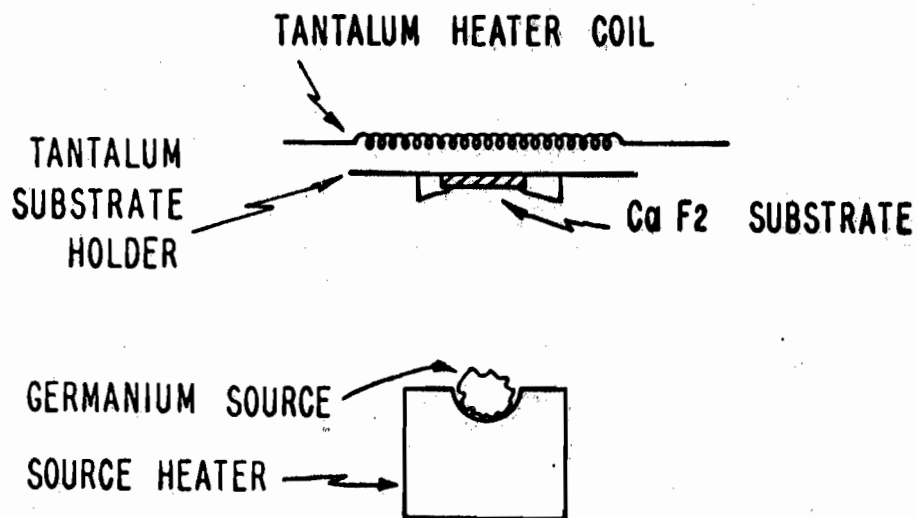
2. The Apparatus of Via

The apparatus designed and used by G. Via of the IBM Components Division for the production of the first high quality epitaxial films of germanium on CaF_2 was also used for the fabrication of the films used in the early stages of this research. This apparatus is described in references 11 and 3. It consists essentially of a vacuum chamber which accommodates an electron microscope gun along with the usual evaporation jigging. Its uniqueness lies in its ability to examine the growth of the epitaxial film by reflection electron diffraction, thereby allowing one to watch the actual pattern transitions as the film grew. Unfortunately, all of the films grown during this period were made on polished CaF_2 substrates before it was realized how rough they were. Therefore, none of the optical measurements could be used for the calculation of optical constants. However, the electron diffraction studies made at that time are still useful.

3. The Harvard Apparatus. Deposition Procedures.

The first epitaxial films of germanium on CaF_2 were made by Via and Thun [11] and Marucchi and Nifontoff [12]. The most extensive investigation to date into the formation conditions and structure of this film-substrate system has been done by Sloope and Tiller [13], although several other works have also been reported [14-16]. In each of these efforts, essentially the same technique was used that is about to be discussed here in conjunction with our work. What will be referred to as the Harvard apparatus has actually undergone a continuous evolution during the course of this work. The changes made were not in technique but were rather improvements in the convenience of operation. Hence, for purposes of general discussion we will refer to the schematic of Fig. 2-1. The actual apparatus is shown in Fig. 2-2 with the components relating to Fig. 2-1 designated therein.

The substrate is mounted on a .020 inch Ta plate with .005 inch Ta spring clips. This assembly is then heated by placing it under a series of .015 inch diameter Ta wire heater coils. Figure 2-3 shows the actual substrate holder with a piece of CaF_2 in place. The substrate temperature was measured by holding a Pt-Pt 10% Rh thermocouple on the substrate surface with one of the Ta clips as indicated in Fig. 2-3. The Ta heater coils were energized electrically from outside the vacuum chamber where the current flow, hence temperature, was regulated.



DEPOSITION PARAMETERS
NECESSARY FOR THE
EPITAXIAL DEPOSITION OF
GERMANIUM ON Ca F₂.

AMBIENT PRESSURE: $1 \cdot 10^{-6}$ TORR
SUBSTRATE
TEMPERATURE: $> 550^{\circ}\text{C}$
DEPOSITION RATE: $0.1-100 \text{ \AA/SEC}$

FIG. 2-1 SCHEMATIC DIAGRAM OF THE ARRANGEMENT OF THE COMPONENTS
IN THE EVAPORATION CHAMBER



In order to obtain a partial pressure suitable for evaporation, the temperature of the germanium source material must be raised to the vicinity of 1300°C and higher. This can be achieved in several different ways; however, for our purposes we found it convenient to use either a tungsten boat of .005 inch thickness or a boron nitride crucible with an embedded Ta resistance heater. The W boat has the advantage that high temperatures can be attained. On the other hand, Ge wets W and slowly dissolves it. Use of the BN crucible circumvented this problem; however, it was difficult to obtain high temperatures with this configuration. Figure 2-2 shows the W boat in place.

The vacuum system was comprised of an NRC model HS 4-750, type 0161 oil diffusion pump together with a Welch model 1402 Duo-seal mechanical forepump. The diffusion pump, manufactured by the NRC Corp., Newton, Mass., has a 4-inch diameter column, a pumping speed of 750 l/s at 10^{-4} torr, and is equipped with a liquid nitrogen cold trap. With the evaporation jigging shown in Fig. 2-2 covered by a 12-inch glass bell jar, this system was capable of reaching pressures as low as $7 \cdot 10^{-7}$ torr using the cold trap. This pressure, however, was read by an ionization gauge situated at the top of the cold trap; therefore, the pressure in the bell jar was probably somewhat higher. After reaching a minimum pressure, the procedure was usually to bring the substrate up

to temperature as fast as the thermal inertia of the heater would allow. For epitaxy to result, the temperature would have to exceed 550°C as read by the substrate thermocouple. During this time there would be little or no rise in pressure. The substrate would then undergo bake-out for a short period, usually 15 minutes to an hour. The source would next be heated to an appropriate level to produce a desired deposition rate. This could be estimated by observing the darkening of a monitor microscope slide at the same distance from the source as the substrate. The power dissipation of the source and substrate heaters was recorded in order to maintain resetability. When the desired evaporation rate was reached, the shutter shown in Fig. 2-2 was opened by means of a rotary mechanical feedthru in the vacuum system baseplate. The shutter remained opened for a predetermined time interval before being closed. Then the source heater would be shut down and the film would be given a short 5-minute post-anneal treatment at its formation temperature before being cooled. During the evaporation, the pressure would usually rise to 1 to $3 \cdot 10^{-6}$ torr. The procedure described above, with minor variations, was the one used to produce the films from which the optical data reported in this work were taken.

4. Physical Appearance of the Deposited Film.

The appearance of a typical film is shown in Fig. 2-4. In daylight or room light the film appears shiny and lustrous; however, when one examines the thicker films in a darkened room with a unidirectional source such as a flashlight, one finds that the film takes on a bluish, milky cast when the light is incident at about 45 degrees. One has to look carefully for this effect and just casual observation will not suffice. This effect is caused by the scattering of light due to the presence of surface roughness in the deposited film. This will be discussed more extensively in Section D of this chapter.

The color of the light transmitted by the film when it is held before a source of white light can be an important clue to its crystalline perfection. We recall that the absorption coefficient at the optical gap of germanium, which occurs at roughly 1.5μ , is around $5 \cdot 10^3 \text{ cm}^{-1}$. For films of a few hundred angstroms, this edge would hardly be noticed in their transmission spectra. However, the next strong transition is the Λ transition at 5900 \AA where the absorption coefficient suddenly reaches $5 \cdot 10^5 \text{ cm}^{-1}$ causing strong attenuation at shorter wavelengths. Therefore, a film whose band structure is that of the bulk material should have a red color when observed before white light. Indeed, this turns out to be a surprisingly good way to quickly judge the crystalline

TABLE 2-1

The pertinent physical properties of possible substrate materials suitable for the epitaxial deposition of germanium films.

Material	Lattice Configuration†	Lattice Constant (Å)†	Melting Point (°C)‡	Thermal Expansion (°C ⁻¹)‡	UV Cutoff (Å)‡
Ge	7 O _h	5.647	910 ††	5.8 · 10 ⁻⁶ (0°C) ††	—
CaF ₂	5 O _h	5.451	1360	24 · 10 ⁻⁶ (20°C-60°C)	1250
BaF ₂	5 O _h	6.184	1320	18 · 10 ⁻⁶ (0°C-300°C)	1300
SrF ₂	5 O _h	5.86	1400		1200
LiF	5 O _h	4.01	848	37 · 10 ⁻⁶ (0°C-200°C)	1040
KC	5 O _h	6.28	776	36 · 10 ⁻⁶ (20°C-60°C)	2000
KBr	5 O _h	6.578	730	43 · 10 ⁻⁶ (20°C-60°C)	2300
NaF	5 O _h	4.62	997	36 · 10 ⁻⁶ (25°C)	1900
NaCl	5 O _h	5.627	801	44 · 10 ⁻⁶ (-50°C-200°C)	2000

† See reference 8.

See reference 9.

†† See reference 10.

quality of the film. Epitaxial films have this characteristic red color, while polycrystalline ones are brownish, with amorphous films being more or less neutral.

C. REFLECTION ELECTRON DIFFRACTION (RED) ANALYSIS

The geometric theory of crystal diffraction phenomena is fully discussed in Barrett [17] and Pinsker [18]. In our discussion, we will apply, without proof, the results of this theory to the case of epitaxial and polycrystalline films.

The Bragg condition may be written as:

$$2\mathbf{k} \cdot \mathbf{G} + G^2 = 0 \quad (2-1)$$

where \mathbf{G} is a reciprocal lattice vector and \mathbf{k} is the wave vector of the incident radiation, in this case a monochromatic electron beam.

The usual way of interpreting equation (2-1) is through the construction of the so-called Ewald sphere in the reciprocal lattice.

Figure 2-5 shows a cross section of Ewald's construction in a simple cubic reciprocal lattice. This is done by drawing a vector parallel to \mathbf{k} , and of equal magnitude, which terminates on a reciprocal lattice point. The length of this vector now defines the radius of a sphere whose surface passes through the above lattice point. Wherever this sphere intersects another reciprocal lattice point, we construct a vector to it from the sphere origin which then indicates the direction of reflection. If we position a film to

intercept the reflected beams we will obtain the well-known Laue pattern. For the very high energy electron beams that are used for RED, the wave vector of the beam becomes very much longer than the distance between points of the reciprocal lattice. For example, the magnitude of a 75 kV electron beam is about 100 times greater than the reciprocal lattice constant of germanium. Therefore, with respect to any given portion of the reciprocal lattice, the Ewald sphere may be considered a plane. This means that for an electron beam incident along a symmetry direction there will appear on the film a projection of the reciprocal lattice points lying in the plane normal to this direction. In the RED technique, the incident electron beam strikes the surface of the sample at a glancing angle and penetrates only a small distance normal to the surface before undergoing reflection. However, the total path traveled in the crystal is much greater than this depth; therefore, because of this fact and the very small angle of incidence it is possible to discuss RED patterns as actually transmission diffractograms.

Figure 2-6 shows the RED pattern for an epitaxial Ge film whose surface vector is of the $\langle 111 \rangle$ type with the electron beam incident in a $\langle 110 \rangle$ type direction. If one had a polycrystalline film whose surface vector was mainly $\langle 111 \rangle$ but whose azimuthal vectors were randomly distributed among the individual crystallites, one would

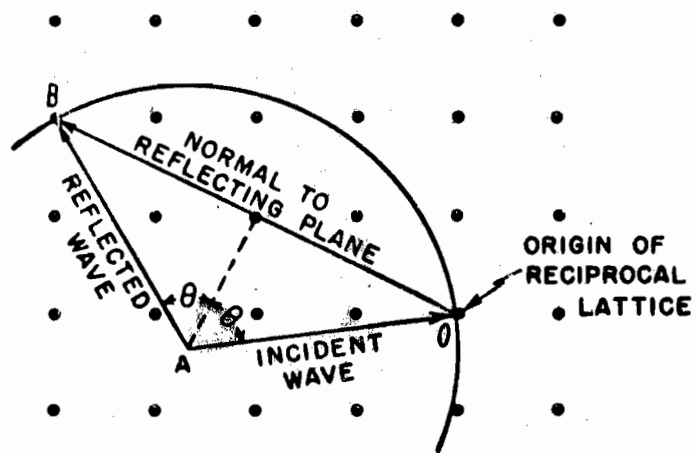


FIG. 2-5 EWALD'S CONSTRUCTION IN THE RECIPROCAL LATTICE

obtain the spot and ring patterns typical of Figs. 4-6 and 4-8. That this is so, can be seen by imagining the projection pattern caused by randomly rotating the reciprocal lattice about the $\langle 111 \rangle$ direction and noting the various intersections with the Ewald plane. In addition, if we randomly rotate the reciprocal lattice in all possible directions, including $\langle 111 \rangle$, we will generate the well-known ring pattern common to powder x-ray diffraction analysis.

In Fig. 2-6, we have a sequence of RED patterns showing various stages in the growth of the epitaxial film. These were made with the Via apparatus described above during the initial period of this research. We see that the start of epitaxy is immediate and continues throughout the growth of the film. The substrate pattern is rather obscure because CaF_2 is a dielectric and tends to become charged and repel the incident electron beam. The sudden appearance of the germanium Laue pattern when the substrate is exposed to the germanium vapor stream is probably due to the rapid development of nucleations on the crystal substrate surface. As the film grows and becomes more or less continuous, the Laue pattern spots should become slightly elongated. Figure 2-6 indicates that this is the case. The elongation may be attributed to a refractive shift of the pattern caused by some sort of wavy surface on a thin layer of finite thickness, whereas the sharp spots are caused by transmission through discrete nucleations. This

interpretation is discussed at length in Pashley's review paper, The Study of Epitaxy in Thin Surface Films [4].

D. FILM SURFACE TOPOGRAPHY STUDIES

According to the nucleation theory of crystalline film growth outlined in Section A-2, one would expect the resulting film surface to possess some sort of structure or texture arising from the nucleation centers. We have mentioned that the RED patterns suggest that such is the case, and in fact studies show that the surfaces of many epitaxial films have a definite texture or roughness. The main tool for the observation of this structure has been the use of the electron microscope on uranium-shadowed carbon replicas of the film surface. Although this technique shows any film granularity or discontinuity, it does not give a clear idea of the cross section of the surface irregularities.

Sloope and Tiller [19] have studied the effect of substrate temperature, deposition rate, and film thickness on the surface roughness of epitaxial germanium films on CaF_2 . These same workers have also studied the Ag-NaCl system [20] along with other germanium systems [13]. In addition, the texture of Ag films deposited on amorphous substrates as a function of the deposition parameters was investigated by Sennett and Scott [21]. Their observations can be summarized as follows:



(a) For a given deposition rate, the films become more and more aggregated, hence rougher, the higher the substrate temperature.

(b) Conversely, for a given substrate temperature, the films become more porous, hence rougher, the lower the deposition rate.

(c) On the other hand, the conditions for epitaxy or improved orientation are made more favorable by high substrate temperatures and low deposition rates.

At this juncture, we should remark that the results of Chapter Four will indicate that the optical response of the films is very strongly influenced by both crystalline perfection and surface roughness. Therefore, we see that any selection of deposition parameters for the production of a film with optimum optical response must result in a compromise between these two factors. We shall see that films with excellent crystalline properties can have a poor optical response because of surface roughness scattering. The range of substrate temperatures and deposition rates we have been discussing above is of course a function of the film-substrate system as are the conditions for epitaxy. For the Ge-CaF₂ system, substrate temperatures from 400°C to 700°C and deposition rates from 10Å/min to 3000Å/min have been investigated [13]. In our work, we have selected those deposition parameters which were felt to offer a good compromise between crystallinity

and roughness. However, we should point out that, to date, no one has claimed to make a smooth epitaxial film of germanium on CaF_2 .

The effect of ambient pressure on the surface topography and crystallinity of the films has not been extensively studied and those results that have been reported seem to be in conflict. Catlin, *et al.* [14], report that ambient pressures of 10^{-9} torr allow epitaxial deposition at lower substrate temperatures for a given deposition rate than had been previously observed. Conversely, it has also been reported that a poor vacuum enhances epitaxy [22].

Figure 2-7 is a photomicrograph of the surface of one of our films. The dark area is the substrate and the speckled area is the germanium film. Dark field illumination was used to bring out the surface detail. This film was grown at a substrate temperature of about 700°C and with a deposition rate around $100\text{\AA}/\text{min}$; that is, under conditions favorable for the formation of a rough growth. To the casual observer, the film looks quite shiny; however, more intensive investigation reveals the effect discussed in Section A-4. It is hard to estimate the size of the aggregates from Fig. 2-7 alone, but they appear to be at least a few thousand \AA in width. The height is even more difficult to resolve. Sloope [19] indicates that for some films the thickness variation may be

as much as 200\AA . Finally, we should mention that it has been established through microscopic and optical investigations of aluminized CaF_2 cleaved surfaces that this surface roughness is definitely a film growth effect and not merely a replication of any substrate roughness. Also, we do not mean to imply that all films will have a surface roughness detectable by observation with an optical microscope. However, in Chapter Four we will see that even quite small roughnesses, beyond the resolution limit of optical microscopy, can still affect the ultraviolet optical response.

E. MEASUREMENT OF FILM THICKNESS

The various methods of measuring film thickness are discussed by Heavens [1, 23]. Of these, the interference method, either the technique of Fizeau fringes or fringes of equal chromatic order (FECO), ranks high as a method which can provide accurate results without requiring the use of any material constants, such as film density and refractive index. Unfortunately, it requires very smooth surfaces for film and substrate, a condition which is not met by our films on cleaved CaF_2 . The cleavage steps obscure the very thin films that we used for our measurements. In fact, in view of the findings of Section D, we must realize that there are certain difficulties connected with the usual concept of film thickness. These arise from the aggregate structure of the film,

particularly when the height of the aggregates approaches the average film thickness. When the mean thickness is only a few dozen atoms, the picture of a film as an isotropic, homogeneous, plane parallel-sided layer is no longer valid. Hence, any reference to "film thickness" will always imply some sort of average thickness.

We used simply the infrared transmission of the film to obtain its thickness. In this region $k = 0$, and because the films are epitaxial, the bulk refractive index can be used with a high degree of confidence. The index of refraction of bulk single crystal germanium has been measured by Cardona in the wavelength region 1.8μ to 5.5μ [24], and there is evidence that these values hold also for polycrystalline germanium [25]. We measured the transmission at 1.8μ and 2.0μ , used Cardona's values for n , and inverted equation (3-6b) to find the thickness. Measurements were made at several different positions on the film surface and the results averaged. (The rms deviation was usually about 10\AA to 20\AA). Fortunately, the transmission varied quite rapidly over the thickness range of interest -- the films were much too thin for interference fringe methods -- so that the thickness to transmission variation was about $10\text{\AA} / \%$ with T being measurable to within one percent. We feel that this method gave satisfactory results.

Chapter Two

BIBLIOGRAPHY

- [1] O. S. Heavens, Optical Properties of Thin Solid Films (Butterworths Scientific Publications, London, 1953).
- [2] L. Holland, Vacuum Deposition of Thin Films (John Wiley and Sons, Inc., New York, 1960).
- [3] R. E. Thun, Structure of Thin Films, Physics of Thin Films, vol. 1, ed. by G. Hass (Academic Press, New York, 1963).
- [4] D. W. Pashley, Advances in Physics 5, 173 (1956); Single Crystal Films, ed. by M. H. Francombe and H. Sato (MacMillan, New York, 1964).
- [5] E. S. Wajda and R. Glang, Proceedings of the AIME Conference on Semiconductor Materials, Aug. 1960.
- [6] E. Krikorian in Single Crystal Films, ed. by M. H. Francombe and H. Sato (MacMillan, New York, 1964).
- [7] See tables in Pashley, reference 4.
- [8] Handbook of Chemistry and Physics (Chemical Rubber Publishing Co., Cleveland, 1955).
- [9] Optovac Optical Crystals Bulletin No. 50, Optovac Inc., North Brookfield, Mass.
- [10] Selected Constants Relative to Semiconductors, ed. by P. Aigrain and M. Balkanski (Pergamon Press, New York, 1961).
- [11] G. G. Via and R. E. Thun, Natl. Symposium on Vacuum Technol. Trans. 8, 950 (1962).
- [12] J. Marucchi and N. Nifontoff, Compt. Rend. 249, 435 (1959).
- [13] B. W. Sloope and C. O. Tiller, J. Appl. Phys. 33, 3458 (1962).
- [14] A. Catlin, A. J. Bellemore, Jr., and R. R. Humphris, J. Appl. Phys. 35, 251 (1964).

- [15] R. L. Schalla, L. H. Thaller, and A. E. Potter, Jr.,
J. Appl. Phys. 33, 2554 (1962).
- [16] A. L. Pundsack, J. Appl. Phys. 34, 2306 (1963).
- [17] C. S. Barrett, Structure of Metals (McGraw-Hill, New York
1952).
- [18] Z. G. Pinsker, Electron Diffraction (Butterworths, London,
1953).
- [19] B. W. Sloope and C. O. Tiller, Japan. J. Appl. Phys. 2,
308 (1963).
- [20] B. W. Sloope and C. O. Tiller, J. Appl. Phys. 32, 1331
(1961).
- [21] R. S. Sennett and G. D. Scott, J. Opt. Soc. Am. 40,
203 (1950).
- [22] H. G. F. Wilsdorf, Bull. Am. Phys. Soc. 10, 342 (1965).
- [23] O. S. Heavens, see reference 22 of Chapter One.
- [24] M. Cardona, Technical Report No. HP-5, Gordon McKay
Laboratory of Applied Science, Harvard University,
1959 (unpublished). See Fig. 6-8.
- [25] C. Salzberg and J. Villa, J. Opt. Soc. Am. 48, 579 (1958).

Chapter Three

THE THEORY OF THE DETERMINATION OF THE OPTICAL CONSTANTS OF SEMICONDUCTOR THIN FILMS FROM PHOTOMETRIC MEASUREMENTS

A. THE REFLECTIVITY - TRANSMISSIVITY (RT) METHOD

1. Theoretical Development.

In Chapter One, Section D-3, some of the various photometric techniques used for the determination of the optical constants of solids were discussed. The RT method for thin absorbing films on **thick nonabsorbing** substrates will now be considered in detail. The particular case to be covered will be that of germanium films on CaF_2 substrates. The index of refraction of CaF_2 between 2000\AA and 6000\AA may be obtained from the data of Martens [1], while the optical constants of germanium that are used in the theoretical calculations are those derived by H. R. Philipp [2] by a dispersion analysis of the reflectivity data of Donovan, et al. [3].

Referring to Fig. 3-1, we have directly from the principle of superposition of electromagnetic waves the following equations for the reflectivity and transmissivity coefficients of the normally incident electric field vector for the case of an absorbing thin film separating two semi-infinite dielectric media, one being air and the other the substrate:

$$r_{FA} = \frac{\rho_{FA} + \rho_{SF} e^{+2i\tilde{k}_F a}}{1 + \rho_{FA} \rho_{SF} e^{+2i\tilde{k}_F a}} \quad (3-1a)$$

$$r_{FS} = \frac{\rho_{FS} + \rho_{AF} e^{+2i\tilde{k}_F a}}{1 + \rho_{FA} \rho_{SF} e^{+2i\tilde{k}_F a}} \quad (3-1b)$$

$$t_{FS} = \frac{\tau_{FS} \tau_{AF} e^{+i\tilde{k}_F a}}{1 + \rho_{FA} \rho_{SF} e^{+2i\tilde{k}_F a}} \quad (3-1c)$$

$$t_{SF} = \frac{\tau_{FA} \tau_{SF} e^{+i\tilde{k}_F a}}{1 + \rho_{FS} \rho_{SF} e^{+2i\tilde{k}_F a}} = \frac{(\tilde{n})^2}{n_s} t_{FS} \quad (3-1d)$$

where we have made use of the following results of Chapter One,

Section B-1:

$$\rho_{FA} = \frac{1 - \tilde{n}}{1 + \tilde{n}} = -\rho_{AF} \quad (3-2a)$$

$$\rho_{SF} = \frac{\tilde{n} - n_s}{\tilde{n} + n_s} = -\rho_{FS} \quad (3-2b)$$

$$\tau_{FS} = \frac{2\tilde{n}}{\tilde{n} + n_s} = \frac{\tilde{n}}{n_s} \tau_{SF} \quad (3-2c)$$

$$\tau_{AF} = \frac{1}{1 + \tilde{n}} = \frac{1}{\tilde{n}} \tau_{FA} \quad (3-2d)$$

$$\tau_{FS} - \rho_{SF} = 1 \quad (3-2e)$$

$$\tau_{AF} - \rho_{FA} = 1 \quad (3-2f)$$

From equations (1-16a) and (1-23) we obtain the following rules for the intensity reflectivity and transmissivity coefficients of the model in Fig 3-1.

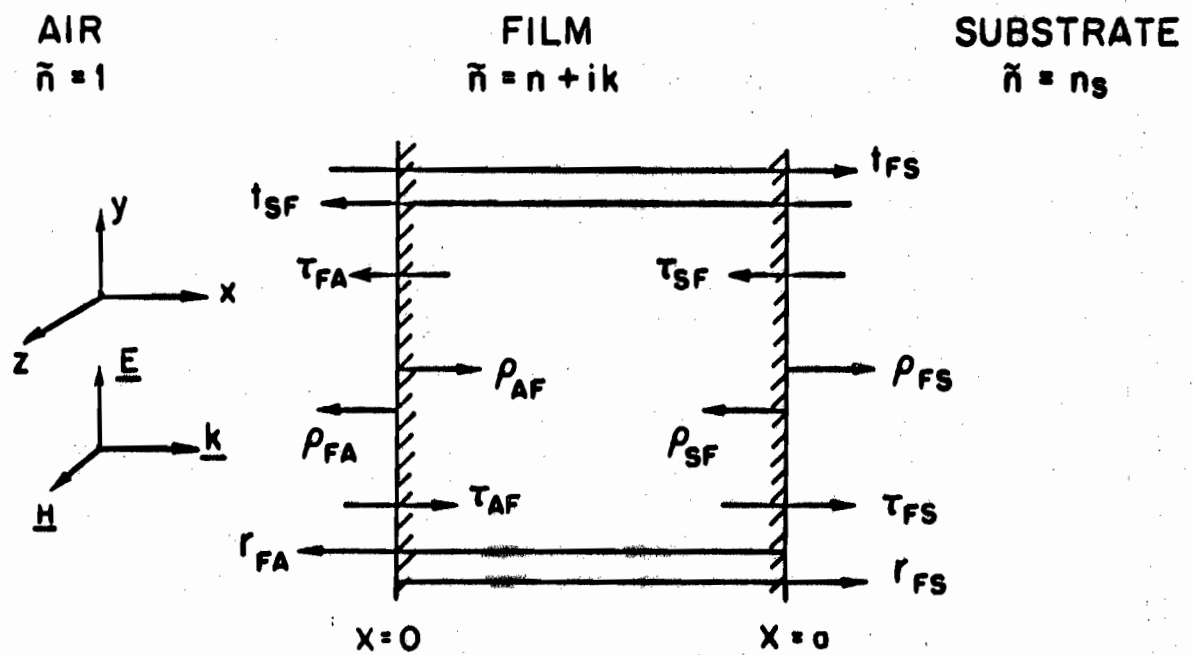


FIG. 3-1 MODEL FOR THE CASE OF AN ABSORBING THIN FILM ON A SEMI-INFINITE NON-ABSORBING SUBSTRATE.



$$R_{FA} = r_{FA} r_{FA}^* \quad (3-3a)$$

$$R_{FS} = r_{FS} r_{FS}^* \quad (3-3b)$$

$$T_{FS} = n_s t_{FS} t_{FS}^* = T_{SF} \quad (3-3c)$$

It is now desirable to cast equations (3-3) in a form which shows more explicitly the dependence on the optical constants. A particularly convenient way in which to do this is to use the polar form of ρ expressed by equations (1-32), obtaining:

$$R_{FA} = R_{FA}^N \frac{\left\{ e^{\frac{\alpha a}{2}} - \left(\frac{R_{FS}^N}{R_{FA}^N} \right)^{\frac{1}{2}} e^{-\frac{\alpha a}{2}} \right\}^2 + 4 \left(\frac{R_{FS}^N}{R_{FA}^N} \right)^{\frac{1}{2}} \sin^2 \left(\varphi + \frac{\psi_{FS} - \psi_{FA}}{2} \right)}{\left(e^{\frac{\alpha a}{2}} - (R_{FA}^N R_{FS}^N)^{\frac{1}{2}} e^{-\frac{\alpha a}{2}} \right) + 4 (R_{FA}^N R_{FS}^N)^{\frac{1}{2}} \sin^2 \left(\varphi + \frac{\psi_{FA} + \psi_{FS}}{2} \right)} \quad (3-4a)$$

$$R_{FS} = R_{FS}^N \frac{\left\{ e^{\frac{\alpha a}{2}} - \left(\frac{R_{FA}^N}{R_{FS}^N} \right)^{\frac{1}{2}} e^{-\frac{\alpha a}{2}} \right\}^2 + 4 \left(\frac{R_{FA}^N}{R_{FS}^N} \right)^{\frac{1}{2}} \sin^2 \left(\varphi + \frac{\psi_{FA} - \psi_{FS}}{2} \right)}{\left(e^{\frac{\alpha a}{2}} - (R_{FA}^N R_{FS}^N)^{\frac{1}{2}} e^{-\frac{\alpha a}{2}} \right) + 4 (R_{FA}^N R_{FS}^N)^{\frac{1}{2}} \sin^2 \left(\varphi + \frac{\psi_{FA} - \psi_{FS}}{2} \right)} \quad (3-4b)$$

$$T_{FS} = \frac{n_s}{[(1+n)^2 + k^2][(n+n_s)^2 + k^2]} \times \frac{16(n^2 + k^2)}{\left(e^{\frac{\alpha a}{2}} - (R_{FA}^N R_{FS}^N)^{\frac{1}{2}} e^{-\frac{\alpha a}{2}} \right) + 4 (R_{FA}^N R_{FS}^N)^{\frac{1}{2}} \sin^2 \left(\varphi + \frac{\psi_{FA} - \psi_{FS}}{2} \right)} \quad (3-4c)$$

where:

$$R_{FA}^N = \frac{(1-n)^2 + k^2}{(1+n)^2 + k^2} \quad (3-4d)$$

$$R_{FS}^N = \frac{(n_s - n)^2 + k^2}{(n_s + n)^2 + k^2} \quad (3-4e)$$

$$\psi_{FA} = \tan^{-1} \frac{2k}{n^2 + k^2 - 1} \quad (3-4f)$$

$$\psi_{FS} = \tan^{-1} \frac{2n_s k}{n^2 + k^2 - n_s^2} \quad (3-4g)$$

$$\alpha = \frac{4\pi k}{\lambda} \quad (3-4h)$$

$$\varphi = \frac{2\pi n a}{\lambda} \quad (3-4i)$$

This is the form usually found in the literature [4, 6]. An even more explicit form is that derived by Harris and Loeb [5][†]:

$$R_{FA} = \frac{|\tilde{n}(1 - n_s) \cos \frac{2\pi\tilde{n}a}{\lambda} - i(n_s - \tilde{n}^2) \sin \frac{2\pi\tilde{n}a}{\lambda}|^2}{|\tilde{n}(1 + n_s) \cos \frac{2\pi\tilde{n}a}{\lambda} - i(n_s + \tilde{n}^2) \sin \frac{2\pi\tilde{n}a}{\lambda}|^2} \quad (3-5a)$$

$$R_{FS} = \frac{|\tilde{n}(n_s - 1) \cos \frac{2\pi\tilde{n}a}{\lambda} - i(n_s - \tilde{n}^2) \sin \frac{2\pi\tilde{n}a}{\lambda}|^2}{|\tilde{n}(1 + n_s) \cos \frac{2\pi\tilde{n}a}{\lambda} - i(n_s + \tilde{n}^2) \sin \frac{2\pi\tilde{n}a}{\lambda}|^2} \quad (3-5b)$$

$$T_{FS} = \frac{4 n_s |\tilde{n}|^2}{|\tilde{n}(1 + n_s) \cos \frac{2\pi\tilde{n}a}{\lambda} - i(n_s + \tilde{n}^2) \sin \frac{2\pi\tilde{n}a}{\lambda}|^2} \quad (3-5c)$$

[†] It should be pointed out that the denominator of equation (4) of reference [5] contains a rather obvious sign error.

We must now consider the fact that the substrate is not semi-infinite. We will derive the appropriate equations taking the substrate-air interface into account and then determine the extent of the error involved in neglecting it. The problem has been extensively investigated by Harris, Beasley, and Loeb [7]. They have considered in detail the treatment of a dielectric slab whose thickness is many times the wavelength of the incident radiation. By assuming an appropriate **linewidth and thickness distribution** function, they have shown that through an averaging process one obtains the same result as if one had summed the intensities of the radiation inside the slab instead of the amplitudes and phases. They also considered this same case when one side of the slab was covered with a thin absorbing film. Although they could not prove formally that the result of the averaging process was identical to the use of intensity addition in the substrate, their numerical calculations showed the two to be equal for all practical purposes. We shall proceed on the assumption that their work has justified intensity addition for our film configuration. Hence, we obtain directly from Fig. 3-2 the following equations:

$$R = R_{FA} + T_{FS} R_{AS} T_{SF} + T_{FS} R_{AS} R_{FS} R_{AS} T_{SF} + \dots$$

or

$$R = R_{FA} + \frac{T_{FS}^2 R_{AS}}{1 - R_{AS} R_{FS}} \quad (3-6a)$$

and

$$T = T_{FS}(1 - R_{AS}) + T_{FS} R_{AS} R_{FS}(1 - R_{AS}) + T_{FS} R_{AS} R_{FS} R_{AS} R_{FS}(1 - R_{AS}) + \dots$$

or

$$T = \frac{T_{FS}(1 - R_{AS})}{1 - R_{AS} R_{FS}} \quad (3-6b)$$

where

$$R_{AS} = \frac{(1 - n_s)^2}{(1 + n_s)^2} \quad (3-7)$$

For the materials studied in this work, we may put typically for the purpose of ascertaining the degree to which the finite substrate correction influences the results $T_{FS} = 10^{-1}$, $R_{FS} = .50$, $R_{AS} = .03$. We then have an additive factor of $3 \cdot 10^{-4}$ to the reflectivity R and the multiplicative factor .97 to the transmissivity T . Only the factor for T can possibly be expected to amount to anything greater than the experimental error; however, since the inclusion of the finite substrate effect does not complicate any of the analysis to follow, we will keep it for the sake of completeness.

Figure 1-3b shows the optical constants of germanium derived by Philipp [2]. The result of substituting these constants into equations (3-6) is given for T in Fig. 3-3 and for R in Fig. 3-4. The curves are calculated for films ranging in thickness from 50\AA to 500\AA in intervals of 50\AA . This covers the usable thickness range in which one can perform transmission experiments. These curves prove to be invaluable for planning experiments and for quickly interpreting the measurements.

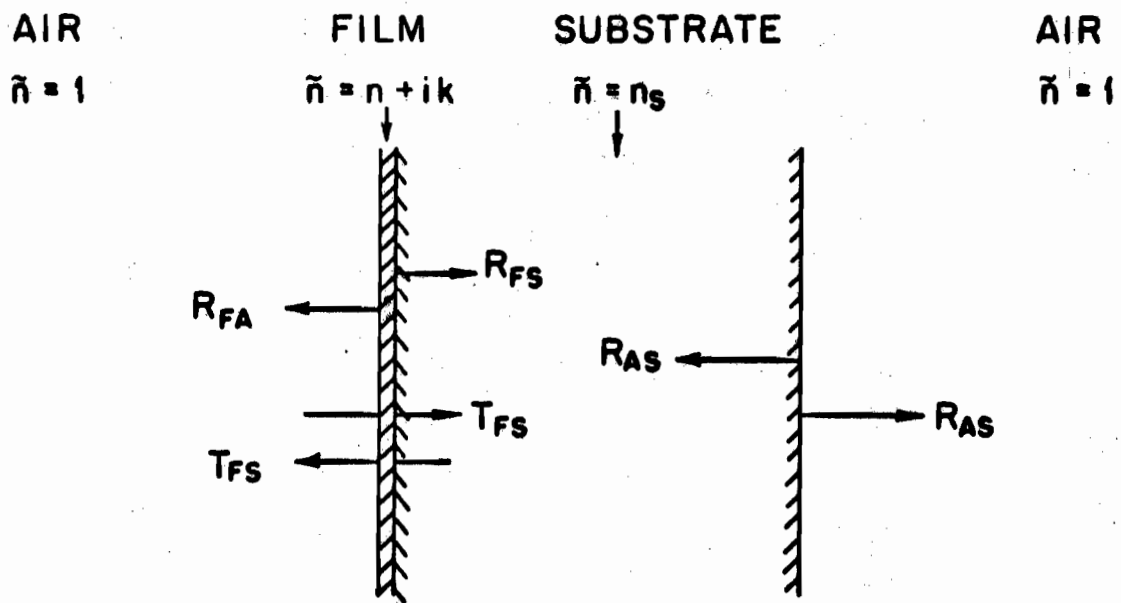


FIG. 3-2 INTENSITY ADDITION MODEL FOR A THIN ABSORBING FILM ON A THICK NON-ABSORBING SUBSTRATE.

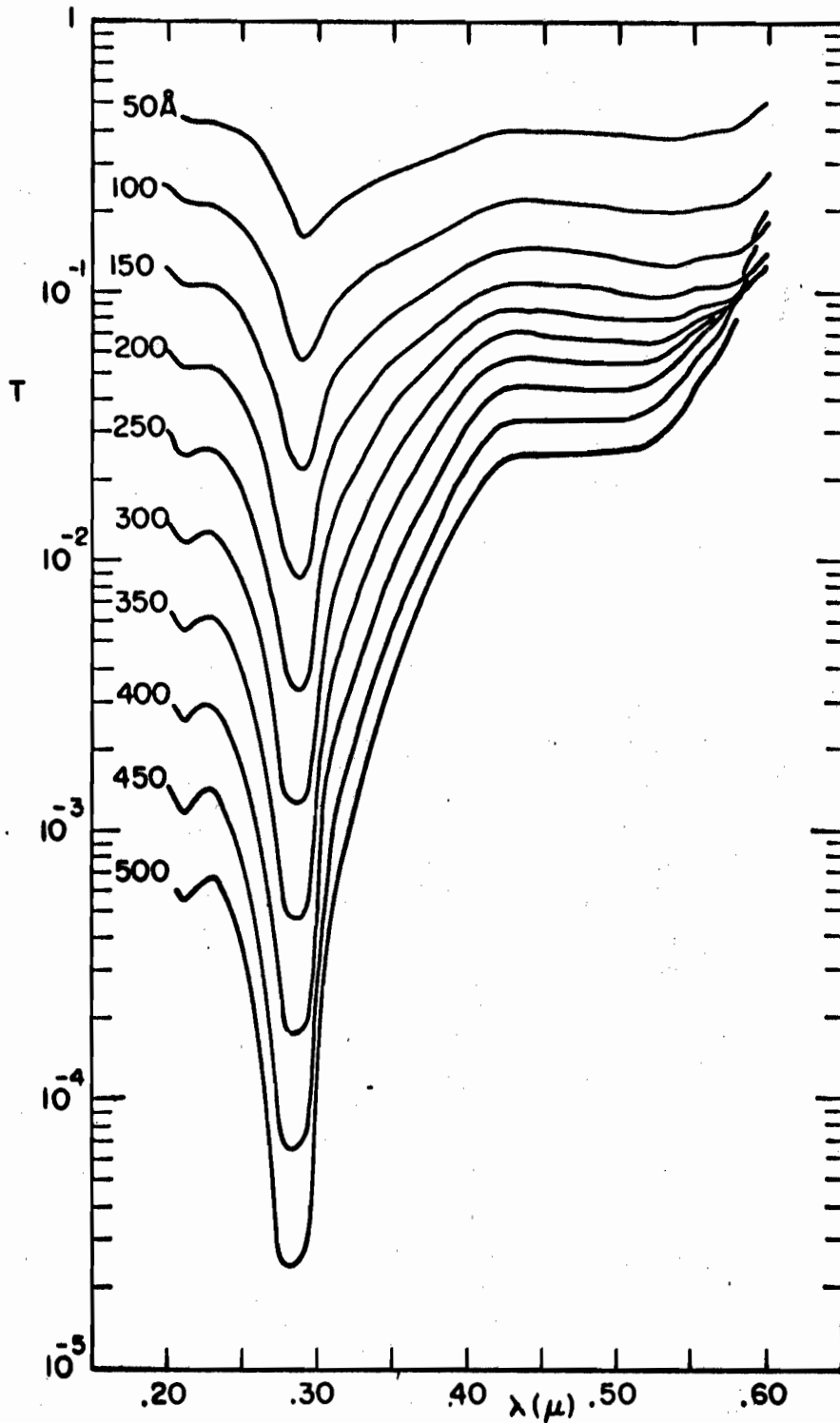


FIG. 3-3 THE TRANSMISSION OF GERMANIUM THIN FILMS ON CdF_2 SUBSTRATES USING THE OPTICAL CONSTANTS DERIVED BY PHILIPP(2). THE FILM THICKNESS IS INDICATED FOR EACH CURVE.

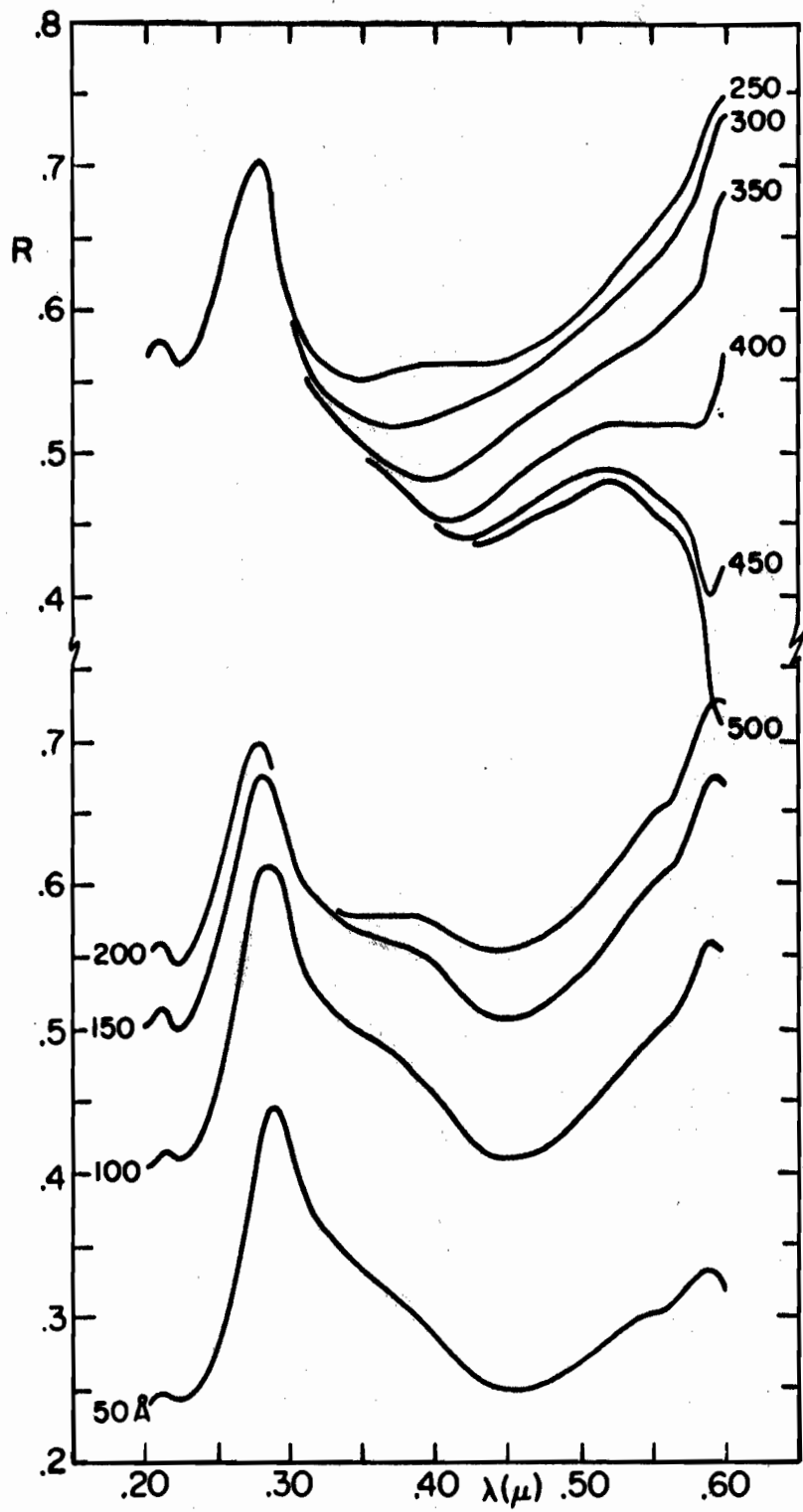


FIG. 3-4 THE REFLECTIVITY OF GERMANIUM THIN FILMS ON CoF_2 SUBSTRATES USING THE OPTICAL CONSTANTS DERIVED BY PHILIPP (2). THE FILM THICKNESS IS INDICATED FOR EACH CURVE.

We shall now state two important approximations to equations (3-4) in order to discuss qualitatively some of the results to be derived numerically and empirically from these equations. In doing this, the presence of the substrate backing will be neglected completely as it has no importance in any qualitative discussions. Equations (3-4a) and (3-4c) become, respectively:

$$R = R^N \frac{\left(\frac{\alpha a}{2} - e^{-\frac{\alpha a}{2}} \right)^2 + 4 \sin^2 \varphi}{\left(\frac{\alpha a}{2} - R^N e^{-\frac{\alpha a}{2}} \right)^2 + 4R^N \sin^2(\varphi + \psi)} \quad (3-8a)$$

$$T = \frac{16(n^2 + k^2)}{[(1+n)^2 + k^2]^2} \times \frac{1}{\left(\frac{\alpha a}{2} - R^N e^{-\frac{\alpha a}{2}} \right)^2 + 4R^N \sin^2(\varphi + \psi)} \quad (3-8b)$$

where R^N , ψ , φ , and α are given by equations (3-4d), (3-4f), (3-4i), and (3-4h), respectively. One important approximation deals with the case of very strong absorption where the absorption damps out interference effects. This is the case where k is of the order of n and $e^{\alpha a} \gg 4$. In the wavelength region below 3500\AA for a 300\AA germanium film, this is a very good approximation. Applying these considerations yields:

$$R = R^N = \frac{(1-n)^2 + k^2}{(1+n)^2 + k^2} \quad (3-9a)$$

$$T = \frac{16(n^2 + k^2)e^{-\alpha a}}{[(1+n)^2 + k^2]^2} = [(1-R)^2 + 4R \sin^2 \psi] e^{-\alpha a} \quad (3-9b)$$

If we further stipulate $k \ll n$ while keeping $e^{\alpha a} \gg 4$, we obtain for (3-9b):

$$T = (1 - R)^2 e^{-\alpha a} \quad (3-10)$$

This form is particularly useful for the infrared spectroscopy of semiconductors and admits of an explicit solution for n and k as follows:

$$k = \frac{\lambda}{4\pi a} \ln \frac{(1 - R)^2}{T} \quad (3-11a)$$

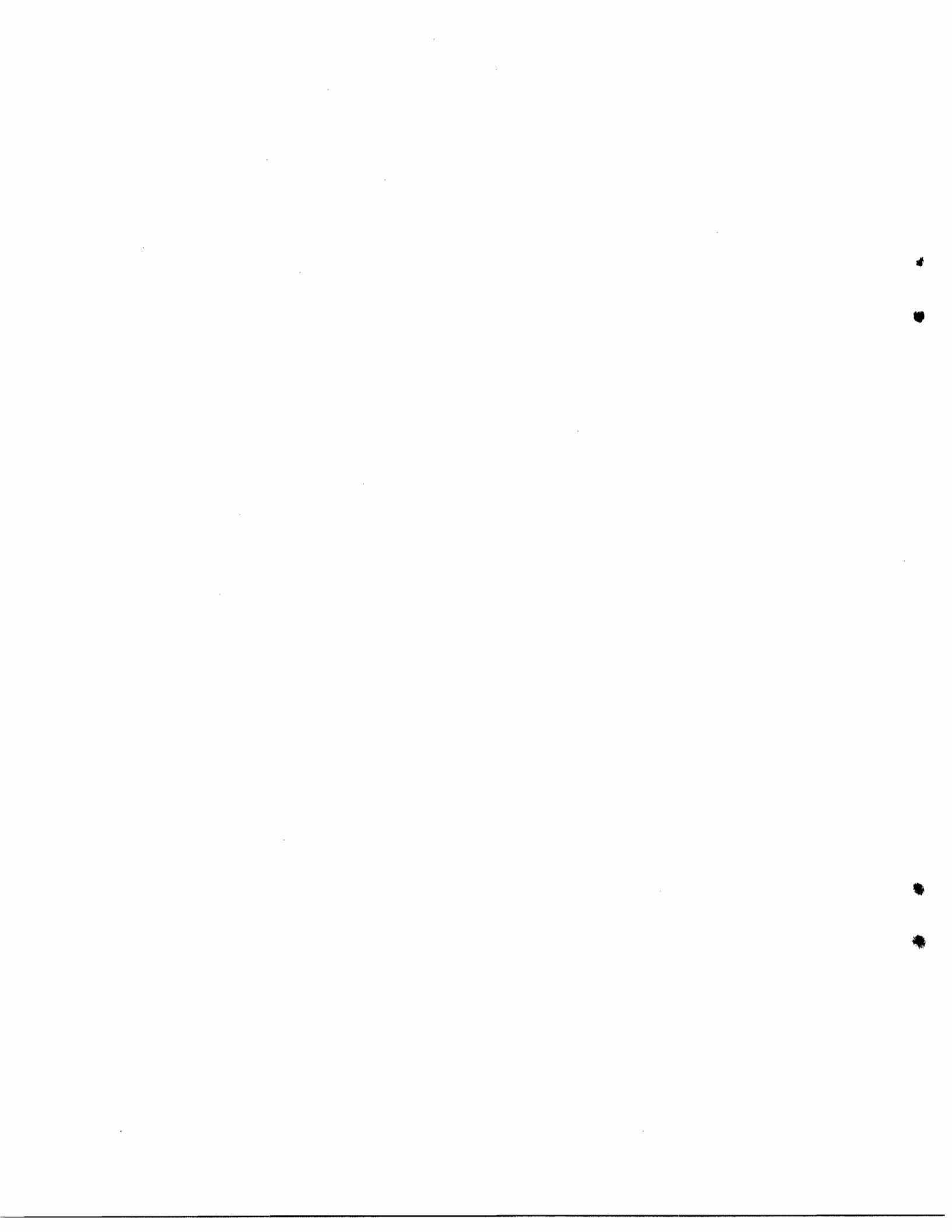
$$n = \frac{1+R}{1-R} + \left\{ \frac{4R}{(1-R)^2} - \frac{\lambda^2}{16\pi^2 a^2} \left[\ln \frac{(1-R)^2}{T} \right]^2 \right\}^{\frac{1}{2}} \quad (3-11b)$$

In general, however, some sort of numerical procedure must be invoked to obtain n and k for less extreme situations. This will be covered in Chapter Five. From equation (3-11b) it is clear that any pair of numbers R and T need not correspond to a real n .

Thus errors in the experimental determination of R and T may make (3-11b) insoluble for a real n . In fact, the criterion for real n can be written as an inequality between R and T :

$$T \geq (1 - R)^2 \exp \left[- \frac{4\pi a}{\lambda} \frac{2\sqrt{R}}{1-R} \right] \quad (3-12)$$

If one plots (3-12) as an equality in a T vs. R representation, the $T - R$ plane is essentially divided into two parts, one having n real and the other n complex. Plotting the experimentally



determined T and R for each wavelength on the same plane yields another curve. Wherever this curve crosses the curve of relation (3-12) into the complex n region will determine the wavelength range for which no real n can be obtained for the given experimental data. Of course, if the experimental conditions were such that the boundary conditions (1-16) and the assumptions leading to equations (3-9a) and (3-10) were obeyed exactly, and R and T were measured perfectly, then such an intersection could never occur. Although in principle the inequality (3-12) cannot be violated, there is no reason why the discriminant of equation (3-11b) cannot vanish if the optical constants of the material permit. If there is such a wavelength where this condition is satisfied, then there may exist a situation where small uncertainties in the experimental values of R and T will cause large uncertainties in n. Algebraic manipulation of equations (3-11) yields the following condition on the optical constants for the vanishing of the discriminant in (3-11b):

$$n^2 = k^2 + 1 . \quad (3-13)$$

We observe that (3-13) violates our assumption that $n \gg k$, necessary for the validity of equation (3-10). Nevertheless, we are encouraged to examine the consequences of equation (3-13) in more general circumstances when an explicit solution for n and k is not

possible. If we examine the germanium optical constant curves of Figs. 1-3b we see that equation (3-13) is satisfied near $\lambda = 3000\text{\AA}$, and that the T vs. R representation plot shown in Fig. 3-5 for a 300\AA film indicates that near this wavelength small changes in the experimental values of R and T may determine whether or not n is real. We might add that the equivalent to (3-13) for the dielectric constant $\tilde{\epsilon}$ is $\epsilon_1 = 1$ and $\epsilon_2 = 2k\sqrt{k^2 + 1}$.

2. The First Order Error Derivatives for Germanium Thin Films.

In general, we are not able to obtain n and k in terms of R and T explicitly as we did in equations (3-11), and some sort of numerical operations must be performed in order to find the optical constants. However, regardless of the numerical procedure actually used, we shall want to know in principle how experimental errors in R and T affect the error in the derived optical constants. Therefore, we write the following equations in terms of the first-order error differentials:

$$dn = \frac{\partial n}{\partial R} dR + \frac{\partial n}{\partial T} dT + \frac{\partial n}{\partial a} da \quad (3-14a)$$

$$dk = \frac{\partial k}{\partial R} dR + \frac{\partial k}{\partial T} dT + \frac{\partial k}{\partial a} da . \quad (3-14b)$$

It is to be remembered that in the mathematical context of the problem we treat R and T as the dependent variables, n and k as the independent variables, and a and λ as parameters. Now, because

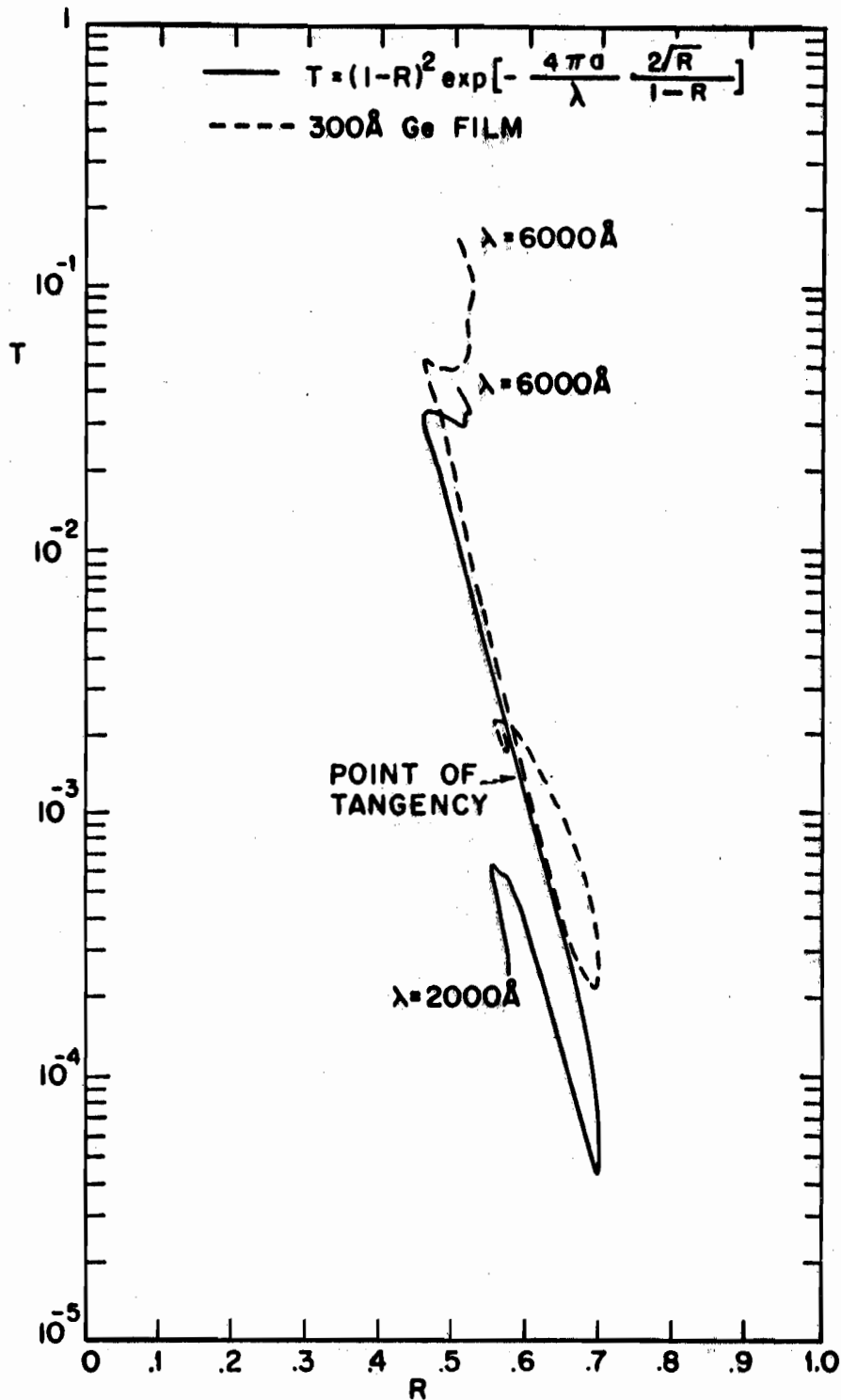


FIG. 3-5 A T VS. R REPRESENTATION USING RELATION (3-12) AND R AND T FOR A 300 Å Ge FILM CALCULATED FROM EQUATIONS (3-9a) AND (3-10).



of the complexity of equations (3-4) and (3-6), the partial derivatives of equation (3-14) must be calculated implicitly. To effect this, we must make use of the machinery of the partial differential calculus, which in turn yields the following set of equations:

$$\frac{\partial n}{\partial R} = \frac{\partial T}{\partial k} / J \quad (3-15a)$$

$$\frac{\partial n}{\partial T} = - \frac{\partial R}{\partial k} / J \quad (3-15b)$$

$$\frac{\partial k}{\partial R} = - \frac{\partial T}{\partial n} / J \quad (3-15c)$$

$$\frac{\partial k}{\partial T} = \frac{\partial R}{\partial n} / J \quad (3-15d)$$

$$\frac{\partial n}{\partial a} = \left(\frac{\partial R}{\partial k} \frac{\partial T}{\partial a} - \frac{\partial R}{\partial a} \frac{\partial T}{\partial k} \right) / J \quad (3-15e)$$

$$\frac{\partial k}{\partial a} = \left(\frac{\partial R}{\partial a} \frac{\partial T}{\partial n} - \frac{\partial R}{\partial n} \frac{\partial T}{\partial a} \right) / J \quad (3-15f)$$

where

$$J = \frac{\partial R}{\partial n} \frac{\partial T}{\partial k} - \frac{\partial R}{\partial k} \frac{\partial T}{\partial n} \quad (3-16)$$

The derivatives on the left-hand side of equations (3-15) will henceforth be referred to as the error derivatives, those on the right-hand side as the explicit derivatives, and J as the Jacobian of the transformation. In searching for the cause of any large increases in the magnitude of the error derivatives that may appear, we can reason physically that since R and T are rather smooth functions of n, k, and a, we may discount the explicit derivatives. This means that large error derivatives will probably be caused by

the vanishing of the Jacobian, and that it is this quantity we should scrutinize. Although the above formalism has been developed primarily for the more intractable film formulas, it will be instructive to examine briefly the explicit derivatives and the Jacobian for equations (3-9a) and (3-10) which are:

$$\frac{\partial R}{\partial n} = 4(n^2 - k^2 - 1)/[(1+n)^2 + k^2]^2 \quad (3-17a)$$

$$\frac{\partial R}{\partial k} = 8nk/[(1+n)^2 + k^2]^2 \quad (3-17b)$$

$$\frac{\partial T}{\partial n} = -32 e^{-\alpha a} n^2 (n^2 - k^2 - 1)/[(1+n)^2 + k^2]^3 \quad (3-17c)$$

$$\frac{\partial T}{\partial k} = -64 e^{-\alpha a} n^2 \left[k + \frac{\pi a}{\lambda} [(1+n)^2 + k^2] \right] / [(1+n)^2 + k^2]^3 \quad (3-17d)$$

$$\frac{\partial R}{\partial a} = 0 \quad (3-17e)$$

$$\frac{\partial T}{\partial a} = - \frac{64\pi n^2 k}{\lambda} e^{-\alpha a} / [(1+n)^2 + k^2]^2 \quad (3-17f)$$

$$J = - \frac{256\pi a}{\lambda} e^{-\alpha a} n^2 (n^2 - k^2 - 1) / [(1+n)^2 + k^2]^4 \quad (3-17g)$$

The corresponding error derivatives are:

$$\frac{\partial n}{\partial R} = \frac{\lambda k}{\pi a} + [(1+n)^2 + k^2] [(1+n)^2 + k^2] / 4(n^2 - k^2 - 1) \quad (3-18a)$$

$$\frac{\partial n}{\partial T} = \frac{\lambda k}{\pi a} [(1+n)^2 + k^2]^2 e^{\alpha a} / 32n(n^2 - k^2 - 1) \quad (3-18b)$$

$$\frac{\partial k}{\partial R} = - \frac{\lambda}{8\pi n a} [(1+n)^2 + k^2] = - \frac{\lambda}{2\pi a(1-R)} \quad (3-18c)$$

$$\frac{\partial k}{\partial T} = - \frac{\lambda}{64\pi n^2 a} [(1+n)^2 + k^2]^2 e^{\alpha a} = - \frac{\lambda}{4\pi a T} \quad (3-18d)$$

$$\frac{\partial n}{\partial a} = 2nk^2/a(n^2 - k^2 - 1) \quad (3-18e)$$

$$\frac{\partial k}{\partial a} = -\frac{k}{a} \quad (3-18f)$$

We see that the Jacobian (3-17g) vanishes for $n^2 = k^2 + 1$ and causes singularities in the error derivatives $\frac{\partial n}{\partial R}$, $\frac{\partial n}{\partial T}$, and $\frac{\partial n}{\partial a}$. The error derivatives $\frac{\partial k}{\partial R}$, $\frac{\partial k}{\partial T}$, and $\frac{\partial k}{\partial a}$ remain unaffected due to the cancellation of the term causing the singularity. The fact that this is so is directly related to the observation in equation (3-11) that near $n^2 = k^2 + 1$ trouble develops only in n and not k ; however, when one considers a more complex model such as represented by equations (3-4) and (3-6) this may no longer remain true.

Before proceeding further, we will make some general comments concerning the geometrical interpretation of the Jacobian. Let us begin by writing equations (3-6) in the form:

$$R(n, k) - R = 0 \quad (3-19a)$$

$$T(n, k) - T = 0 \quad (3-19b)$$

where R and T are the experimentally determined quantities. It is obvious that not all pairs of n and k are going to satisfy equations (3-19); however, considering each equation by itself, it is apparent that there is a series of pairs for each one separately which can be found by solving each for n as a function of k . That is, we have in principle for (3-19a) the one equation:

$$n = n_R(k) \quad (3-20a)$$

and for (3-19b) another:

$$n = n_T(k) . \quad (3-20b)$$

Equations (3-20) are curves in the $n - k$ plane, and the points at which they intersect are the simultaneous solutions to equations (3-19). The equations (3-20) will be called the root-locus equations. The root-locus of equation (3-9a) is a circle of radius $2\sqrt{R}/(1-R)$ and center at $n = (1+R)/(1-R)$, $k = 0$. On the other hand, the root-locus of equation (3-9b) or (3-10) has no simple form. However, if the absorption is high enough, n has roughly a decaying exponential dependence on k . Let us now recall that the magnitude of the vector product of two unit vectors is equal to the sine of the angle between them. Applying this fact to equations (3-19), we obtain:

$$\sin \theta_{RT} = \frac{|\nabla R \times \nabla T|}{|\nabla R| |\nabla T|} = \frac{J}{\left(\left[\left(\frac{\partial R}{\partial n} \right)^2 + \left(\frac{\partial R}{\partial k} \right)^2 \right] \left[\left(\frac{\partial T}{\partial n} \right)^2 + \left(\frac{\partial T}{\partial k} \right)^2 \right] \right)^{\frac{1}{2}}} . \quad (3-21)$$

Thus we see that when $J = 0$, $\theta_{RT} = 0$, or that curve (3-20a) ceases to intersect curve (3-20b). Instead, the two curves become tangent to each other thus leading to a highly unstable condition with regard to the dependence of the derived n and k on the experimental errors in R and T . If the errors are such as to prevent any intersection or tangency at all, then we have no real roots. This is

the analogy for the general case to the special case of equations (3-9a) and (3-10) when the discriminant of (3-11b) becomes negative.

In Figs. 3-6, 3-7, 3-8, and 3-9 are depicted the root-locus diagrams for germanium films on CaF_2 substrates for thicknesses of 50 \AA , 150 \AA , 300 \AA , and 500 \AA , respectively. Three representative wavelengths, namely, 2500 \AA , 3000 \AA , and 5500 \AA , are plotted for each thickness with the exception of the 300 \AA case where 3900 \AA is given also. These curves were calculated using the data from references 1 and 2 and Figs. 3-3 and 3-4 in addition to equations (3-4) and (3-6). We note immediately that there is in general more than one simultaneous solution to equations (3-20), in fact, because of interference effects the actual number is indeterminate. However, we observe that all but one solution changes with thickness at a given wavelength. This solution is obviously the physical one and is the one given by the dispersion relations also. We see that for the most part the curves of equations (3-20) have the same qualitative behavior predicted by our analysis above for the simpler cases except for the fact that $n_R(k)$ has multiple "loops" due to the effect of phase interference. Quite outstanding, however, and also mildly surprising is the observation that near $\lambda = 3000\text{ \AA}$ for all thicknesses one finds $n_R(k)$ almost tangent to $n_T(k)$, and it is easy to see that small variations in the measurement of R and T can lead to large variations in n and k, especially n. This is

just what is predicted by the simpler model, even though $n^2 = k^2 + 1$ violates one of the assumptions of its derivation. On the other hand, that interference is not entirely without its effects is demonstrated by the 300Å film for $\lambda = 3900\text{Å}$. Here we have a condition of near tangency for $n^2 \neq k^2 + 1$.

Figures 3-10, 3-11, and 3-12 present θ_{RT} and the magnitude of the error derivatives as functions of wavelength for the four thicknesses mentioned above. These figures confirm in detail our previous discussion on the root-locus diagrams. In addition, we see that for short wavelengths the behavior is fairly independent of thickness, except for the 300Å case where the error derivative singularity is shifted to longer wavelengths. At these longer wavelengths, the effects of interference become more apparent. Note that for the complex model of equations (3-4) and (3-6), singularities can appear in all the error derivatives.

In order to gain some feeling for the wavelength ranges over which reasonable experimental errors in R, T, and θ would lead to, unreasonable errors in n and k the bar diagrams Figs. 3-13, 3-14, and 3-15 were constructed. The choice of a "reasonable experimental error" is somewhat arbitrary. However, one can generally conclude that an absolute error in n and k of no greater than .5 is necessary if one is to approach the accuracy of the dispersion analysis. For

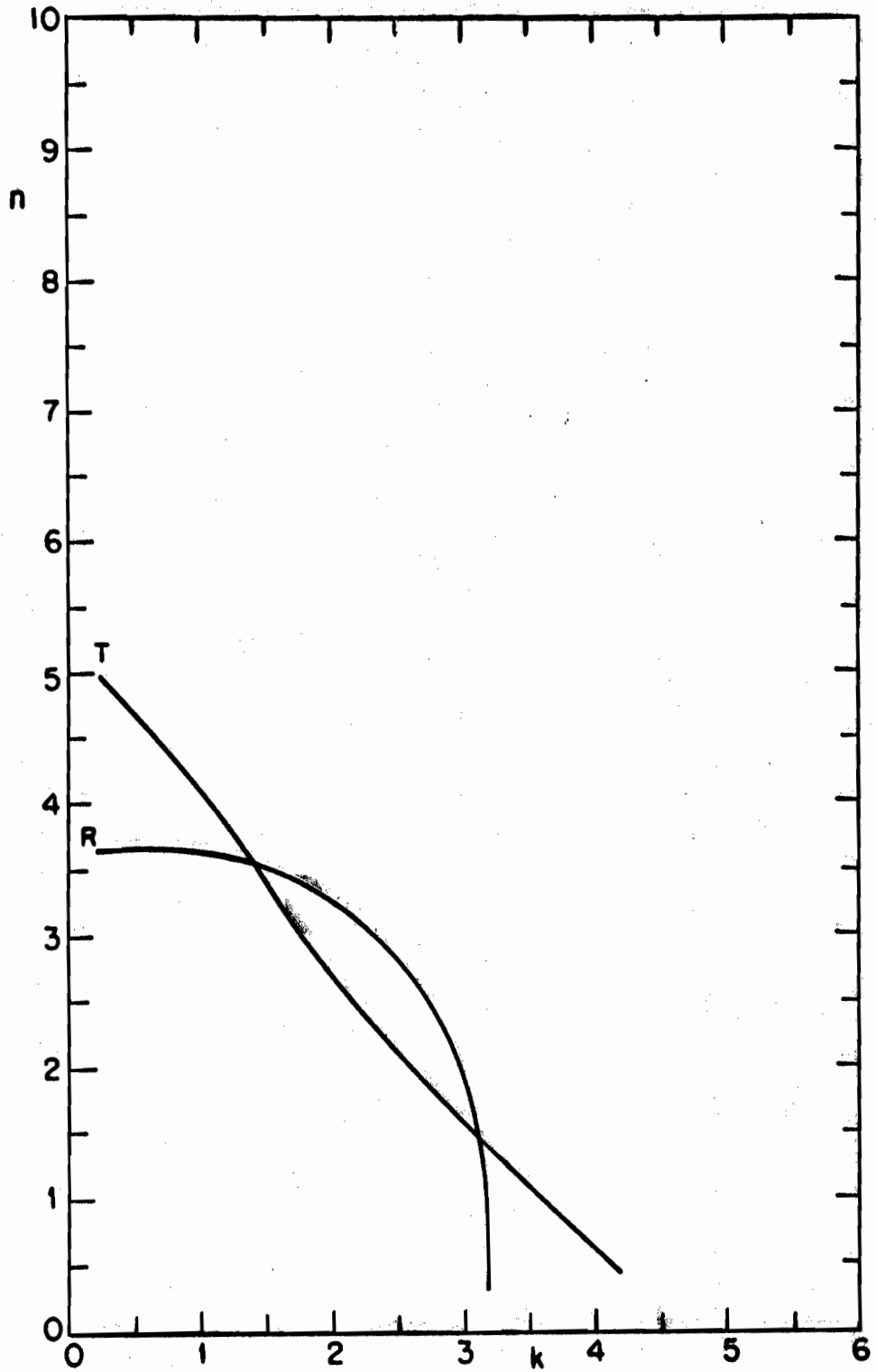


FIG. 3-6a THE ROOT-LOCUS DIAGRAM FOR THE R-T MODEL OF A 50Å Ge FILM ON CoF₂. $\lambda = 2500\text{\AA}$.

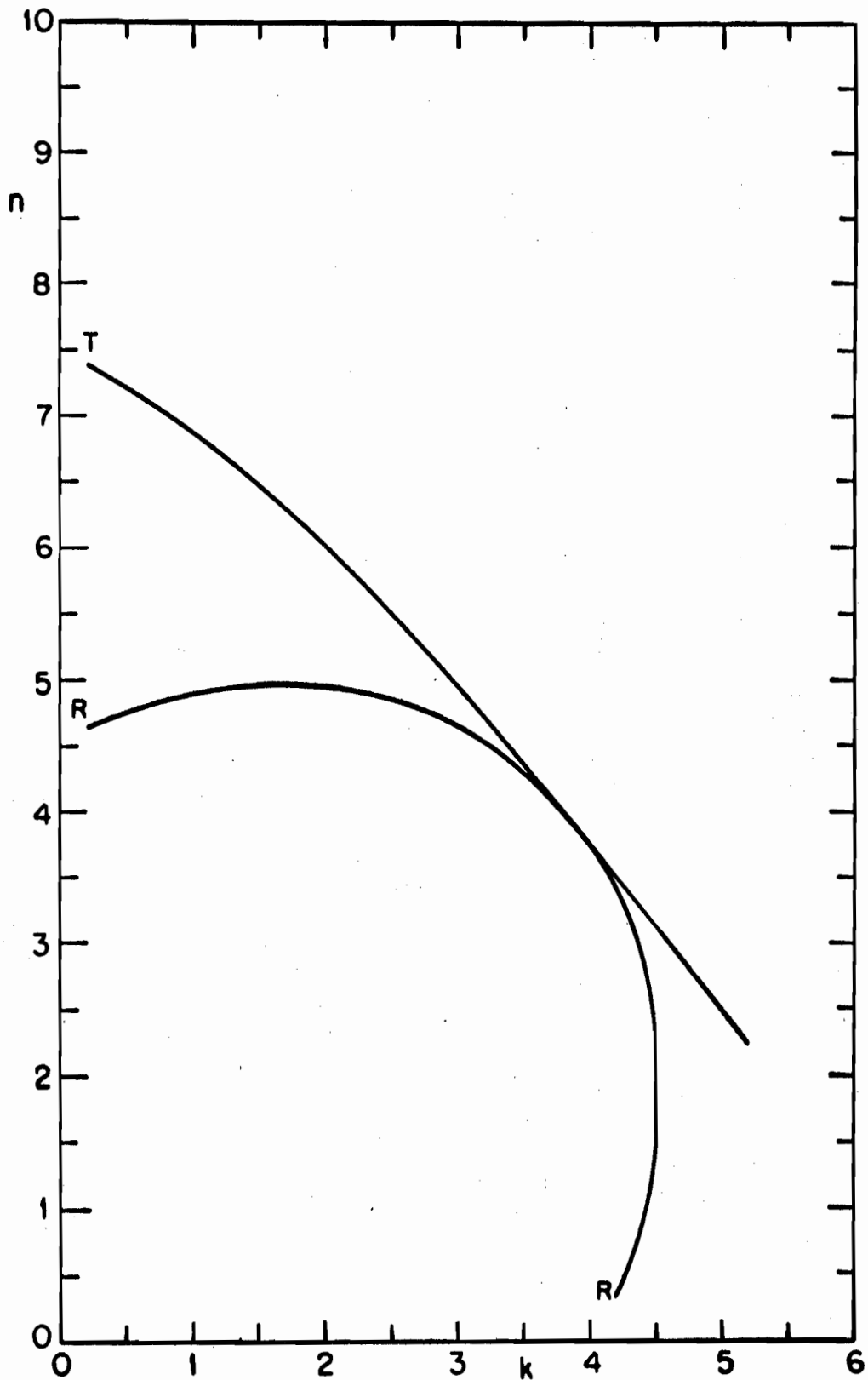


FIG. 3-6b $\lambda = 3000\text{\AA}$, $\sigma = 50\text{\AA}$.

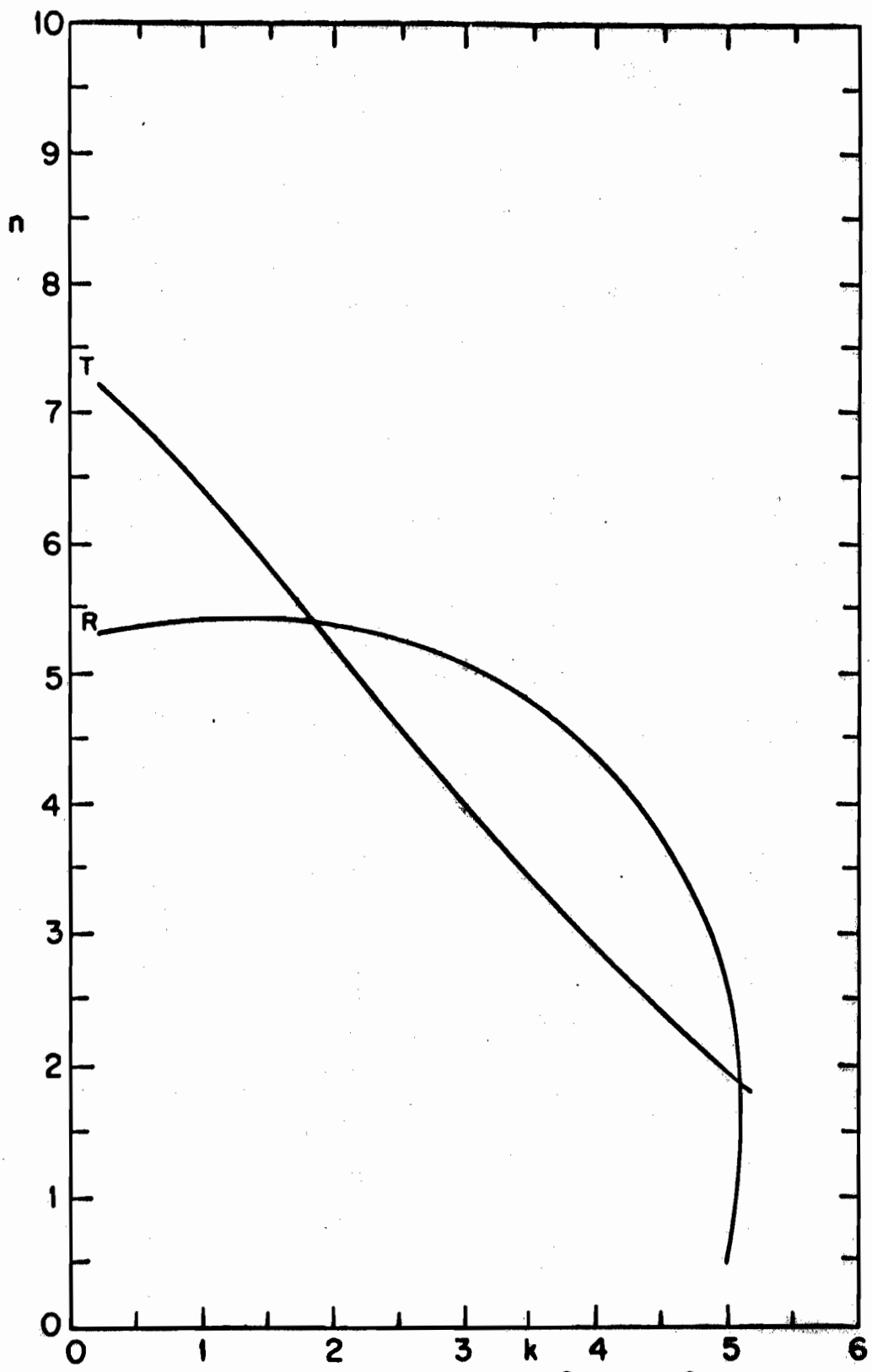


FIG. 3-6c $\lambda = 5500\text{\AA}$, $a = 50\text{\AA}$.

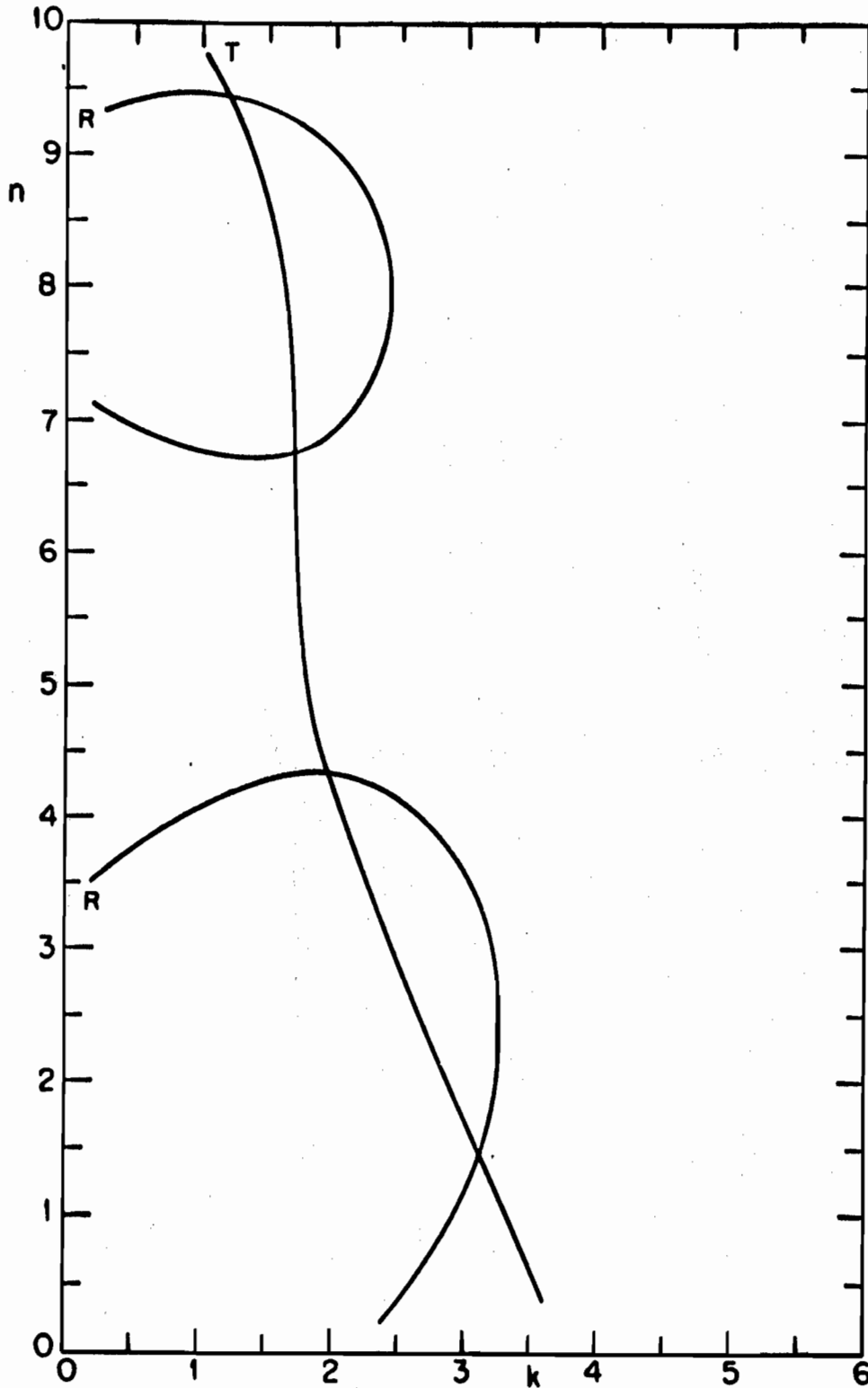


FIG. 3-70 THE ROOT-LOCUS DIAGRAM FOR THE R-T MODEL OF A 150 Å Ge FILM ON CoF₂. $\lambda = 2500 \text{ \AA}$.

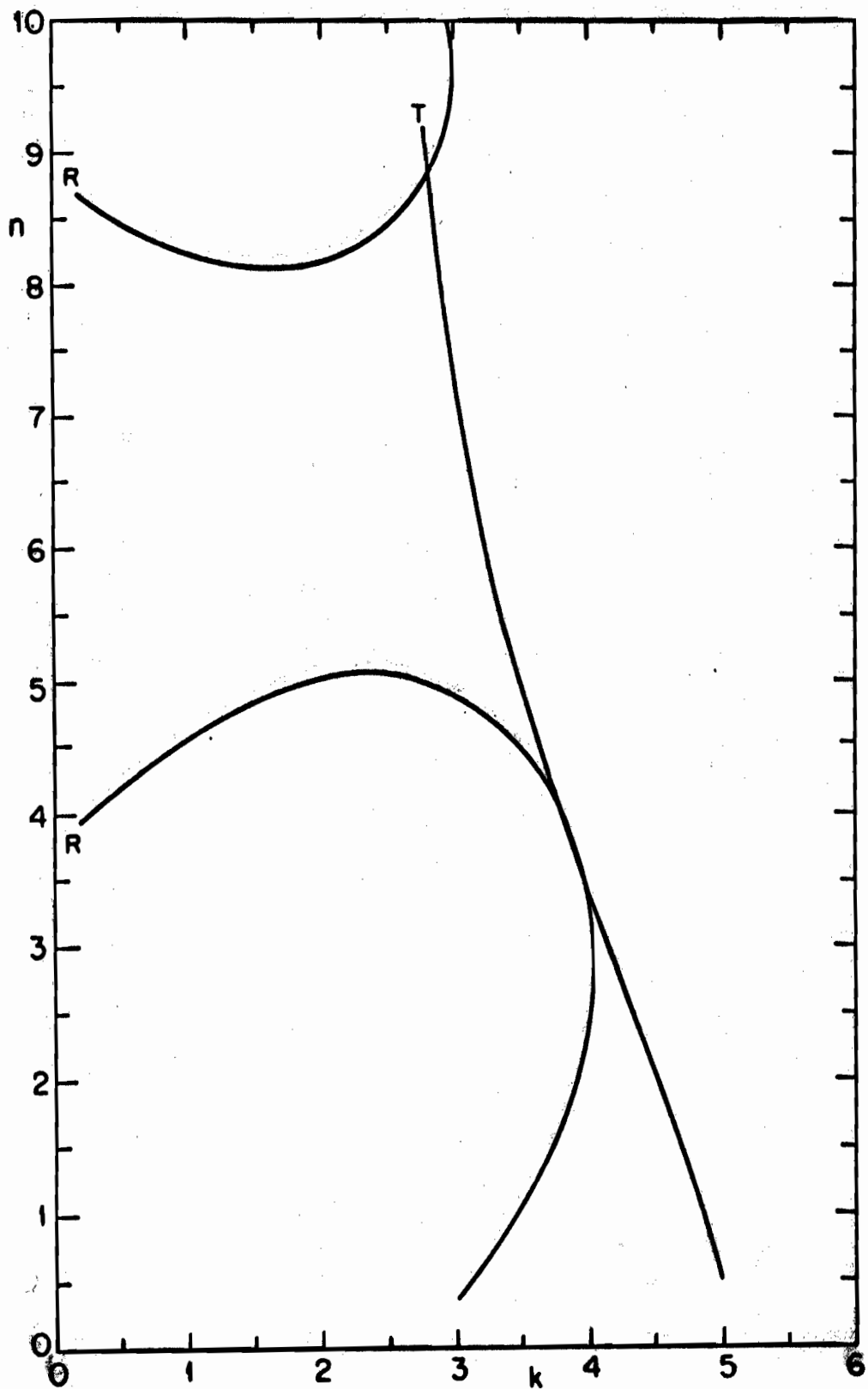


FIG. 3-7b $\lambda = 3000\text{\AA}$, $\sigma = 150\text{\AA}$.

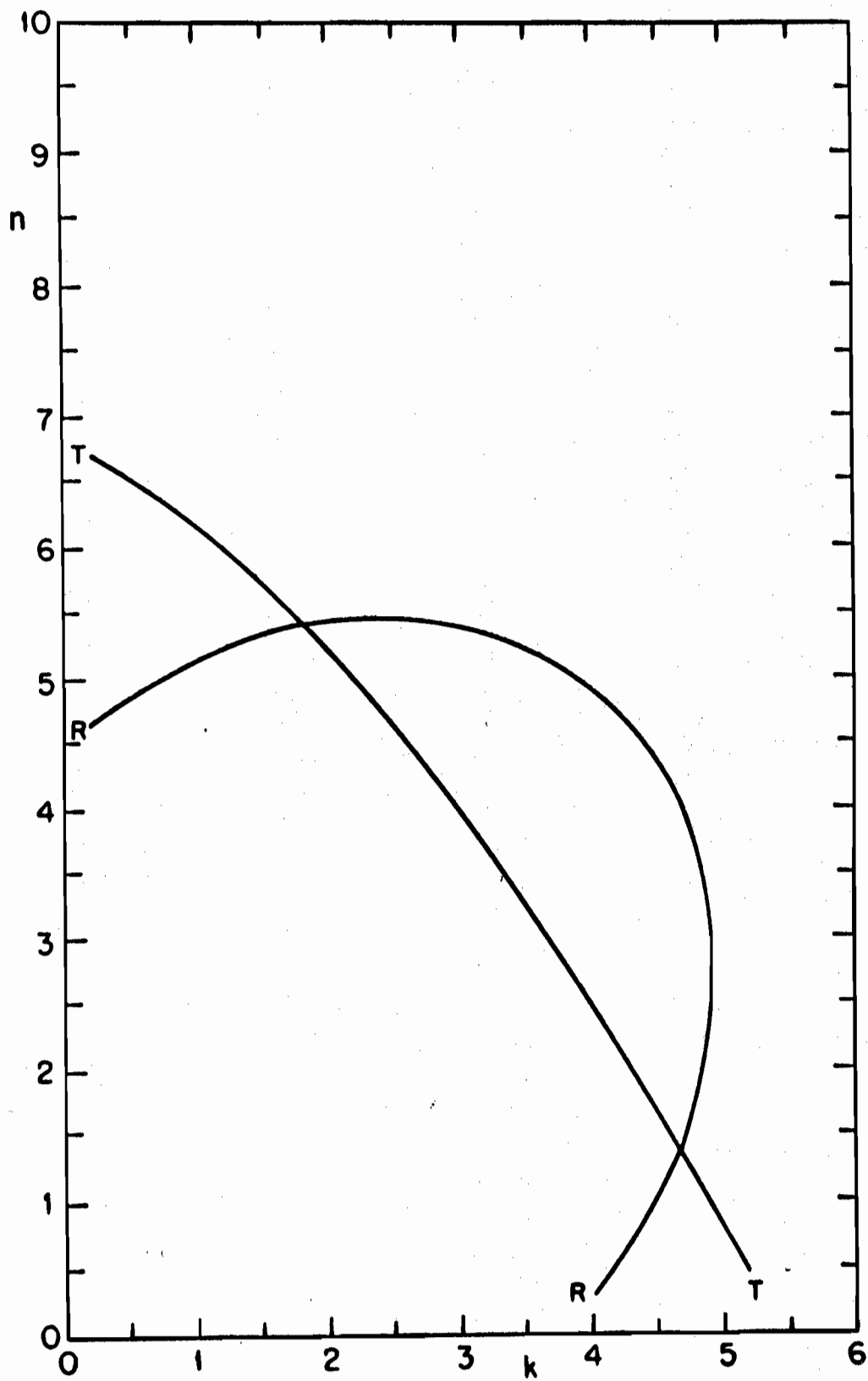


FIG. 3-7c $\lambda = 5500\text{\AA}$, $a = 150\text{\AA}$.

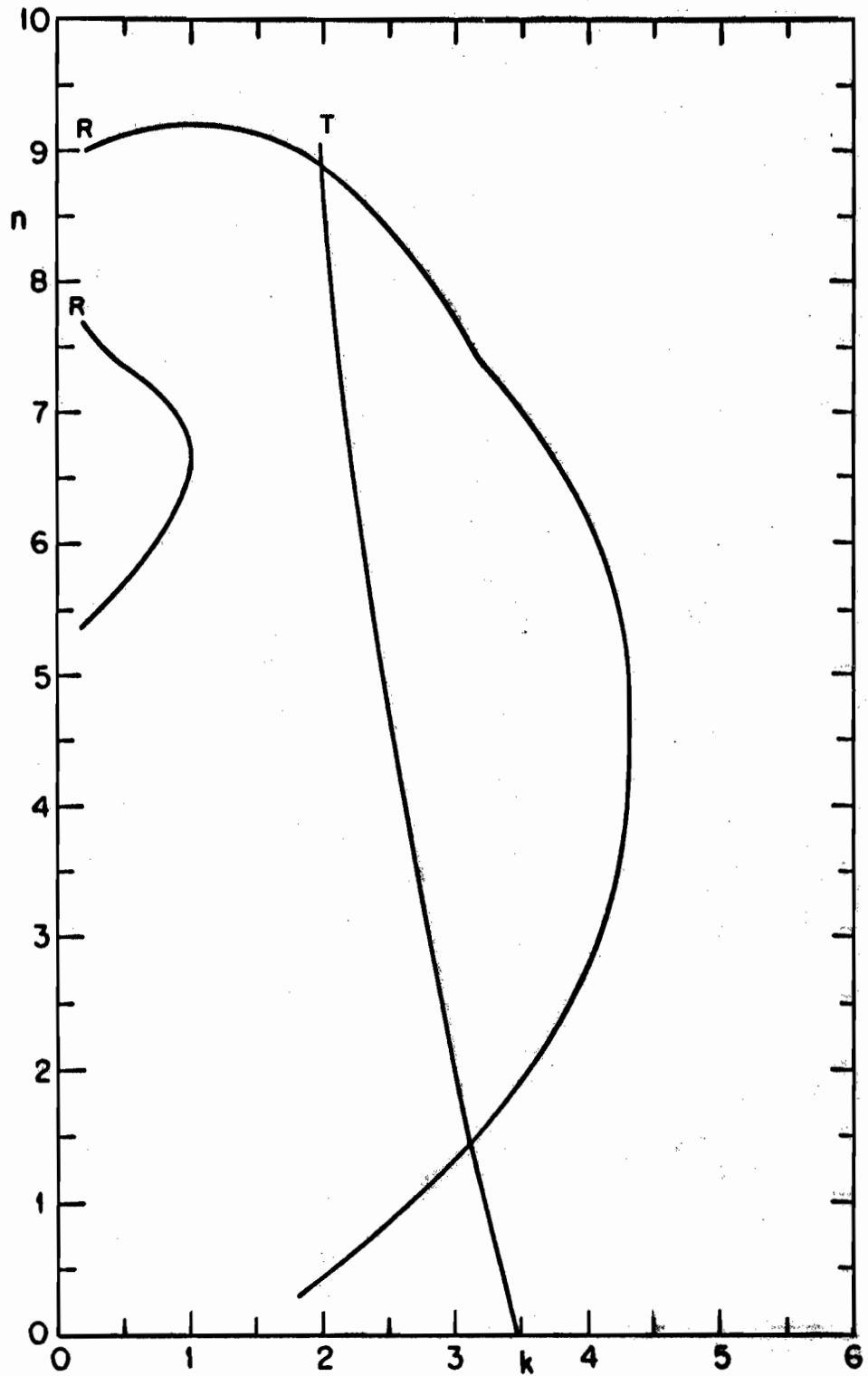


FIG. 3-80 THE ROOT-LOCUS DIAGRAM FOR THE R-T MODEL OF A 300 Å Ge FILM ON CaF₂. $\lambda = 2500 \text{ Å}$.

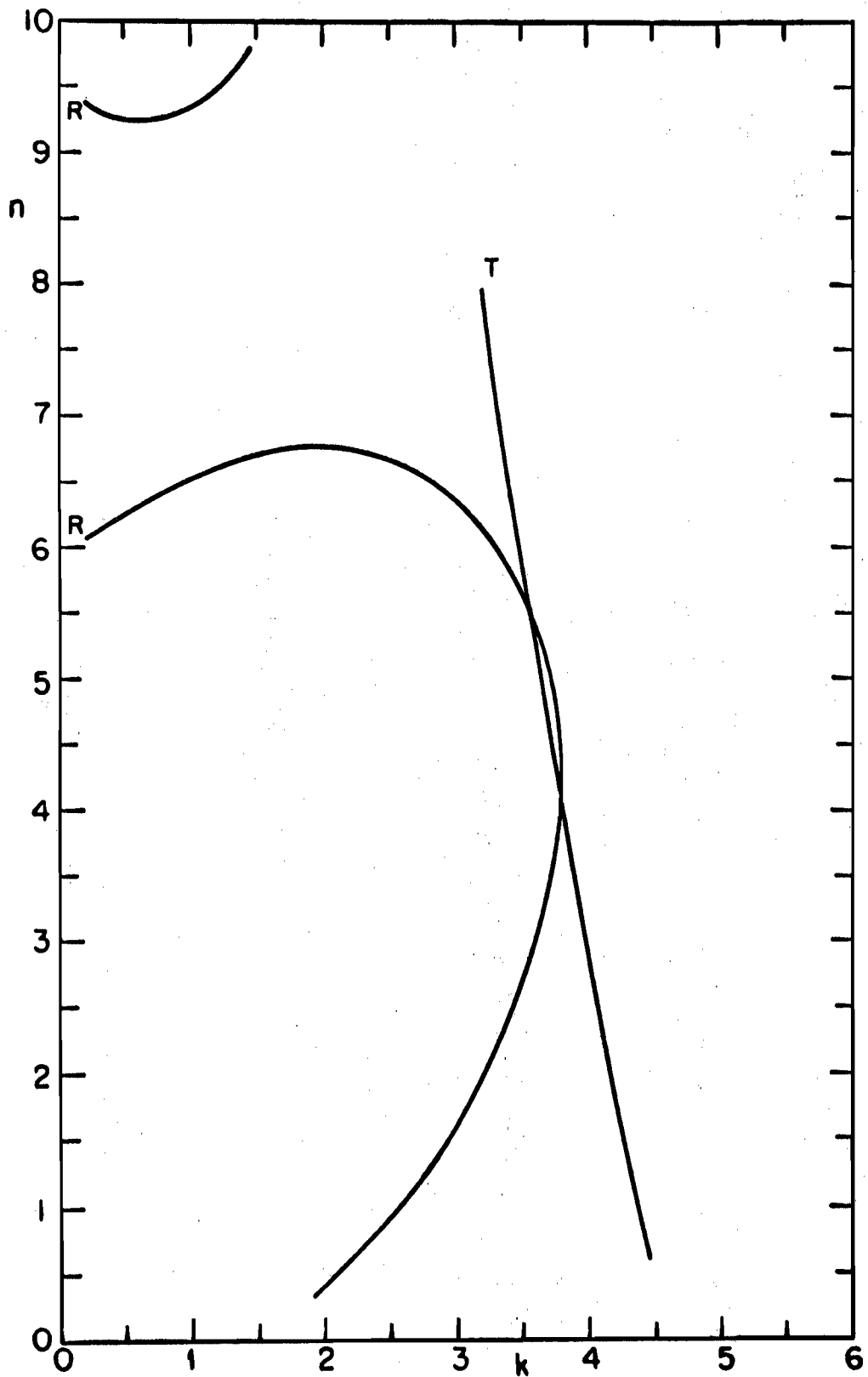


FIG. 3-8b $\lambda = 3000\text{\AA}$, $a = 300\text{\AA}$.

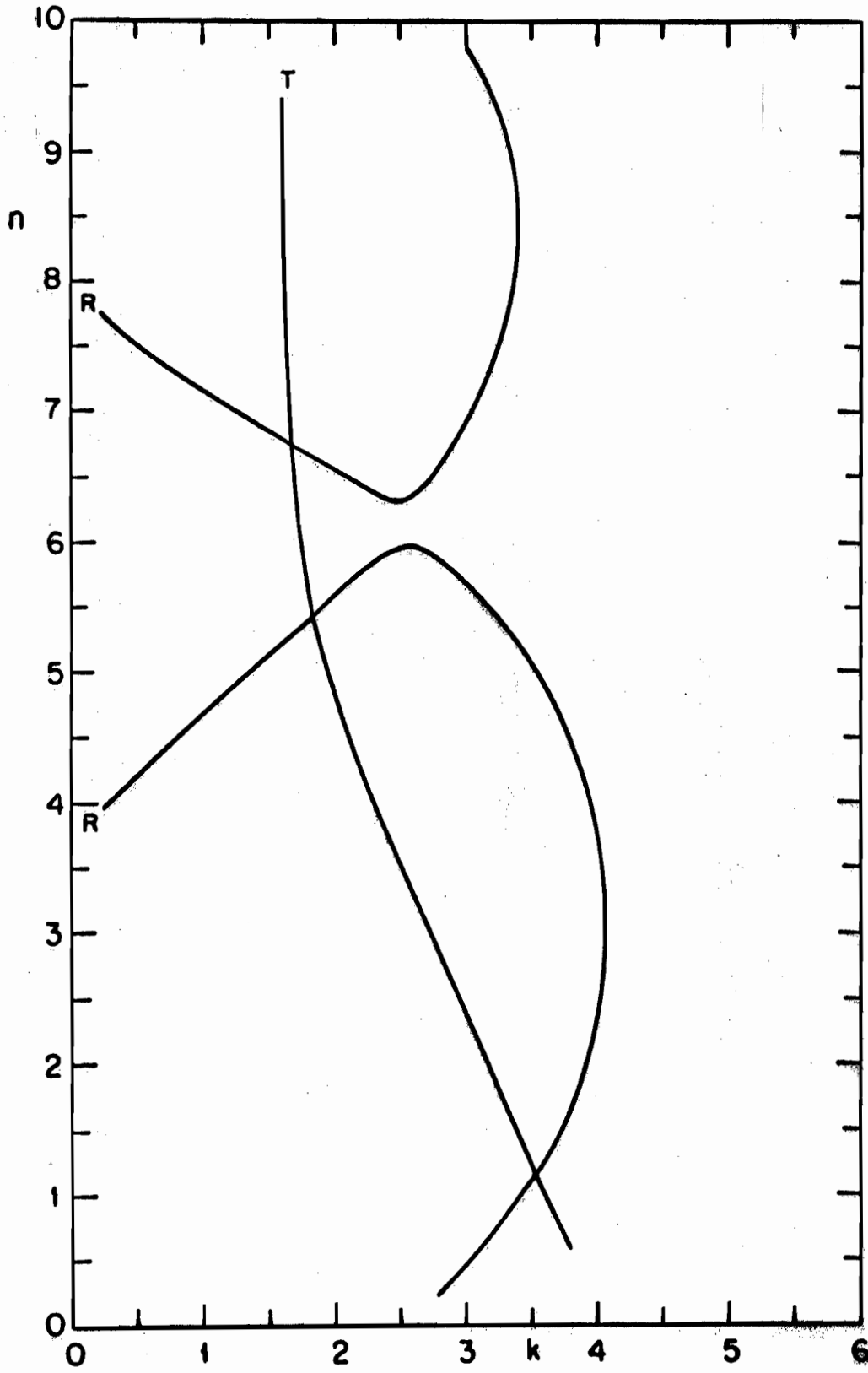


FIG. 3-8c $\lambda = 5500\text{\AA}$, $\sigma = 300\text{\AA}$.

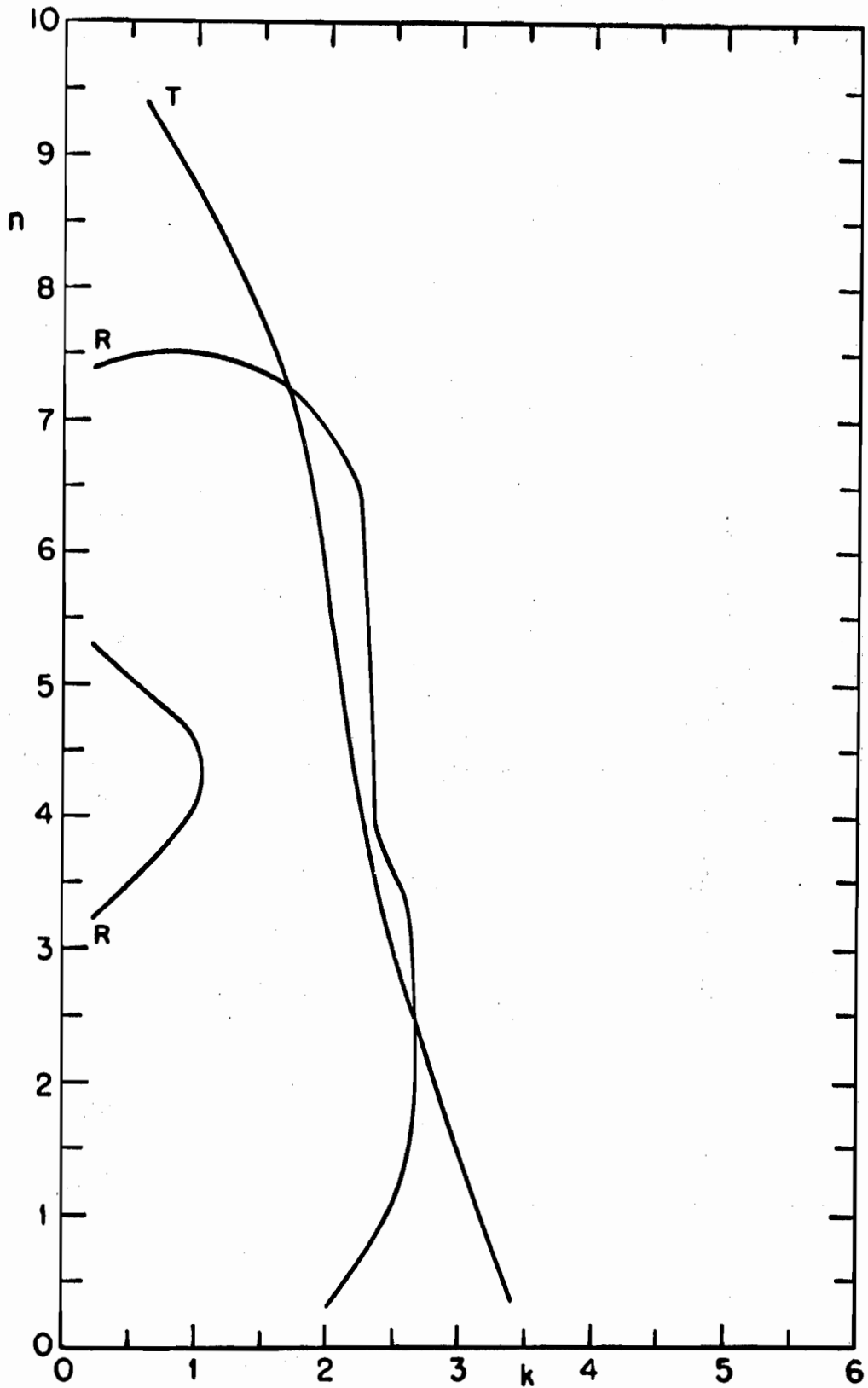


FIG. 3-8d $\lambda = 3900\text{\AA}$, $a = 300\text{\AA}$.

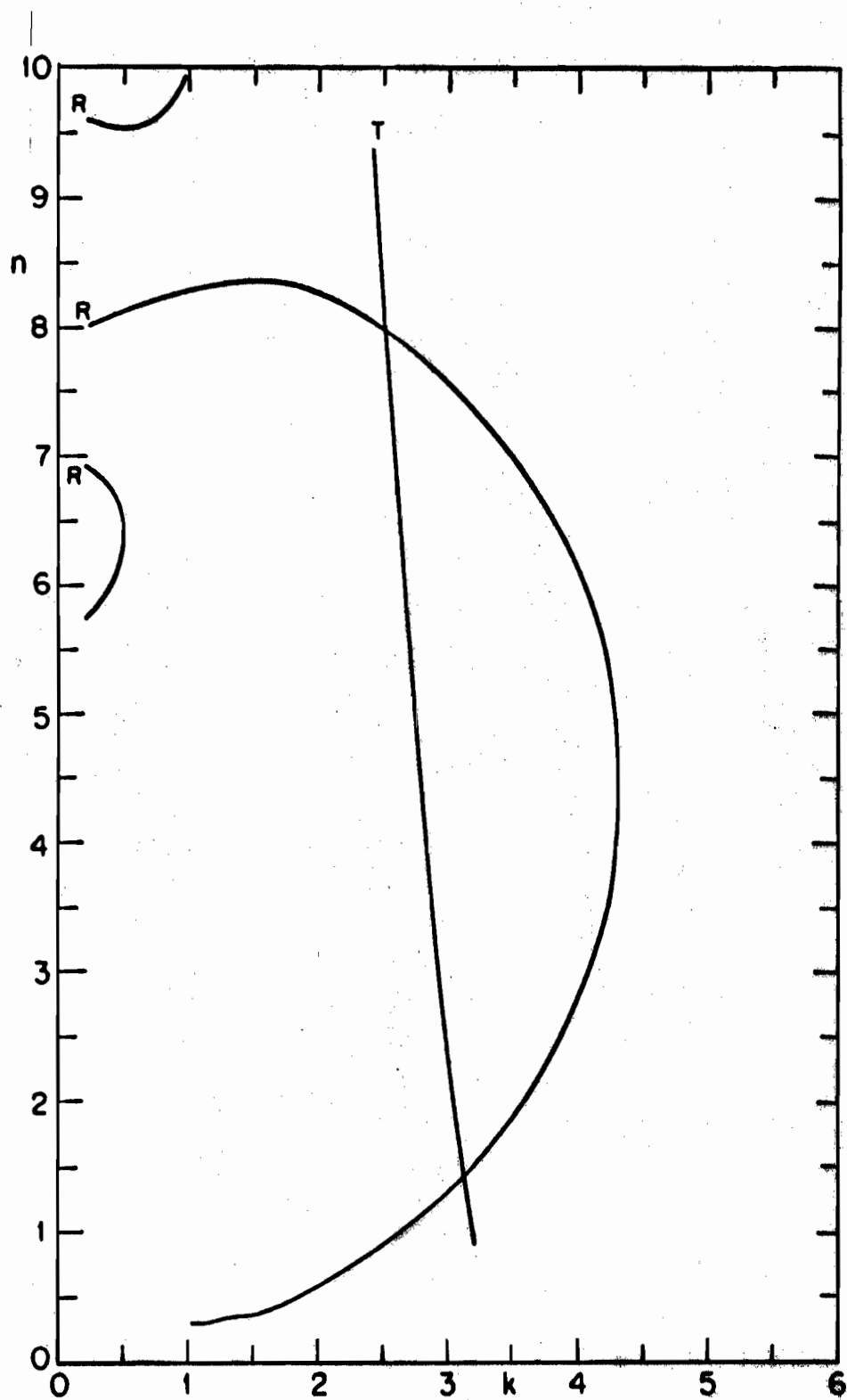


FIG. 3-9a THE ROOT-LOCUS DIAGRAM FOR THE R-T MODEL OF A 500Å Ge FILM ON CoF₂. $\lambda = 2500\text{\AA}$.

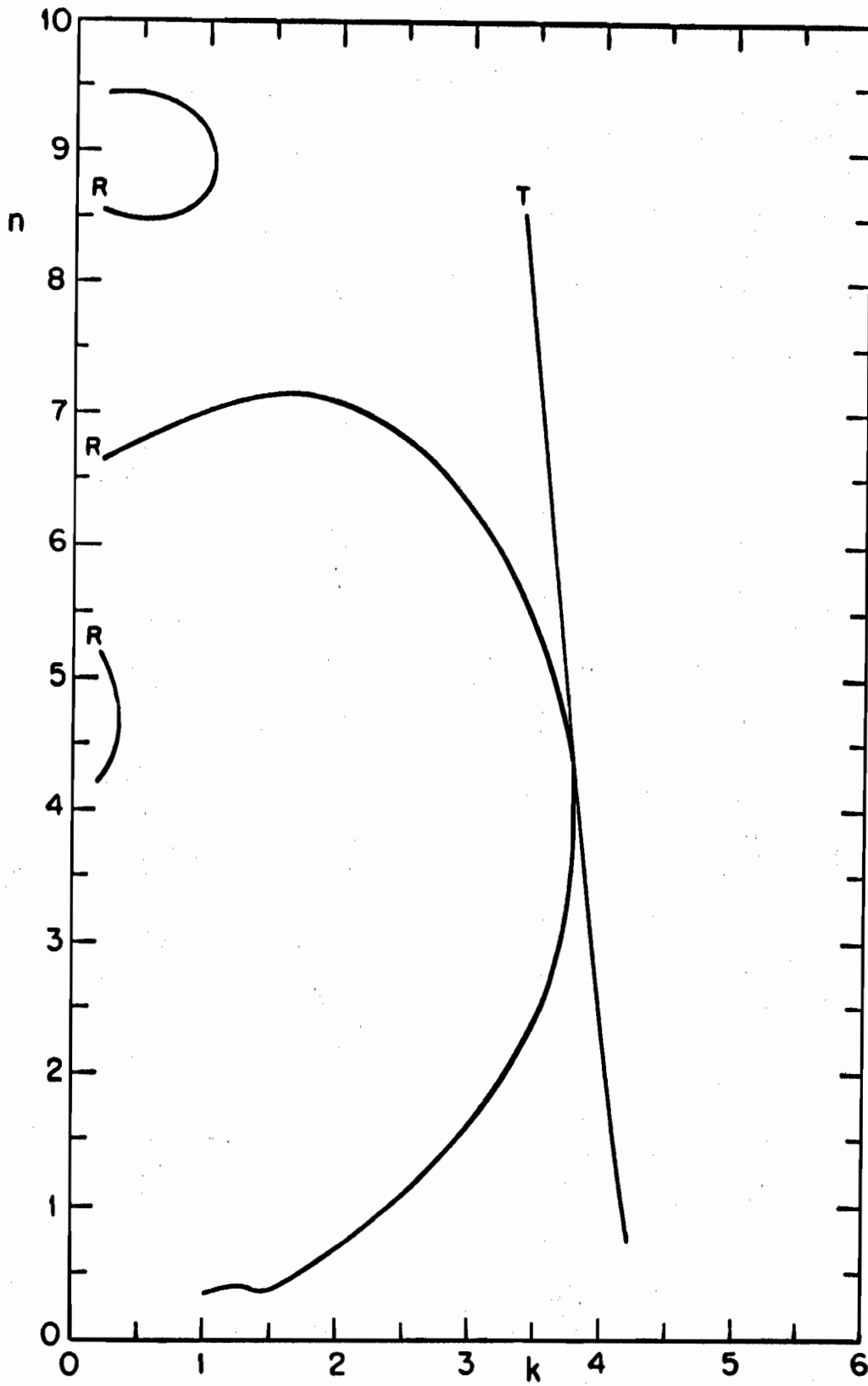


FIG. 3-9b $\lambda = 3000\text{\AA}$, $\sigma = 500\text{\AA}$.

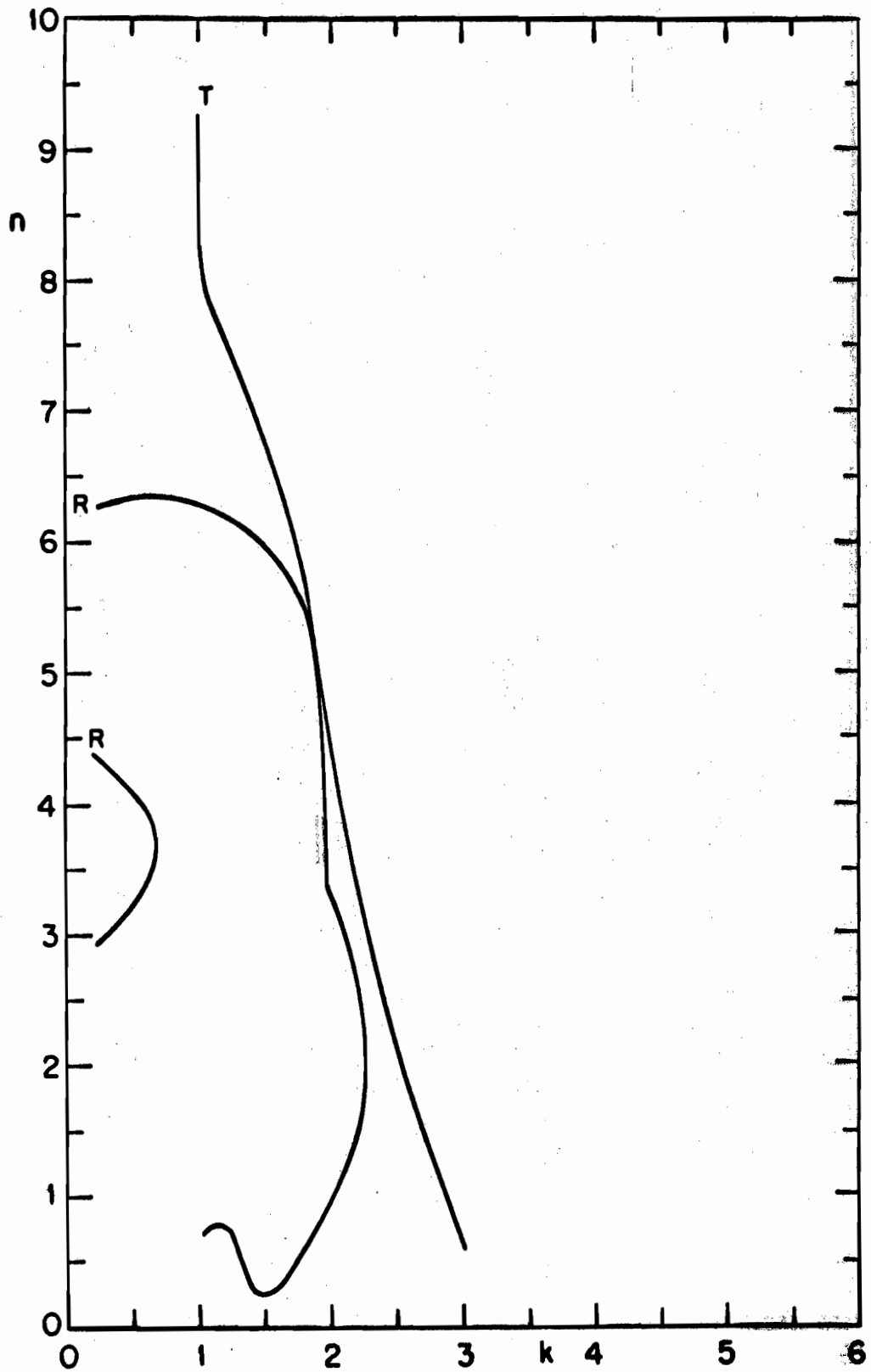


FIG. 3-9c $\lambda = 5500\text{\AA}$, $\sigma = 500\text{\AA}$.

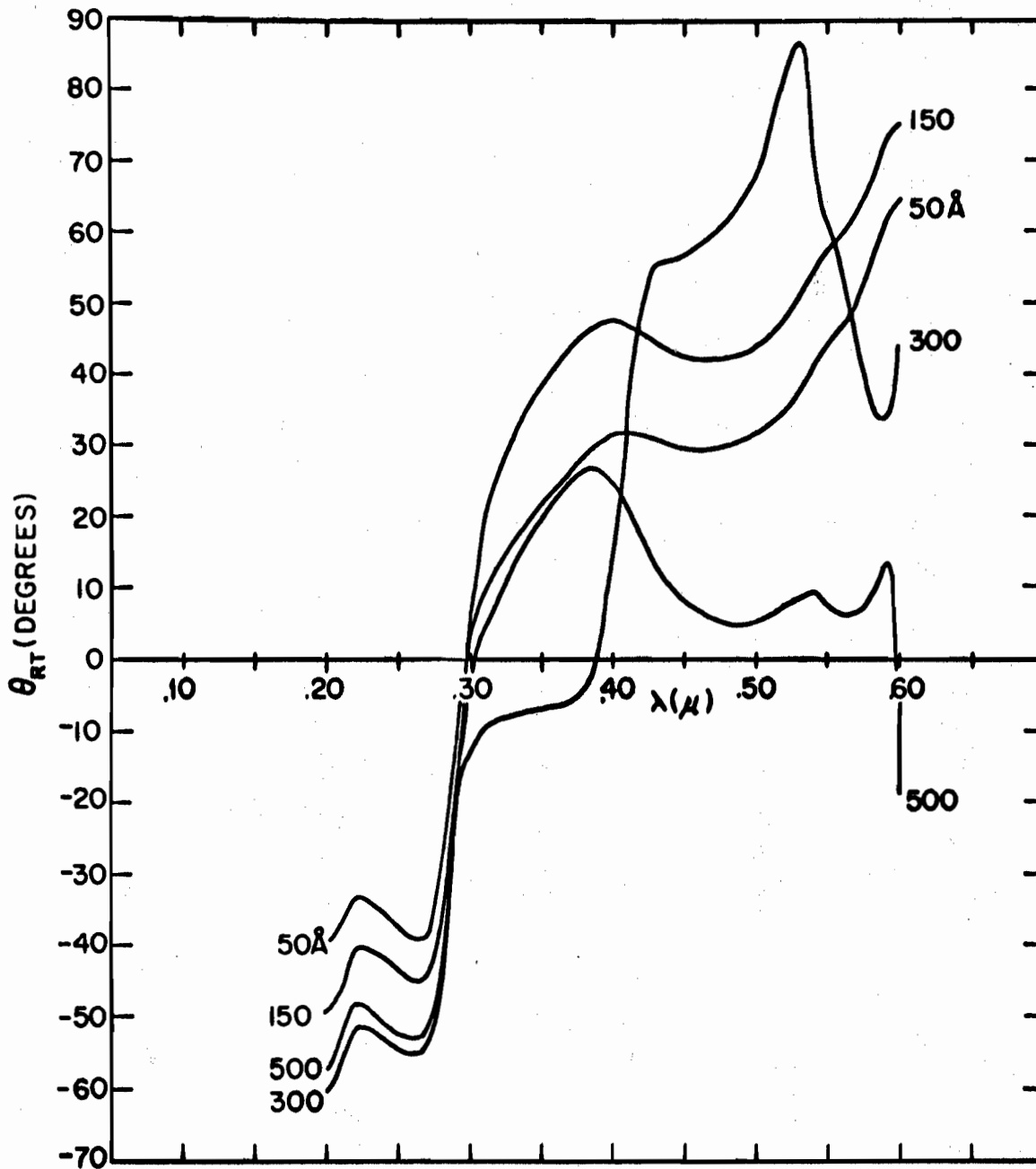


FIG. 3-10 THE ANGLE OF ROOT-LOCUS INTERSECTIONS, θ_{RT} , VS. λ FOR THE R-T MODEL OF A Ge FILM ON CaF_2 . FILM THICKNESS IS INDICATED ON EACH CURVE.

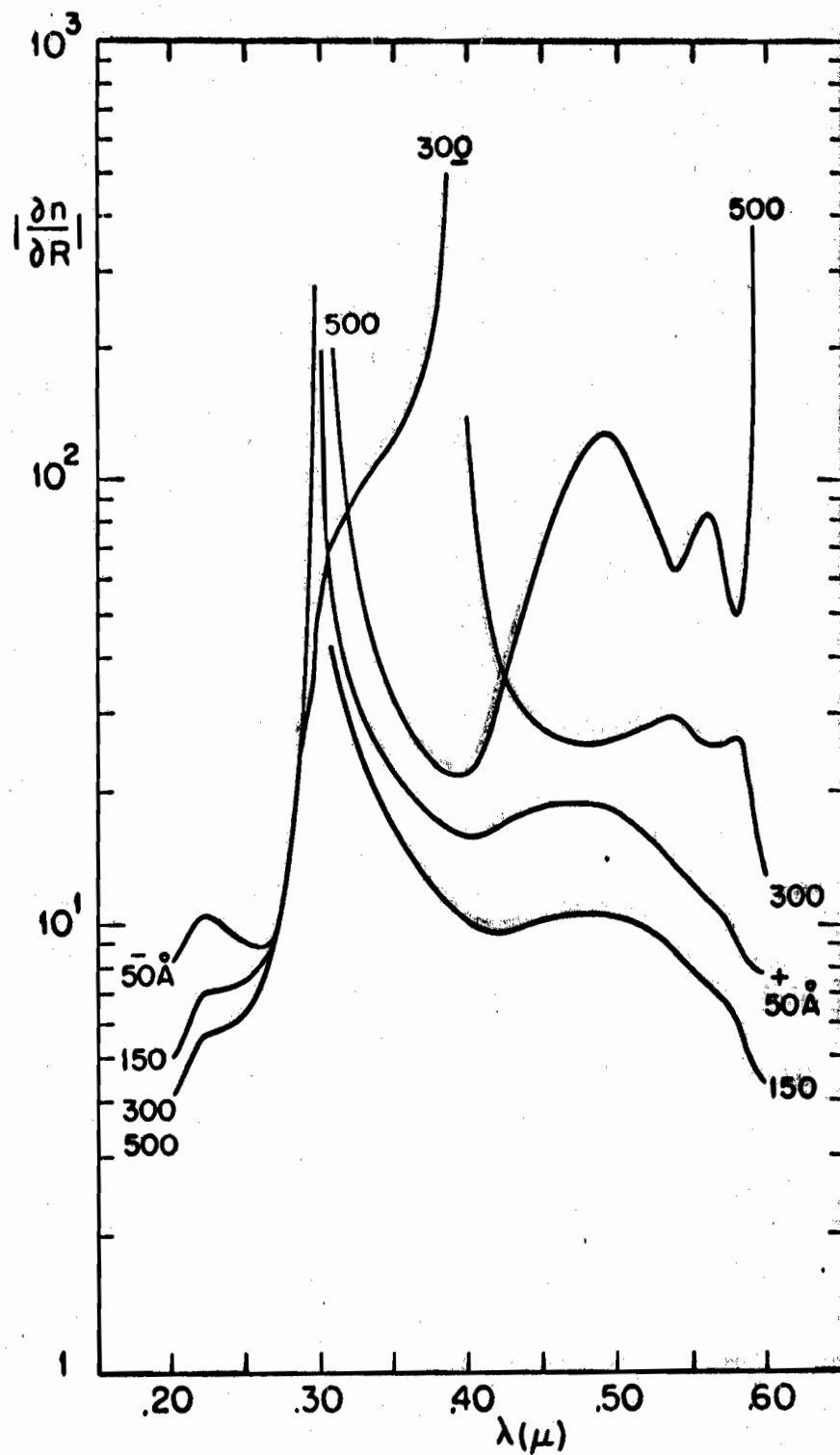


FIG. 3-110 THE INDEX OF REFRACTION ERROR DERIVATIVES VS. λ FOR THE R-T MODEL OF A Ge FILM ON CoF_2 .
 $\alpha. |\frac{\partial n}{\partial R}|$

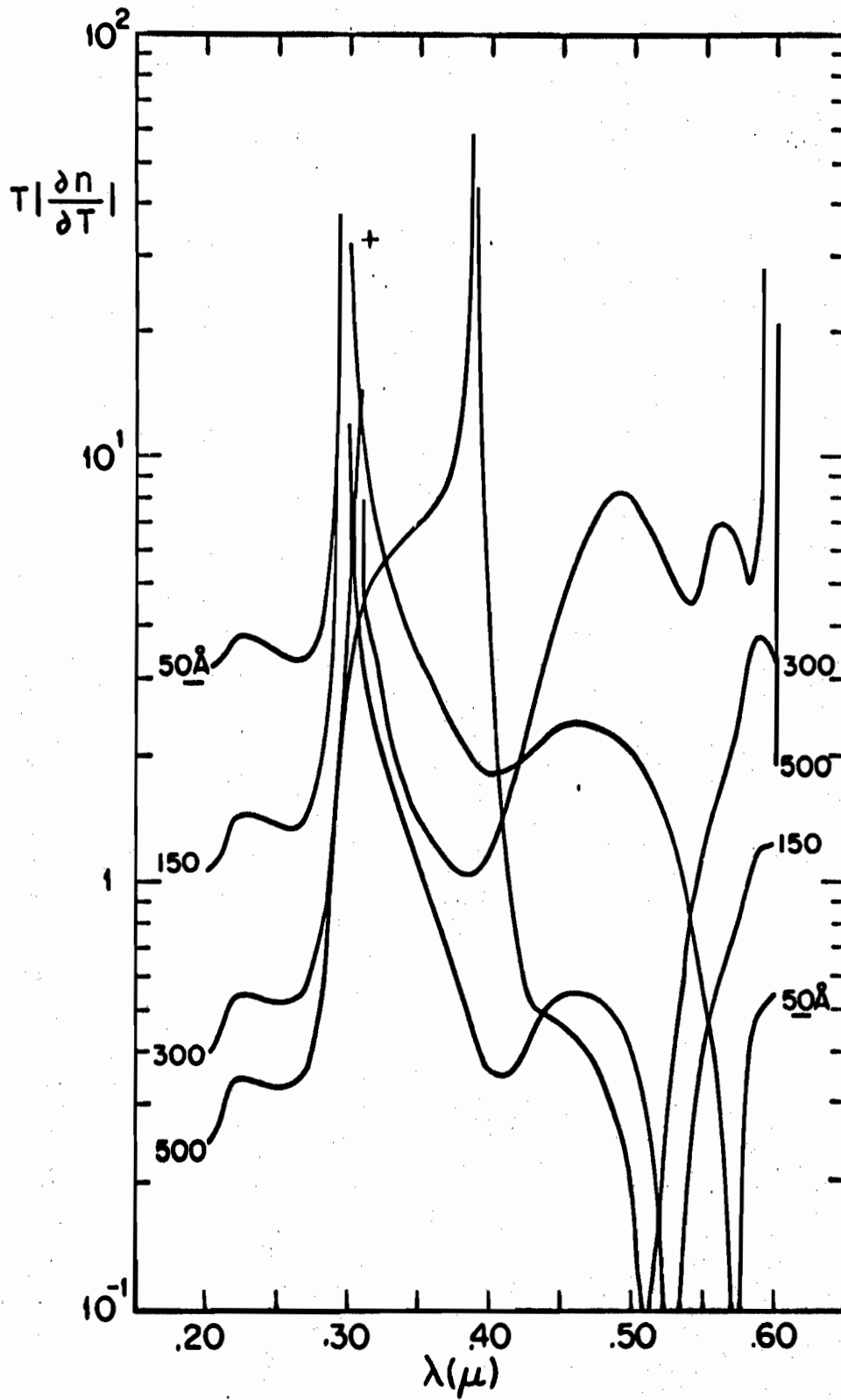


FIG. 3-11b $T \left| \frac{\partial n}{\partial T} \right|$.

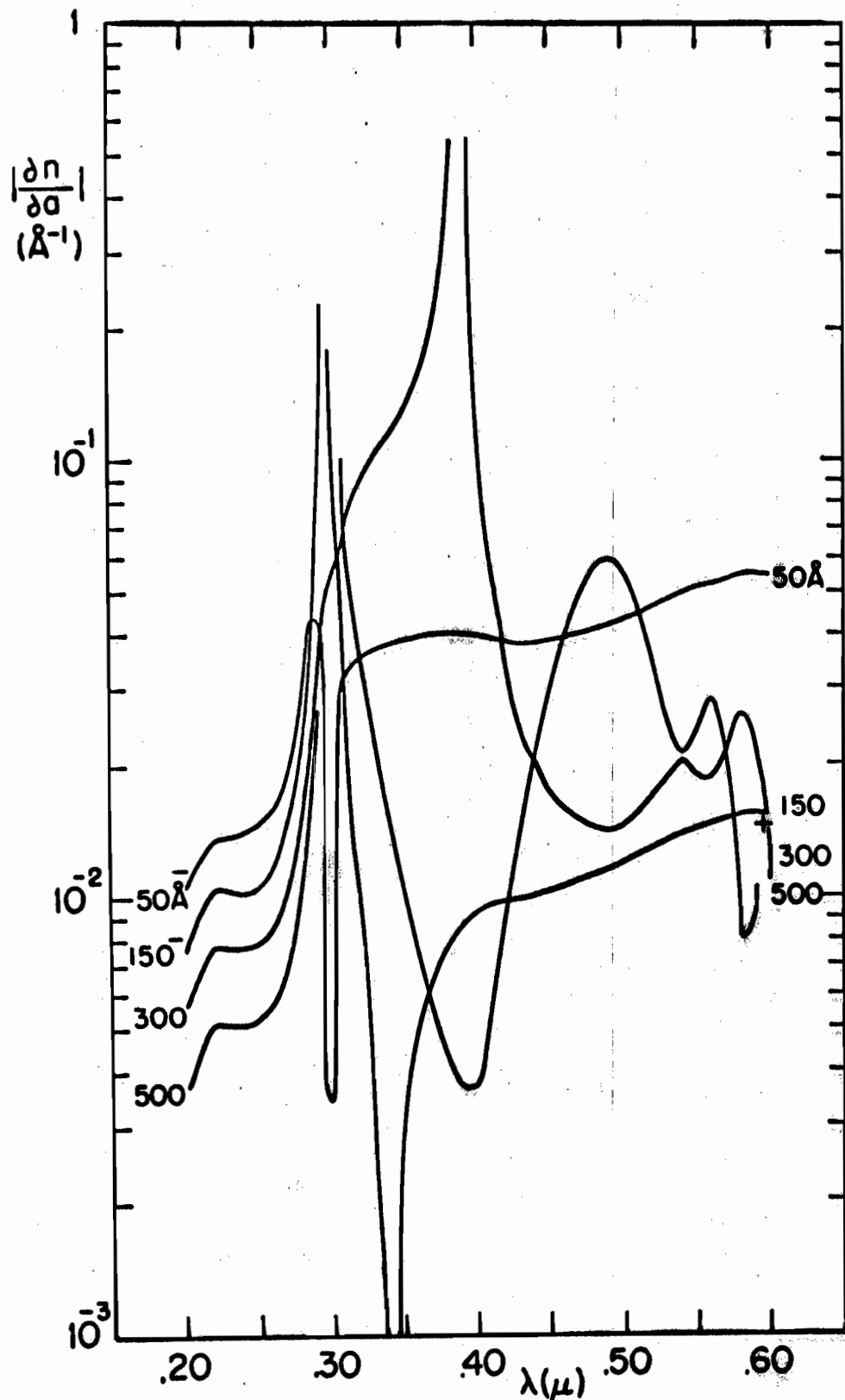


FIG. 3-11c $|\frac{\partial n}{\partial \alpha}|$.

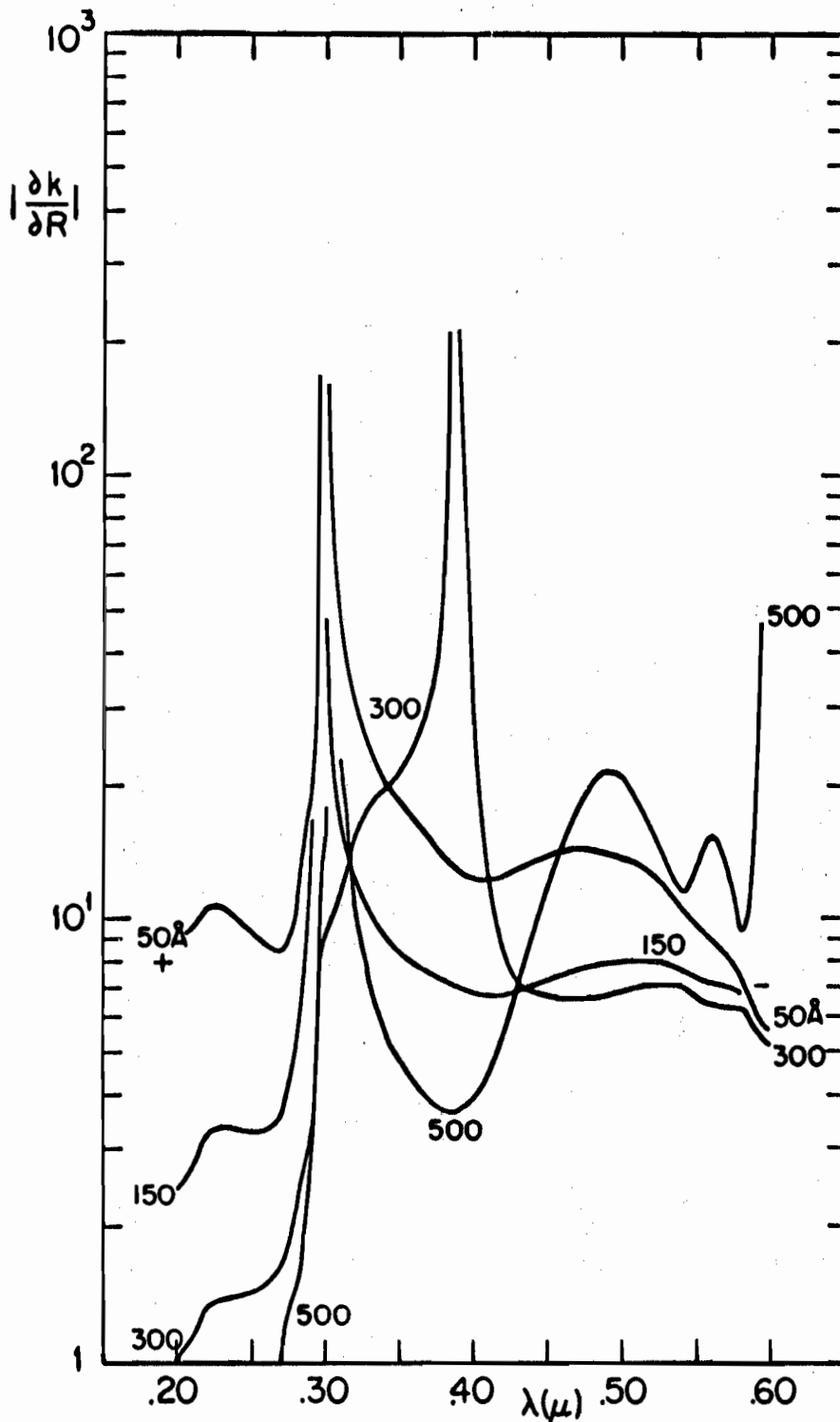


FIG. 3-12a THE EXTINCTION COEFFICIENT ERROR DERIVATIVES VS. λ FOR THE R-T MODEL OF A Ge FILM ON CaF_2 .

a. $|\frac{\partial k}{\partial R}|$.

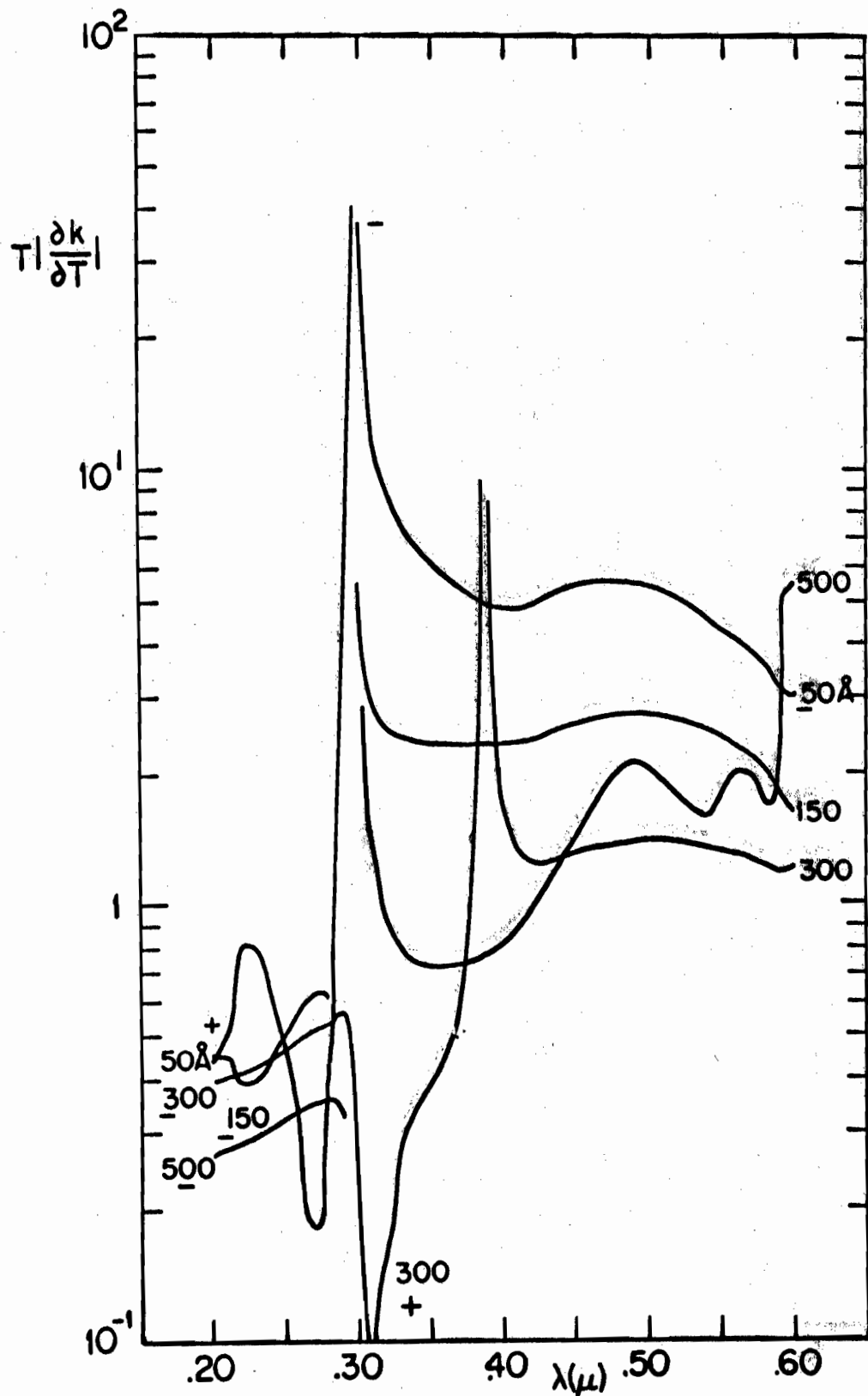


FIG. 3-12b $T \left| \frac{\partial k}{\partial T} \right|$.

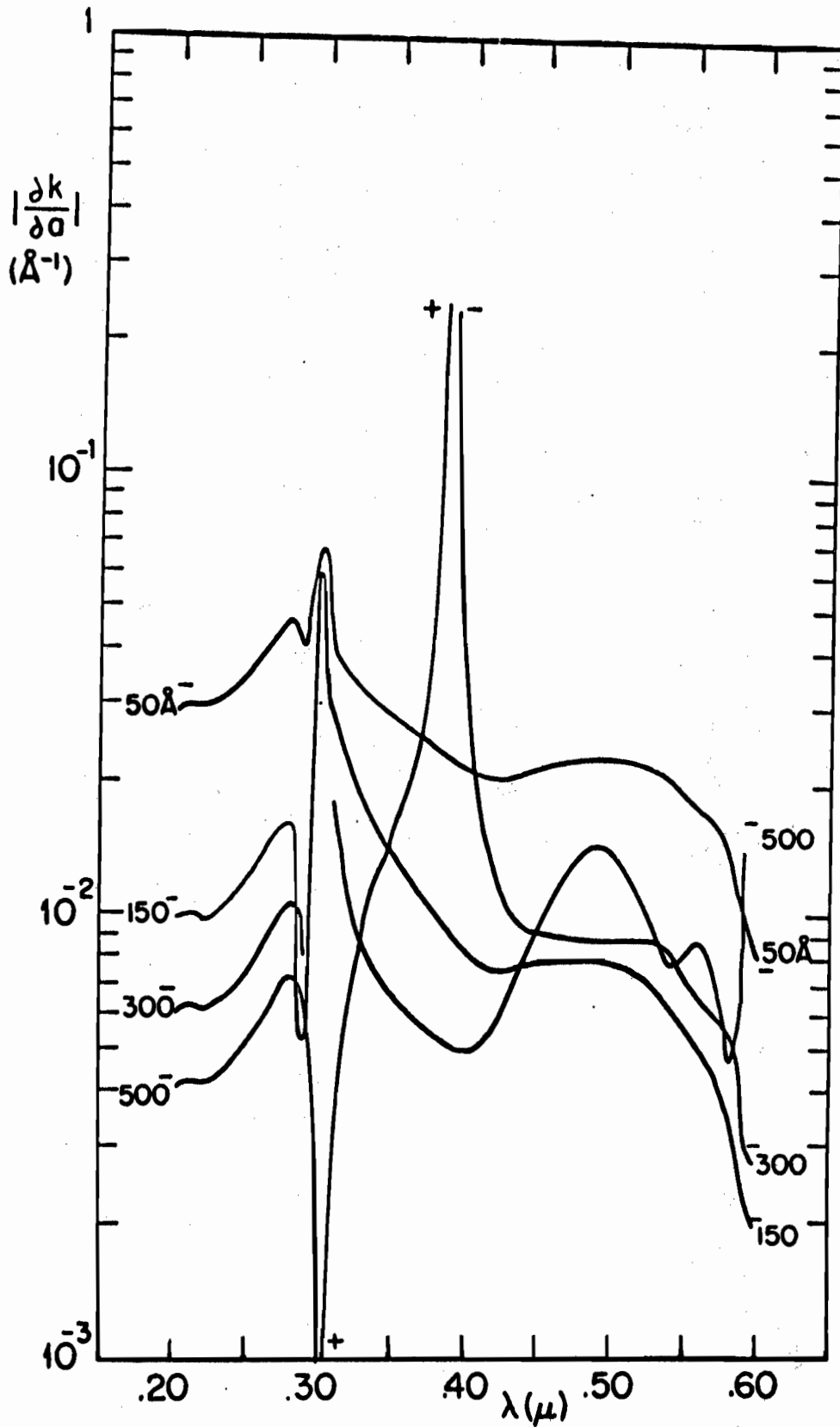


FIG. 3-12c $|\frac{\partial k}{\partial \alpha}|$.

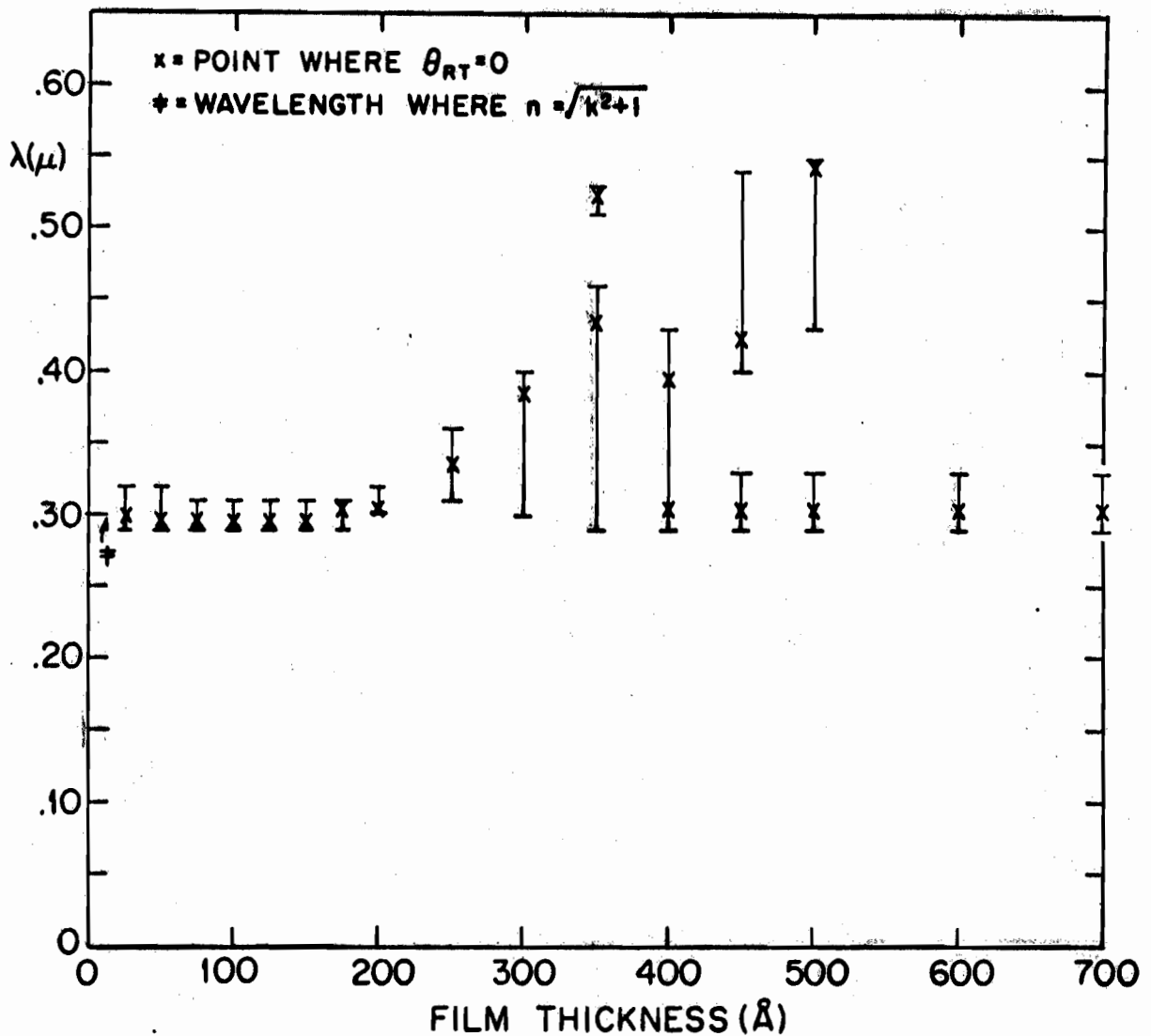


FIG. 3-13 WAVELENGTH REGION WHERE $|\theta_{RT}| \leq 10^\circ$ FOR THE R-T MODEL OF A Ge FILM ON GeF_2 .

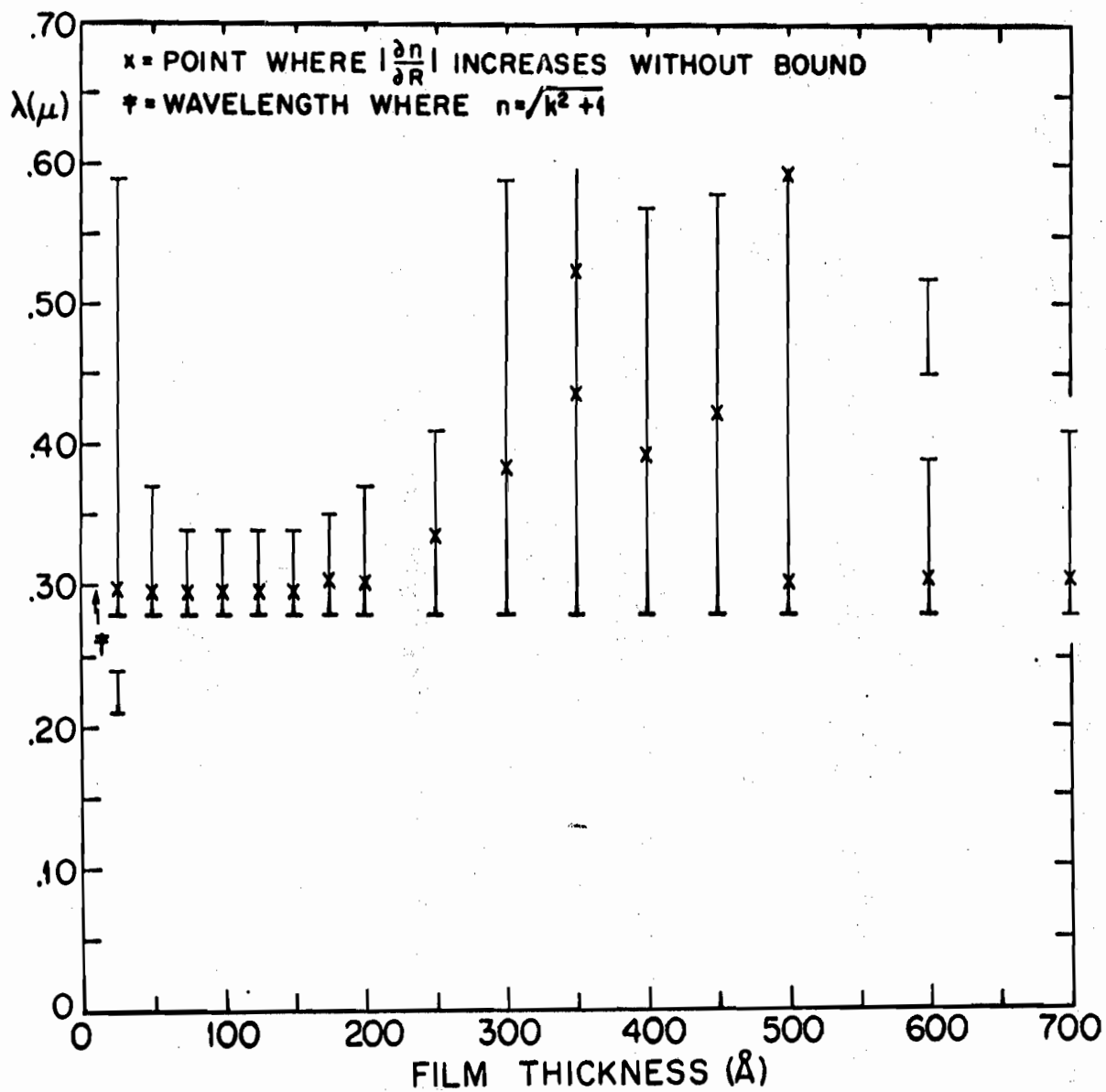


FIG. 3-14a WAVELENGTH REGION WHERE $|\frac{\partial n}{\partial R}| \geq 20$ FOR THE R-T MODEL OF A Ge FILM ON CaF_2 .

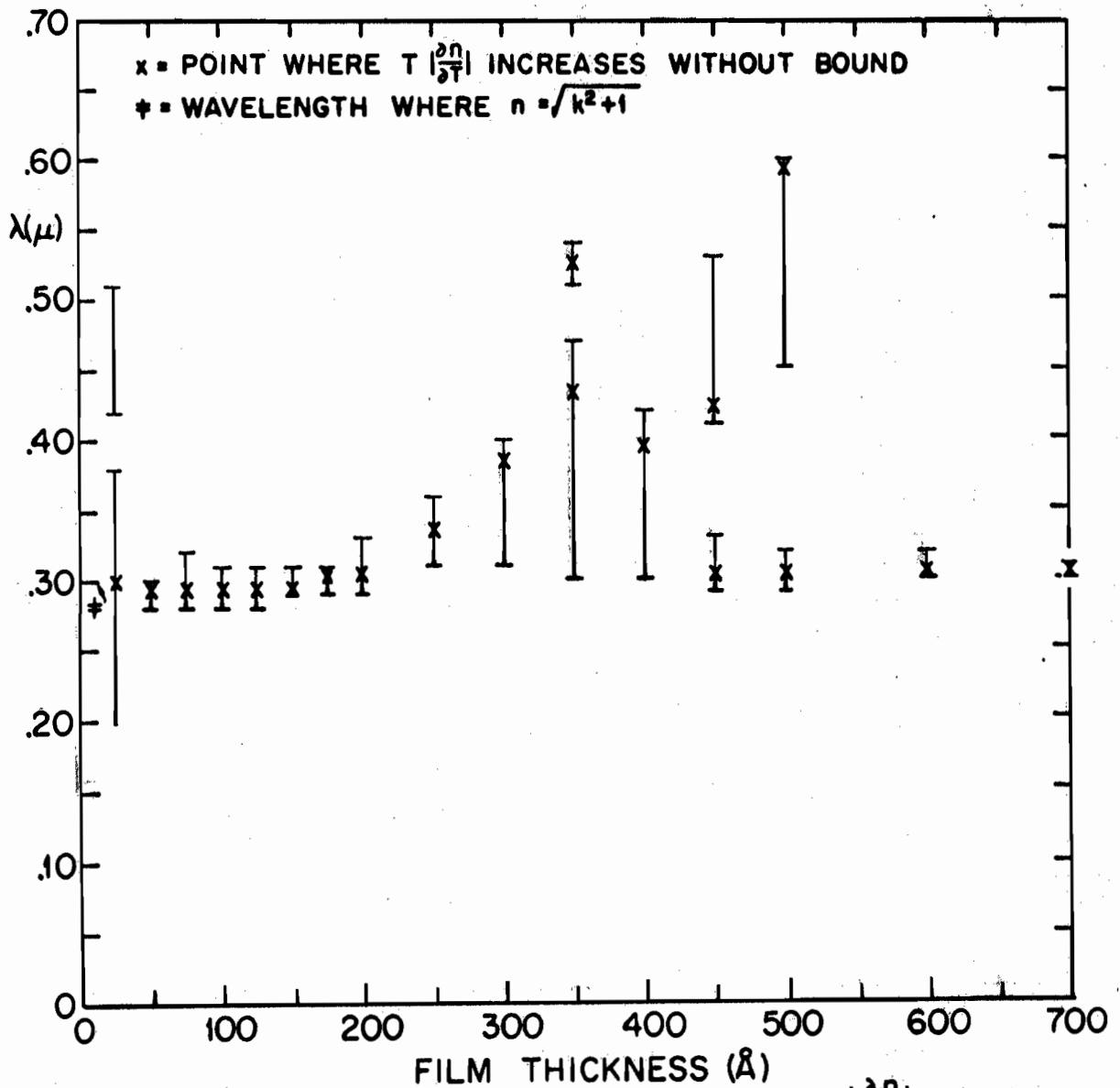


FIG. 3-14b WAVELENGTH REGION WHERE $T \left| \frac{\partial n}{\partial T} \right| \geq 5$ FOR THE R-T MODEL OF A Ge FILM ON CaF_2 .

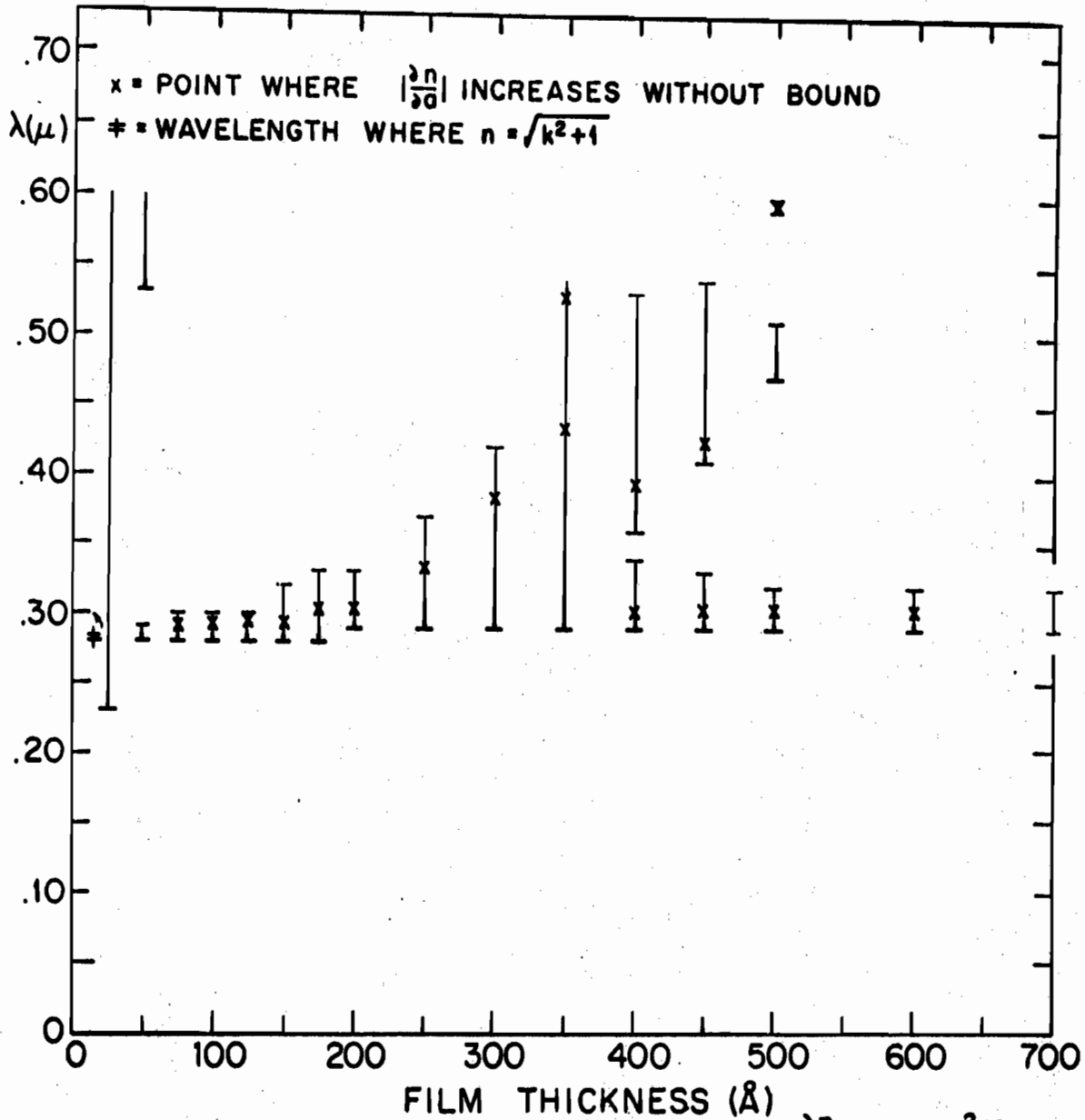


FIG. 3-14c WAVELENGTH REGION WHERE $|\frac{\partial n}{\partial a}| > 5 \cdot 10^{-2}/\text{\AA}$
 FOR THE R-T MODEL OF A Ge FILM ON CaF₂.

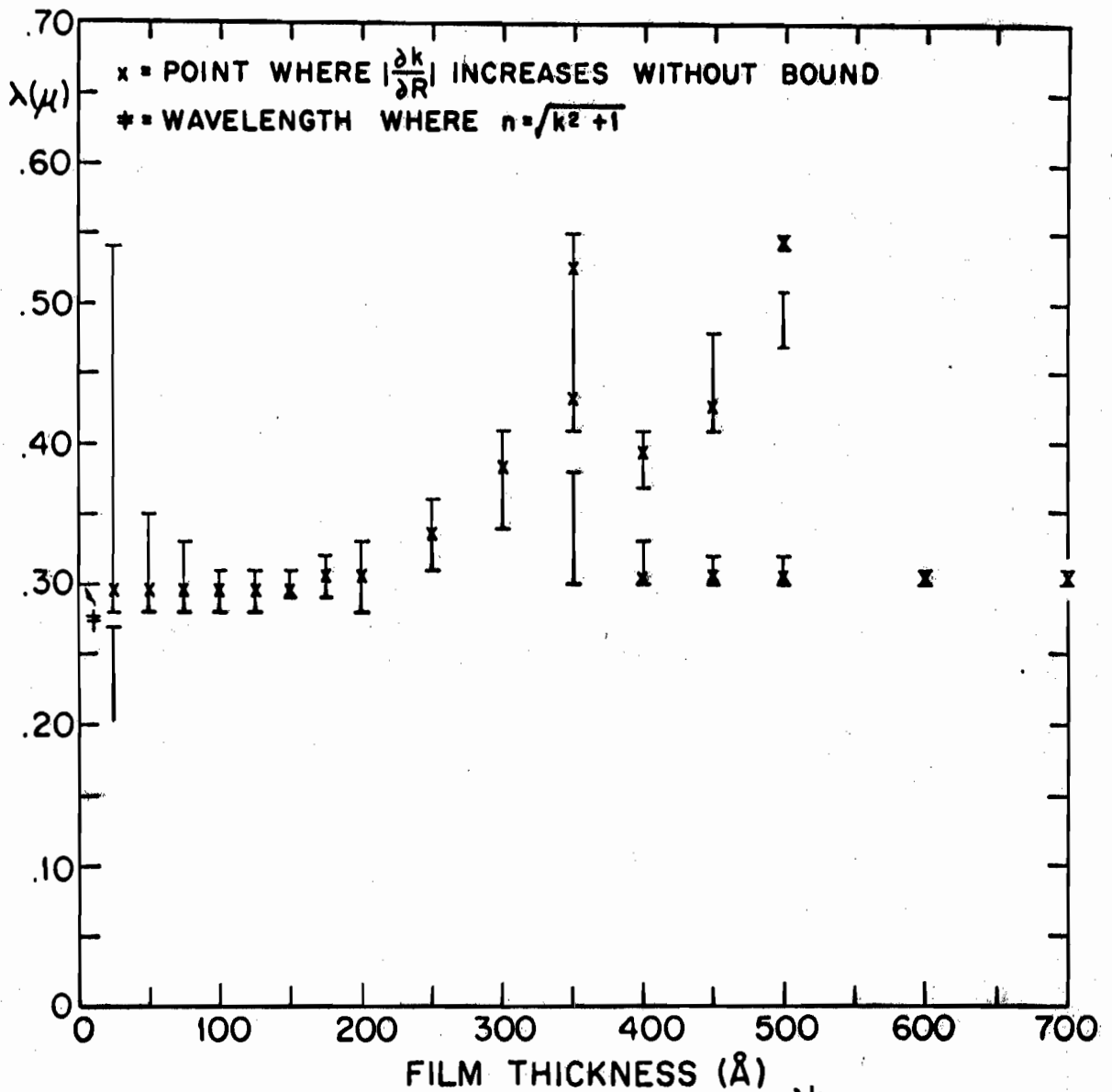


FIG. 3-15a WAVELENGTH REGION WHERE $|\frac{\partial k}{\partial R}| \geq 20$ FOR THE R-T MODEL OF A Ge FILM ON CaF_2 .

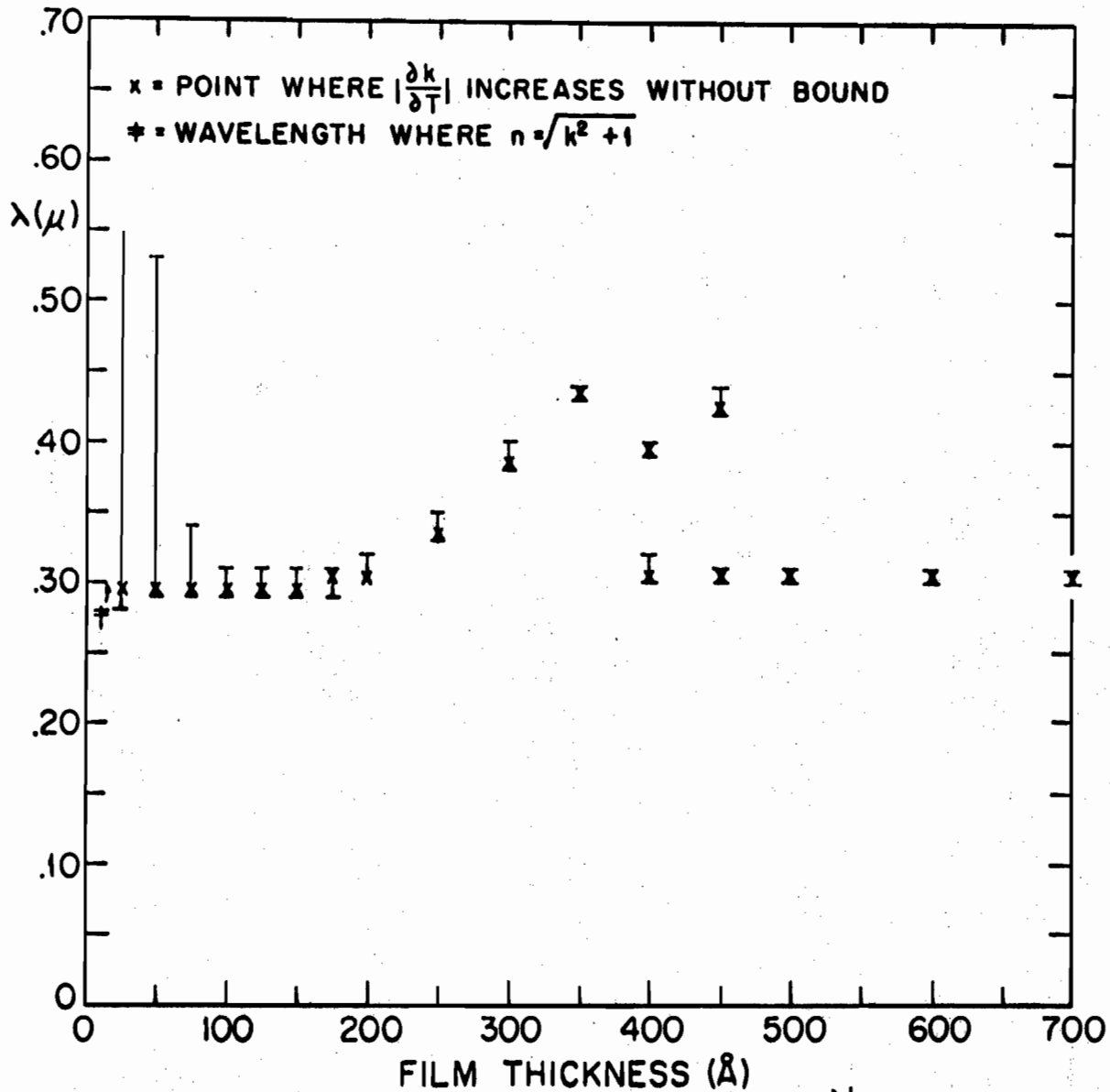


FIG. 3-15b WAVELENGTH REGION WHERE $T|\frac{\partial k}{\partial T}| \geq 5$ FOR THE R-T MODEL OF A Ge FILM ON CaF_2 .

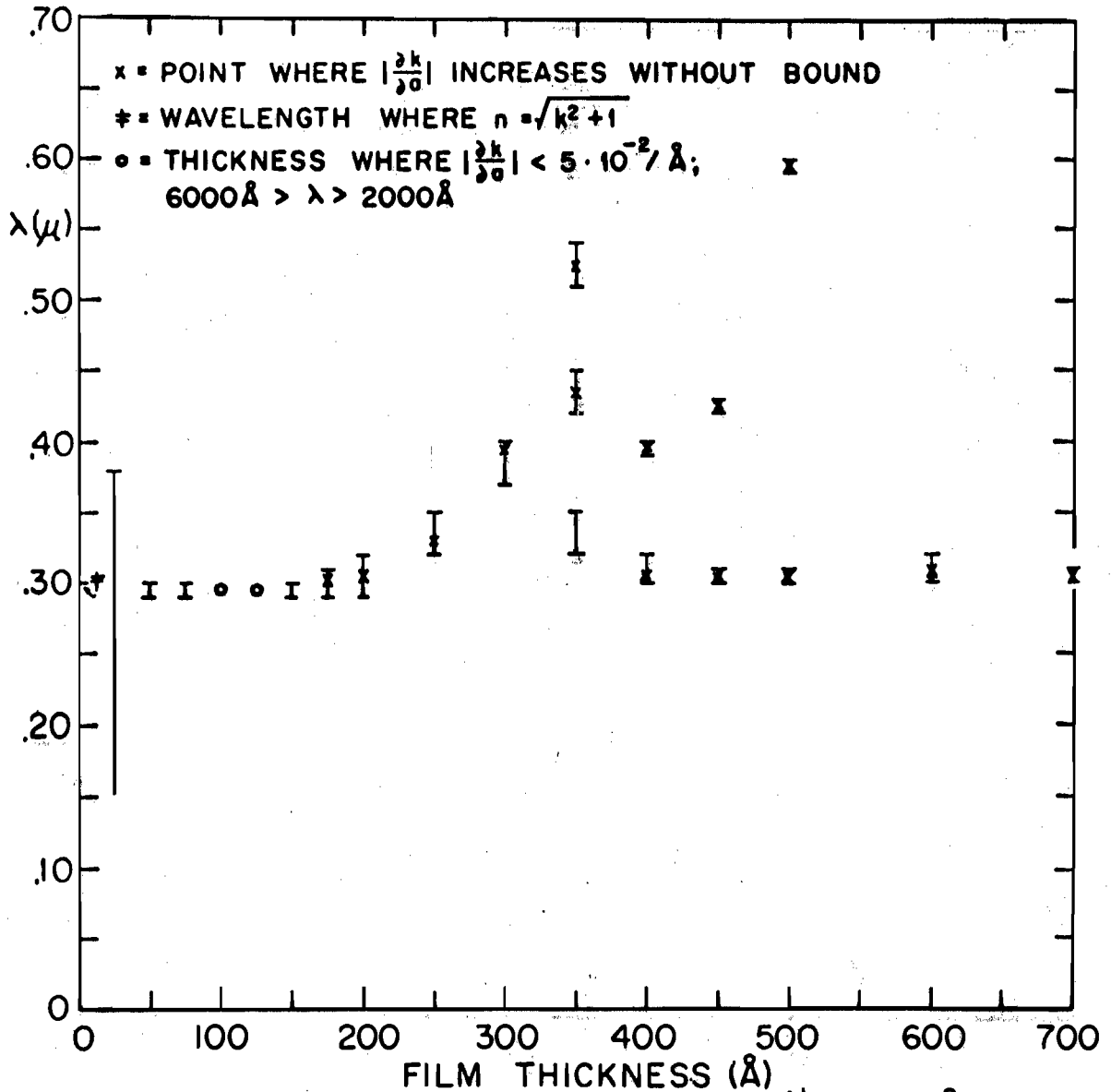


FIG. 3-15c WAVELENGTH REGION WHERE $|\frac{\partial k}{\partial \sigma}| > 5 \cdot 10^{-2} / \text{\AA}$ FOR THE R-T MODEL OF A Ge FILM ON CaF_2 .



the experimental conditions of this work, we can assign an absolute error of $\pm 2.5\%$ to R, a relative error of $\pm 10\%$ to T, and an absolute error of $\pm 10\text{\AA}$ to a. This last figure may be somewhat optimistic. These criteria result in the minimal values of the error derivatives indicated on the bar diagrams. For θ_{RT} , the value of 10 degrees was chosen arbitrarily. The two most significant facts to arise from these diagrams are that there is apparently an optimum thickness range in which to choose films for the determination of the optical constants, and that there is no way in which one may choose two films of different thicknesses in an attempt to circumvent the troublesome wavelength range. **As before, we note that our most sensitive error derivatives are those involving the index of refraction n.**

At the conclusion of this chapter, we shall discuss the implications of these results for the best choice of experimental method and for the experimental determination of the optical constants for semiconductors other than germanium.

B. THE TWO THICKNESS, TWO TRANSMISSION METHOD

1. Theoretical Development.

Let us now consider another method for the determination of the optical constants from photometric measurements on thin films, namely, the method in which one obtains the necessary two independent measurements by measuring the transmission of two films of different

thicknesses. This was the approach used by Brattain and Briggs [8] and Gebbie [9] to obtain the optical constants of germanium films. In reality the method requires four measurements altogether as one must also determine the thicknesses of the two films involved.

The appropriate equations are:

$$T = T(n, k; \lambda; a) \quad (3-22a)$$

$$T' = T(n, k; \lambda; a') \quad (3-22b)$$

where the functional dependence of the right-hand side is given by equations (3-4) and (3-6b). The left-hand side represents the experimental or measured quantities.

2. Error Derivatives

Following the method of Section A-2 we may write the appropriate differentials as:

$$dn = \frac{\partial n}{\partial T} dT + \frac{\partial n}{\partial T'} dT' + \frac{\partial n}{\partial a} da + \frac{\partial n}{\partial a'} da' \quad (3-23a)$$

$$dk = \frac{\partial k}{\partial T} dT + \frac{\partial k}{\partial T'} dT' + \frac{\partial k}{\partial a} da + \frac{\partial k}{\partial a'} da' \quad (3-23b)$$

Almost the entire discussion of Section A-2 as it applies to the method of finding the error derivatives is valid here. Also, the root-locus approach as given in Section A-2 may be brought over to this method if so desired. Furthermore, we could consider the two thickness, two transmission technique with the aid of the simpler film models; however, such an attack does not seem to yield any

simple interpretation of the behavior of the error derivatives that can be extended into the more complex case. Therefore, we shall proceed immediately to a discussion of this case using error derivatives calculated from the data of reference 2. We observe that there are eight such error derivatives to be calculated and many possible thickness pairs to be considered. Hence, some way must be found to condense the results. Fortunately, if one applies as a criterion the tolerable experimental errors as set forth in Section A-2, we may immediately eliminate discussion of the error derivatives $T \frac{\partial k}{\partial T}$, $T' \frac{\partial k}{\partial T'}$, $\frac{\partial k}{\partial a}$, and $\frac{\partial k}{\partial a'}$, because they turn out to be far too small to cause an error of ± 5 in the optical constants at any wavelength. We may reduce our presentation further by observing that any relative errors in the measurement of the two transmissivities are likely to be systematic. That is, experimentally the error in a transmission measurement will probably be due to misalignment or substrate refraction (see Chapter Four, Section A-2) which will be common to all samples. Therefore, we may posit $dT/T \approx dT'/T'$. This allows us to consider as the error derivative the quantity $|T \frac{\partial n}{\partial T} + T' \frac{\partial n}{\partial T'}|$. However, it must be pointed out that $T \frac{\partial n}{\partial T}$ and $T' \frac{\partial n}{\partial T'}$ are usually of approximately equal magnitude but of opposite sign; therefore, the results presented here may unrealistically favor the two thickness, two transmission method. It often happens that $T \frac{\partial n}{\partial T}$ and $T' \frac{\partial n}{\partial T'}$ are by themselves more than large

enough to cause errors greater than ± 0.5 in the deduced optical constants, but that their sum almost completely cancels any effect. We have also assumed that we can combine the thickness error derivatives into a single quantity $\left| \frac{\partial n}{\partial a} + \frac{\partial n}{\partial a'} \right|$ by considering $da = da'$. The experimental motivation in this case, however, is less clear than in the former, although if we measure the thickness by infrared transmission, the justification becomes the same as above. Again we have the possibility that our means of presentation unduly favors the two thickness, two transmission method because $\left| \frac{\partial n}{\partial a} \right| \approx \left| \frac{\partial n}{\partial a'} \right|$ with their signs opposing. Figures 3-16 and 3-17 show the behavior of the combined error derivatives with wavelength. They are plotted as a family of curves for **representative thickness pairs**. Note that, although there are no **singularities in the region near $n^2 = k^2 + 1$** , almost every curve has at least a relative maximum in this area.

We see that there exists the possibility of choosing an optimum thickness pair with which the effect of experimental errors on the deduced optical constants will be minimized. In fact, for $a = 100 \text{ \AA}$, $a' = 300 \text{ \AA}$ or 400 \AA , the combined error derivatives have values below the limits imposed by the considerations of Section A-2. Therefore, it appears that measurements on pairs of films with the above thicknesses would yield reasonably accurate values of the optical constants.

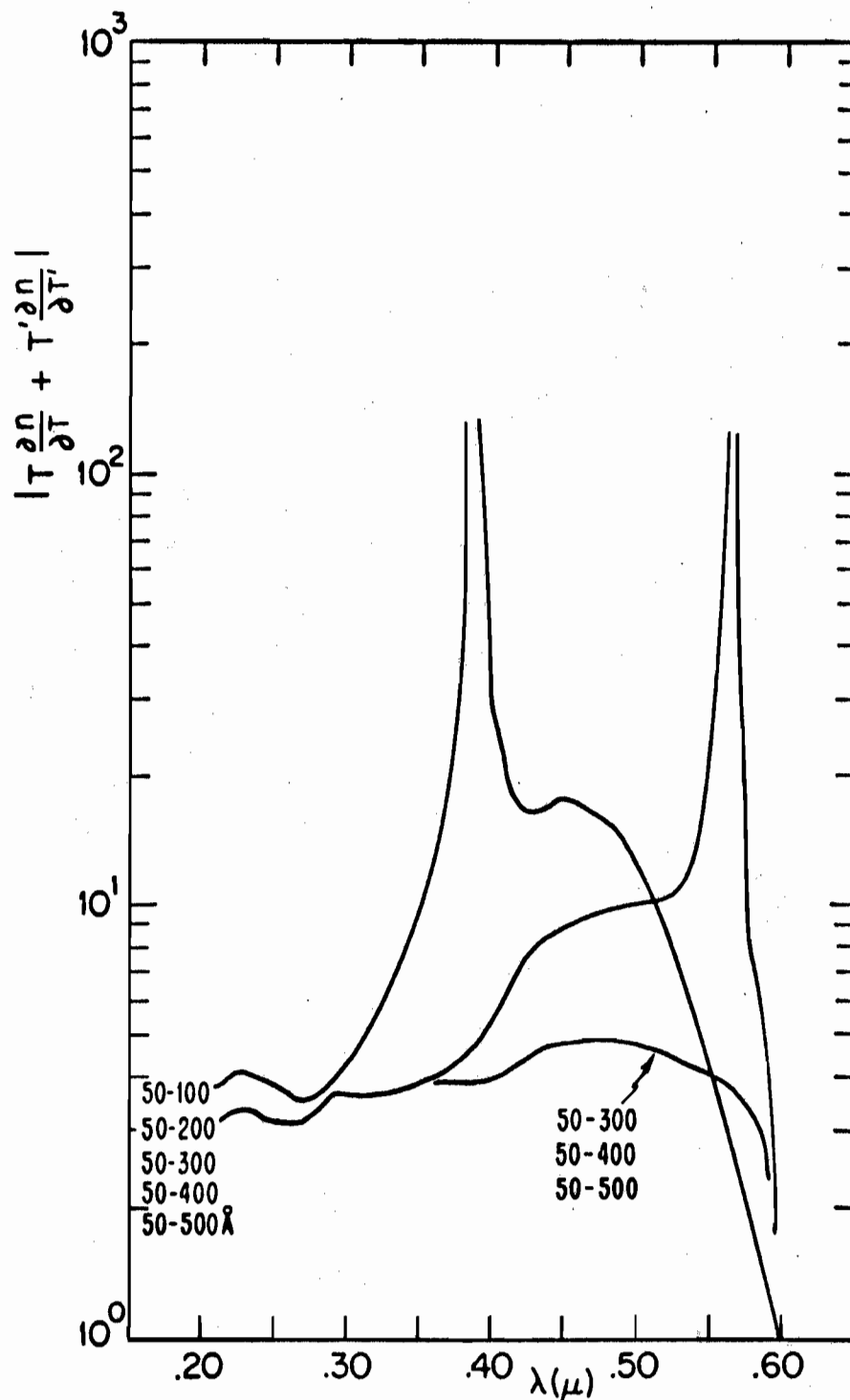


FIG. 3-16a THE INDEX OF REFRACTION COMBINED TRANSMISSION ERROR DERIVATIVES VS. λ FOR TWO THICKNESS, TWO TRANSMISSION METHOD FOR Ge FILMS ON CaF_2 .
 α : α' PAIRED WITH $\alpha = 50\text{\AA}$.

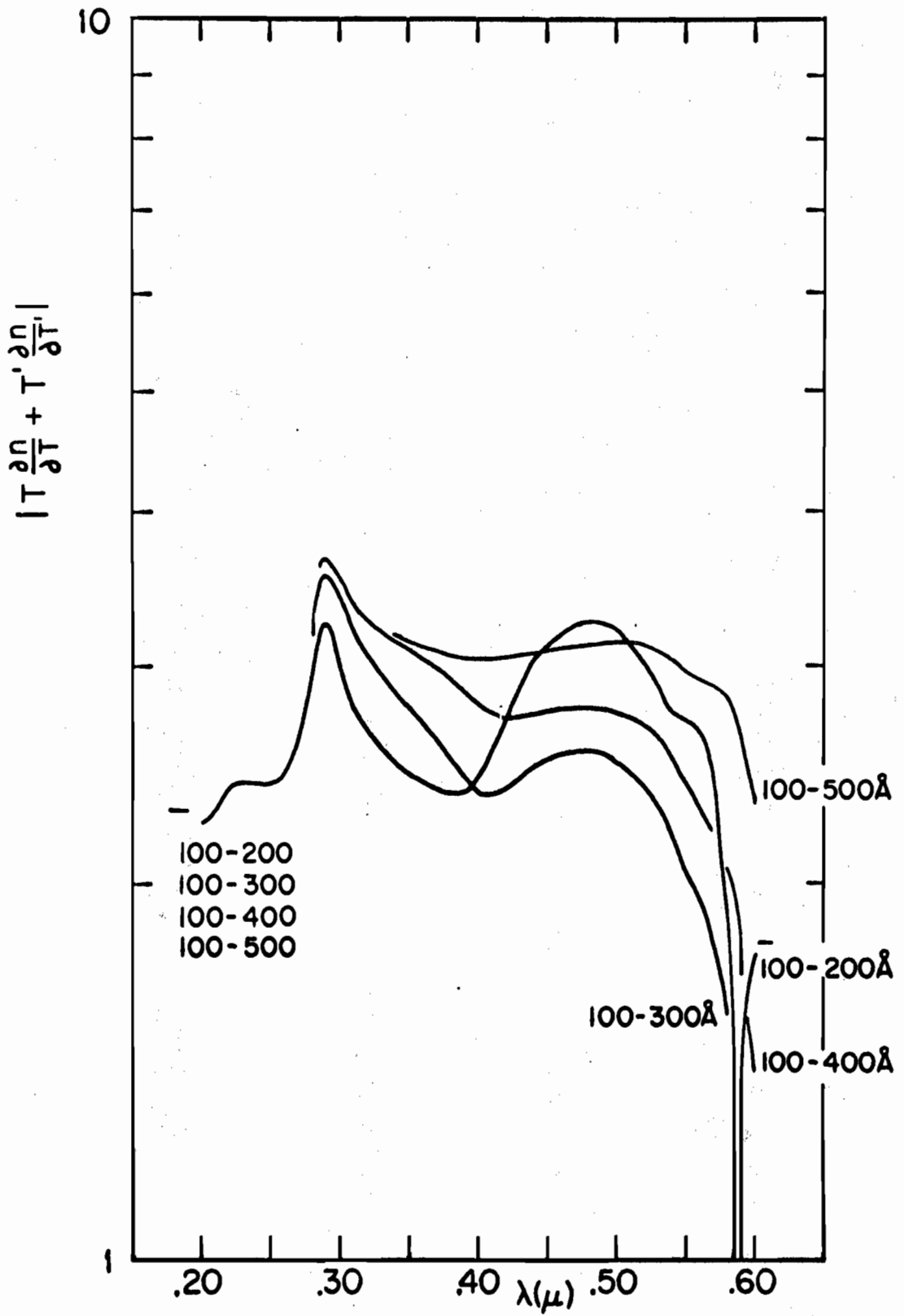


FIG. 3-16b a' PAIRED WITH $a = 100 \text{ \AA}$.

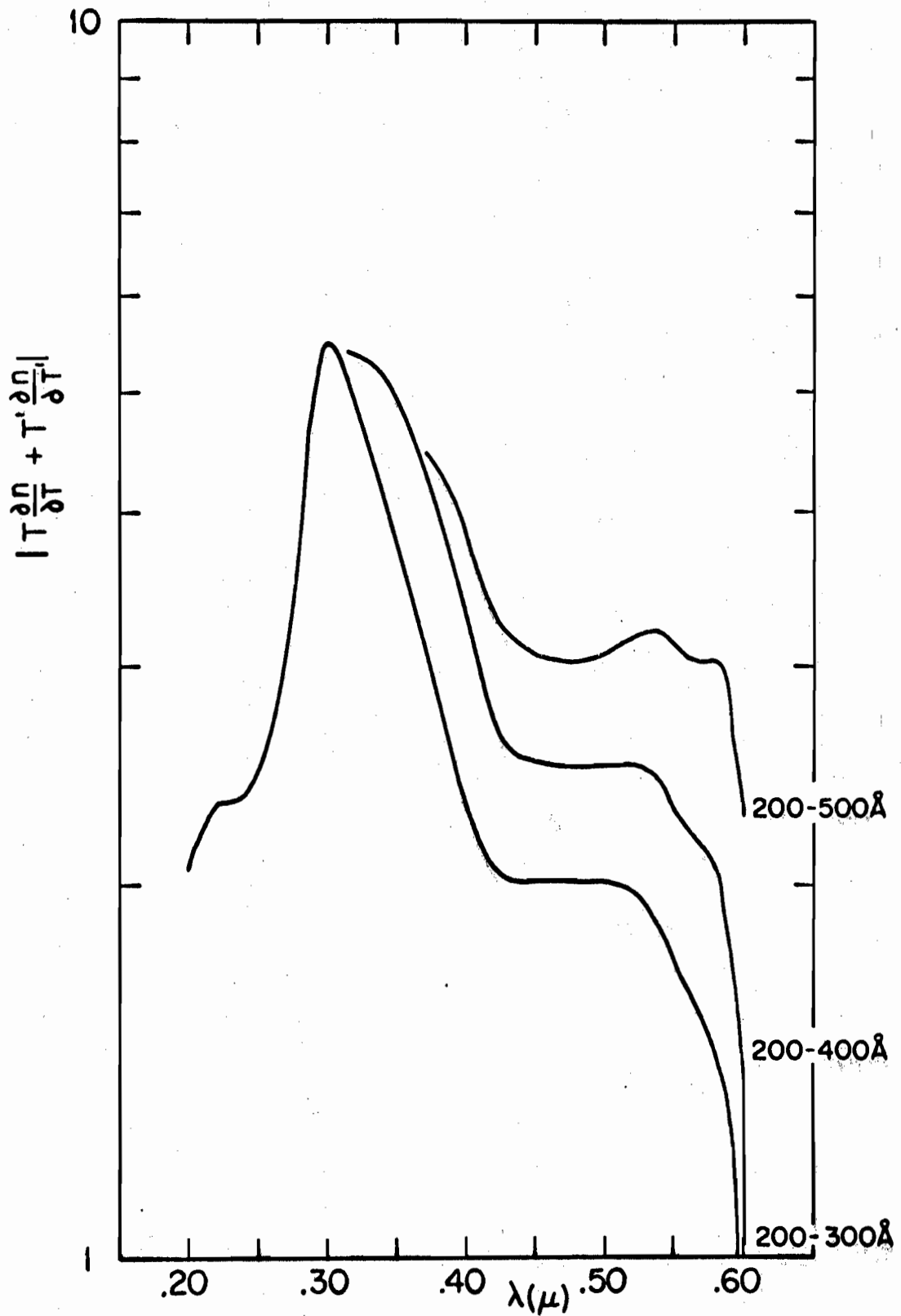


FIG. 3-16c σ' PAIRED WITH $\sigma = 200\text{\AA}$.

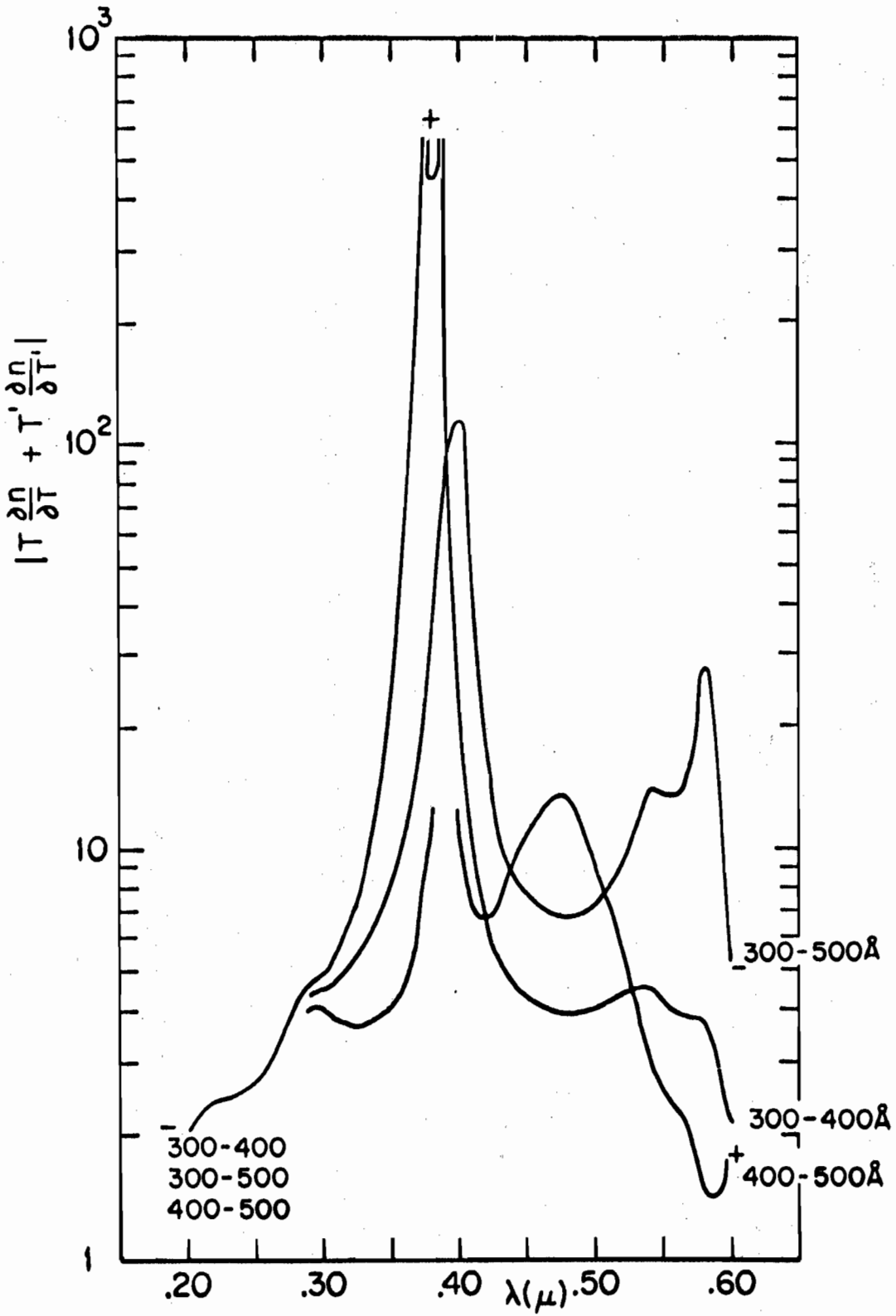


FIG. 3-16d σ' PAIRED WITH $\sigma = 300\text{\AA}$ AND 400\AA .

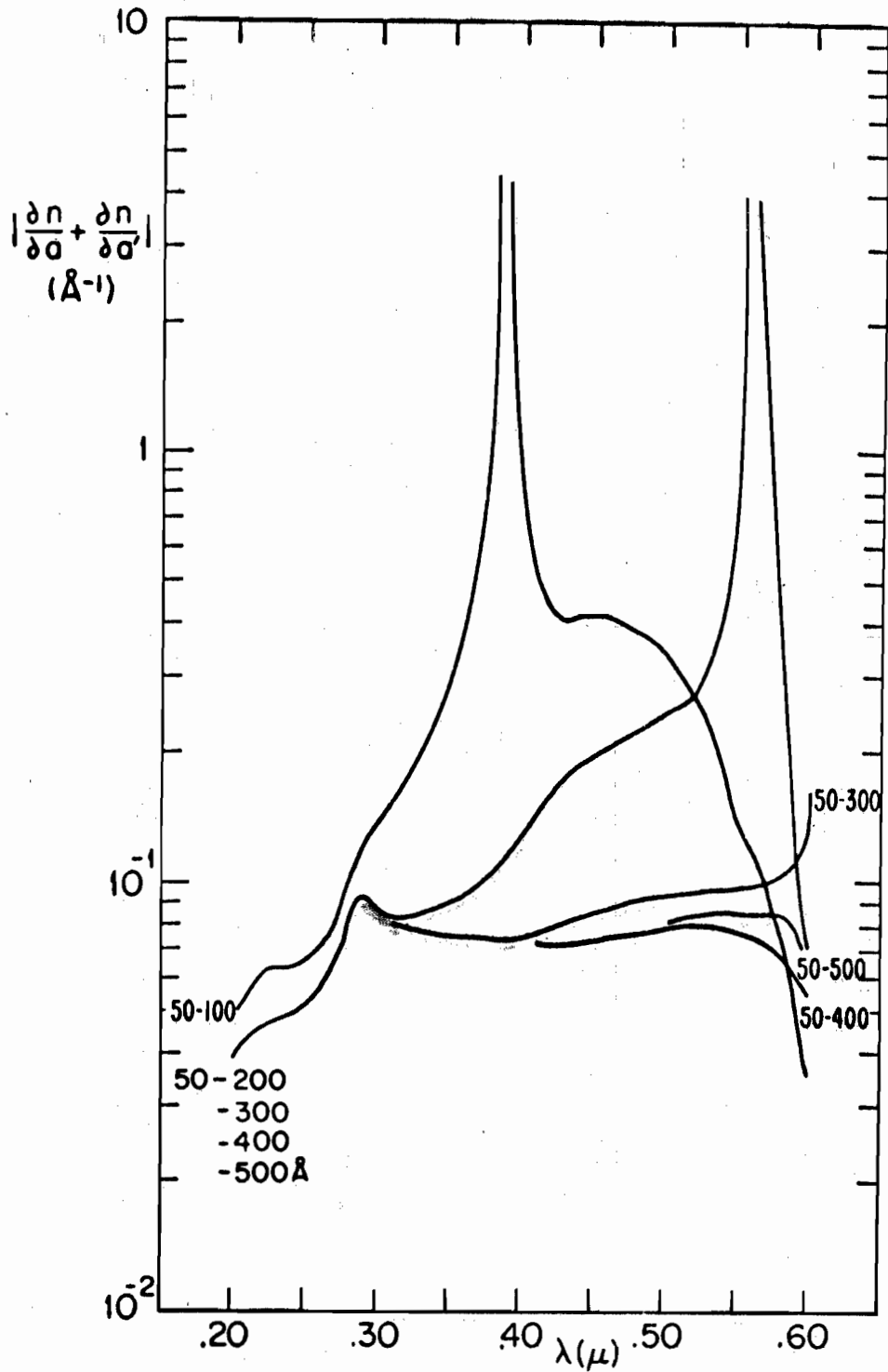


FIG. 3-17a THE INDEX OF REFRACTION COMBINED THICKNESS ERROR DERIVATIVES VS. λ FOR TWO THICKNESS, TWO TRANSMISSION METHOD FOR Ge FILMS ON CaF_2 .
 $\sigma: \sigma'$ PAIRED WITH $\sigma = 50 \text{ \AA}$.

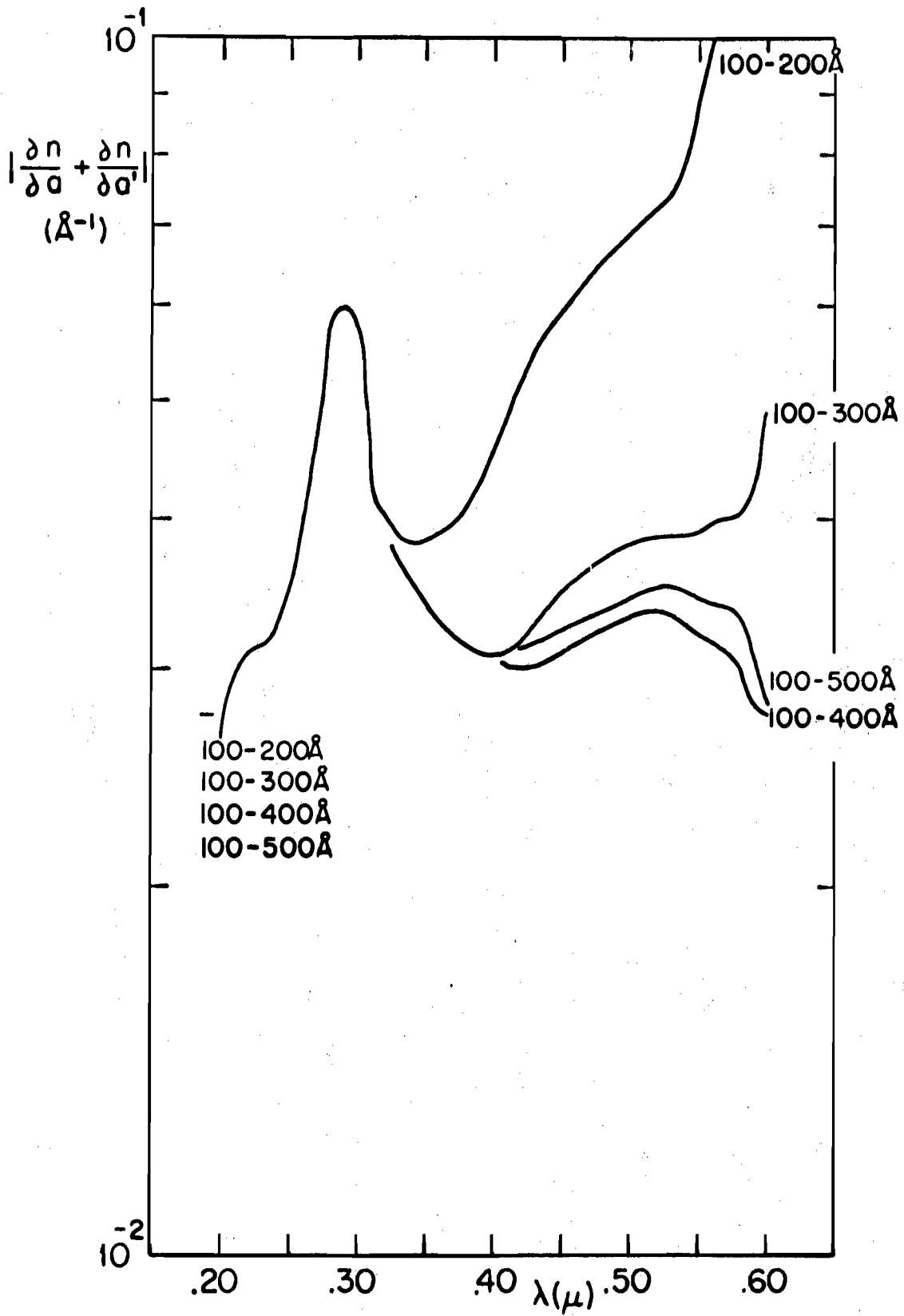


FIG. 3-17b σ' PAIRED WITH $\sigma = 100\text{\AA}$.

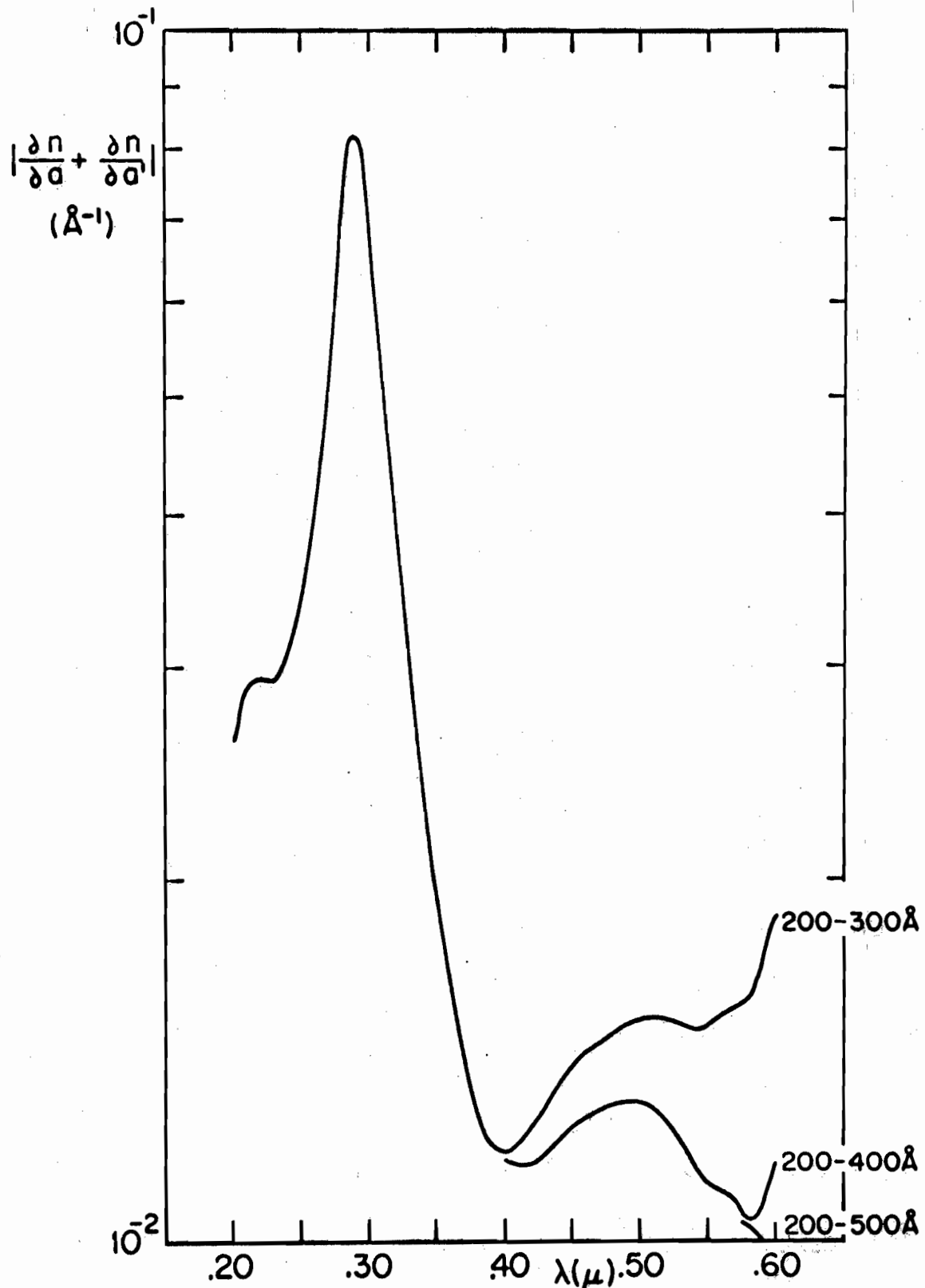


FIG. 3-17c α' PAIRED WITH $\alpha = 200\text{\AA}$.

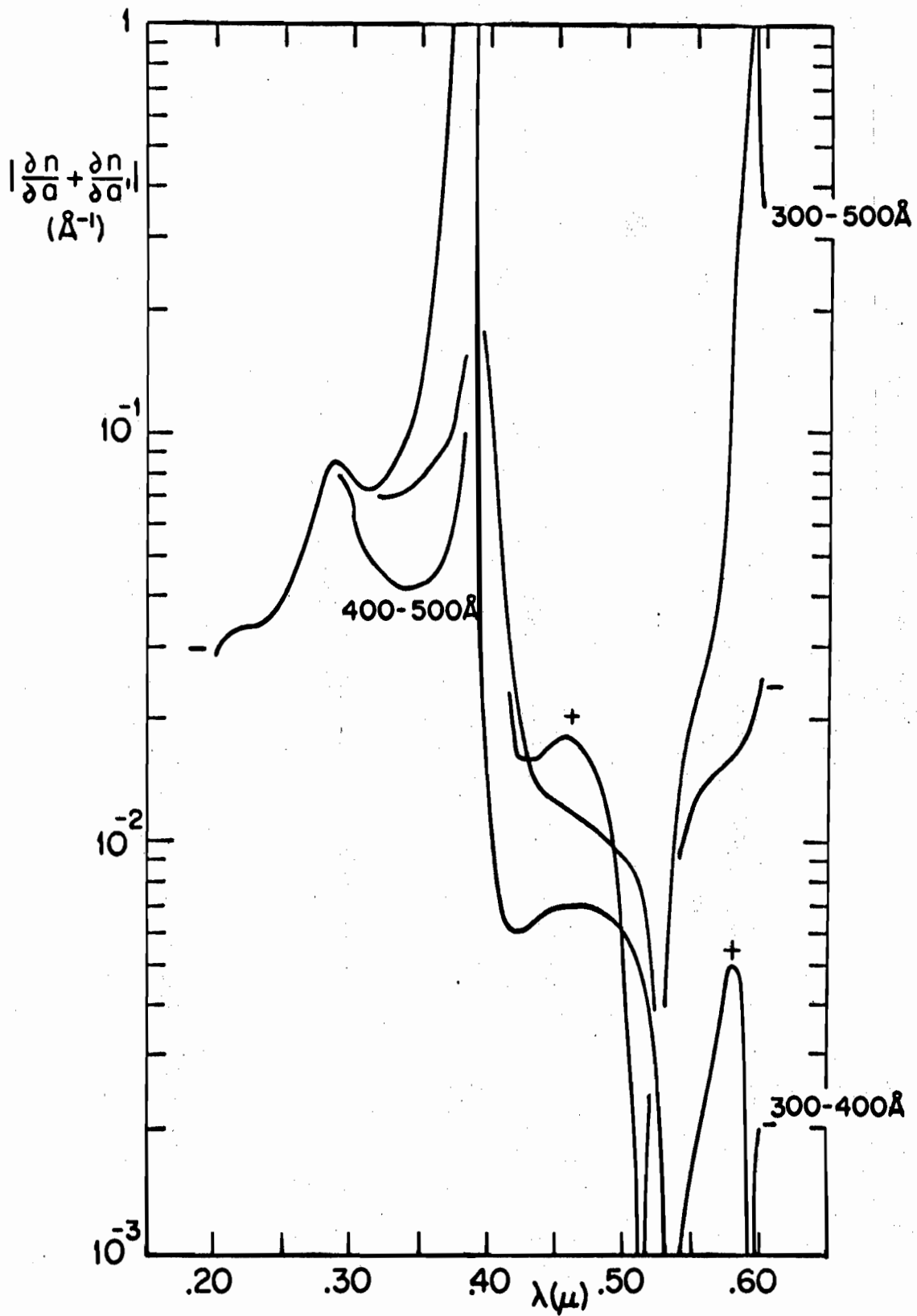


FIG. 3-17d α' PAIRED WITH $\alpha = 300\text{\AA}$ AND 400\AA .

C. CONCLUSIONS

Historically there have been two interpretations placed on optical constants obtained from thin film measurements. One has been to regard the results as representing only the optical properties of a particular film formed under certain conditions and not necessarily representing the bulk material. The availability of epitaxial films makes it more likely that the deduced optical constants express the properties of the bulk material. A firm knowledge of the constants obtained from bulk reflectivity measurements now enables us to test for film conditions that minimize experimental and interpretive errors [14].

For the RT method, it has been shown that there exists a range of thicknesses for which intolerable sizes of the error derivatives are limited to a minimum wavelength range. However, for the thicknesses under consideration here there will always be some wavelength range in which the error derivatives are very large. Such will very likely be the case for most semiconductor materials. Table 3-1 gives the energy and wavelength at which $n^2 = k^2 + 1$ or $\epsilon_1 = 1$ for several well-known semiconductors. Although this table is incomplete, one would expect that, from similarities in band structure, $n^2 = k^2 + 1$ at some wavelength for all of the usual semiconductors. Indeed, this point may well obey

the λ^2 law of the isoelectronic sequence [15].[†] Also there is evidence that SnTe, GeTe, and the semimetals As, Sb, and Bi may have such an energy [11] in addition to some metals [12, 13].

On the other hand, it appears possible with the two transmission, two thickness method to choose a pair of films that will reduce the error derivatives to a tolerable size for all wavelengths to be considered in this work. Thus it seems that this method is superior to the RT method. However, it was pointed out that our method of presentation would probably favor this technique; therefore, it still remains a matter to be decided by experiment in order to see which of the two techniques is the better.

[†] It is interesting to note that the relation $\epsilon_1 = 1$ has the following connection with the fundamental processes of a material. From the definition $\tilde{\epsilon} = 1 + 4\pi\tilde{\chi}$, we see that if $\epsilon_1 = 1$, $\chi_1 = 0$. Now if we consider an electromagnetic wave with frequency ω incident on a collection of N classical harmonic oscillators with charge-mass ratio e/m , characteristic frequency ω_0 , and damping time τ , we have:

$$\chi_1 = Ne^2/m \frac{\omega_0^2 - \omega^2}{(\omega_0^2 - \omega^2)^2 + \frac{\omega^2}{\tau^2}}$$

$$\chi_2 = Ne^2/m \frac{\omega/\tau}{(\omega_0^2 - \omega^2)^2 + \frac{\omega^2}{\tau^2}}$$

We see that this implies that when $\epsilon_1 = 1$, our incident light frequency is passing through the resonance frequency of the oscillators. We note also that in the region of plasma oscillations, $n \approx k$.

TABLE 3-1

Wavelength and Energy at which $n^2 = k^2 + 1$ or $\epsilon_1 = 1$
for several common semiconductor materials.

Material	Energy (eV)	Wavelength (Å)
Ge	4.13	3000
Si [†]	4.0	3100
InSb [†]	3.8	3250
InAs [†]	4.5	2750
GaAs [†]	4.7	2650
GaP [†]	5.1	2450
PbS [‡]	3.1	4000
PbTe [‡]	1.8	6900
PbSe [‡]	2.2	5650

[†] See reference 10.

[‡] See reference 11.

Chapter Three

BIBLIOGRAPHY

- [1] F. Martens, Ann. Physik 6, 606 (1901).
- [2] H. R. Philipp, **private communication**, Nov. 16, 1964.
- [3] T. M. Donovan, E. J. Ashley, and H. E. Bennett, J. Opt. Soc. Am. 53, 1403 (1963).
- [4] J. F. Hall and W. F. C. Ferguson, J. Opt. Soc. Am. 45, 714 (1955).
- [5] L. Harris and A. L. Loeb, J. Opt. Soc. Am. 45, 179 (1955).
- [6] P. R. Wessel, to be published.
- [7] L. Harris, J. K. Beasley, and A. L. Loeb, J. Opt. Soc. Am. 41, 604 (1951).
- [8] W. H. Brattain and H. B. Briggs, Phys. Rev. 75, 1705 (1949).
- [9] H. A. Gebbie, Ph.D. Thesis (unpublished), Reading, 1952.
- [10] H. R. Philipp and H. Ehrenreich, Phys. Rev. 129, 1550 (1963).
- [11] M. Cardona and D. L. Greenaway, Phys. Rev. 133, A1685 (1964).
- [12] H. Ehrenreich and H. R. Philipp, Phys. Rev. 128, 1622 (1962).
- [13] H. Ehrenreich, H. R. Philipp, and B. Segall, Phys. Rev. 132, 1918 (1963).
- [14] P. M. Grant, Bull. Am. Phys. Soc. 10, Series II, 546 (1965).
- [15] F. Herman, J. Electronics 1, 103 (1955); M. Cardona, Phys. Rev. 129, 69 (1963).

Chapter Four

MEASUREMENT OF THE REFLECTIVITY AND TRANSMISSIVITY COEFFICIENTS OF THIN GERMANIUM FILMS

A. SPECTROPHOTOMETRIC APPARATUS

1. Principles of Design and Operation.

This section contains a general description of the design of the spectrophotometric system used to make measurements of the film optical response coefficients, along with its sources of error, and methods of calibration. Figure 4-1 is a schematic diagram of both the optical and electronic signal paths, while Figs. 4-2, 4-3, and 4-4 relate the schematic to the actual apparatus. Figure 4-1a shows the optical arrangement. For purposes of clarity this diagram is not to scale. Some of the light emitted by the lamp L passes through the limiting aperture and filter-holder F to the plane mirror M_1 where it is reflected to spherical mirror M_2 and thence focused on the entrance slit of a model 82-000 1/2 meter Ebert grating monochromator manufactured by the Jarrell-Ash Co. The magnification of the entrance optics is unity so that an exact image of the source appears at the entrance slit. Also, the effective aperture of the entrance optics is matched to that of the monochromator in order to obtain high efficiency and reduce scattered radiation. The grating used for all of the optical measurements taken with this instrument was a 30,000 grooves/inch

Bausch and Lomb grating blazed at 5000\AA producing a linear dispersion of $16\text{\AA}/\text{mm}$ at the exit slit. The lamps used as sources were a General Electric instrument lamp, type 9A/T8 $\frac{1}{2}$ /1, and a high pressure deuterium discharge lamp, model D-100-S, manufactured by Quarzlampe G.m.B.H., Hanau, West Germany. The GE lamp, with a $1\text{ mm} \times 1\text{ in.}$ tungsten filament, was used for the spectral range 6000 to 3500\AA , while the deuterium lamp, with a 1 mm circular aperture, was used for the spectral range 4000\AA to 2000\AA . For most of the optical experiments, an entrance and exit slit width of $100\ \mu$ and a slit height of 5 mm , giving a resolution of 1.6\AA , were found to provide sufficient light intensity without overloading the detector and electronics or unduly increasing the scattered light. Also, a scanning rate of $125\text{\AA}/\text{m}$ in for the entire spectral range covered was found to be a good compromise in that it provided data for the over-all picture fairly rapidly, and was sufficiently slow that any fine structure present would be observed.

Upon emerging from the monochromator exit slit, the light is chopped at a frequency of 1080 cps by a rotating slotted wheel. Attached to the chopper C is a panel light-photodiode combination whose purpose is to provide an electronic signal with a constant phase relationship to the chopped optical beam. The chopper light is now reflected by mirror M_3 to the "mirror lens" system comprised of mirrors M_4 , M_5 , and M_6 . The magnification of the mirror

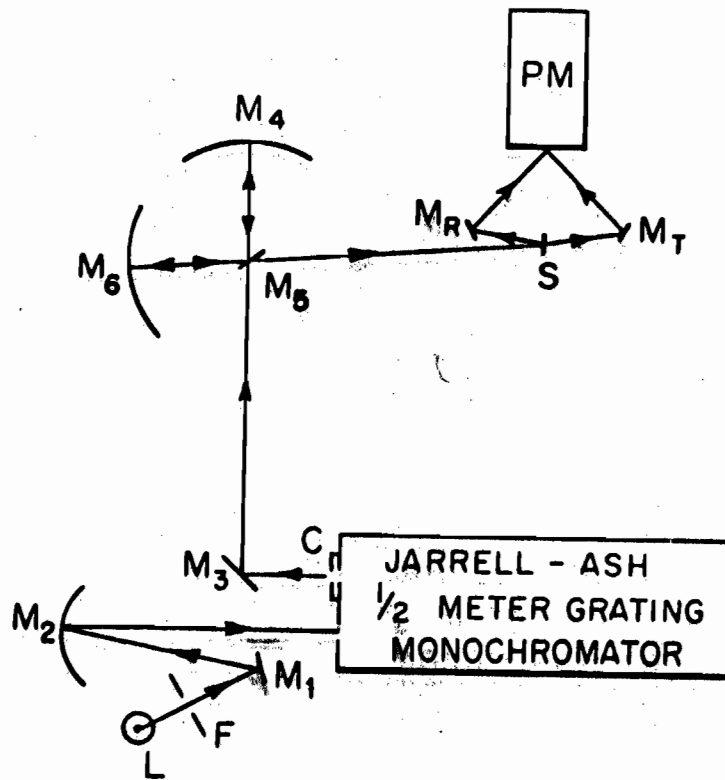


FIG. 4-10 SCHEMATIC DIAGRAM OF THE OPTICAL SIGNAL PATH.

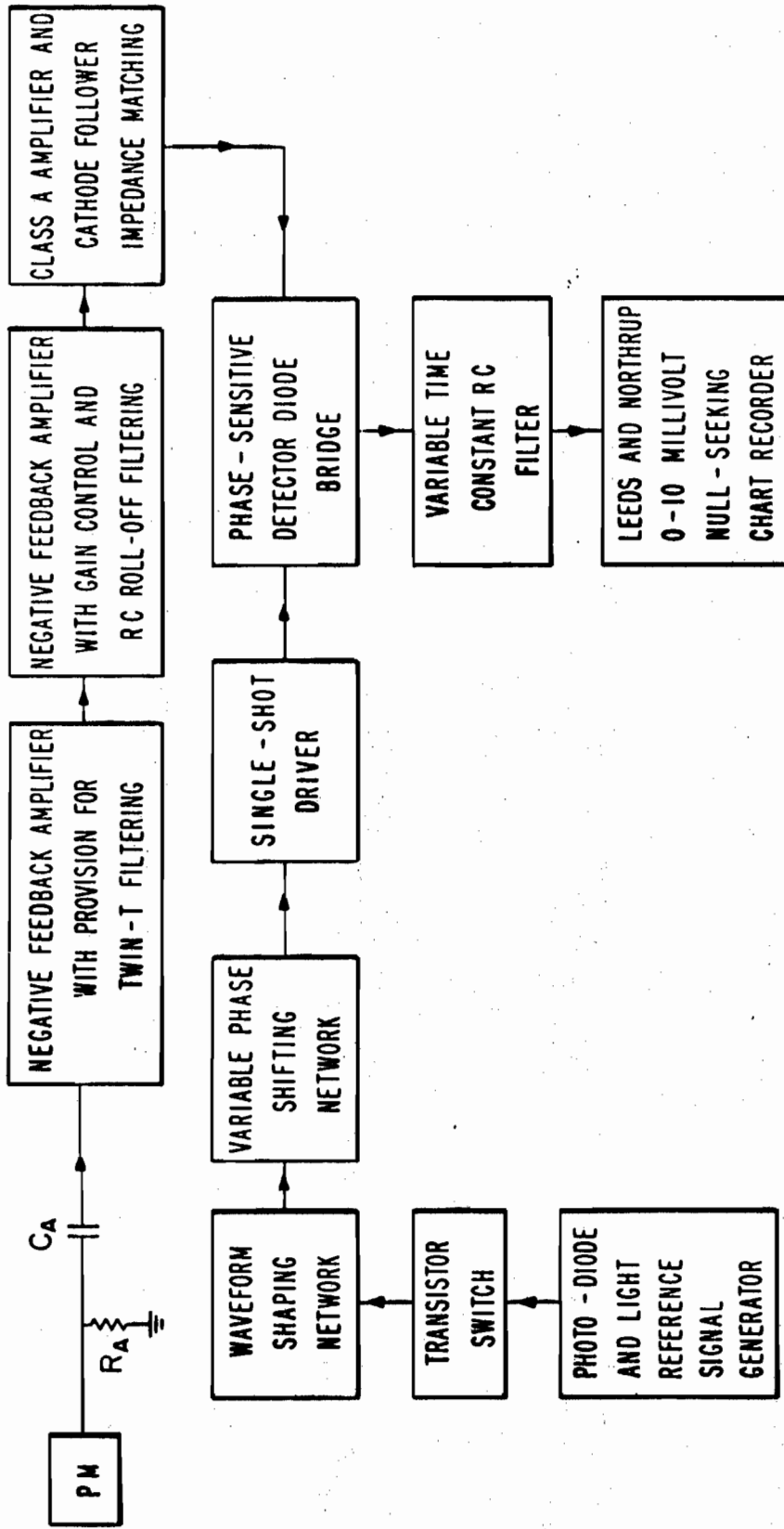


FIG. 4-1b BLOCK DIAGRAM OF THE ELECTRONIC SIGNAL PATH.

lens is $1/2$. Mirror M_6 , slightly off-axis in order to accommodate the sample optics design, focuses the light on the sample S.

There are essentially two **distinct methods of operation** for the sample optics, one for transmission and one for reflection. Let us first consider transmission. If S is removed from the path of the beam, the light is reflected from M_T into the photomultiplier PM, thus giving a measure of the radiation incident on the sample. When S is placed in the beam, the ratio of the signal now received by PM to the previous signal is obviously the sample transmission. In order to measure the reflectivity of S, mirror M_R is put into position and the light from M_T is blocked out. The ratio of the signal now recorded by PM to the incident signal is the sample reflectivity provided that: (a) the reflectivities of mirrors M_R and M_T are identical, and (b), the optical paths $S \rightarrow M_T \rightarrow PM$ and $S \rightarrow M_R \rightarrow PM$ are equal. Neither of these conditions can ever be achieved in practice. However, one can approach condition (a) by cutting the mirror substrates from the same slab, and cleaning and aluminizing them in the same operation. Condition (b) may be approximated through careful experimental procedure. One will note that normal incidence is not used with this technique; however, the angle of incidence is actually only 7 degrees and this can be considered as very close to normal incidence. Further consideration of measurement technique will be deferred to Section A-2 of this chapter. We will only mention that the photomultiplier

used for all optical measurements in the spectral range 6000\AA - 2000\AA was a model 6256B manufactured by EMI, Ltd. of the United Kingdom. This tube has a 1 cm diameter quartz window with an S-13 response cathode. It has a particularly **low dark current and very high gain.**

Let us now consider Fig. 4-1b which shows the flow paths of the electronic signals from the photomultiplier and the chopper photodiode. Because a photomultiplier is principally a constant current source, the usual practice is to convert the current signal into a voltage signal with the anode resistor R_A . This also provides a means of controlling the system gain. In our system, we used two values of R_A , 1K and 10K, providing a gain or attenuation capability of 10 in the input voltage signal. This signal is fed through the coupling capacitor C_A into a negative feedback amplifier tuned with a twin T filter to a narrow passband around 1080 cps. The open loop gain of this amplifier is high enough so that the closed loop gain is dependent only on the passive elements of the twin T filter. The second stage of amplification is another negative feedback amplifier with RC cutoffs on both the high and low frequency sides of 1080 cps in order to complement the twin T filter of the first stage. The purpose of this extensive filtering is to reduce the amount of noise in the signal eventually to be detected. The "intelligence" in the incoming signal consists

of a 1080 cps carrier with very low frequency sidebands. By the use of a 1080 cps carrier, we can circumvent most of the $1/f$ noise, thus leaving Johnson noise and photomultiplier shot effects and dark current noise as the main noise components in the input signal. As our "intelligence" is carried in a very narrow band of frequencies and the noise has an essentially white spectrum, the logical thing to do is to use narrow band amplification. The second stage of amplification contains the gain control. This control is a 20 position, 4 dB/step potentiometer identical to the gain control of the Perkin-Elmer model 107 amplifier. The third and last stage of amplification is a simple class A amplifier followed by a cathode follower whose function is to drive the signal side of the diode bridge of the phase sensitive detector.

We use the technique of phase sensitive detection in order to take advantage of the well-known noise rejection features of this method. In this system, noise components which are out of phase with an independently generated reference signal tend to be suppressed. That is, the transfer function of a phase sensitive detector depends on the cosine squared of the phase difference between the input signal and the reference signal. The usual practice in spectrophotometric instruments is to make this phase difference zero with regard to the "intelligence" portion of the input signal. Hence, this portion undergoes optimum transfer while

the randomly distributed phase of the input noise causes it to be attenuated to a greater or lesser degree. In our system, the appropriate reference signal is generated by a photodiode-panel light assembly mounted on the chopper wheel housing. The light from the panel light is chopped and then detected by the photodiode. The phase difference between this signal and the chopped light signal from the monochromator exit slits is controlled by mechanically moving the photodiode-panel light assembly along the circumference of the chopper wheel housing. The output of the photodiode is now symmetrized by a transistor switching circuit. It is then fed to a waveform shaping filter whose function is to isolate the fundamental sinusoidal harmonic of the reference signal so that it can be operated on by the phase shifting network which follows the filter. This circuit provides an additional means for adjusting the phase difference between the input signal and the reference signal. The reference signal next triggers a single-shot multivibrator whose purpose is to provide a large amplitude square wave with fast rise and fall times to be used in switching the diodes of the phase sensitive detector. This detector has been so designed that in effect it full-wave rectifies the "intelligence" portion of the input signal and yields an output which is independent of the amplitude of the reference signal. The average value of the phase sensitive detector output is found by passing

this signal through a double L-section RC filter with variable time constants. The values and variety of the available time constants are identical to those of the Perkin-Elmer 107. The resulting DC signal is finally displayed on a Leeds and Northrup 0-10 millivolt null-seeking chart recorder.

Extensive use of this photometric system has shown that its dynamic range is limited by the scattered light in the monochromator and not by any residual noise levels. We define scattered light as the ratio of the radiation measured at the exit slits of the monochromator with the wavelength set below the edge of a sharp cut-off filter placed before the entrance slits to the radiation at the exit slits when the wavelength is set above the filter cut-off edge. The resulting number is dependent on the type of source used and the wavelength of the cut-off edge of the filter and also on the slit width. The sensitivity range of the detector is an important additional factor. For our instrument, the scattered light was measured under the following conditions:

- (a) The source was a tungsten filament lamp.
- (b) The cut-off edge of the filter was about 5400Å.
- (c) The two wavelengths used were 5800Å and 5100Å .
- (d) The detector was a photomultiplier and the slit width was 25 μ .

These conditions closely approximate those under which transmission measurements on germanium films were made. The scattered light determined in this way was found to be .08%. This effectively limited the dynamic range of the spectrophotometer to about three orders of magnitude.

2. Description of Experimental Procedure. Test and Calibration by Measurement of Bulk Reflectivity.

As was mentioned above, the measurement of absolute reflectivity by our apparatus depends on whether or not the optical paths $S \rightarrow M_T \rightarrow PM$ and $S \rightarrow M_R \rightarrow PM$ are equivalent. Also, from Fig. 2-4 we see that we are seeking the reflectivity of a highly irregular surface caused by the presence of cleavage steps in the substrate. Therefore, the following experimental procedure was used:

(a) With the sample removed, light with wavelength 5300\AA was allowed to fall upon mirror M_T . Since the light is focused at S, a short distance from M_T , M_T collects all of the incident light. M_T is now rotated until it floods the photomultiplier cathode with the maximum amount of light as found by optimizing the photomultiplier output.

(b) The sample, mounted in a sample holder as shown in Fig. 4-4, is now placed into position. It is then situated so that the film surface stands halfway between mirrors M_T and M_R . M_R is then rotated in order to optimize the signal output as in (a).

(c) The sample surface is then searched for the highest available reflectivity by moving it back and forth in the plane halfway between M_T and M_R .

(d) Steps (a), (b), and (c) are then repeated until one is satisfied that the alignment is optimized.

However, in order to assure that this procedure led to consistent results, it was necessary to devise a reflectivity **standard**. In view of the accurate measurement of the reflectivity of germanium reported by Donovan, Ashley, and Bennett [1], and because we would be measuring the reflectivity of films of this material, it was decided to adopt their measurements as our standard. In reference 1 the sample surfaces were prepared by electropolishing; however, our sample was prepared by polishing and etching techniques as electropolishing equipment was not available. According to the results of reference 1 and those of Philipp and Ehrenreich [2], the difference in surface topography arrived at by these two methods may lead to a difference in absolute reflectivity that is as much as 7% absolute in the ultraviolet region. This is because an etched surface invariably has ripples and pits which scatter the reflected light, while electropolishing leaves the surface much more flat and still retains the crystalline perfection of an etched surface. On the other hand, it appears possible to improve on the etching procedure so that the magnitude of the reflectivity

approaches that of reference 1. Our method was to obtain a 1 cm × 1 cm × 1 mm slab of 40 Ω·cm high purity single crystal of germanium with its surface parallel to the {111} planes of the crystal. This slab was then attached to a lapping dop and the following procedure used:

- (a) The sample was first lapped with 12 μ Buehler #1200 lapping compound.
- (b) Lapping was completed with 3 μ Al₂O₃.
- (c) Polishing commenced with .3 μ Linde "A" using a beeswax polishing platform.
- (d) Polishing was completed with .1 μ Linde "B", also on beeswax. Great care was taken during this step not to bear undue pressure on the sample and hence to minimize the depth of the amorphous surface layer left by polishing. Each step was continued for such time as was felt necessary to remove the damaged layer incurred by the previous step.

After polishing, the sample was removed from the dop for etching. A fresh batch of CP-4 was prepared, the sample placed in a Teflon dish, and about 15 cc of the solution poured over it. The acid was gently sloshed over the sample for one minute, whereupon the etching was stopped with distilled H₂O. The sample was then cleaned in three changes of fresh acetone and finally swabbed with a benzene soaked Q-tip. The sample was immediately placed in a sample holder, alignment made through use of the above procedure,

and the reflectivity measured. The result is shown in Fig. 4-5. The over-all reflectivity is about $\frac{1}{2}\%$ greater than that reported in reference 1. Repetition of the alignment and measurement procedure indicates a scatter in the over-all reflectivity amplitude of +0%, -2% absolute in the wavelength region 3500Å to 6000Å and +0%, -4% absolute in the wavelength region 2000 Å to 3500 Å. In addition, repetition of the measurement over a period of one or two weeks indicated a steady decrease in the amplitude of the 2800Å peak to a level of about 64%. However, the amplitude could be restored to a high value by bathing the sample in HF, acetone, and they drying carefully. This indicates that the degradation of the reflectivity was probably due to the formation of an oxide layer.

This sample then became the calibration standard for all reflectivity measurements. Before making measurements on the reflectivity of a film sample, we invariably checked out our procedure by making reflectivity measurements on our standard at three or four different wavelengths.

With regard to the measurement of the film transmissivity, there appears to be only a small chance of the introduction of error due to alignment procedures. The major cause of error is thought to be due to refraction by the substrate (care was taken to make measurements in a pinhole-free region). This is possible

because the light is converging to a focus on the sample and also because of the irregular substrate surface. The error due to these effects is estimated to be approximately $\pm 10\%$ relative.

B. RESULTS FOR THE REFLECTIVITY AND TRANSMISSIVITY COEFFICIENTS

1. Results for Fused Quartz Substrates.

It was decided to study the reflectivity of germanium films deposited on fused quartz substrates for the following reasons:

(a) To ascertain whether or not such films might possibly make more suitable vehicles for the calculation of the optical constants than those on CaF_2 .

(b) To check our experimental methods by comparing our results with a similar, but less complete study by T. M. Donovan and E. J. Ashley [3].

Two sets of experiments were performed, one being the maintenance of a reasonably constant deposition rate, denoted by Δ , while the substrate temperature, denoted by T_S , was varied considerably, and the other being of the same type except that T_S was held constant and Δ varied. Figure 4-6 gives the RED patterns and Fig. 4-7 the reflectivity as T_S was varied, while Figs. 4-8 and 4-9 hold for the case in which Δ was varied. The method of deposition was the same as outlined in Chapter Two, Section B-3. However, the substrate preparation differed in that all substrates

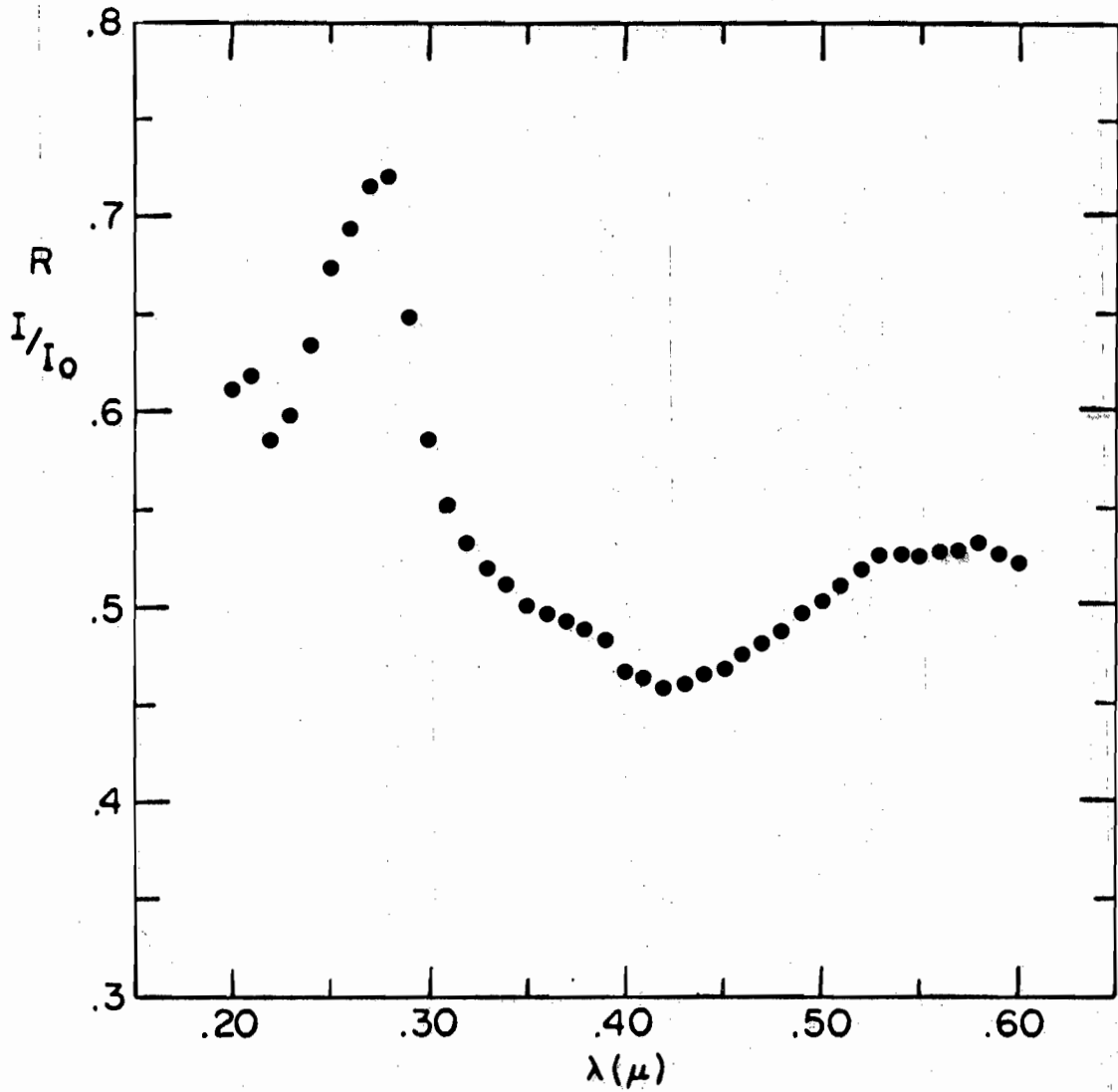


FIG. 4-5 REFLECTIVITY OF ETCHED SINGLE CRYSTAL BULK GERMANIUM.

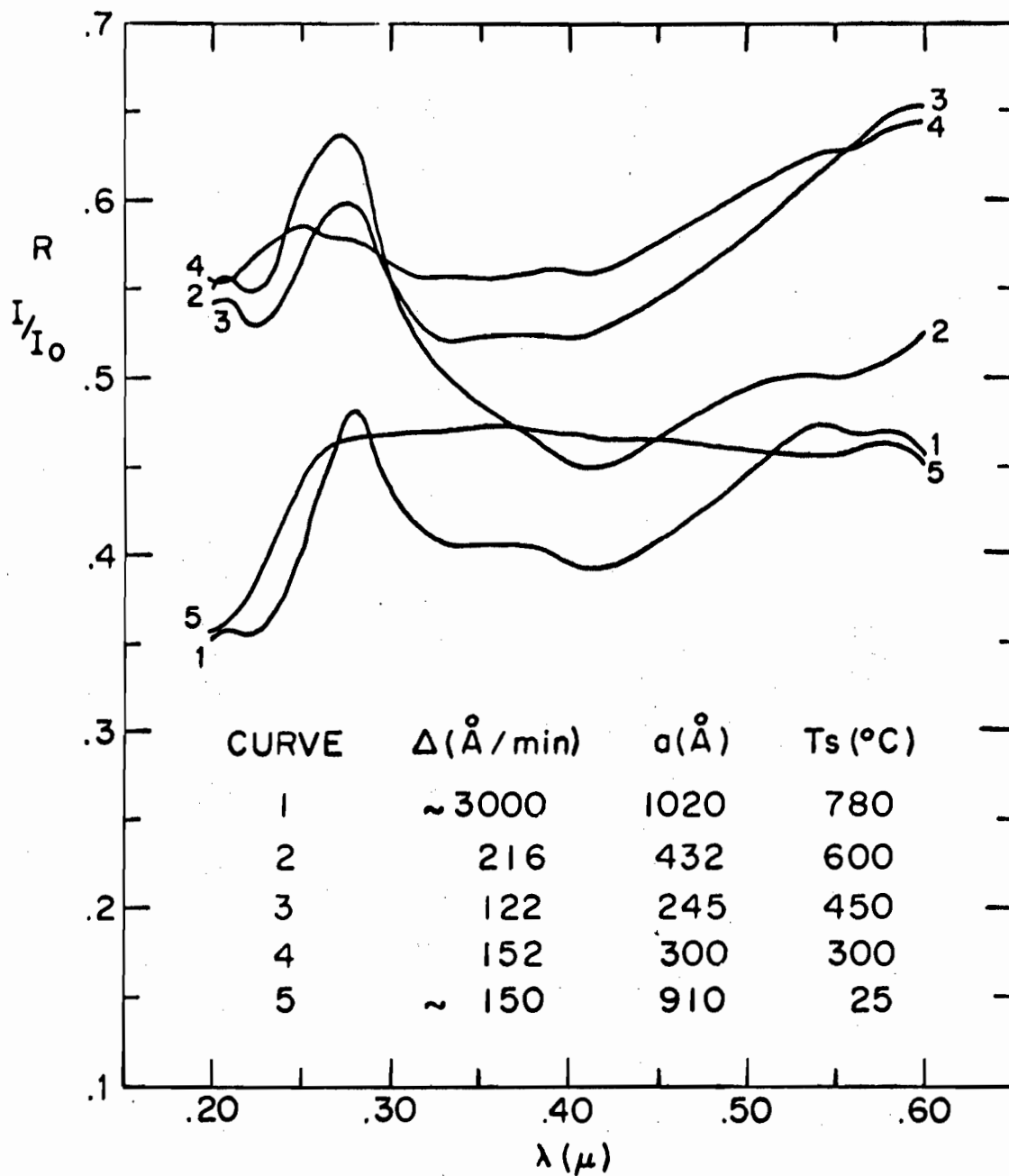


FIG. 4-7 REFLECTIVITY OF Ge FILMS ON FUZED QUARTZ FOR VARIOUS SUBSTRATE TEMPERATURES, T_s .

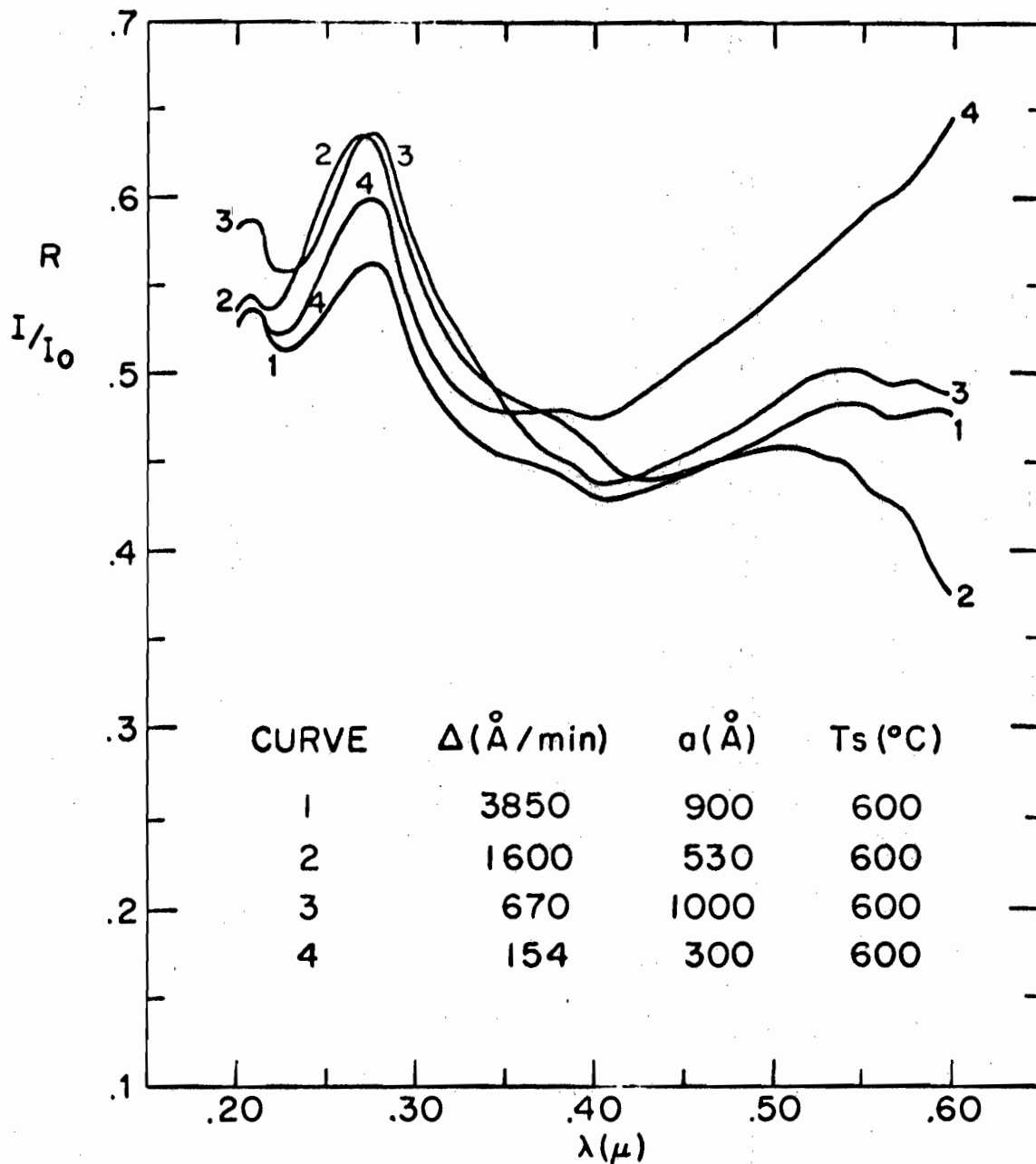


FIG. 4-9. REFLECTIVITY OF Ge FILMS ON FUZED QUARTZ FOR VARIOUS DEPOSITION RATES, Δ .

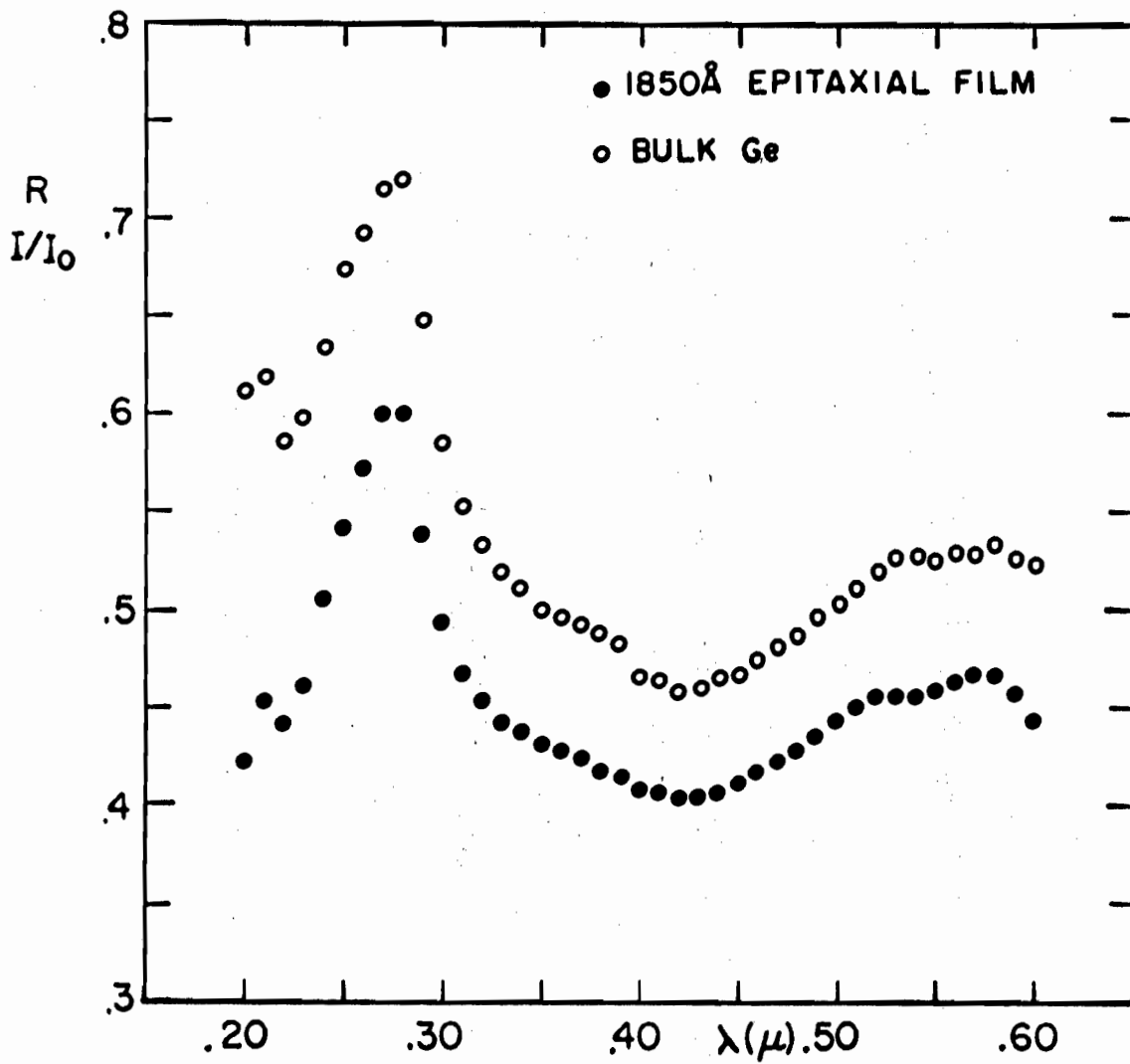


FIG. 4-11 REFLECTIVITY OF A 1850Å EPITAXIAL GERMANIUM FILM COMPARED WITH THAT OF BULK GERMANIUM.

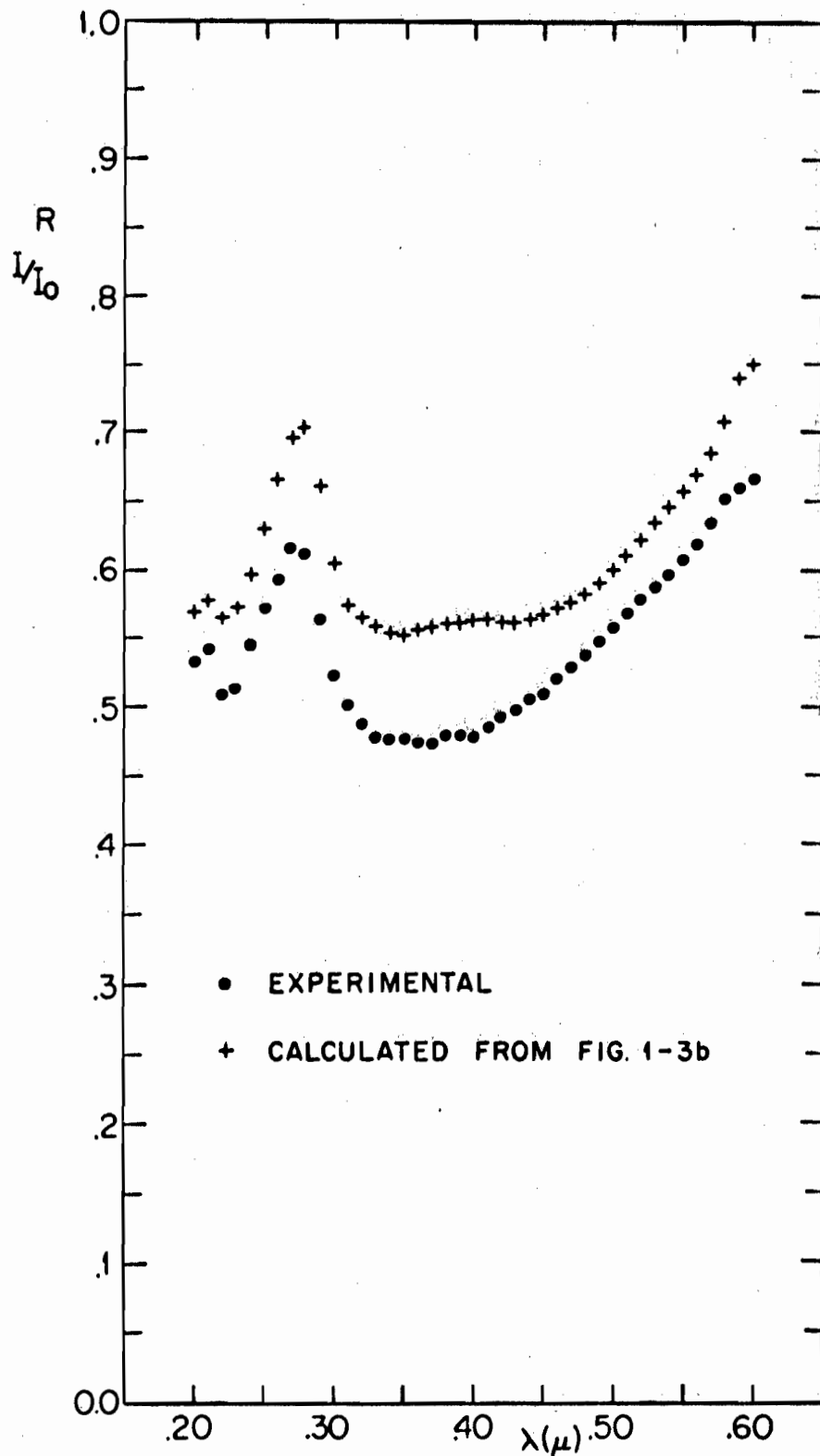


FIG. 4-12a REFLECTIVITY OF A 250Å EPITAXIAL GERMANIUM FILM ON CaF₂.

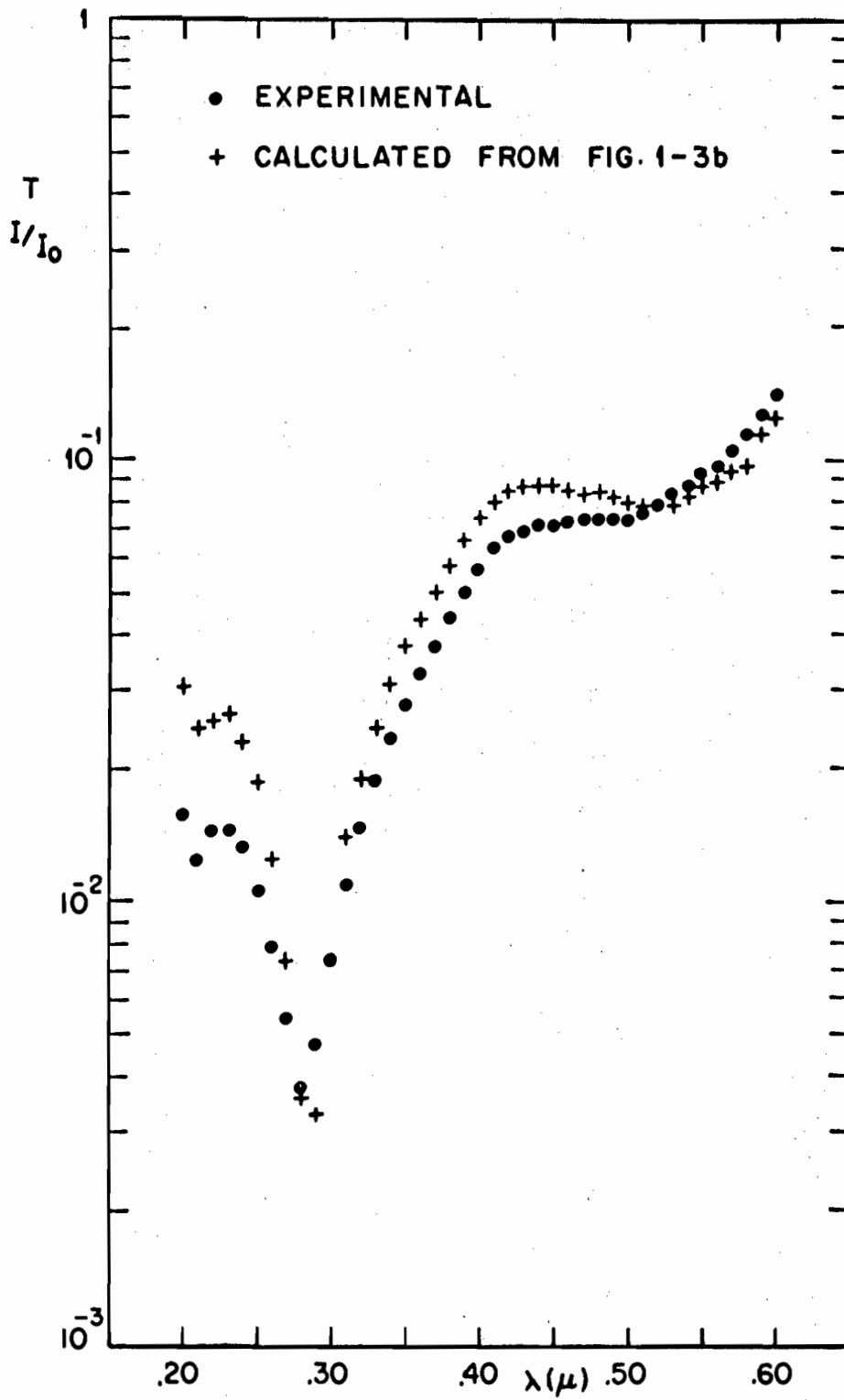


FIG. 4-12b TRANSMISSION OF A 250Å EPITAXIAL GERMANIUM FILM ON CaF₂.

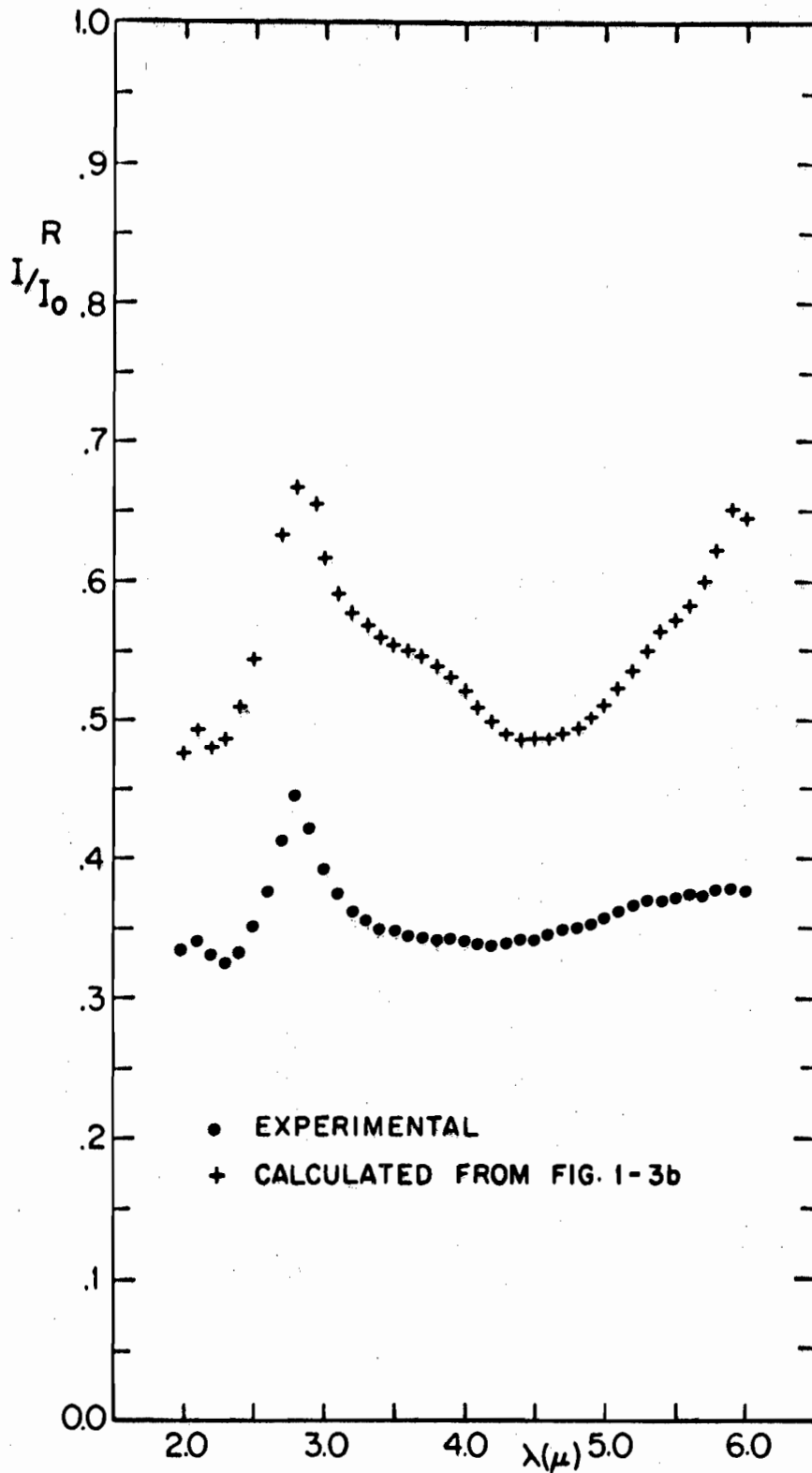


FIG. 4-13a REFLECTIVITY OF A 135 Å EPITAXIAL GERMANIUM FILM ON CaF₂.

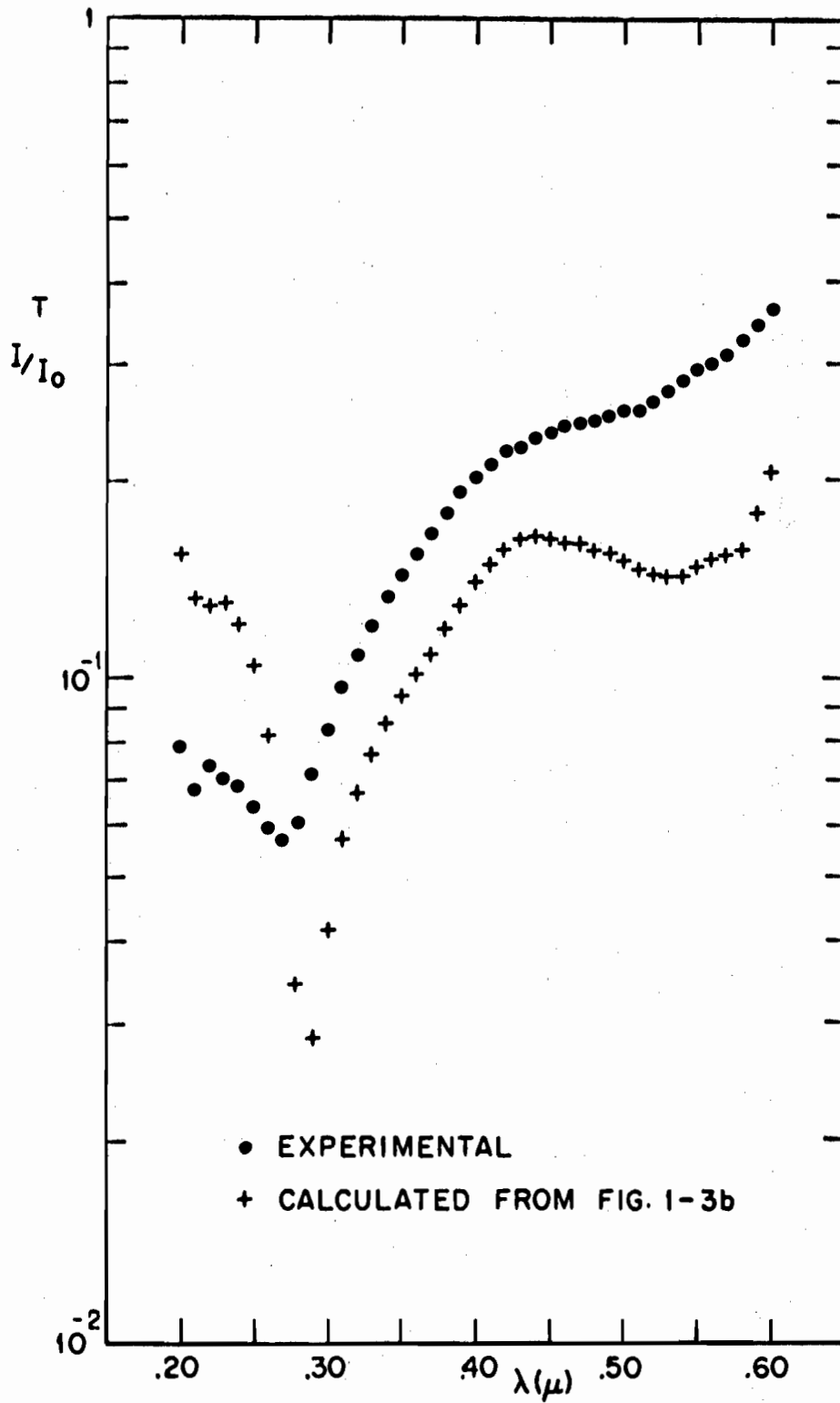


FIG. 4-13b TRANSMISSION OF A 135 Å EPITAXIAL GERMANIUM FILM ON CaF₂.

used were cut from the same fused quartz slide, washed in HNO_3 and two baths of acetone and then dried in an N_2 stream. During the experiment where T_S was varied, reasonable efforts were made to keep Δ constant; however, when the substrate temperature was raised to 780°C , re-sublimation from the substrate was rapid enough to require the increase of Δ to a higher value in order to form a film. In addition, the variation of the deposition parameters produced films of different thickness. This means that the difference in reflectivities among the films in the longer wavelength regions will in large part be due to differences in interference effects. However, at the Σ , X peak all films are thick enough so that comparisons of their reflectivities in this region are meaningful. The interpretation of Figs. 4-6 through 4-9 will be given in Section C.

2. Results for Cleaved CaF_2 Substrates.

Altogether 47 epitaxial films deposited on CaF_2 were examined. Forty-four were produced in this laboratory and three were obtained from workers elsewhere. The films were examined visually for evidence of surface roughness according to the recipe of Chapter Two, Section A-4. When such roughness was apparent, no further measurements were made. For those not displaying this effect, reflectivity measurements were taken at wavelengths of 5300 \AA , 3500 \AA , and 2800 \AA

and the data recorded. Films having relatively high reflectivity at 2800 \AA were scanned to obtain their entire reflectivity spectrum from 2000 \AA to 6000 \AA , and, if thin enough, their transmissivities were also measured. Figure 4-10 shows the RED patterns and Figs. 4-11, 4-12, and 4-13 the optical response of three typical films differing widely in thickness. These films are by no means to be regarded as unique occurrences; in fact, in each case other films were made under identical conditions and they displayed nearly the same optical response as those shown. Deposition rates and substrate temperatures were kept reasonably constant at values thought to produce films with minimum roughness yet good crystalline quality (see Chapter Two).

Optical measurements were also made on three films received from the University of Virginia Materials Science Department [4]. These films were grown under conditions of substrate temperature 300°C and ambient pressure $5 \cdot 10^{-8}$ torr. When these films were examined by RED, they were epitaxial but contained a superposed twin patterns whose spots were almost as intense as the basic {111} Laue pattern. The usual interband transition structure in the reflectivity spectrum was quite weak and none of the films displayed distinctly the spin-orbit split Λ peaks. None of the films was thin enough for transmission measurements.

The effect of ambient pressure on film perfection was mentioned briefly in Chapter Two, Section D where it was stated that the results are at present inconclusive. We have made independent experiments using a Varian Vac-Ion vacuum system capable of attaining pressures of $\sim 10^{-9}$ torr before deposition and $\sim 10^{-7}$ torr during deposition. The source material was heated by electron beam bombardment and the substrate temperature was kept at $\sim 500^{\circ}\text{C}$. This system was made available to us through the courtesy of Dr. M. G. Holland of the Research Division of the Raytheon Corporation, Waltham, Mass. The optical response of the films produced in this system under the above conditions did not differ appreciably from those presented here, even when the substrate was cleaved in high vacuum prior to deposition.

C. INTERPRETATION OF RESULTS

1. Effect of Film Crystalline Perfection.

In this subsection we will discuss structure in the film R and T spectrum as opposed to over-all optical response amplitudes which will be discussed in the next subsection. Using the reflectivity spectrum of bulk single crystal germanium as our standard, we would expect that the greater the crystalline order of the film, the closer the structure will duplicate that of bulk material. An examination of Figs. 4-5 through 4-13 shows that this is definitely true. Each of our epitaxial films has all of the principal

structure indicated by the bulk reflectivity, including the Λ spin-orbit splitting. This is most strikingly brought out by Fig. 4-11 for the 1850 Å film (the shift of the Λ peaks will be discussed later in Subsection 3). Even the 135 Å film, which is only about 25 atoms thick, reveals the structure predicted by bulk measurements, and, in fact, the proper structure was also observed in still thinner epitaxial films. The RED patterns indicate the presence of stacking faults and twins in each of our epitaxial films; however, their effect on the film optical response is not known at the present time.

The RED results for the **multisubstrate temperature series** on fused quartz show a progression from sharp, textured Debye-Scherrer-Hull rings at 780°C to broad, diffuse DSH rings at 25°C, as indicated in Fig. 4-6. At the higher temperatures, one can see regular intensification of the rings which signify the presence of $\langle 110 \rangle$ preferred orientation in the film normal to the substrate. Thus, we see that the higher the substrate temperature, the greater the crystalline ordering, in agreement with the discussions of Chapter Two. The reflectivity structure of this series shows a strong temperature dependence. Referring to Fig. 4-7, the 780°C film, curve 1, possesses all of the bulk structure, except that the Λ spin-orbit split peaks are severely distorted. As T_S decreases, clear evidence of these peaks disappears; however, the

Σ , X peak retains its identity until $T_S = 300^\circ\text{C}$, where pronounced distortion sets in. From Fig. 4-6, we see that at this temperature all indications of preferred orientation are gone and the DSH rings begin to broaden considerably, pointing out the breakdown of long-range crystalline order. At 25°C , the RED pattern shows that long-range order is gone, which results in the complete deterioration of the Σ , X peak.

The interpretation of the behavior of the reflectivity on crystalline order will center on the Λ peaks and the over-all reflectivity structure. It might be expected that polycrystalline germanium would have the same optical response as single crystal germanium and this is true up to a point. However, it is clear that ultimately the crystallite size can become so small that long-range order is drastically reduced. Tauc, et al. [5], interpret the resulting reflectivity spectrum as that which would occur for interband transitions with only energy conserved. That is, strong singularities in the joint density of states no longer appear due to the breakdown of symmetry and all interband transitions can be considered as indirect. This interpretation would account for the loss of sharp reflectivity structure as one proceeds to the amorphous state. **However, it is well known that relatively** small distortions in the crystalline order can affect the amplitudes of Λ spin-orbit split peaks [3, 6]. Donovan and

Ashley [3] have studied this problem using polycrystalline films and polished bulk surfaces, and on the basis of their results have suggested that in the bulk material "the observed structure in the reflectance in the region of 2 eV results from a combination of the L and Λ transitions or that the 2.3 eV peak corresponds to transitions at the Λ point and the peak at 2.1 eV corresponds to transitions at the L point." That neither of these deductions is wholly correct can be reasoned as follows:

(a) Neither explanation accounts in a clear manner for the theoretically predicted spin orbit splitting [7].

(b) The calculations of Brust [8] indicate that the $L_3' \rightarrow L_1$ transition has a joint density of states of Type M_0 which has the wrong shape to cause a peak in the reflectivity spectrum.

(c) Pressure measurements of Zallen [9] show that both peaks have the same pressure coefficient, as would be expected if they arose at the same point in the band.

(d) The L transitions have actually been observed apart from the Λ transitions by Greenaway [10] for GaAs and by Cardona and Greenaway [11] for ZnTe and CdTe.

In the case where the peaks are distorted due to polycrystalline film structure or polished bulk surfaces, a simpler explanation of either increasing the relative difference between the amplitudes of the two peaks or reversing their magnitudes is

that induced stresses, or reduction of long-range order, cause small changes in the respective density of states of the Λ transitions which bring about the above observations.

2. Effect of Surface Topography and Film Thickness.

From the discussion of Chapter Two, Section D, we should expect to find the reflectivity amplitudes affected by surface roughness scattering which in turn can be correlated with deposition parameters. The Σ , X peak amplitudes of the films shown in Fig. 4-7 clearly indicate this correlation. The 780 Å film had a surface roughness visible under an optical microscope in addition to sharp DSH rings denoting large grain size, and we see that its Σ , X amplitude is considerably depressed from the approximately 70% of Fig. 4-5, whereas the smoother 600°C film has a value of 64%. The amplitude of the 600°C film 2 of Fig. 4-7 agrees well with Donovan and Ashley's [3] best result for fused quartz substrates of 66% with the remaining difference between these values and the bulk value being most likely a residual roughness effect. The difference between the 780°C film and the 600°C film is consistent with the conclusions of Chapter Two, Section D, namely, the higher the substrate temperature for a given deposition rate, the greater the agglomeration and roughness and hence the poorer the reflectivity. For substrate temperatures below 600°C, loss of long-range order as

well as roughness degrade the reflectivity. However, according to Chapter Two, Section D, amorphous films should be smoothest of all. If this is true, then the reflectivity of amorphous films should be the same as that of smooth bulk crystalline surfaces in the far ultraviolet, as the optical response in this region is due to valence band plasma oscillations which are relatively independent of long-range order. This has been observed to be the case by Tauc, et al. [5], who also explain the deviation of the Σ , X peak amplitude (whose reflectivity was 55%) of their polycrystalline film from the bulk value as due to surface roughness scattering.

Figures 4-8 and 4-9 give the results of the **multideposition** rate series of films on fused quartz. We see that this parameter does not influence either crystalline quality or reflectivity as strongly as does T_S . All of the RED patterns appear identical except for intensity differences caused by variations in exposure times. The differences in amplitude among the Σ , X peaks may or may not be significant. Their magnitudes and shapes are **nearly** identical. The most cautious conclusion would seem to be that over the range of Δ shown, the film crystalline and optical properties are reasonably constant.

In Chapter Two, Section D, evidence for the presence of surface roughness for epitaxial films on CaF_2 was given. In Fig. 4-11, we see that the reflectivity of the 1850Å film, thick enough to

suppress interference for $\lambda < 6000 \text{ \AA}$, falls below that of bulk material by an amount which increases with decreasing λ . It has been shown by Porteus and Bennett [12] that the following relation for the reflectance of a rough surface

$$R = R_0 \exp[-(4\pi\sigma/\lambda)^2], \quad (4-1)$$

where R_0 is the reflectivity of a perfectly smooth surface of the same material and σ , the RMS value of the deviations from mean thickness, is valid under the following assumptions:

- (a) The surface irregularity distribution must be gaussian.
- (b) The reflected light must be coherently scattered from the surface, a condition which holds for $\sigma/\lambda \ll 1$.

The reader interested in further experimental and theoretical details should consult reference 12. The ratio of the reflectivity of the 1850 \AA film to that of the bulk reflectivity given in Fig. 4-5 as a function of $1/\lambda^2$ is shown in Fig. 4-14. It is seen to yield approximately a straight line in agreement with equation (4-1) and its attendant conditions and gives a value for σ of 76 \AA . By way of comparison, we might point out that the RMS roughness of the usual variety of microscope slide is about 10 \AA to 15 \AA . Equation (4-1) predicts that as $\lambda \rightarrow \infty$, $R \rightarrow R_0$; however, Fig. 4-14 shows that $R \rightarrow .91 R_0$. This 9% difference can be explained as a constant systematic error in the film reflectivity due to misalignment and

poor optical imaging because of the cleaved surface. For the 250\AA film of Figs. 4-12 we may perform a similar analysis by using only the reflectivity in the region below 3500\AA where interference is **small** and extrapolating to infinite wavelength. This procedure leads to $\sigma = 50\text{\AA}$ and $R_{\infty} = .95 R_0$. In addition, we see from Fig. 4-12b that the roughness is not without its effect on the UV transmittance where T of the film falls below its theoretically predicted value by about 50% at $\lambda = 2000\text{\AA}$.

Figure 4-13 shows the optical response of a film whose thickness was measured by infrared transmission to be 135\AA . We see that the experimental values of R and T depart considerably from the corresponding theoretical values for this thickness, T measured being higher than T calculated (except in the far UV region) with the reverse true for R . This behavior was observed in each of our very thin films, thus the film of Fig. 4-13 is not a mere variant. The RED pattern for this film shows sharp Laue spots indicating epitaxy, and Fig. 4-13 confirms the presence of the appropriate interband structure. The disparity in amplitudes is probably due to the breakdown of coherent interference effects when the RMS roughness of the film approaches an appreciable fraction of the mean film thickness. This results in phase averaging or intensity addition (discussed in Chapter Three) for the theoretical R and T expressions. The scattering will not be as strong for IR

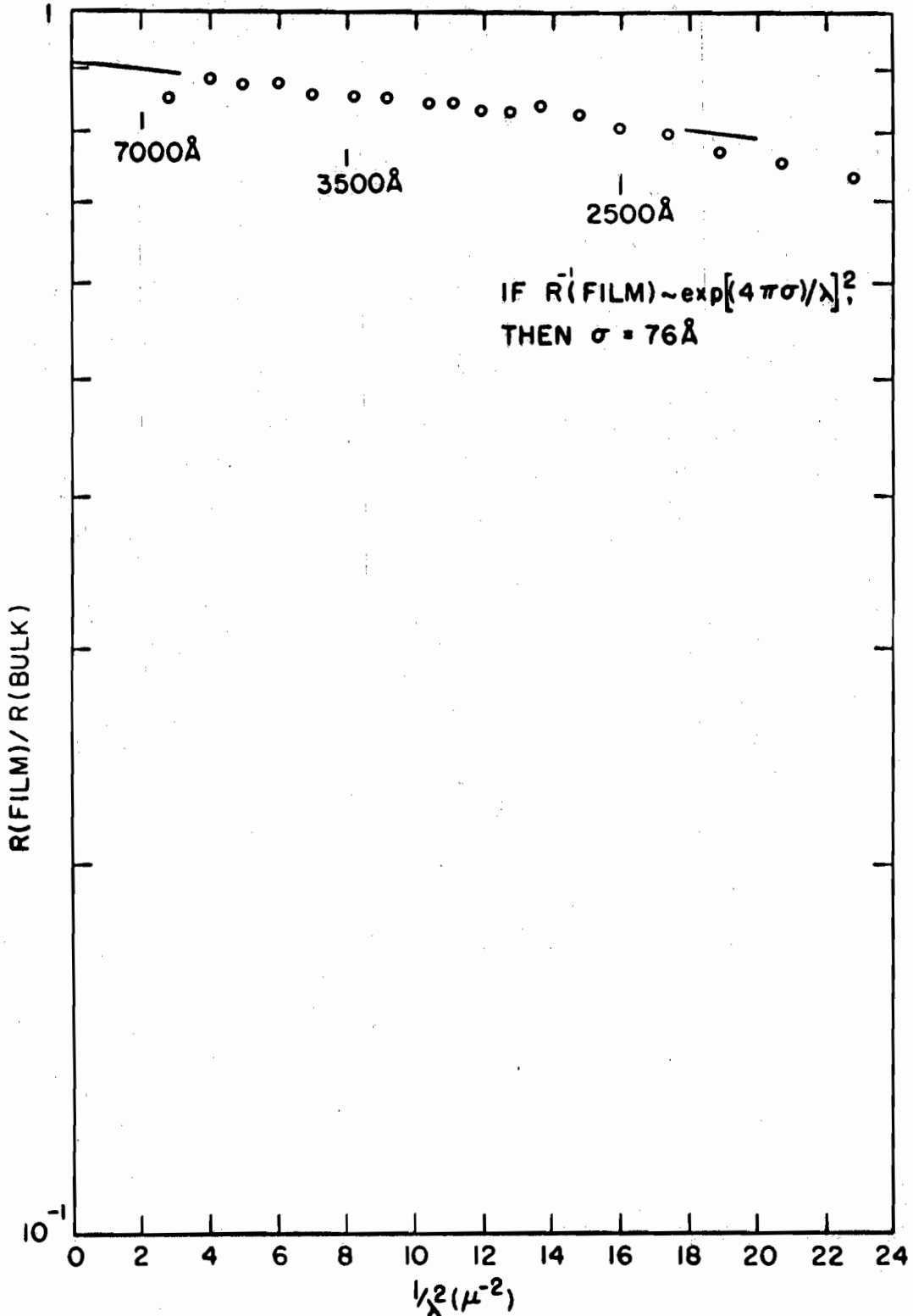


FIG. 4-14 ROUGHNESS PLOT FOR THE 1850 Å EPITAXIAL Ge FILM ON CoF2.



wavelengths; therefore, a measurement of transmission in this region will contain interference effects. However, for the small film thicknesses under consideration ($\sim 100 \text{ \AA}$), a small change of -2% in T can cause a change of $+30 \text{ \AA}$ in the derived thickness. When phase averaged theoretical values of R and T were calculated, their effect was to shift the IR transmission to lower values (higher thicknesses) and the visible to higher. Essentially our difficulty is this: the IR and visible measurements of transmissivity are incompatible with each other for any assumed thickness and we must fix on one or the other as being more in accord with theory. In addition to reasons already mentioned, it seems plausible to accept the IR measurement and derive the thickness therefrom because its measured T was $.880$ at 2.0μ compared with a calculated phase averaged T of $.519$, implying interference effects are still strongly present. On the other hand, phase averaged calculations at 6000 \AA give $T = .287$ showing that the effect of interference in this range is to make T lower than the phase averaged value, whereas in the IR the opposite was true. Hence, we see that the observed behavior can be in part explained as due to the progressive loss of interference as one moves to shorter wavelengths.

The effect of thickness on film optical constants has, as far as is known, never been theoretically treated. We were unable to

investigate the effect experimentally because of the roughness-coherence difficulties discussed above; however, we would like to make a few conjectures about what might be expected should suitable samples become available. The problem seems to be divided into two aspects: (1) the perturbative effect of the finite boundary on the bulk energy levels, and (2) the "quantitization" of k space in the direction normal to the film surface into intervals of $2\pi/Na$ where N is the number of atoms and a the lattice constant. Of these, the second has the interesting possibility of giving the joint density of states a two-dimensional character and of splitting interband transitions which occur between bands of non-zero slope.

3. Effect of Induced Strains in the Films.

Because of the difference in thermal expansion between the film and the substrate, there will appear an induced strain in the film as it is cooled from its formation temperature. The effect of this strain is clear from Fig. 4-5 where it is apparent that both the Λ peaks and the Σ , X peak are shifted to higher energies in the film. In treating this phenomenon, we will make the following idealizations:

(a) The film and substrate will be assumed to be isotropic, homogeneous, and temperature independent in their thermal expansion properties.

(b) The substrate will be taken as much more massive than the film so that the film will be assumed not to constrain the expansion of the substrate in any way.

(c) We will consider the resulting induced stress in the film as if it arose from forces applied at faces of the film edges or sides.

The basis for finding the induced effective stress is that elongations of both film and substrate are necessarily equal.

This leads to a stress of the form:

$$X = \frac{(\alpha_{\text{Ge}} - \alpha_{\text{CaF}_2})\Delta T}{S} \quad (4-2)$$

where the α 's are the appropriate linear thermal expansion coefficients. ΔT the temperature change, and S and X are the appropriate Young's modulus and induced stress, respectively, for the direction of elongation under consideration. For a film whose axis of epitaxy is [111], the [1 -10] and [-1 -12] directions along with [111] form a mutually orthogonal set of which [1 -10] and [-1 -12] may be considered the direction of the applied stress given by equation (4-2). For each of these directions, S becomes:

$$S = \frac{1}{2} \left(s_{11} + s_{12} + \frac{s_{44}}{2} \right) \quad (4-3)$$

where s_{11} , s_{12} , and s_{44} are the compliance constants. For room temperature values of $\alpha_{\text{Ge}} = 5.75 \cdot 10^{-6}/^{\circ}\text{C}$ [13], $\alpha_{\text{CaF}_2} = 19.5 \cdot 10^{-6}/^{\circ}\text{C}$ [14]; $s_{11} = .97 \cdot 10^{-6}/\text{atm}$, $s_{12} = -2.63 \cdot 10^{-7}/\text{atm}$, and $s_{44} = 1.50 \cdot 10^{-6}/\text{atm}$

[12], with $\Delta T = -575^\circ\text{C}$, equations (4-2) and (4-3) give $X = 10,800$ atm compression.

Brooks's equation for the shift of an energy band under strain may be written as [15]:

$$\delta E = E_1 \text{Tr } \underline{u} + E_2 \hat{k} \cdot \left(\underline{u} - \frac{1}{3} \underline{1} \text{Tr } \underline{u} \right) \cdot \hat{k} . \quad (4-4)$$

Here E_1 and E_2 are deformation potentials (E_1 is directly related to the hydrostatic pressure coefficient), \hat{k} is the unit vector in k space to the band edge in question and \underline{u} is the strain tensor. In the following discussion, we will take δE , E_1 , and E_2 to refer to differences in energy transitions instead of band edges. For purposes of discussion, we note that the stress tensor for hydrostatic pressure is

$$\underline{\sigma}_{\text{HSP}} = -X \begin{pmatrix} 1 & 0 & 0 \\ 0 & 1 & 0 \\ 0 & 0 & 1 \end{pmatrix} \quad (4-5)$$

for which the generalized Hooke's Law in conjunction with (4-4) gives:

$$\delta E = -3 E_1 (s_{11} + 2 s_{12}) X \quad (4-6)$$

where X is of course the pressure. This relates E_1 to $\partial E / \partial P$.

For applied biaxial stress X in the $[1 -10]$ and $[-1 -12]$ directions, the stress tensor is:

$$\underline{\sigma} = \frac{X}{3} \begin{pmatrix} 2 & -1 & -1 \\ -1 & 2 & -1 \\ -1 & -1 & 2 \end{pmatrix} . \quad (4-7)$$

Hooke's Law and (4-4) yield for the $\Lambda_3 \rightarrow \Lambda_1$ transition in the [111] direction:

$$\delta E_{[111]}^{\Lambda} = 2 E_1^{\Lambda} (s_{11} + 2 s_{12}) X - \frac{1}{3} E_2^{\Lambda} s_{44} X \quad (4-8)$$

On the other hand, for Λ transitions in [1 -11] type directions, we have:

$$\delta E_{[1 -11]}^{\Lambda} = 2 E_1^{\Lambda} (s_{11} + 2 s_{12}) X + \frac{1}{9} E_2^{\Lambda} s_{44} X \quad (4-9)$$

A similar analysis for the Σ , X transition gives:

$$\delta E_{[100]}^X = 2 E_1^X (s_{11} + 2 s_{12}) X \quad (4-10)$$

$$\delta E_{[110]}^{\Sigma} = 2 E_1^{\Sigma} (s_{11} + 2 s_{12}) X - \frac{1}{6} E_2^{\Sigma} s_{44} X \quad (4-11)$$

$$\delta E_{[1 -10]}^{\Sigma} = 2 E_1^{\Sigma} (s_{11} + 2 s_{12}) X + \frac{1}{6} E_2^{\Sigma} s_{44} X \quad (4-12)$$

We see that there is always a part related to hydrostatic pressure in addition to the shear component which lifts the degeneracy of otherwise equivalent transitions. The detection of this splitting was beyond the resolution of our experiments and its principal effect was probably to broaden slightly the reflectance peaks of the films.

Philipp, Dash, and Ehrenreich [16] have performed uniaxial stress measurements on the Λ transition of Ge. Using their value of $E_2^{\Lambda} = -2.0 \text{ eV}^\dagger$ and $E_1^{\Lambda} = -5.6 \text{ eV}$ calculated from Zallen's [9] value of the hydrostatic pressure coefficient, we obtain

[†]This number was calculated from data contained in references 16 and 9. The value of E_2^{Λ} actually given in reference 16 is believed to be in error.

$$\delta E_{[111]}^{\Lambda} = (-4.0 \times 10^{-6} \text{ eV/atm}) X \text{ and } \delta E_{[1-11]}^{\Lambda} = (-5.3 \times 10^{-6} \text{ eV/atm}) X.$$

As there are three times as many $\langle 1-11 \rangle$ transitions as $\langle 111 \rangle$, we will take the over-all shift to be the weighted average of $\delta E_{[111]}^{\Lambda}$ and $\delta E_{[1-11]}^{\Lambda}$ or $\delta E^{\Lambda} = (-5.0 \times 10^{-6} \text{ eV/atm}) X$. From Fig. 4-15, we have $\delta E^{\Lambda} = 44 \pm 10$ millieV as the observed mean shift of the Λ doublet which implies a value of 8800 ± 2000 atm for the induced biaxial compressive stress, as compared with the previously calculated value of 10300 atm from thermal expansion.

E_1 and E_2 for the Σ , X transition are not known at present. However, an estimate can be made of E_1 from the pressure coefficient for the Σ , X transition in silicon measured by Zallen to be $3 \cdot 10^{-6}$ eV/atm [9]. There is an empirical rule which states that among semiconductors with similar band structures, the pressure coefficients for transitions at identical symmetry points of their Brillouin zones are approximately equal [17]. We therefore take Zallen's result to hold for germanium also. For purposes of calculation, we will assume $E_1^X = E_1^{\Sigma}$ and $E_2^{\Sigma} = 0$. From Fig. 4-15, $\delta E^{X,\Sigma} = 33 \pm 12$ millieV which results in $X = 16500 \pm 6000$ atm compressive biaxial stress. The factor of two difference in the Λ and Σ , X results cannot, at present, be attributed to anything except experimental error. Although the shift of the reflectivity was observed in all of our films, it was carefully measured only in the 1850 Å film of Figs. 4-11 and 4-15.

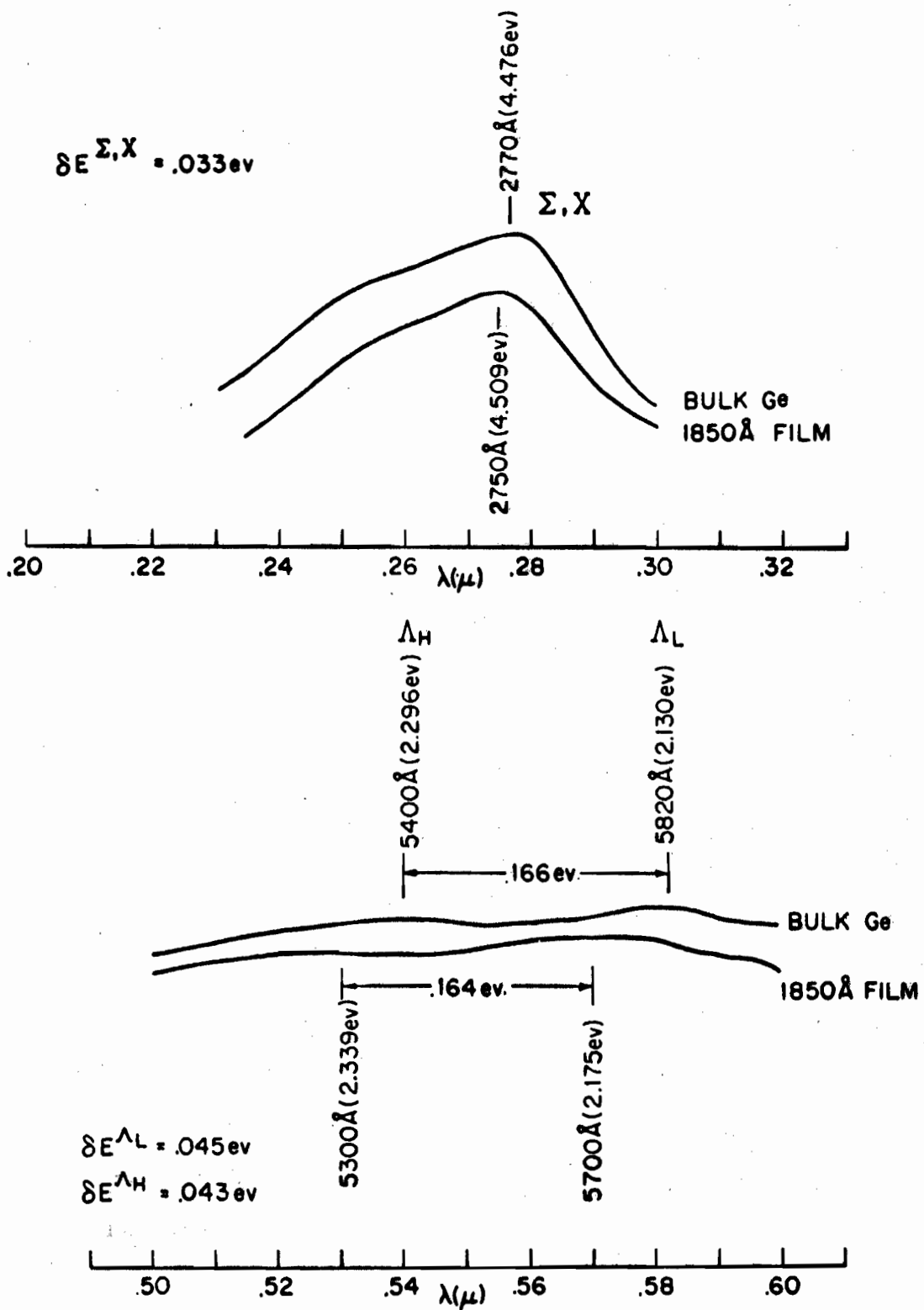


FIG. 4-15 EFFECT OF FILM STRESS ON REFLECTIVITY PEAKS.

It is interesting to note that because the force which effects the stress in the film is actually applied at the film-substrate interface, a bending moment arises which tends to lift the film away. This bending moment increases with film thickness until rupture takes place, thus setting an upper limit on the film thickness for a given substrate temperature. For $T_S = 600^\circ\text{C}$, the critical thickness appears to be around 3000\AA to 4000\AA as deduced from observations of thick films that rapidly broke up immediately after deposition.

4. Comparison with Other Work.

The most recent works on the optical response of thin germanium films have been by Donovan and Ashley [3], Tauc, et al. [5], and Cardona and Harbeke [18]. The relationship of our work to that of references 3 and 5 has been discussed above. However, in these two the film transmission was not measured. Cardona and Harbeke have measured the transmission (but not reflectivity) of several rather thick epitaxial films on CaF_2 . Although their total results account for the proper structure, only one film was thin enough (500\AA) for measurements down to the Σ , X transition (which appeared quite weak) and this film did not display the Λ doublet. Also, the magnitude of their transmissivities is in great disagreement with those calculated from bulk optical constants for

the stated thicknesses; however, it must be conceded that the accurate measurement of such magnitudes was not the object of their work and to belabor their inaccuracies would be unfair. In conclusion, then, we may state that the results for R and T presented for epitaxial films in this chapter are the first in which close attention has been paid to obtaining film optical response which matches that predicted by bulk results in both structural and amplitude aspects.



Chapter Four

BIBLIOGRAPHY

- [1] T. M. Donovan, E. J. Ashley, and H. E. Bennett, *J. Opt. Soc. Am.* 53, 1403 (1963).
- [2] H. Philipp and H. Ehrenreich, *Phys. Rev.* 129, 1550 (1963).
- [3] T. M. Donovan and E. J. Ashley, *J. Opt. Soc. Am.* 54, 1141 (1964).
- [4] A. Catlin, A. J. Bellemore, Jr., and R. R. Humphries, *J. Appl. Phys.* 35, 251 (1964).
- [5] J. Tauc, A. Abraham, L. Pajasova, R. Grigorovici, and A. Vancu, Optical Properties of Non-Crystalline Semiconductors (Proceedings of the International Conference on Physics of Non-Crystalline Solids, Delft, 1964).
- [6] J. Tauc and E. Antoncik, *Phys. Rev. Letters* 5, 253 (1960).
- [7] L. Roth and B. Lax, *Phys. Rev. Letters* 3, 217 (1959).
- [8] D. Brust, *Phys. Rev.* 134, A1337 (1964).
- [9] R. Zallen, W. Paul, and J. Tauc, *Bull. Am. Phys. Soc.* 7, 185 (1962);
R. Zallen, Technical Report No. HP-12 (Contract Nonr-1866 (10), NR-017-308), Gordon McKay Laboratory of Applied Science, Harvard University, 1964 (unpublished).
- [10] D. Greenaway, *Phys. Rev. Letters* 9, 97 (1962).
- [11] M. Cardona and D. Greenaway, *Phys. Rev.* 131, 98 (1963).
- [12] H. Bennett, *J. Opt. Soc. Am.* 53, 1389 (1963); J. Porteus, *J. Opt. Soc. Am.* 53, 1394 (1963); H. Bennett and J. Porteus, *J. Opt. Soc. Am.* 51, 123 (1961).
- [13] See Chapter Two, reference 10.
- [14] See Chapter Two, reference 8.

- [15] H. Brooks, Advances in Electronics and Electron Physics, ed. by L. Larton (Academic Press, New York, 1956), vol. 7; R. W. Keyes, Solid State Physics, ed. by F. Seitz and D. Turnbull (Academic Press, New York, 1960), vol. 11.
- [16] H. Philipp, W. Dash, and H. Ehrenreich, Phys. Rev. 127, 762 (1962).
- [17] W. Paul, J. Appl. Phys. 32, 2082 (1961); R. Zallen and W. Paul, Phys. Rev. 134, A1682 (1964).
- [18] M. Cardona and G. Harbeke, J. Appl Phys. 34, 813 (1963).

Chapter Five

ANALYSIS OF EXPERIMENTAL RESULTS

A. NUMERICAL ANALYSIS AND PROGRAMMING TECHNIQUES

1. The Newton-Raphson Method.

The Newton-Raphson method is an iterative procedure for finding the real roots of an algebraic or transcendental equation [1]. We will make use of the form which applies to multivariate simultaneous equations. In Chapter Three we constructed the theory necessary for the determination of the optical constants. We now describe a way in which these optical constants can be obtained rapidly from the experimental data. In the discussion to follow, we will frame our remarks in terms of the RT model; the extension to the two thickness, two transmission method will be obvious.

We recall from equations (3-19) that:

$$R(n, k) - R = 0 \quad (5-1a)$$

$$T(n, k) - T = 0 \quad (5-1b)$$

where $R(n, k)$ and $T(n, k)$ represent the functional dependence on n and k given by the right-hand sides of equations (3-6) while R and T are the observed quantities. As far as is known there is no explicit solution to equations (5-1). Therefore, we must find the roots n and k by some numerical procedure. Let us assume that we know the approximate values of the roots, namely n_0 and k_0 ,

and that the roots are given by:

$$n = n_o + \Delta n \quad (5-2a)$$

$$k = k_o + \Delta k \quad (5-2b)$$

where Δn and Δk are the necessary corrections to n_o and k_o .

Applying Taylor's theorem to equations (5-1) yields:

$$\begin{aligned} R(n, k) - R &= R(n_o, k_o) - R + (n - n_o) \left(\frac{\partial R}{\partial n} \right)_o \\ &+ (k - k_o) \left(\frac{\partial R}{\partial k} \right)_o + O(\Delta n^2, \Delta k^2) = 0 \end{aligned} \quad (5-3a)$$

$$\begin{aligned} T(n, k) - T &= T(n_o, k_o) - T + (n - n_o) \left(\frac{\partial T}{\partial n} \right)_o \\ &+ (k - k_o) \left(\frac{\partial T}{\partial k} \right)_o + O(\Delta n^2, \Delta k^2) = 0. \end{aligned} \quad (5-3b)$$

If we further assume Δn and Δk to be small enough to neglect their higher-order terms, then we have immediately:

$$n - n_o = \left((R - R(n_o, k_o)) \left(\frac{\partial T}{\partial k} \right)_o - (T - T(n_o, k_o)) \left(\frac{\partial R}{\partial k} \right)_o \right) / J \quad (5-4a)$$

$$k - k_o = \left((T - T(n_o, k_o)) \left(\frac{\partial R}{\partial n} \right)_o - (R - R(n_o, k_o)) \left(\frac{\partial T}{\partial n} \right)_o \right) / J \quad (5-4b)$$

where

$$J = \left(\frac{\partial R}{\partial n} \right)_o \left(\frac{\partial T}{\partial k} \right)_o - \left(\frac{\partial R}{\partial k} \right)_o \left(\frac{\partial T}{\partial n} \right)_o \quad (5-5)$$

The roots may now be found to any desired degree of accuracy by repeated applications of these **formulas with the improved values** of n and k substituted at each step. We see that equation (5-5)

corresponds identically to equation (3-16) We also see that when n and k are such that singularities occur in the error derivatives, **the above iteration procedure diverges.**

2. Programming Operations.

In order to carry out the Newton-Raphson iteration efficiently, the services of a digital computer are needed. Figure 5-1 shows the flow chart of a program which was written in the FORTRAN language for the IBM 7094 data processing system in order to perform this calculation. However, there is nothing unique about this particular data processing system which disqualifies any other for application to this problem. In fact, a similar program was written in 1955 by Loeb and Denman [2] for the M.I.T. Whirlwind I digital computer.

Referring to Fig. 5-1, the program begins by reading in a card which supplies the film thickness for all data to follow. This data consists of a group of cards containing trial values of the optical constants and the experimental R and T for a given wavelength. The trial n and k are used as the initial guesses in the iteration procedure. They are usually the Kramers-Kronig results. If, however, these trial values are left blank, the program switches to an automatic root-finding mode as shown in the figure. The purpose of this feature is to allow the procurement of all possible pairs of real roots within a given range of n and k. Examination

of equations (3-19) and (3-6) reveals that the number of possible roots is generally indeterminate. This is also shown by the root-locus diagrams Figs. 3-6 through 3-9. The area of n and k to be searched by the program is 0 to 10 for both constants. The program was almost always run in the automatic mode.

Enough iterations were performed so that by using the results of the most recent iteration, the calculated values R' , T' would equal the experimental values R , T to within three significant figures. If this did not occur by the 20th iteration, the program would assume that divergence was taking place and print out a statement to this effect along with the results of the last iteration. When the work for the wavelength under consideration was finished, the data for the succeeding one would be read in. After the data had been exhausted, the FORTRAN monitor system automatically terminated the program. The running time to compute the optical constants for 41 wavelengths (6000 Å to 2000 Å in 100 Å intervals) in the automatic mode was approximately two minutes. The calculations for Chapter Three were effected by separately using the arithmetic subroutine which calculates R' , T' , and the various derivatives.

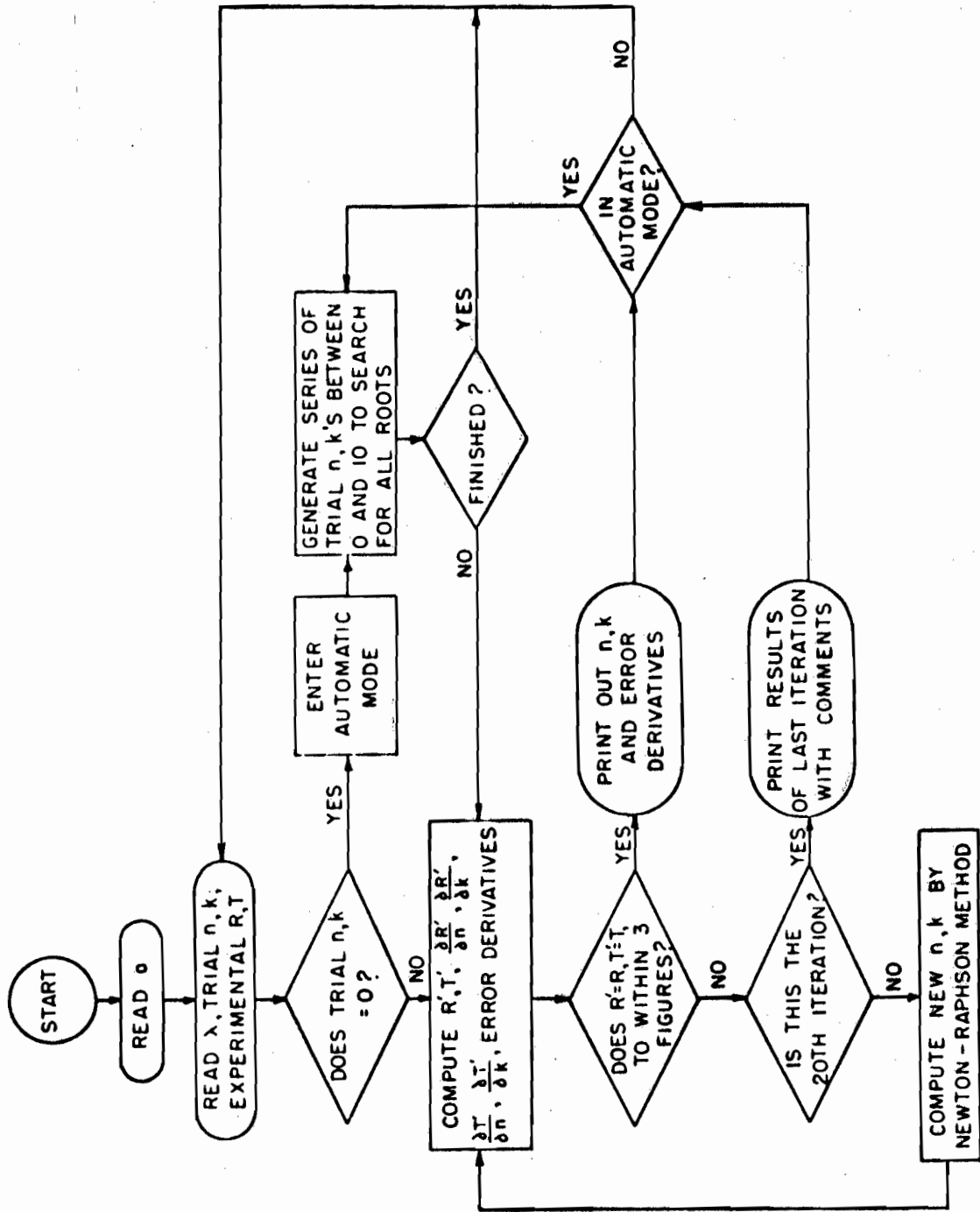


FIG 5-4 FLOW CHART OF OPTICAL CONSTANT CALCULATION PROGRAM.



B. THE OPTICAL CONSTANTS OF THIN GERMANIUM FILMS

The results of Chapters Two, Three, and Four dictate the following criteria for the selection of a film sample from which to calculate the optical constants:

(a) The film crystallinity should replicate that of a bulk single crystal as closely as possible; hence, use should be made of epitaxial films.

(b) The film thicknesses should be chosen so that they fall in the region where experimental error has its minimum effect as indicated by the bar diagrams of Chapter Three.

(c) Deposition conditions should be selected to insure a film with minimal roughness.

Conditions (a) and (b) alone would result in the choice of a 125 Å film for use with the R-T method or of two films, one with thickness $\sim 100\text{Å}$ and the other $\sim 300\text{Å}$, for use with the two thickness, two transmission method. However, the results of Chapter Four show that the optical response of very thin films suffers greatly from scattering effects; therefore, specification (c) forces a compromise choice for the R-T method and practically rules out the use of the two thickness, two transmission method for germanium (although it certainly should be strongly considered for those materials, such as the lead salts, where roughness does not seem to be a serious problem [5]). This compromise is represented by the

250 Å film of Fig. 4-12. The optical constants calculated for the film are shown in Fig. 5-2, where, in performing the calculation, the reflectivity was corrected for roughness according to the experimental quantities $R_{\infty} = .95 R_0$ and $\sigma = 50 \text{ \AA}$. The bars indicate the error spread in n and k for an absolute error in R of $\pm 2.5\%$ and in a of $\pm 10 \text{ \AA}$ and a relative error in T of $\pm 10\%$. We see that the discrepancy between the film values of the optical constants and those of bulk Ge (taken from Fig. 1-3b) can be included, for the most part, within the span of these conservative experimental error estimates. We see also that the region in which no roots appeared, namely, 3000 Å to 4100 Å, corresponds almost exactly to the region predicted by Fig. 3-14a for a 250 Å film as having very high sensitivity to experimental errors in R and T . Reference to Figs. 1-5 will show that the present results are far superior to previous film optical constant work, primarily because of the use of epitaxial films.

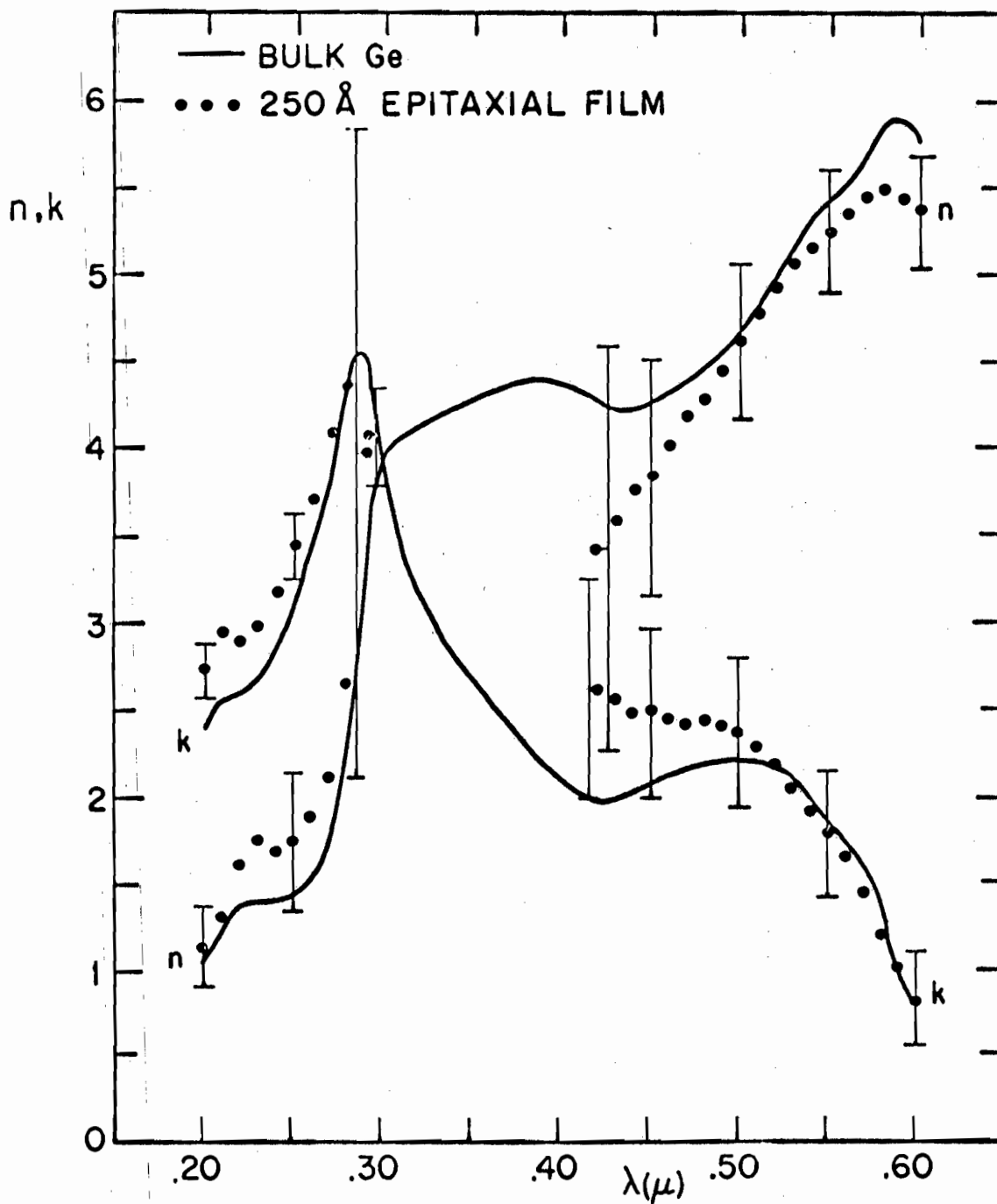


FIG. 5-2 OPTICAL CONSTANTS OF A 250Å EPITAXIAL GERMANIUM FILM.



C. CONCLUSIONS

In Chapter One it was stated that the purpose of this thesis is to demonstrate that the use of epitaxial films now allows the measurement of the optical properties of materials in the film state which can be extended to and correlated with the optical properties of materials in the bulk state. The problem undertaken for detailed study was the determination of the optical constants of germanium from measurements of the reflection and transmission of thin epitaxial films. Before undertaking a discussion of the results, we will state what we believe to be the two main conclusions of this research.

(a) We feel our measurements of R and T and calculation of n and k indicate that, after experimental difficulties have been taken into account, the epitaxial films have essentially the same optical properties as bulk material. Hence we may begin to consider the use of epitaxial films as reliable vehicles for investigation into the optical properties of semiconductors in the high absorption regions.

(b) However, because the theoretical developments of Chapter Three indicate that there will invariably be a region of high sensitivity in the derived n and k to errors in R and T, we may conclude that film determinations of n and k will not supplant, but rather will supplement, other methods such as polarimetry

and dispersion analyses. We have shown that in the region where roots are obtained, the film optical constants compare favorably with the Kramers Kronig result.

With regard to the statement in (a) concerning experimental difficulties, we feel these to be of four types:

(1) Roughness scattering. In Chapters Two and Four we have seen how the presence of granular structure in the film produces scattering effects which reduce reflectivity and destroy coherence. For germanium it appears to be difficult to obtain epitaxial films that do not possess residual roughness. This is because, as pointed out in Chapter Two, Section D, the deposition conditions for epitaxial films are in opposition to the requirements for smooth films. However, there is evidence that the situation is not so severe in the case of epitaxial lead salt films [5]. Roughness is the most serious problem confronting the calculation of the optical constants. However, if the mean film thickness is much larger than the rms surface roughness, its effect may be ignored in transmission and experimentally compensated in reflection. When thickness and roughness are of the same order, coherence is destroyed and it is for this reason that we were unable to apply the two thickness, two transmission method for germanium. Extensions of this research should concentrate on devising methods of producing smooth films, possibly through techniques other than vacuum deposition.

(2) Cleaved surfaces. Our inability to produce high quality polished surfaces on CaF_2 led us to use cleaved surfaces. These cleaved surfaces were smooth microscopically but rough macroscopically. Their result was to produce systematic errors in the reflectivity and transmissivity amplitudes (less so in the latter than in the former). Careful selection of the portion of the sample area to be studied helped minimize this difficulty.

(3) Reflectometer misalignment. The alignment of the sample optics for measuring reflectivity was described in Chapter Four, Section A-1. Because the reflected light ray does not follow the same optical path as the incident ray, there is always some difficulty in aligning to measure absolute reflectivity. In our work, we used as an alignment standard a very carefully etched sample of bulk germanium. In this way we were able to reduce errors associated with this problem by periodically checking our film alignment procedures with our standard.

(4) Stress effects. In Chapter Four, Section C-3, we discussed the energy shift in the characteristic film reflectivity peaks due to the difference in the thermal expansion coefficients of the film and substrate. As a result, we must be cautious in ascribing structure appearing in film optical spectra as being precisely at the same energy as it would appear in the bulk material. However, in relation to the entire film optical response spectrum considered here (2-6 eV) the effect is small (~ 40 millieV) and may be neglected.

In Chapter Four, Section B, we gave the results for the effect of deposition parameters on the reflectivity and crystallinity of films on fused quartz. These results show that both reflectivity and crystallinity have a strong dependence on substrate temperature and a weak dependence on deposition rate. The crystallinity and reflectivity structure improves with increasing substrate temperature; however, the magnitude of the reflectivity becomes degraded beyond a certain substrate temperature due to increasing roughness effects. In this same section, we also presented the optical response of three epitaxial germanium films on CaF_2 . These results indicate interband transition structure corresponding closely to that observed in bulk material, even in the case of films ~ 25 atoms thick.

The results of Chapter Three relating to conclusion (b) above lead us to believe that similar analyses should be undertaken for the dispersion method, polarimetric methods, and other photometric methods in order to determine the efficacy of each for calculating optical constants. The results for the RT method and the two thickness, two transmission method argue eloquently for the necessity of investigating in detail whatever other methods may be chosen in order that experimental conditions may be arranged for optimum results.

It has become apparent since the inception of this research that interest has begun to grow in the optical properties of epitaxial semiconductor thin films. This has been particularly true recently

of the lead salt semiconductors (3-5). It is possible to conceive of several experiments in the range 2 eV to 6 eV for which epitaxial films would be particularly suitable; for example, magneto-optic measurements such as magnetoabsorption and Faraday and Voigt effects, hydrostatic pressure shifts, and photoconductivity investigations are a few of the possible extensions of the research begun in this thesis.

In addition, it may prove more feasible to produce certain transition metal oxides and semiconductor alloys in epitaxial film form than in the bulk state. In fact, it may be possible to control the crystallographic phase of the film by the choice of substrate.

Chapter Five

BIBLIOGRAPHY

- [1] J. B. Scarborough, Numerical Mathematical Analysis (The Johns Hopkins Press, Baltimore, 1950) 2nd ed.
- [2] A. L. Loeb and H. H. Denman, J. Soc. Indust. Appl. Math. 3, 1 (1955).
- [3] R. B. Schoolar and J. R. Dixon (Accepted for publication in Phys. Rev., received Aug. 3, 1964); R. B. Schoolar, Bull. Am. Phys. Soc., Ser. II, 8 516 (1963); P. R. Wessel, Ibid., 516; P. R. Wessel (to be published).
- [4] M. Cardona and D. L. Greenaway, Phys. Rev. 133, A1685 (1964).
- [5] C. E. Rossi (to be published).

ACKNOWLEDGEMENTS

I would like to express my appreciation to the IBM Corporation for the personal financial assistance rendered me during the entire period of my graduate study. I am very much indebted to many kind and generous individuals in this company who have assisted me with advice and counsel in past years. In particular, I would like to mention Mr. Robert A. Reynolds who was the administrator of my IBM graduate study program.

The equipment portion of this project was financed by the Office of Naval Research and I want to record my thanks to this organization for their vital and necessary support.

I learned the technique of epitaxial deposition of germanium from Dr. George Via of the IBM Corporation and I am grateful for his assistance during the initial stages of this research.

The help received from the technical staff of the Semiconductor Group of Harvard is much appreciated. Mr. James Inglis and Mr. Albert Manning constructed much of the experimental apparatus while Mr. David MacLeod assisted in sample preparation.

I am very much in debt to my colleagues for their suggestions and advice. Mr. Bernard Kosicki assisted in the design and construction of the electronic circuitry of the spectrophotometer. Mr. Paul McElroy made several useful suggestions with regard to the spectrophotometer. Discussions of the experimental results with Mr. C. E. Rossi were very much appreciated, as were similar discussions with Dr. Richard Zallen and Mr. Rudolph Ludeke.

I have also enjoyed a stimulating and beneficial correspondence concerning various aspects of this research with Billy W. Sloope of the Virginia Institute for Scientific Research and T. M. Donovan of the China Lake Laboratories.

If a student comes into contact with one or two very fine teachers during his years of formal schooling, he is to be considered quite fortunate. It has been my good luck to have had several. Some who influenced my career at an early stage are members of the faculty of Clarkson College of Technology. However, in this instance I refer to Professor William Paul who has been my thesis advisor at Harvard. I shall always be grateful for his editorial assistance in the preparation of this thesis and for his guidance and advice on the experimental problems that arose during the course of this work. The example he has provided of a highly competent research scientist formed a very valuable part of my educational experience at Harvard.

Unclassified
Security Classification

DOCUMENT CONTROL DATA - R&D

(Security classification of title, body of abstract and indexing annotation must be entered when the overall report is classified)

1. ORIGINATING ACTIVITY (Corporate author) Division of Engineering and Applied Physics Harvard University Cambridge, Massachusetts		2a. REPORT SECURITY CLASSIFICATION Unclassified	
		2b. GROUP	
3. REPORT TITLE THE OPTICAL PROPERTIES OF THIN GERMANIUM FILMS			
4. DESCRIPTIVE NOTES (Type of report and inclusive dates) Interim technical report			
5. AUTHOR(S) (Last name, first name, initial) Grant, Paul Michael			
6. REPORT DATE June, 1965		7a. TOTAL NO. OF PAGES 190	7b. NO. OF REFS 90
8a. CONTRACT OR GRANT NO. None-1866(10)		8a. ORIGINATOR'S REPORT NUMBER(S) Technical Report No. EE-14	
b. PROJECT NO. NR-017-308		8b. OTHER REPORT NO(S) (Any other numbers that may be assigned this report)	
c.			
d.			
10. AVAILABILITY/LIMITATION NOTICES Qualified requesters may obtain copies of this report from DDC. All other persons or organizations should apply to the Clearinghouse for Federal and Scientific Information, 5285 Port Royal Road, Springfield, Virginia 22151.			
11. SUPPLEMENTARY NOTES Supported in part by the Division of Engineering and Appl. Phys., Harvard University, Cambridge, Massachusetts		12. SPONSORING MILITARY ACTIVITY Office of Naval Research Department of the Navy Washington, D. C.	
13. ABSTRACT This report describes an investigation into the optical properties of thin germanium films. The central topic is the deduction of the optical constants from photometric measurements on epitaxial films on CaF_2 in the wavelength range 2000-6000 Å. Methods of film production are discussed and the effect of deposition parameters on the crystallinity and reflectivity of films on fused quartz and CaF_2 are reported. The principal conclusion is that epitaxial films give excellent agreement with bulk single crystal material as regards interband transition structure in their reflectivity and transmissivity coefficients R and T. However, the overall amplitudes of R and T for films are strongly governed by residual surface roughness effects. These cause the magnitude of R, in the region 2000-3500 Å, to depart considerably from that of carefully prepared bulk surfaces. Theoretical studies are carried out on the accuracy of derivation of the optical constants n and k from measurements of normal incidence R and T on a single film. Another model also considered is the recovery of n and k from measurements of the transmissivities of two films of different thicknesses. For each of these methods, the first-order dependence of n and k on the photometric quantities was calculated using appropriate theoretical equations and optical constants from dispersion analyses. The results indicate that for the R and T method, in the wavelength regions where $n \approx k$, the error in the derived optical constants becomes intolerably large for the usual experimental errors in R and T. For the two-thickness, two-transmission method, however, certain judicious choices of thicknesses can reduce the sensitivity to experimental error to reasonable values over the entire wavelength range considered here. (Continued)			

14. Key Words

Link A		Link B		Link C	
Role	Wt	Role	Wt	Role	Wt

Thin films
Semiconductors
Germanium
Optical properties
Epitaxial films
Optical constants

ABSTRACT, Continued

A review is given of previous investigations and measurements of the optical properties and constants of germanium thin films. This review shows that the results are much at variance among themselves, due to lack of crystalline perfection in the samples studied. The results for n and k reported in this work were computed from measurements of R and T on a 250 Å epitaxial germanium film on CaF_2 . They are shown to give much better agreement with optical constants from dispersion analysis than those of earlier workers. In addition, with the inclusion of experimental error, the present results overlap those of the dispersion analysis in those wavelength ranges in which it was possible to obtain roots.

Thus, the conclusion of this research may be summarized as follows:

(1) The optical properties of epitaxial germanium films replicate bulk single crystals to a degree sufficient to justify their consideration as vehicles for further optical research into the high energy, high absorption spectral regions.

(2) The use of epitaxial semiconductor films to calculate optical constants will supplement, but not supplant, other methods such as polarimetry and dispersion analysis. (Author)

Non-1866(10) DISTRIBUTION LIST

Defense Documentation Center
Cameron Station [20]
Alexandria, Virginia 22314

Chief, Bureau of Naval Weapons
Department of the Navy
Washington, D. C. 20360
Attn: P. M. Goodwin, RRMA-10

Chief, Bureau of Ships
Code 140
Department of the Navy
Washington, D. C. 20360

Chief of Naval Research
Office of Naval Research [3]
Washington, D. C. 20360
Attn: Physics Branch

Director [6]
U. S. Naval Research Laboratory
Washington, D. C. 20390
Attn: Code 4000

Commanding Officer
Office of Naval Research
1205 East Green Street
Pasadena, California 91101

Commanding Officer
Office of Naval Research
500 Geary Street
San Francisco, California 94109

Office of Naval Research
Branch Office Chicago
130 N. Michigan Avenue
Chicago, Illinois 60601

Director, Research Department
U. S. Naval Ordnance Laboratory
White Oak
Silver Spring, Maryland 20910

U. S. Naval Ordnance Laboratory
White Oak
Silver Spring, Maryland 20910
Attn: Dr. J. Dixon

Commanding Officer
Office of Naval Research
413 Sumner Street
Boston, Massachusetts 02110

Commanding Officer
Office of Naval Research
427 West 44 Street
New York, New York 10011

Air Force Office of Scientific Research
Washington, D. C. 20333

Air Force Weapons Laboratory
Kirtland AF Base, New Mexico 87117
Attn: Miles, WLPX

Air Force Cambridge Research Laboratories
Laurence G. Hanscom Field
Bedford, Massachusetts 01731
Attn: CRXL-R, Research Library

U. S. Army Research Office-Durham
Box CM, Duke Station
Durham, North Carolina 27706

Commanding Officer
U. S. Army Materials Research Agency
Wetmore, Massachusetts 02172
Attn: AMXMR-ATL

Director
Advanced Research Projects Agency
Department of Defense
Washington, D. C. 20301

Director
National Bureau of Standards
U. S. Department of Commerce
Washington, D. C. 20234

Director
U. S. Army Electronics Laboratories
Hq., U. S. Army Electronics Command
AMSEL-RD/XE
Fort Monmouth, New Jersey 07703
Attn: Dr. A. A. Glavin

Director
Institute for Exploratory Research
Hq., U. S. Army Electronics Command
Fort Monmouth, New Jersey 07703
Attn: Dr. S. Benedict Levin

Prof. John Bardeen
Department of Physics
University of Illinois
Urbana, Illinois 61803

Dr. A. C. Beer
Bastille Memorial Institute
595 King Avenue
Columbus, Ohio 43201

Dr. J. M. Beason
511 Gordon McKey Laboratory
Harvard University
Cambridge, Massachusetts 02138

Prof. A. Blasenstock
Pierce Hall 227
Harvard University
Cambridge, Massachusetts 02138

Prof. Joseph L. Birman
Department of Physics
New York University
University Heights
New York, New York 10453

Prof. N. Bloembergen
Pierce Hall 331
Harvard University
Cambridge, Massachusetts 02138

Dr. R. Brunstein
RCA Laboratories
David Sarnoff Research Center
Princeton, New Jersey 08540

Prof. Harvey Brooks [5]
Dean, Div. Engineering and Applied Physics
Pierce Hall 217
Harvard University
Cambridge, Massachusetts 02138

Prof. Edmund Brown
Department of Physics
Massachusetts Polytechnic Institute
Troy, New York 12181

Prof. Elias Bustein
Department of Physics
University of Pennsylvania
Philadelphia, Pennsylvania 19104

Prof. N. Cabrera
Department of Physics
University of Virginia
Charlottesville, Virginia 22903

Prof. J. Callaway
Department of Physics
University of California
Riverside, California 92502

Prof. H. B. Callen
Department of Physics
University of Pennsylvania
Philadelphia, Pennsylvania 19104

Dr. Manuel Cardona
Department of Physics
Brown University
Providence, Rhode Island 02912

Dr. R. O. Carlson
General Electric Research Laboratory
P. O. Box 1088
Schenectady, New York 12301

Dr. E. M. Conwell
General Telephone and
Electronics Laboratories, Inc.
Bayside, New York 11360

Dr. Michael DeMeis
559 Gordon McKey Laboratory
Harvard University
Cambridge, Massachusetts 02138

Mr. B. Danison
501 Gordon McKey Laboratory
Harvard University
Cambridge, Massachusetts 02138

Dr. Thomas F. Deutsch
Research Division
Raytheon Company
12 Bay Street
Waltham, Massachusetts 02154

Prof. H. O. Dickmar
Department of Chemistry and
Chemical Engineering
University of Illinois
Urbana, Illinois 61803

Prof. Henry Ehrenreich
Pierce Hall 105-F
Harvard University
Cambridge, Massachusetts 02138

Prof. A. W. Ewald
Department of Physics
Northwestern University
Evanston, Illinois 60201

Prof. H. Y. Fan
Department of Physics
Purdue University
Lafayette, Indiana 47907

Dr. J. Feinberg
Massachusetts Institute of Technology
Lincoln Laboratory, P. O. Box 73
Lexington, Massachusetts 02173

Prof. R. Farrell
Prof. J. R. Toll
Department of Physics
University of Maryland
College Park, Maryland 20742

Prof. H. Frisvold
Institute for the Study of Metals
University of Chicago
5640 South Ellis Avenue
Chicago, Illinois 60637

Dr. H. P. R. Fredericks
National Bureau of Standards
U. S. Department of Commerce
Washington, D. C. 20234

Dr. Murray Gershenson
Bell Telephone Laboratories
Murray Hill, New Jersey 07971

Dr. Paul Grant
557 Gordon McKey Laboratory
Harvard University
Cambridge, Massachusetts 02138

Dr. S. Croves
Massachusetts Institute of Technology
Lincoln Laboratory, P. O. Box 73
Lexington, Massachusetts 02173

Dr. Robert N. Hall
General Electric Research Laboratory
P. O. Box 1088
Schenectady, New York 12301

Dr. P. Herman
Dept. 18-48, Building 201
Lockheed Missile and Space Company
3251 Hanover Street
Palo Alto, California 94304

Dr. C. Herring
Dr. J. Barston
Bell Telephone Laboratories
Murray Hill, New Jersey 07971

Prof. K. F. Herzfeld
Department of Physics
The Catholic University of America
Washington, D. C. 20017

Prof. R. W. Hoffmann
Department of Physics
Case Institute of Technology
10900 Euclid Avenue
Cleveland, Ohio 44106

Dr. M. G. Holland
Research Division
Raytheon Company
Waltham, Massachusetts 02154

Dr. Wabataz E. Howard
Thomas J. Watson Research Center
IBM, P. O. Box 218
Yorktown Heights, New York 10598

Prof. R. V. Jones
Pierce Hall 233
Harvard University
Cambridge, Massachusetts 02138

Prof. G. Jura
Department of Chemistry
University of California
Berkeley, California 94720

Dr. E. O. Kane
Bell Telephone Laboratories
Murray Hill, New Jersey 07971

Dr. R. W. Keyes
Thomas J. Watson Research Center
IBM, P. O. Box 218
Yorktown Heights, New York 10598

Prof. C. Kittel
Department of Physics
University of California
Berkeley, California 94720

Prof. Leonard Kliffman
Department of Physics
University of Southern California
Los Angeles, California 90007

Prof. J. S. Koehler
Department of Physics
University of Illinois
Urbana, Illinois 61803

Prof. W. Kohn
Department of Physics
University of California
La Jolla, California 92038

Mr. B. Kozicki
551 Gordon McKey Laboratory
Harvard University
Cambridge, Massachusetts 02138

Dr. L. C. Kravitz
General Electric Research Laboratory
P. O. Box 1088
Schenectady, New York 12301

Prof. J. A. Krumboltz
Laboratory of Atomic and
Solid State Physics
Rockefeller Hall, Cornell University
Ithaca, New York 14850

Mr. J. A. Ladd
529 Gordon McKey Laboratory
Harvard University
Cambridge, Massachusetts 02138

Prof. A. W. Lawson
Department of Physics
University of California
Riverside, California 92502

Prof. B. Lau
Director, National Magnet Laboratory
NW 14-3220
Massachusetts Institute of Technology
Cambridge, Massachusetts 02139

Dr. M. Lee
Bell Telephone Laboratories
Murray Hill, New Jersey 07971

Mr. R. Ludke
509 Gordon McKey Laboratory
Harvard University
Cambridge, Massachusetts 02138

Dr. J. L. Mazin, Technical Director
U. S. Army Materials Research Agency
Watertown, Massachusetts 02172

Dr. L. Marton
Room 311, South Building
National Bureau of Standards
Washington, D. C. 20234

Massachusetts Institute of Technology
Engineering Library
Building 10 - Room 350
Cambridge, Massachusetts 02139
Attn: Technical Reports Collection

Massachusetts Institute of Technology
Lincoln Laboratory, P. O. Box 73
Lexington, Massachusetts 02173
Attn: Library

Prof. R. J. Maurer
Department of Physics
University of Illinois
Urbana, Illinois 61803

Mr. Paul Mc Elroy
525 Gordon McKey Laboratory
Harvard University
Cambridge, Massachusetts 02138

Prof. H. Meyer
Department of Physics
Duke University
Durham, North Carolina 27706

Mr. F. J. Morin
Associate Director
North American Aviation Science Center
1049 Chennet Drive
Northbrook, Illinois 60062

Dr. George A. Morton
RCA Laboratories
David Sarnoff Research Center
Princeton, New Jersey 08540

Prof. S. Mrozowski
Department of Physics
State University of New York at Buffalo
Hochstetler Hall, Administration Road
Buffalo, New York 14244

Dr. M. L. Nathan
Thomas J. Watson Research Center
IBM, P. O. Box 218
Yorktown Heights, New York 10598

Dr. Roger Newman
Sperry Rand Research Laboratory
Sudbury, Massachusetts 01776

Dr. R. H. Parmenter
RCA Laboratories
David Sarnoff Research Center
Princeton, New Jersey 08540

Prof. William Paul [10]
Pierce Hall 229
Harvard University
Cambridge, Massachusetts 02138

Prof. G. L. Pearson
Stanford Electronics Laboratories
Stanford University
Stanford, California 94305

Prof. P. S. Pappas
Pierce Hall 205-C
Harvard University
Cambridge, Massachusetts 02138

Dr. Herbert R. Philipp
General Electric Research Laboratory
P. O. Box 1088
Schenectady, New York 12301

Prof. James C. Phillips
Department of Physics
University of Chicago
Chicago, Illinois 60637

Dr. Vignit Prakash
529 Gordon McKey Laboratory
Harvard University
Cambridge, Massachusetts 02138

Dr. R. H. Rediker
Massachusetts Institute of Technology
Lincoln Laboratory, P. O. Box 73
Lexington, Massachusetts 02173

Mr. Charles Rose
509 Gordon McKey Laboratory
Harvard University
Cambridge, Massachusetts 02138

Prof. L. M. Roth
Department of Physics
Tufts University
Medford, Massachusetts 02155

Dr. A. Sagar
Westinghouse Electric Corporation
Research and Development Center
Bantah Road, Churchill Boro.
Pittsburgh, Pennsylvania 15235

Prof. Allan B. Scott
Department of Chemistry
Oregon State College
Corvallis, Oregon 97331

Prof. Frederick Seitz, Dean
Credentia College
308 Administration East
University of Illinois
Urbana, Illinois 61803

Mr. Thomas Shankland
513 Gordon McKey Laboratory
Harvard University
Cambridge, Massachusetts 02138

Prof. John C. Slater
Department of Physics
5-180
Massachusetts Institute of Technology
Cambridge, Massachusetts 02139

Prof. A. C. Smith
Department of Electrical Engineering
10-079
Massachusetts Institute of Technology
Cambridge, Massachusetts 02139

Prof. C. S. Smith
Department of Physics
Case Institute of Technology
Cleveland, Ohio 44106

Prof. C. S. Smith
Department of Humanities and Metallurgy
140-317
Massachusetts Institute of Technology
Cambridge, Massachusetts 02139

Prof. R. A. Smith
Center for Materials Science and
Engineering
13-202
Massachusetts Institute of Technology
Cambridge, Massachusetts 02139

Prof. R. Smoluchowski
Solid State and Materials Program
Engineering Quadrangle
Princeton, New Jersey 08540

Dr. William C. Spitzer
Electronics Sciences Laboratory
School of Engineering
University of Southern California
University Park
Los Angeles, California 90007

Dr. R. L. Sproull, Director
Advanced Research Projects Agency
Department of Defense
Washington, D. C. 20301

Prof. Julius Taylor
Morgan State College
Baltimore, Maryland 21212

Dr. D. O. Thomas
Bell Telephone Laboratories
Murray Hill, New Jersey 07971

Dr. W. W. Tyler
Assistant Vice-President
Xerox Corporation
P. O. Box 1840
Rochester, New York 14640

Prof. A. R. Von Hippel
Department of Electrical Engineering
4-243
Massachusetts Institute of Technology
Cambridge, Massachusetts 02139

Dr. W. C. Walker
Department of Physics
University of California
Santa Barbara, California 93106

Dr. D. M. Warshawer
Research Division
Raytheon Company
Waltham, Massachusetts 02154

Dr. Ernst Weber
President
Polytechnic Institute of Brooklyn
31 Jay Street
Brooklyn, New York 11201

Dr. F. K. Willenbrack
Associate Dean
Division of Engineering and Applied Physics
Harvard University
Cambridge, Massachusetts 02138

Dr. George B. Wright
Massachusetts Institute of Technology
Lincoln Laboratory, P. O. Box 73
Lexington, Massachusetts 02173

Dr. R. Zallen
513 Gordon McKey Laboratory
Harvard University
Cambridge, Massachusetts 02138

Dr. Herbert J. Ziegler
Massachusetts Institute of Technology
Lincoln Laboratory, P. O. Box 73
Lexington, Massachusetts 02173

Gordon McKey Library [2]
Pierce Hall
Harvard University
Cambridge, Massachusetts 02138
Attn: Technical Reports Collection

Editorial Office [2]
Pierce Hall 210
Harvard University
Cambridge, Massachusetts 02138
Attn: Technical Reports Reserve

Prof. J. F. Gibson
Department of Physics
University of Essex
Colchester, Essex
ENGLAND

Dr. C. Hillson
Ministry of Aviation
Royal Radar Establishment
St. Andrews Road
Great Malvern, Worcestershire
ENGLAND

Dr. T. B. Moore
R. A. E.
Farnborough, Hants.
ENGLAND

Prof. P. Algrin
Ecole Normale Supérieure
24, Rue Lhomond
Paris 5
FRANCE

Prof. Antonin De Luarche
Institut de Chimie
2 Rue Coehne
Strasbourg 67
FRANCE

Prof. B. Vodar
BP 50
Billereu
FRANCE

Prof. H. Wulker
Stamm-Schuetterwerk
880 Erlangen 2
GERMANY

Dr. H. J. O. Meyer
PHILIPS Research Laboratories
Eindhoven
NETHERLANDS

Mr. C. J. M. Rooymans
PHILIPS Research Laboratories
Eindhoven
NETHERLANDS

Department of Scientific and
Industrial Research
National Engineering Laboratory
East Kilbride, Glasgow
SCOTLAND
Attn: Mr. R. J. P. Franklin

*One copy to each address, unless otherwise indicated by numbers enclosed in brackets.

17

17

The change in boundary values due to moderate gain should produce small inaccuracies, of the order of a few percent, if the low-gain model is used to describe giant-pulse laser energy release.

Of the assumptions used in proving minor differences between the two cases, the assumption of uniform

photon density and distribution of the effect of standing waves is the greatest source of potential inaccuracy. This is because higher gain values reduce the influence of the standing wave and the spatially varying part of inversion and thereby change the value of \bar{N} rather than altering Eq. (B26) because of moderate values of \bar{N} .

Optical Properties of Thin Germanium Films in the Wavelength Range 2000–6000 Å*

PAUL M. GRANT† AND WILLIAM PAUL

Division of Engineering and Applied Physics, Harvard University, Cambridge, Massachusetts

(Received 3 February 1966; in final form 1 April 1966)

Measurements have been made of the normal incidence reflectivity and transmissivity coefficients R and T of thin germanium films. Films were deposited *in vacuo* on fused quartz substrates where the crystalline perfection of the film was controlled by varying the substrate temperature so that the effect of crystalline order on reflectivity could be observed. Epitaxial films were grown on cleaved CaF_2 substrates to thicknesses in the range 100–3000 Å. Structure in the reflectivity and transmission spectra showed these films to possess bulk band properties. However, the amplitudes of R and T were affected by the presence of film surface roughness believed to originate from nucleation and growth phenomena. Also, compressive strain induced by the difference in thermal expansion coefficients between Ge and CaF_2 shifted interband transition structure to slightly higher energies. Values of the optical constants were deduced from R and T . When experimental and calculational difficulties peculiar to the film method are accounted for, the results correspond closely to those of the Kramers–Kronig analyses of bulk reflectivity data.

I. INTRODUCTION

IN this paper we examine the degree to which optical properties derived from measurements of semiconductors in the form of films can be correlated with optical properties of the materials in the bulk state. The problem chosen for detailed study was the determination of the optical properties of germanium films from reflection and transmission measurements. Much is known concerning the band structure of bulk crystalline germanium, which, in addition to the fact that films of this material are easily prepared in a variety of stages of crystalline perfection, makes it ideally suited for this investigation. This section summarizes the results of reflectivity measurements on bulk crystals and also previous film work. Section II contains a discussion of the film preparation techniques and optical apparatus used in this work. Section III presents results for the reflectivity and transmissivity coefficients of polycrystalline and epitaxial films. Section IV includes the calculation of the optical constants from the data of Sec. III, and Sec. V contains a discussion of the over-all results and conclusions.

* This research was supported by the U. S. Office of Naval Research and formed part of a thesis submitted by P. M. Grant to the Division of Engineering and Applied Physics, Harvard University, in partial fulfillment of the requirements for the Ph.D. degree.

† IBM Pre-doctoral Fellow. Present address: IBM Research Laboratory, San Jose, California.

Energy band calculations^{1–3} in conjunction with reflectivity experiments^{4–8} have led to an understanding of the nature of interband transitions at energies up to 20 eV greater than the forbidden gap. The pseudopotential energy bands of germanium have been calculated by Brust² and are shown in Fig. 1 along with the important critical point transitions. M_0 , M_1 , and M_2 designate the type of critical point behavior and are explained in Ref. 2. Figure 2 depicts the reflectivity of bulk single-crystal germanium in the region of 2000 to 6000 Å as found by several workers.^{4,7,8} The ($L_3' \rightarrow L_1$) and ($\Lambda_3 \rightarrow \Lambda_1$) transitions are responsible for the reflectivity peaks near 6000 Å; the L transition is thought to cause the onset of these peaks, while the peaks themselves are due to the Λ transition. Two peaks occur in the spectrum because of the spin-orbit splitting (not shown in Fig. 1) of the Λ_3 valence band. The main peak near 2800 Å is due to the combined effect of the ($X_4 \rightarrow X_1$)

¹ J. C. Phillips and L. Kleinman, *Phys. Rev.* **116**, 287 (1959).

² D. Brust, *Phys. Rev.* **134**, A1337 (1964).

³ D. Brust, J. C. Phillips, and F. Bassani, *Phys. Rev. Letters* **9**, 94 (1962).

⁴ H. R. Philipp and E. A. Taft, *Phys. Rev.* **113**, 1002 (1959).

⁵ J. Tauc and E. Antoncik, *Phys. Rev. Letters* **5**, 253 (1960).

⁶ H. Philipp and H. Ehrenreich, *Phys. Rev.* **129**, 1550 (1963).

⁷ J. Tauc and A. Abraham, *Proceedings of the International Conference on Semiconductor Physics, Prague, 1960* (Czechoslovakian Academy of Sciences, Prague, 1961), p. 375; *J. Phys. Chem. Solids* **20**, 190 (1961).

⁸ T. M. Donovan, E. J. Ashley, and H. E. Bennett, *J. Opt. Soc. Am.* **53**, 1403 (1963).

and ($\Sigma_4 \rightarrow \Sigma_1$) transitions,² and the small peak near 2100 Å has been assigned to the ($L_3' \rightarrow L_3$) transition which is not explicitly designated in Fig. 1. As Fig. 2 shows, agreement exists among the various workers as regards structure in the reflectivity spectrum; however, there are differences in the absolute amplitudes due to differences in sample surface preparation. Donovan *et al.*⁸ have obtained the best reflectivity values yet by using electropolished surfaces, and their results are used as the standard in this paper. By using dispersion theory (Kramers-Kronig analysis), the optical constants have been deduced from the reflectivity data of Philipp and Taft⁴ and more recently by Philipp⁹ from that of Ref. 8. The results are given in Fig. 3 and will be compared to those obtained from film data. Figure 4 gives the skin depth δ ($\delta \equiv 1/\alpha \equiv \lambda/4\pi k$) for germanium from which one can see that very thin samples are necessary to perform transmission measurements in the range of 2–6 eV.

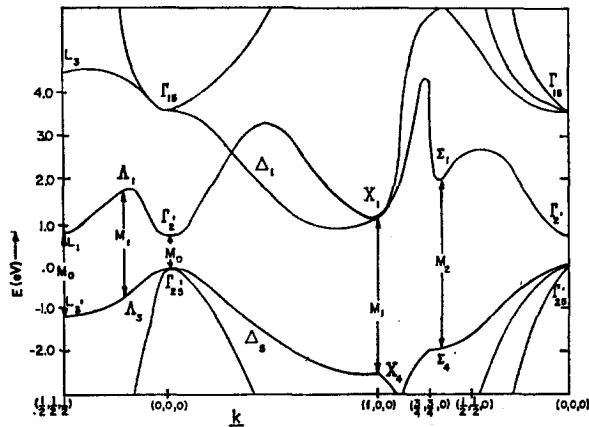


FIG. 1. The pseudopotential energy bands of germanium as calculated by Brust with some of the principal transitions indicated.

Previous measurements^{10–13} of the optical properties of thin germanium films showed little resemblance to those of bulk material. Gebbie¹² appears to have been first to appreciate the importance of crystalline perfection and its effect on optical properties. He found that annealing his films after deposition for several hours at temperatures up to 525°C produced an electron diffraction pattern of fine Debye-Scherrer-Hull rings characteristic of the polycrystalline state. The optical constants for such a film are shown in Fig. 5 along with those of Ref. 9. Here the qualitative agreement among the values of k is tolerable, but n appears to oscillate wildly. Since this work is unpublished, we cannot be sure of the method used to obtain n and k . However, it

⁹ H. R. Philipp (private communication).

¹⁰ H. M. O'Bryan, *J. Opt. Soc. Am.* **26**, 122 (1936).

¹¹ W. H. Brattain and H. B. Briggs, *Phys. Rev.* **75**, 1705 (1949).

¹² H. A. Gebbie, Ph.D. thesis, Reading, 1952 (unpublished), according to Ref. 13.

¹³ F. Lukeš, *Czech. J. Phys.* **B10**, 59 (1960).

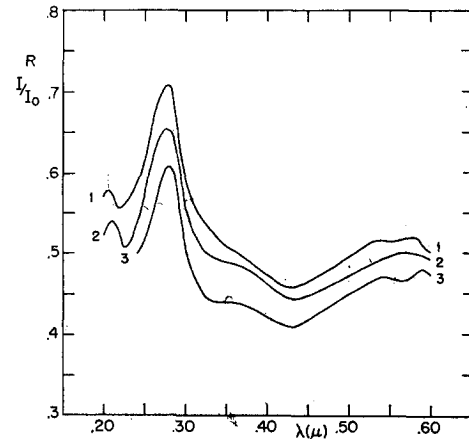


FIG. 2. Reflectivity of bulk germanium. 1. Donovan *et al.* (Ref. 8); 2. Philipp and Taft (Ref. 4); 3. Tauc and Abraham (Ref. 7).

is reported by Heavens¹⁴ that Gebbie employed the transmittances of two or more films to deduce the optical constants. If this is the case, then the theory of Ref. 15 provides an explanation for the oscillatory behavior of n which shows it to be an effect of the method of calculation and not an intrinsic property of the material.

The most recent optical constant results are those of Lukeš,¹³ shown in Fig. 6. These display fair qualitative agreement with the dispersion results over a common

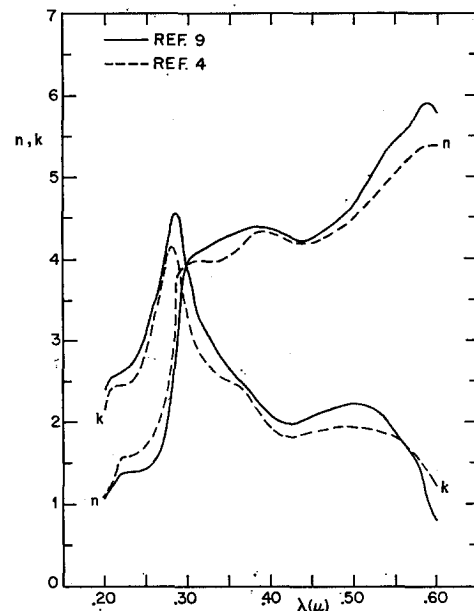


FIG. 3. The optical constants of germanium as obtained by Kramers-Kronig analyses.

¹⁴ O. S. Heavens, *Optical Properties of Thin Solid Films* (Butterworths Scientific Publications Ltd, London, 1953).

¹⁵ P. M. Grant, *J. Opt. Soc. Am.* (to be published); P. M. Grant, *Bull. Am. Phys. Soc.* **10**, 546 (1965); P. M. Grant, Gordon McKay Laboratory of Applied Science, Harvard University, Technical Report No. HP-14, 1965 (unpublished), CFSTI AD-619071.

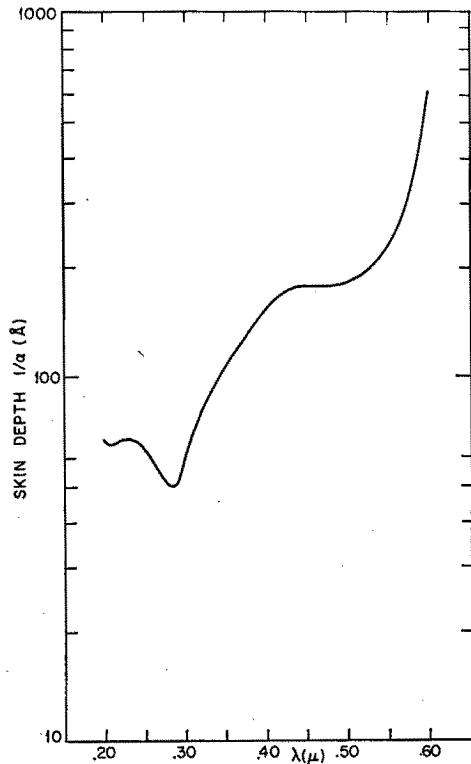


FIG. 4. Skin depth of germanium as a function of wavelength.

wavelength region. This is somewhat surprising because his films were neither deposited on hot substrates nor post-annealed to improve their crystallinity. That the crystallinity was indeed poor can be seen from his Fig. 5 which shows the reflectivity of one of his films. It cor-

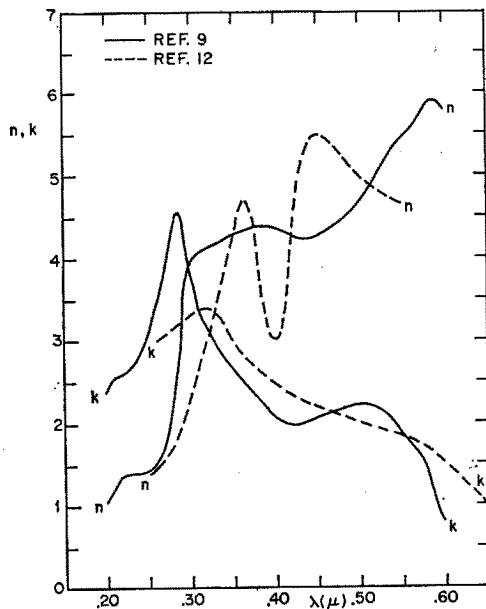


FIG. 5. Optical constants obtained by Gebbie from germanium thin films, shown by the broken line. The solid line indicates Philipp's calculations from the data of Donovan *et al.*

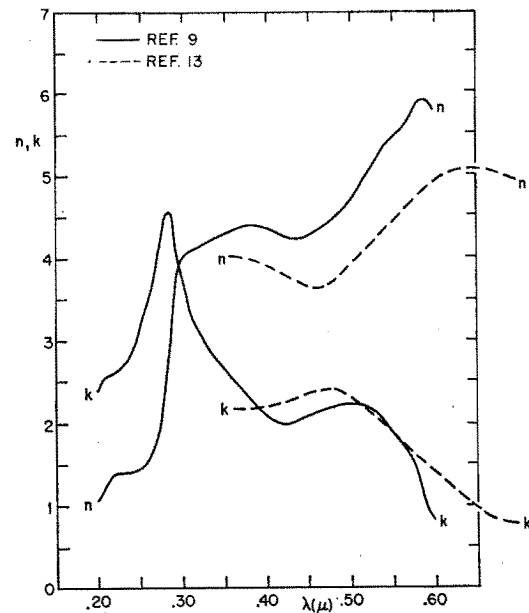


FIG. 6. Optical constants obtained by Lukeš from germanium thin films, shown by the broken line. The solid line indicates Philipp's calculations from the data of Donovan *et al.*

responds roughly to our result for a film on fused quartz shown by curve 4 of Fig. 9 which was definitely known to be of poor crystalline quality.

Measurements of either the transmissivity or reflectivity (but not both) of thin germanium films have been reported by Donovan and Ashley,¹⁶ Tauc *et al.*,¹⁷ and Cardona and Harbeke.¹⁸ In the case of Refs. 16 and 17, only the reflectivity was measured and the relationship of their work to ours is studied in Sec. III. Cardona and Harbeke have measured the transmissivity (but not reflectivity) of several rather thick epitaxial films on CaF₂. Their total results account for the proper interband transitional structure; however, the magnitude of their transmissivities is in great disagreement with those calculated from bulk optical constants for the stated thicknesses.

II. EXPERIMENTAL PROCEDURES

A. Film Preparation

Vacuum deposition techniques were used to prepare film samples on both fused quartz and CaF₂ substrates. The vacuum system was comprised of a 4-in. oil diffusion pump together with a mechanical forepump and liquid-nitrogen cold trap. Using the cold trap, this system was capable of maintaining pressures of $1-3 \times 10^{-6}$

¹⁶ T. M. Donovan and E. J. Ashley, *J. Opt. Soc. Am.* **54**, 1141 (1964).

¹⁷ J. Tauc, A. Abraham, L. Pajasova, R. Grigorovici, and A. Vancu, in *Proceedings of the International Conference on Physics of Non-Crystalline Solids, Delft, 1964*, J. A. Prins, Ed. (Interscience Publishers, New York, 1965).

¹⁸ M. Cardona and G. Harbeke, *J. Appl. Phys.* **34**, 813 (1963).

Torr during evaporation. The germanium source material was heated to evaporation temperatures in a tungsten boat of 0.005-in. thickness. The substrates were held about 6 in. above the source and were clipped to a 0.020-in. Ta plate with 0.005-in. Ta spring clips. This assembly was then heated from above by a series of 0.015-in.-diam Ta wire heater coils. The substrate temperature was measured by a Pt-Pt 10% Rh thermocouple held on the substrate surface with one of the Ta clips. The general procedure was to outgas the source and bake out the substrate for about 5 min before releasing a shutter and exposing the substrate to the evaporant beam.

A survey was made of possible substrate materials suitable for heteroepitaxial deposition of germanium. The following factors were taken into consideration:

(a) The substrate must be transparent to radiation with wavelength between 2000 and 6000 Å so that optical transmission measurements could be made on the deposited film.

(b) The present data on heteroepitaxy appear to suggest that the film and substrate lattice structure and lattice constants must match each other to a degree depending on the extent to which the bonding of the film material is ionic. That is, it seems that the greater the ionicity of the valence bonds of the film, the greater is the lattice mismatch with the substrate that can be tolerated. Therefore, as the germanium bond is non-ionic in character, a reasonable match of its lattice constant to that of the substrate is to be demanded.

(c) Because the substrate must be heated, it has to be able to withstand the temperature necessary for epitaxial growth without undue deterioration. Since this temperature runs between 500° and 700°C, the melting point of the substrate should be considerably above this range.

(d) Again, because the substrate must be heated, its linear thermal expansion coefficient becomes an important parameter. If the difference between the film and substrate thermal expansion coefficients is large, then large stresses are induced into the film on cooling to room temperature. This effect is discussed in Sec. III.

Of the presently available optical crystals, CaF₂ and SrF₂ come closest to satisfying all of the above criteria. We chose CaF₂ for our work primarily because of the abundance of experience with this material as a substrate for germanium films.¹⁹⁻²² The substrates were prepared by cleavage in air from a large single crystal. The resulting slab was 1 cm square by 1-2 mm thick. Sometimes several attempts were required to obtain a fairly smooth substrate surface. That is, the substrates, although being smooth on an atomic scale, would usually display a proliferation of cleavage steps on a macro-

¹⁹ J. Marucchi and N. Nifontoff, *Compt. Rend.* **249**, 435 (1959).
²⁰ G. G. Via and R. E. Thun, *Natl. Symp. Vac. Technol. Trans.* **8**, 950 (1962).

²¹ B. W. Sloope and C. O. Tiller, *J. Appl. Phys.* **33**, 3458 (1962).

²² A. Catlin, A. J. Bellemore, Jr., and R. R. Humphris, *J. Appl. Phys.* **35**, 251 (1964).

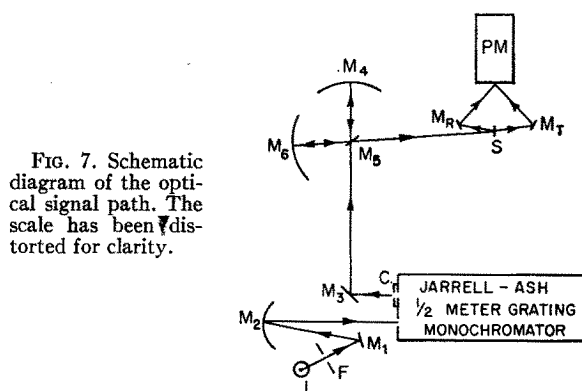


FIG. 7. Schematic diagram of the optical signal path. The scale has been distorted for clarity.

scopic level. The substrates were usually used immediately, but at other times several days would elapse. This did not seem to make any difference in the growth of the film. The fused quartz substrates were the same size as those of CaF₂ and were prepared for deposition by washing in HNO₃ and acetone.

The crystal structure of the deposited film was investigated using reflection electron diffraction and its surface topography studied by optical microscopy. The latter revealed the presence of surface roughness in those films deposited at high substrate temperatures and low deposition rates. Such behavior has been observed by several workers^{17,28,24} and leads to degradation of the film optical response. This is further discussed in Sec. III.

Of the various methods available for film thickness measurement we chose infrared transmissivity. In the wavelength region above 1.8 μ, germanium may be treated as a dielectric. In this spectral range, the index of refraction appears to be rather independent of crystalline order so the method was applied to all films, whether epitaxial or polycrystalline. The rms deviation for measurements made on any one film was about 20 Å.

B. Optical Measurements

Figure 7 is a schematic diagram of the optical path of the spectrophotometric system used to make measurements of the optical response coefficients. Light from the lamp L passes through filter F and is focused by the mirror system M₁, M₂ onto the entrance slit of a ½-m Ebert grating monochromator manufactured by Jarrell-Ash Company. Monochromatic light emerges and passes through chopper C and is then focused by the "mirror lens" system M₄, M₅, M₆ onto the sample S. It is easily seen that if the mirrors M_R and M_T are identical and the optical paths S → M_T → PM and S → M_R → PM are equal, then both transmissivity and reflectivity can be measured by a simple sample-in-sample-out technique. The mirrors were aluminized together and care was taken in alignment to keep the

²⁸ B. W. Sloope and C. O. Tiller, *Japan. J. Appl. Phys.* **2**, 308 (1963).

²⁴ R. S. Sennett and G. D. Scott, *J. Opt. Soc. Am.* **40**, 203 (1950).

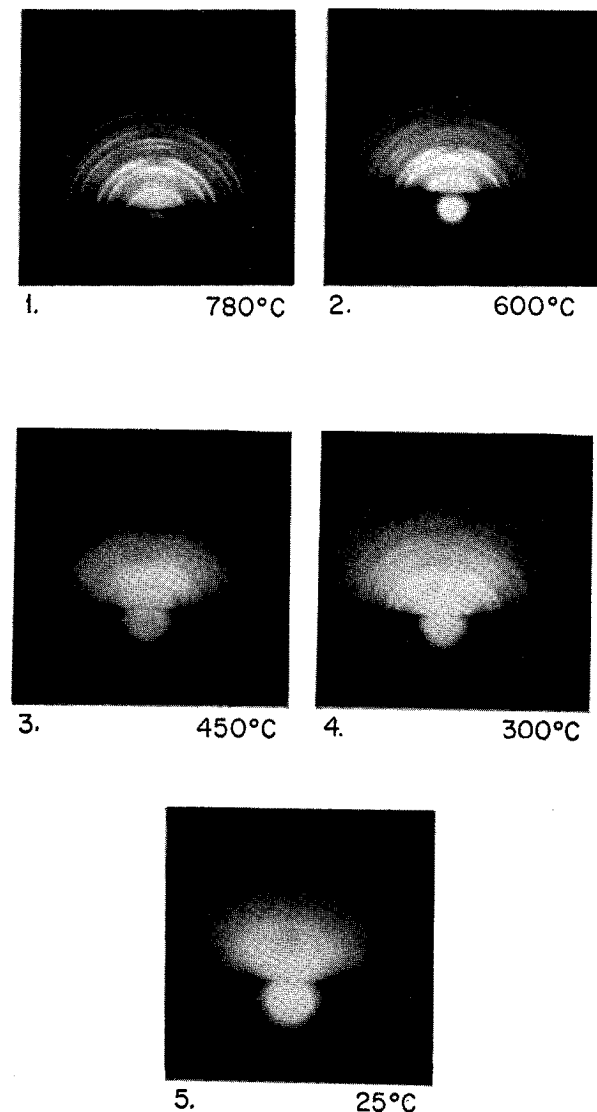


FIG. 8. Reflection electron diffraction patterns of Ge films deposited on fused quartz at various substrate temperatures. The deposition rate was from 120 to 220 Å/min for all films except film 1, where the high substrate temperature made it necessary to raise the deposition rate to 3000 Å/min in order to form a film.

optical path lengths as equal as possible. The average angle of incidence was 7° , essentially normal incidence. A tungsten lamp was used as the light source for the range 6000–3500 Å, while a high-pressure deuterium discharge device provided source energy down to 2000 Å. The photomultiplier detector was an EMI 6256B and the technique of phase sensitive detection was used in the electronic portion of the system.

The most difficult part of the experimental procedure was aligning the optics for the measurement of absolute reflectivity. Use of cleaved substrates made necessary a search for large film areas sufficiently level to allow optical alignment over the whole wavelength region. By carefully scanning the sample surface, we were us-

ually able to find an area flat enough to accommodate the slit image (about $2\text{ mm} \times 0.5\text{ mm}$). In order to assure that absolute reflectivity was being measured, a bulk germanium sample was prepared by careful polishing and etching and its reflectivity taken in order to compare with values found by other workers. With a freshly etched surface, repetition of the alignment and measurement procedure indicated a scatter in the over-all reflectivity amplitude of $+0\%$, -2% absolute in the wavelength region 3500–6000 Å and $+1\%$, -4% absolute in the wavelength region 2000–3500 Å about the values of Ref. 8. For our purposes, this degree of accuracy was considered sufficient.

Alignment errors in the measurement of film transmissivity are thought to be small. Care was taken to keep observations in a pinhole-free region; however, some error was probably caused by substrate refraction. Errors of this type are estimated to be about 10% relative. On the other hand, scattered light considerations limited the transmission measurements to values above 10^{-3} .

III. RESULTS FOR THE FILM REFLECTIVITY AND TRANSMISSIVITY COEFFICIENTS

A. Polycrystalline Films

Figure 8 displays the reflection electron diffraction (RED) patterns for five germanium films deposited on fused quartz substrates held at different substrate temperatures. We see from the broadening of the Debye-Scherrer-Hull rings that there is a progressive decrease in grain size with decreasing substrate temperature. The effect on the film reflectivity can be seen in Fig. 9. Interference effects due to low absorption and film thinness appear at wavelengths above 3500 Å; hence care

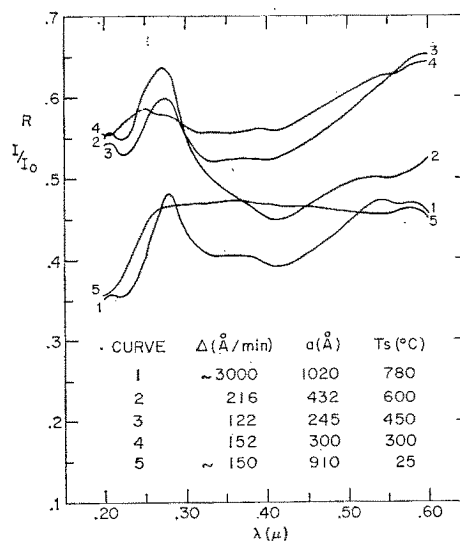


FIG. 9. Reflectivity of Ge films on fused quartz for various substrate temperatures. Δ =deposition rate, a =film thickness, T_s =substrate temperature.

must be exercised in interpreting effects in this region as intrinsic. However, below 3500 Å the absorption is sufficiently high so that the reflectivity is independent of thickness. In this range, we see that the shape of the Σ , X peak deteriorates with decreasing grain size (or with DSH ring broadening) until it completely disappears in the film deposited at room temperature. It might be expected that polycrystalline germanium would have the same optical response as single-crystal germanium and this is true up to a point. However, it is clear that ultimately the crystallite size can become so small or internal strain so great that even short-range order is deeply perturbed. Tauc *et al.*¹⁷ interpret the resulting reflectivity spectrum as that which would occur for interband transitions with only energy conserved. That is, strong singularities in the joint density of states no longer appear due to the breakdown of symmetry and all interband transitions can be considered as indirect. This interpretation accounts for the loss of sharp reflectivity structure as one proceeds to the amorphous state. One notices that the amplitude of the Σ , X peak of film 1 is considerably below those of the other polycrystalline films. This is due to scattering of the incident uv light by a rough film surface arising from deposition at elevated substrate temperatures. The onset of roughness with increasing substrate temperatures is a well-known effect.^{17,24} Trying to optimize the amplitude of the Σ , X peak involves finding a temperature at which long-range order will still be present, yet surface roughness will not. Our best sample in this respect was the 600°C film 2 of Fig. 9 which gave a value of 64%, agreeing well with that of Ref. 16. The remaining difference with the bulk is probably due to a residual roughness effect.

The 780°C film 1 was thick enough to suppress most of the interference effects in the long-wavelength region. It is seen that this film possesses all of the bulk reflectivity structure except that the Λ spin-orbit split peaks are severely distorted. From a similar study of these peaks under different states of disorder, Donovan and Ashley¹⁶ imply that, for bulk crystals, a reassignment from the spin-orbit splitting scheme to one in which the low-energy peak belongs to L -point transitions and the high-energy peak to Λ -point transitions should be considered. In fact, such could be the case for polished bulk surfaces or highly polycrystalline films; however, the former interpretation still seems to be the correct one for the bulk single crystals because:

(a) It accounts in a clear manner for the theoretically predicted spin-orbit splitting.

(b) Λ transitions occur at M_1 -type saddle points while L transitions occur at M_0 -type saddle points.³ The former have the proper shape to produce reflectivity peaks whereas the latter would tend to produce at best weak ones.

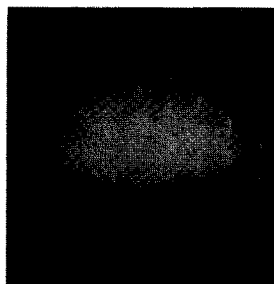
(c) Pressure measurements of Zallen *et al.*²⁵ show that both peaks have the same pressure coefficient, as would be expected if they arose at the same point in k space.

(d) The L transitions have actually been observed apart from the Λ transitions by Greenaway²⁶ for GaAs and by Cardona and Greenaway²⁷ for ZnTe and CdTe.

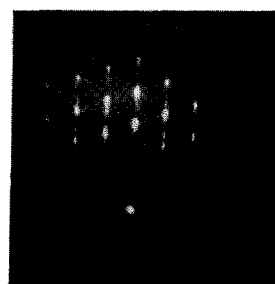
Reflectivity measurements on polycrystalline Ge films evaporated on fused quartz substrates held at 600°C with deposition rates ranging from 154–3850 Å/min have been taken. The results indicated that variations of this parameter within the above range produced changes in the reflectivity spectrum and RED patterns that were much smaller than those caused by changes in substrate temperature and whose interpretation would be very difficult.

B. Epitaxial Films on CaF₂

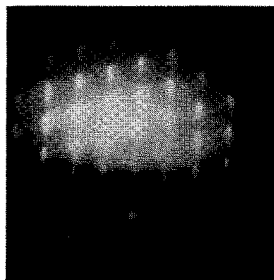
The optical properties of over 40 epitaxial films on CaF₂ were examined. Figures 10–15 show the results for three typical films deposited under conditions felt to give good crystalline quality yet minimize surface roughness. Figure 10 gives the RED patterns for these films and clearly shows their epitaxial behavior. The



$T_s = 600^\circ\text{C}$
 $\Delta = 925 \text{ \AA}/\text{min}$
 $a = 1850 \text{ \AA}$



$T_s = 620^\circ\text{C}$
 $\Delta = 810 \text{ \AA}/\text{min}$
 $a = 135 \text{ \AA}$



$T_s = 600^\circ\text{C}$
 $\Delta = 750 \text{ \AA}/\text{min}$
 $a = 250 \text{ \AA}$

FIG. 10. Reflection electron diffraction patterns of epitaxial Ge films on cleaved CaF₂. The notation is the same as in Fig. 9.

²⁵ R. Zallen, W. Paul, and J. Tauc, *Bull. Am. Phys. Soc.* **7**, 185 (1962); R. Zallen, Technical Report No. HP-12, Gordon McKay Laboratory of Applied Science, Harvard University, 1964 (unpublished).

²⁶ D. Greenaway, *Phys. Rev. Letters* **9**, 97 (1962).

²⁷ M. Cardona and D. Greenaway, *Phys. Rev.* **131**, 98 (1963).

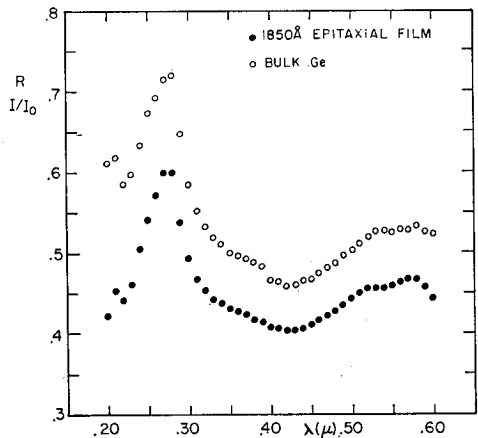


FIG. 11. Reflectivity of a 1850-Å epitaxial germanium film on CaF₂ compared to that of bulk germanium.

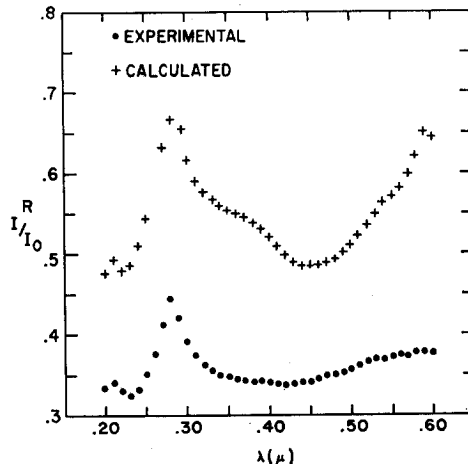


FIG. 14. Reflectivity of a 135-Å epitaxial film on CaF₂ compared to theoretical values calculated from the data of Ref. 9.

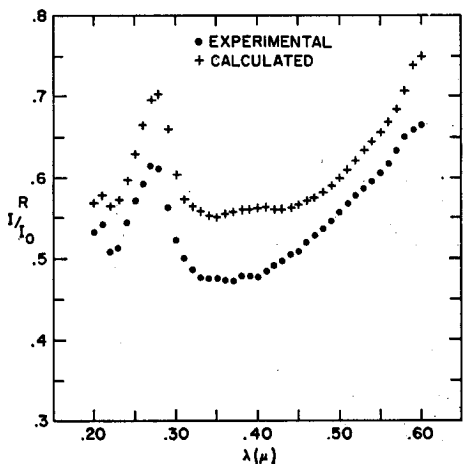


FIG. 12. Reflectivity of a 250-Å epitaxial film on CaF₂ compared to theoretical values calculated from the data of Ref. 9.

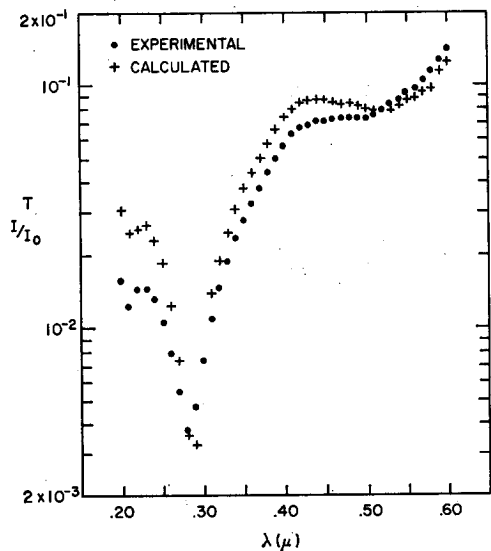


FIG. 13. Transmissivity of the same 250-Å film as in Fig. 12 compared to theoretical values calculated from the data of Ref. 9.

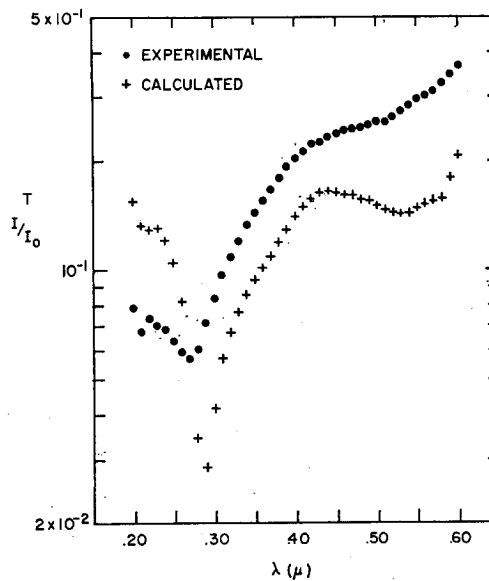


FIG. 15. Transmissivity of the same 135-Å film as in Fig. 14 compared to theoretical values calculated from the data of Ref. 9.

films are grown in the $\langle 111 \rangle$ direction and the electron beam is incident in a $\langle 110 \rangle$ -type direction. For epitaxial films, one would expect structure in the optical response to duplicate closely that of bulk material. Examination of Figs. 11–15 shows this to be true. Each epitaxial film has all the principal structure indicated by bulk reflectivity, including Λ spin-orbit splitting. This is most strikingly brought out in Fig. 11 for the 1850-Å film (the shift of the Λ peaks are discussed below). Even the 135-Å film, which is only about 25 atoms thick, reveals the structure predicted by bulk measurements, and, in fact, the proper structure was observed in still thinner films. Because of the agglomerate character of the films, this indicates that short-range order is far more important than long-range order in the formation of critical points in the band structure.

The RED patterns indicate the presence of stacking-fault and twin types of defects in each of our epitaxial films; however, what their effect should be in producing fine structure in the film optical response is not presently known.

The reflectivity amplitude of the 1850-Å film of Fig. 11 should in principle be equal to that of bulk germanium as its thickness is sufficient to suppress interference below 6000 Å. The reason it does not is due primarily to scattering from a rough surface arising from the agglomerate growth of the film. It has been shown by Porteus and Bennett²⁸ that the following relation for the reflectance of a rough surface,

$$R = R_0 \exp[-(4\pi\sigma/\lambda)^2], \quad (1)$$

where R_0 is the reflectivity of a perfectly smooth surface of the same material and σ is the rms value of the deviations from mean thickness, is valid under the following assumptions:

(a) The surface irregularity distribution must be Gaussian.

(b) The reflected light must be coherently scattered from the surface, a condition which holds for $\sigma/\lambda \ll 1$. The ratio $R(\text{film})/R(\text{bulk})$ for the 1850-Å film vs $1/\lambda^2$ is given in Fig. 16. It is seen to yield approximately a straight line, in agreement with (1), whose slope determines a σ of 76 Å. By way of comparison, we might point out that the rms roughness of the usual variety of microscope slide is about 10–15 Å. Equation (1) predicts that as $\lambda \rightarrow \infty$, $R \rightarrow R_0$; however, Fig. 16 shows that $R \rightarrow 0.091 R_0$. This 9% difference can be explained as a constant systematic error in the film reflectivity due to misalignment and poor optical imaging because of the cleaved surface. For the 250-Å film of Figs. 12 and 13 we may perform a similar analysis by using only the reflectivity in the region below 3500 Å and extrapolating to infinite wavelength. In this region the skin depth is small (see Fig. 4) and interference does not occur. This procedure leads to $\sigma = 50$ Å and $R_\infty = 0.95 R_0$. In addition, we see from Fig. 13 that roughness is not without its effect on the uv transmittance where T of the film falls below its theoretically predicted value by about 50% at $\lambda = 2000$ Å.

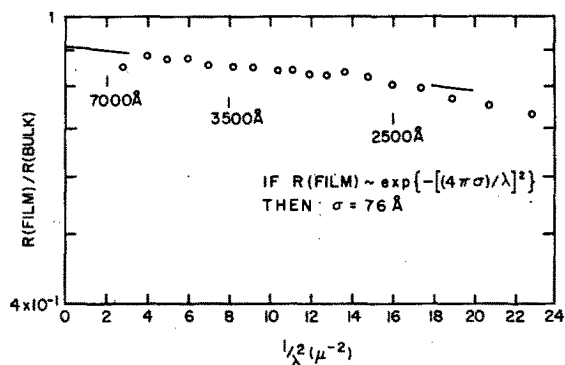


FIG. 16. Plot of $R(\text{film})/R(\text{bulk})$ vs $1/\lambda^2$ for the 1850-Å epitaxial Ge film on CaF_2 .

²⁸ H. Bennett, *J. Opt. Soc. Am.* **53**, 1389 (1963); J. Porteus, *ibid.* **53**, 1394 (1963); H. Bennett and J. Porteus, *ibid.* **51**, 123 (1961).

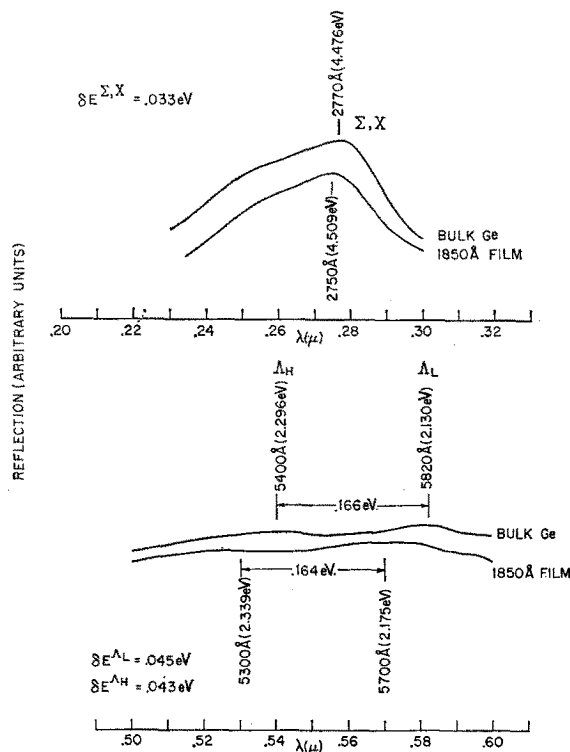


FIG. 17. Effect of film stress on the reflectivity peaks of the 1850-Å epitaxial Ge film on CaF_2 .

Figures 14 and 15 show the optical response of a film whose thickness was measured by infrared transmission to be 135 Å. We see that the experimental values of R and T depart considerably from corresponding theoretical values, T measured being higher than T calculated (except in the far uv region) with the reverse true for R . The theoretical T and R are computed for a given film thickness using the data of Ref. 9 and the equations of Ref. 15. This behavior was observed in each of our very thin films; thus the film of Figs. 14 and 15 is not a mere variant. The disparity in amplitudes is probably due to the breakdown of coherent interference effects when the rms roughness of the film approaches an appreciable fraction of the mean film thickness. This results in phase averaging or intensity addition for the theoretical R and T expressions of Refs. 15 and 29. The effects of such averaging have been calculated and the results confirm the observed behavior. The scattering will not be nearly as strong for ir radiation; hence, measurements of transmission here can still be used to calculate thicknesses.

Surface roughness in epitaxial germanium films on CaF_2 has been studied by Sloope and Tiller.²³ Their investigations indicate that conditions for good epitaxy are also conditions for appreciable roughness, and that the size of the agglomerates is of the order of some thousands of angstroms with thickness variations as much as 200 Å. Surface roughness is the most serious

²³ L. Harris, J. K. Beasley, and A. L. Loeb, *J. Opt. Soc. Am.* **41**, 604 (1951). This paper contains a discussion of the appropriate phase-averaging procedures for thin-film formulas.

problem preventing the fabrication of films with bulk optical properties.

C. Effect of Induced Strains in the Films on Optical Properties

Because of the difference in thermal expansion between film and substrate, there will appear an induced strain in the film as it is cooled from its formation temperature. The effect of this strain is clear from Fig. 17, where it is seen that both the Λ peaks and the Σ , X peak are shifted to higher energies. In the discussion to follow, we make the following idealizations:

(a) The film and substrate are assumed to be isotropic, homogeneous, and temperature-independent in their thermal expansion properties.

(b) The film is assumed not to constrain the expansion of the substrate.

(c) The induced stress is considered as if it arose from forces applied at the faces of the film edges.

The constraining condition that gives us a relation for induced stress is that elongations of both film and substrate are necessarily equal. This leads to

$$X = (\alpha_{Ge} - \alpha_{CaF_2})\Delta T/S, \quad (2)$$

where the α 's are the appropriate linear thermal expansion coefficients, ΔT the temperature change, and S and X are the appropriate inverse Young's modulus and induced stress, respectively, for the direction of elongation under consideration. For a film whose axis of epitaxy is $[111]$, the $[1\bar{1}0]$ and $[\bar{1}\bar{1}2]$ directions along with $[111]$ form a mutually orthogonal set of which $[1\bar{1}0]$ and $[\bar{1}\bar{1}2]$ may be considered the directions of applied stress. For each of these directions, S becomes

$$S = \frac{1}{2}(s_{11} + s_{12} + s_{44}/2), \quad (3)$$

where s_{11} , s_{12} , and s_{44} are the the compliance constants. For room-temperature values of $\alpha_{Ge} = 5.75 \times 10^{-6}/^\circ\text{C}^{30}$ and $\alpha_{CaF_2} = 19.5 \times 10^{-6}/^\circ\text{C}$,³¹ $s_{11} = 0.97 \times 10^{-6}/\text{atm}$, $s_{12} = -2.63 \times 10^{-7}/\text{atm}$, and $s_{44} = 1.50 \times 10^{-6}/\text{atm}$,³⁰ with $\Delta T = -575^\circ\text{C}$, (2) and (3) give $X = 10\,800$ atm compressive.

Brooks' equation for the shift of an energy band under strain may be written as³²

$$\delta E = E_1 \text{Tr } \mathbf{u} + E_2 \hat{k} \cdot (\mathbf{u} - \frac{1}{3} \mathbf{1} \text{Tr } \mathbf{u}) \cdot \hat{k}. \quad (4)$$

Here E_1 and E_2 are deformation potentials, \hat{k} is the unit vector in \mathbf{k} space to the band edge in question, and \mathbf{u} is the strain tensor. We will take δE , E_1 , and E_2 to refer to transitional energy differences instead of band edges. We note that in the case of hydrostatic pressure, Eq. (4) in conjunction with the generalized Hooke's law gives

$$\delta E = -3E_1(s_{11} + 2s_{12})X, \quad (5)$$

³⁰ *Selected Constants Relative to Semiconductors*, P. Aigrain and M. Balkanski, Eds. (Pergamon Press, Inc., New York, 1961).

³¹ *Handbook of Chemistry and Physics* (Chemical Rubber Publishing Company, Cleveland, Ohio, 1955).

³² H. Brooks, in *Advances in Electronics and Electron Physics*, L. Lorton, Ed. (Academic Press Inc., New York, 1956), Vol. 7; R. W. Keyes, in *Solid State Physics*, F. Seitz and D. Turnbull, Eds. (Academic Press Inc., New York, 1960), Vol. 11.

where X is the pressure. This relates E_1 to the hydrostatic pressure coefficient $\partial E/\partial P$.

For applied biaxial stress X in the $[1\bar{1}0]$ and $[\bar{1}\bar{1}2]$ directions, the stress tensor is

$$\sigma = \frac{X}{3} \begin{pmatrix} 2 & -1 & -1 \\ -1 & 2 & -1 \\ -1 & -1 & 2 \end{pmatrix}. \quad (6)$$

Hooke's law and (4) yield for the ($\Lambda_3 \rightarrow \Lambda_1$) transition in the $[111]$ direction

$$\delta E_{[111]}^\Lambda = 2E_1^\Lambda(s_{11} + 2s_{12})X - \frac{1}{3}E_2^\Lambda s_{44}X. \quad (7)$$

On the other hand, for Λ transitions in $[1\bar{1}\bar{1}]$ -type directions, we have

$$\delta E_{[1\bar{1}\bar{1}]}^\Lambda = 2E_1^\Lambda(s_{11} + 2s_{12})X + \frac{1}{3}E_2^\Lambda s_{44}X. \quad (8)$$

A similar analysis for the Σ , X transition gives

$$\delta E_{[100]}^\Sigma = 2E_1^\Sigma(s_{11} + 2s_{12})X, \quad (9)$$

$$\delta E_{[110]}^\Sigma = 2E_1^\Sigma(s_{11} + 2s_{12})X - \frac{1}{6}E_2^\Sigma s_{34}X, \quad (10)$$

and

$$\delta E_{[1\bar{1}0]}^\Sigma = 2E_1^\Sigma(s_{11} + 2s_{12})X + \frac{1}{6}E_2^\Sigma s_{34}X. \quad (11)$$

We see that there is always a part related to hydrostatic pressure in addition to the shear component which lifts the degeneracy of otherwise equivalent transitions. The detection of this splitting was beyond the resolution of our experiments and its principal effect was probably to broaden slightly the reflectance peaks of the films.

Philipp, Dash, and Ehrenreich³³ have performed uniaxial stress measurements on the Λ transition of Ge. Using their value of $E_2^\Lambda = -2.0$ eV³⁴ and $E_1^\Lambda = -5.6$ eV calculated from Zallen's²⁵ value of the hydrostatic pressure coefficient, we obtain $\delta E_{[111]}^\Lambda = (-4.0 \times 10^{-6}$ eV/atm) X and $\delta E_{[1\bar{1}\bar{1}]}^\Lambda = (-5.3 \times 10^{-6}$ eV/atm) X . As there are three times as many $(1\bar{1}\bar{1})$ transitions as (111) , we take the over-all shift to be the weighted average of $\delta E_{[111]}^\Lambda$ and $\delta E_{[1\bar{1}\bar{1}]}^\Lambda$ or $\delta E^\Lambda = (-5.0 \times 10^{-6}$ eV/atm) X . From Fig. 17, we have $\delta E^\Lambda = 44 \pm 10$ meV as the observed mean shift of the Λ doublet which implies a value of 8800 ± 2000 atm for the induced biaxial compressive stress to be compared with $10\,800$ atm calculated from thermal expansion.

E_1 and E_2 for the Σ , X transition are not known at present. However, an estimate can be made of E_1 from the pressure coefficient for the Σ , X transition in silicon found by Zallen²⁵ to be about 3×10^{-6} eV/atm. There is an empirical law which states that among semiconductors with similar band structures, the pressure coefficients for transitions between similar irreducible representations at identical points of their Brillouin zones are approximately equal.^{25,35} We therefore take Zallen's result to hold for germanium also. For purposes of calculation, we will assume $E_1^\Sigma = E_1^\Sigma$ and $E_2^\Sigma = 0$. From

³³ H. Philipp, W. Dash, and E. Ehrenreich, *Phys. Rev.* **127**, 762 (1962).

³⁴ This number was calculated from data contained in Refs. 33 and 25. The value of E_2 actually given in Ref. 33 is believed to be in error.

³⁵ W. Paul, *J. Appl. Phys.* **32**, 2082 (1961).

Fig. 15, $\delta E^{X,\Sigma} = 33 \pm 12$ meV which results in $X = 16\,500 \pm 6000$ atm compressive biaxial stress. The factor of two difference in the Λ and Σ , X results cannot, at present, be attributed to anything except experimental error. Although a shift of reflectivity peaks was observed in all epitaxial films, it was carefully measured only in the 1850 Å film. Rather dramatic evidence of the film stress occurs as the film is made thicker. Since the stress force is applied at the film-substrate interface, a bending moment is created in the film which increases with film thickness until some critical value is reached whereupon the film begins to break away from the substrate. For a substrate temperature of 600°C, the critical thickness appears to be around 3000–4000 Å as deduced from observations of thick films that rapidly broke up immediately after deposition.

IV. CALCULATION OF THE FILM OPTICAL CONSTANTS

The theory necessary for the deduction of the optical constants from measurements of thin-film reflectivity and transmissivity is discussed elsewhere¹⁵ and only the principal conclusions and results are presented here. Using appropriate theoretical expressions for R and T , the optical constants may be recovered through a Newton-Raphson iteration using a high-speed digital computer. In doing this, it is found that there are certain regions in which the derived n and k are very sensitive to small changes in R and T . This fact, however, is shown in Ref. 15 to be intrinsic in the theoretical development and is not connected with any particular method of numerical analysis. The sensitivity to experimental error arises from the existence of at least one branch point in the dependence of n and k on R and T . The branch point originates from the fact that

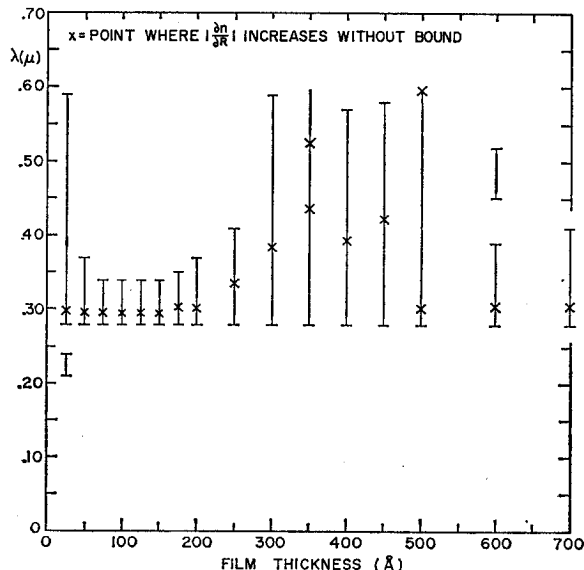


FIG. 18. Wavelength region where $|\partial n/\partial R| \geq 20$ as a function of film thickness. The optical constants of Ge from Ref. 9 were used in Ref. 15 to calculate this bar diagram. The criterion on $|\partial n/\partial R|$ was determined by stipulating that an error of 0.5 absolute in the derived n would be considered intolerable for an error of 2.5% absolute in the measured R .

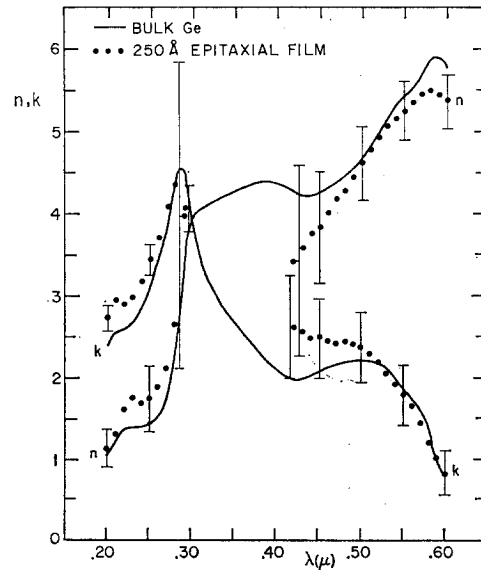


FIG. 19. Optical constants derived from R and T measurements on a 250-Å epitaxial germanium film deposited on CaF_2 .

R and T are intensities and involve squares of the optical constants. It turns out that the most critical behavior is that of the real part of the index of refraction on reflectivity. Figure 18 indicates that there is always some wavelength region for which n is highly sensitive to small experimental errors in R . In fact, there is always at least one singular point in $|\partial n/\partial R|$. However, there appears to be an optimum film thickness range, although experimental considerations may obviate its use. In our work, we found 250 Å to be a workable thickness in both experimental and theoretical aspects and we present the results for this film in Fig. 19. In performing the calculation, the reflectivity in Fig. 12 was corrected for roughness scattering according to the experimental quantities $R_\infty = 0.95R_0$ and $\sigma = 50$ Å. These quantities were calculated by extrapolating from the high absorption region and applying Eq. (1). The bars indicate the error spread in n and k for an absolute error in R of $\pm 2.5\%$ and in a of ± 10 Å, and a relative error in T of $\pm 10\%$. We see that the discrepancy between the film values of the optical constants and those of bulk Ge (taken from Fig. 3) can be included, for the most part, within the span of these conservative experimental estimates. We see also that in the region in which no roots appeared, namely, 3000 to 4100 Å, corresponds almost exactly to the region predicted by Fig. 18 for a 250-Å film as having very high sensitivity to experimental errors in R and T . Reference to Figs. 5 and 6 shows that the present results are far superior to previous film optical constant work, primarily because of the use of epitaxial films.

V. CONCLUSIONS

In Sec. I it was stated that the object of this research was to study the correlation between the optical properties of semiconductors in the film and bulk states using germanium as the investigative medium. We believe the following to be the three main conclusions:

(a) A correspondence can be established between the crystalline perfection of a film as determined by diffraction techniques and the degree to which its optical spectrum approaches that of a bulk single crystal. It is interesting to note that although the grain size of our very thin epitaxial films approximated that of the polycrystalline films, only the former possessed bulk optical structure. This would suggest that it is some other factor, such as large intrinsic strain, rather than small grain size that distorts the optical response of our polycrystalline films. However, the exact nature of the relation between grain size, texturization, intrinsic strain, etc., and the band structure of a disordered material is a subject which remains for future theoretical and experimental development.

(b) We feel our measurements of R and T and calculations of n and k indicate that after experimental difficulties have been taken into account the epitaxial films have essentially the same optical properties as bulk material. Hence we may consider the use of epitaxial films as reliable vehicles for investigation into the optical properties of semiconductors in the high-absorption regions.

(c) However, because the theoretical discussions of Sec. IV indicate that there will invariably be a region of high sensitivity in the derived n and k to errors in R and T , we may conclude that film determinations of n and k will not supplant, but rather will supplement, other methods such as polarimetry and dispersion analyses. We have shown that in the regions where roots are obtained, the film optical constants compare favorably with the Kramers-Kronig result.

With regard to the statement in (b) concerning experimental difficulties, we believe these to be of four types:

(1) *Roughness scattering.* As pointed out in Sec. III, the deposition conditions for epitaxial films are in opposition to the requirements for smooth films and this prevents attainment of bulk single-crystal optical properties. However, there is evidence that the situation is not so severe in the case of epitaxial lead salt films.³⁶ Extensions of this work should concentrate on devising methods of producing smooth films, possibly through techniques other than vacuum deposition.

(2) *Cleaved surfaces.* The result was to produce systematic errors in the reflectivity and transmissivity amplitudes (less so in the latter than in the former). Careful selection of the sample area to be studied helped minimize this difficulty.

(3) *Reflectometer misalignment.* Because the reflected ray does not follow the same optical path as the incident ray, there is always some difficulty in aligning to measure absolute reflectivity. In our work, we used as an alignment standard a very carefully etched sample of bulk germanium. In this way we were able to reduce errors by periodically checking our film alignment procedures with our standard.

³⁶ P. R. Wessel (to be published); C. E. Rossi, Gordon McKay Laboratory of Applied Science, Harvard University (unpublished data.)

(4) *Stress effects.* In Sec. III, the energy shift in the characteristic film reflectivity peaks due to the difference in the thermal expansion coefficients of the film and substrate was discussed. As a result, we must be cautious in ascribing structure appearing in film optical spectra as being precisely at the same energy as it would appear in the bulk material. Particular care is to be exercised in assigning physical significance to energy differences between absorption edges in films and reflectivity peaks in bulk crystals. On the other hand, in relation to the entire film optical response spectrum considered here (2-6 eV) the effect is small (~ 40 meV) and may usually be ignored.

Because of the roughness-coherence difficulties, we were not able to investigate the effect of thickness on the film optical properties. The influence of this parameter seems to be divided into two aspects: (1) the perturbative effect of the finite boundary on the bulk energy levels, and (2) the "quantization" of k space in the direction normal to the film surface into intervals of $2\pi/Na$, where N is the number of atoms and a the lattice constant. Of these, the second has the interesting possibility of giving the density of states a two-dimensional character and of splitting interband transitions which occur between bands of nonzero slope. Such splittings may be hard to observe, however, due to competition from other directions in the Brillouin zone equivalent to the thickness direction.

It is possible to conceive of several experiments in the range 2-6 eV for which epitaxial films would be particularly suitable; for example, magneto-optic measurements such as magnetoabsorption and Faraday and Voigt effects, hydrostatic pressure shifts, and photoconductivity investigations are some that can be considered. In addition, it may prove more feasible to produce certain semiconductor alloys in film form than in the bulk state in order to study their optical properties.

ACKNOWLEDGMENTS

The authors wish to thank Dr. H. R. Philipp, T. M. Donovan, and P. Wessel for providing them with preprints of their work prior to publication and to acknowledge a useful correspondence with B. W. Sloope on the preparation and properties of epitaxial germanium films. Thanks are also due to Dr. G. Via and Dr. M. Holland for the use of their vacuum apparatuses during certain stages of this work.

The authors have also benefited from discussions with colleagues of the Gordon McKay Laboratory and wish to thank B. Kosicki, P. McElroy, and R. Ludeke for suggestions concerning the experimental apparatus and C. Rossi and Dr. R. Zallen for discussion of the experimental results.

The construction of all experimental apparatuses was performed by James Inglis and Albert Manning while David MacLeod assisted in sample preparation.

One of us (PMG) wishes to acknowledge the personal financial assistance provided by the IBM Corporation over the duration of this research.